MODELLING PATTERNS AND DRIVERS OF POST-FIRE FOREST EFFECTS THROUGH A REMOTE SENSING APPROACH

A Thesis Submitted to the College of Graduate Studies
and Research in Partial Fulfillment of the Requirements
for the Degree of Doctor of Philosophy in the
Department of Geography and Planning at the University
of Saskatchewan, Saskatoon, Canada

By

Thuan Chu

Permission to Use

In presenting this thesis in partial fulfillment of the requirements for a Postgraduate degree from the University of Saskatchewan, I agree that the Libraries of this University may make it freely available for inspection. I further agree that permission for copying of this thesis in any manner, in whole or in part, for scholarly purposes may be granted by the professor or professors who supervised my thesis work or, in their absence, by the Head of the Department or the Dean of the College in which my thesis work was done. It is understood that any copying or publication of use of this thesis or parts thereof for financial gain shall not be allowed without my written permission. It is also understood that due recognition shall be given to me and to the University of Saskatchewan in any scholarly use which may be made of any material in my thesis.

Requests for permission to copy or make to other use of material in this thesis in whole or part should be addressed to:

Head of the Department of Geography and Planning

University of Saskatchewan

Saskatoon, Saskatchewan S7N5C8

ABSTRACT

Forests play a significant role in the global carbon budget as they are a major carbon sink. In addition to the deforestation caused by human activities, some forest ecosystems are experiencing detrimental changes in both quantity and quality due to wildfires and climate change that lead to the heterogeneity of forest landscapes. However, forest fires also play an ecological role in the process of forming and functioning of forest ecosystems by determining the rates and direction of forest stand recovery. This process is strongly associated with various biotic and abiotic factors such as: the disturbance regimes, the soil and vegetation properties, the topography, and the regional climatic conditions. However, the factors that influence forest-recovery patterns after a wildfire are poorly understood, especially at broad scales of the boreal forest ecosystems. The study purpose of this research is to use remote sensing approaches to model and evaluate forest patterns affected by fire regimes under various environmental and climatic conditions after wildfires. We hypothesized that the forest regeneration patterns and their driving factors after a fire can be measured using remote sensing approaches. The research focused on the post-fire environment and responses of a Siberian boreal larch *(Larix sibirica)* forest ecosystem. The integration of different remotely sensed data with field-based investigations permitted the analysis of the fire regime (e.g. burn area and burn severity), the forest recovery trajectory as well as the factors that control this process with multi temporal and spatial dimensions. Results show that the monitoring of post-fire effects of the burn area and burn severity can be conducted accurately by using the multi temporal MODIS and Landsat imagery. The mapping algorithms of burn area and burn severity not only overcome data limitations in remote and vast regions of the boreal forests but also account for the ecological aspects of fire regimes and vegetation responses to the fire disturbances. The remote sensing

models of vegetation recovery trajectory and its driving factors reveal the key control of burn severity on the spatiotemporal patterns in a post-fire larch forest. The highest rate of larch forest recruitment can be found in the sites of moderate burn severity. However, a more severe burn is the preferable condition for the area occupied quickly by vegetation in an early successional stage including the shrubs, grasses, conifer and broadleaf trees (e.g. *Betula platyphylla, Populus tremula, Salix spp., Picea obovata, Larix sibirica*). In addition, the local landscape variables, water availability, solar insolation and pre-fire condition are also important factors controlling the process of post-fire larch forest recovery. The sites close to the water bodies, received higher amounts of solar energy during the growing season and a higher pre-fire normalized difference vegetation index (NDVI) showed higher regrowth rates of the larch forest. This suggests the importance of seed source and water-energy availability for the seed germination and growth in the post-fire larch forest. An understanding of the fire regimes, forest-recovery patterns and post-wildfire forest-regeneration driving factors will improve the management of sustainable forests by accelerating the process of forest resilience.

Keywords: *post-fire, fire regime, burned area, burn severity, boreal larch forest, forest trajectory, forest regeneration, driving factors, remote sensing*.

ACKNOWLEDGEMENTS

I would like to express sincere thanks to my supervisor, Dr. Xulin Guo. Without her advice and encouragement, I could not have completed my PhD program. I wish to thank my committee members who are Dr. John Wilmshurst, Dr. Winston Zeng, Dr. Kazuo Takeda, and Dr. Karen Tanino for their valuable support and guidance throughout my whole PhD program. In addition, I really appreciate that Dr. Kazuo Takeda and his research group in Japan for sharing their field data. I want to thank Dr. Guo's research group and her students for knowledge sharing and discussion on my research topic. I also would like to express my gratitude to the Department of Geography and Planning and College of Graduate Studies and Research in the University of Saskatchewan for the training of academic integrity during my PhD program. I wish to give my thanks to Dr. Cherie Westbrook for her valuable comments and suggestions in improving my thesis. Many thanks go to the Vietnam International Education Development (VIED) program, Department of Geography and Planning, and the University of Saskatchewan for their financial support. Finally, I want to deeply express my love and thanks to my family, my parents, and my friends who always support me behind every step of my life. I would like to dedicate this work to my parents, my wonderful wife, Ninh Cao, and my lovely children, Bi and Nhi.

TABLE OF CONTENTS

LIST OF TABLES

LIST OF FIGURES

LIST OF ABBREVIATIONS

AIC	Akaike's Information Criterion
AMSR-E	Advanced Microwave Scanning Radiometer for Earth Observation
AUC	Area Under the Curve
AVHRR	Advanced Very High Resolution Radiometer
CART	Classification and Regression Tree
CBI	Composite Burn Index
dNBR	Differenced Normalized Burn Ratio
dNDMI	Differenced Normalized Difference Moisture Index
dNDVI	Differenced Normalized Difference Vegetation Index
EVI	Enhanced Vegetation Index
fAPAR	Fraction of Absorbed Photosynthetically Active Radiation
FRI	Forest Recovery Index
FVC	Fractional Vegetation Cover
GeoCBI	Geo Composite Burn Index
GEOLAND-2	Global Monitoring for Environment and Security integrating Earth Observation
GFED	Global Fire Emissions Database
GIMMS	Global Inventory Modeling and Mapping Studies
GLOBCARBON	Global Land Products for Carbon Model Assimilation
IFZ	Integrated Forest Z-score
L3JRC	The global vegetation burned area product 2000-2007
LAI	Leaf Area Index
Landsat ETM+	Landsat Satellite 7 Enhanced Thematic Mapper Plus
Landsat TM	Landsat Satellite 5 Thematic Mapper
LiDAR	Light Detecting and Ranging
MOD09A1	MODIS Surface Reflectance 8-day Level-3 Global 500m Product
MOD14A2	MODIS Thermal Anomalies and Fire 8-day Level-3 Global 1km Product
MODIS MCD45A1	MODIS Burned Area Monthly Level-3 Gridded 500m Product
MODIS MCD64A1	MODIS Collection 5.1 Direct Broadcast Monthly Burned Area Product
MODIS	Moderate Resolution Imaging Spectroradiometer

NBR	Normalized Burn Ratio
NDMI	Normalized Difference Moisture Index
NDSWIR	Normalized Difference Shortwave Infrared Index
NDVI	Normalized Difference Vegetation Index
NPP	Net Primary Productivity
PAL	Pathfinder AVHRR Land
RdNBR	Relative differenced Normalized Burn Ratio
SAR	Synthetic Aperture Radar
SAVI	Soil Adjusted Vegetation Index
SMA	Spectral Mixture Analysis
SPOT VEGETATION	Systeme Pour I'Observation de la Terre Vegetation
SRTM	Shuttle Radar Topography Mission
TVDI	Temperature Vegetation Dryness Index
VIF	Variance Inflation Factor
VOD	Vegetation Optical Depth
YSF	Year Since Fire

CHAPTER 1: GENERAL INTRODUCTION

1.1 Preface

Chapter 1 presents the summary of literature review and defines the research hypotheses and objectives. This chapter also outlines the structure of the thesis. The detail of the literature review has been fully published as a review paper:

> Chu, T. & Guo, X. (2014) Remote Sensing Techniques in Monitoring Post-Fire Effects and Patterns of Forest Recovery in Boreal Forest Regions: A Review. *Remote Sensing*, 6(1), 470-520, doi:10.3390/rs6010470.

The first two sections in the published paper have been summarized and re-organized to form sections 1.2 and 1.3 in this chapter. The major findings and conclusions from the literature review of mapping burned area and burn severity and remote sensing based assessment of post-fire forest patterns have been summarized to include in the sections 1.4.1, 1.4.2 and 1.4.3. In addition, the section 1.4.4 that is not included in the published paper has been added to draw the research hypotheses and objectives of this dissertation. Thuan Chu conducted the literature review and wrote the manuscript. Dr. Xulin Guo provided comments and revised the manuscript. The permission to re-use the paper for this thesis has been obtained from the publisher by Thuan Chu.

1.2 Background

Under the effects of climate change, fire is a common factor in many forest ecosystems, particularly in the northern hemisphere (Flannigan et al., 2013). Forest disturbance by fires is a major challenge for forest management in various forest ecosystems due to the loss of lives and infrastructure, greenhouse gas emissions, soil degradation, soil erosion, and the destruction of species, biomass and biodiversity (EARSEL, 2008, FAO, 2010, Flannigan et al., 2006, Carmenta

et al., 2011). On the other hand, the forest fires constitute one major ecological process, especially during the initial stages of the forest regeneration which positively influence a rapid growth in the young trees, an early and abundant seed productivity, and a good dispersal of the seeds (Babintseva and Titova, 1996). Fires, in combination with the variations in topography, soil and climate, also result in the diversity of forest species, forest types and stand ages which in turn influence natural cycles such as the carbon and hydrological cycles (Kasischke and Stocks, 2000). Forest fires and fire regimes, however, are severely underreported at the global and regional scales. Only 78 countries responded to the fire effect surveys, representing 63 percent of the global forest area, reporting that 60 million hectares of land , including forests and other wooded land, were burned per year during the period 2003-2007 (FAO, 2010). Additionally, there has been uncertainty surrounding the characterization of forest fire regimes and its influences on the ecosystem carbon balance, particularly in remote regions (e.g., Eurasian boreal forest) (Kukavskaya et al., 2012).Therefore, it is necessary to have more studies and reports on forest fire to understand how the natural and anthropogenic environments might be affected as well as their responses after the fire disturbances.

Remote sensing techniques for forest fire prevention, assessment and monitoring have been developed since the mid-1980s (Lentile et al., 2006). These techniques have been employed to address the three different temporal fire-effects phases: pre-fire conditions, active fire characteristics, and post-fire ecosystem response (French et al., 2008, Lentile et al., 2006, Veraverbeke et al., 2010a, Seidl et al., 2010). Numerous algorithms and approaches for the first two phases have been developed (Mulder et al., 2011, Hansen and Loveland, 2011, Pierce Jr et al., 2009, Boyd and Foody, 2010, Powell et al., 2010, Wang et al., 2012, Schroeder et al., 2008, Giglio et al., 2008, Wooster et al., 2012, Justice et al., 2011). However, little effort has been dedicated to assess suitable remote sensing data and methods over the widely spatial and temporal ranges of post fire-affected environments, particularly in characterizing and explaining

the patterns of forest ecosystems responding to fire disturbances (e.g. Leon et al., 2012, Eckert et al., 2015, Kane et al., 2015).

The nature and state of the forest recovery after the impact of fire disturbance are a function of the following factors: the size and severity of the disturbances, the pre-disturbance conditions, the climate, the post-disturbance soil nutrient status, the topography, and the process of seedling establishment (Frolking et al., 2009, Shenoy et al., 2010, Zhao et al., 2012, Mansuy et al., 2012). Quantification of forest-regeneration variability as an explanation of the above factors has been used in a number of studies using field-based approaches (e.g.: Furyaev, 2001, Pausas et al., 2004, Jain et al., 2012, Shenoy et al., 2010, Mansuy et al., 2012, Zhao et al., 2012, Veilleux-Nolin and Payette, 2012). To date, however, remote sensing approach is still a potential application, and a number of challenges remain to be solved before researchers and managers in order to look for vegetation responses within a larger context, particularly in Eurasian boreal larch forests.

1.3 Forest fire and forest pattern terminology

Relationships between forest fire, climate and ecotope condition, and forest pattern are complicated. Climate condition, forest fuels, ignition agents, topography and human activities are major factors strongly influencing forest fire regimes and forest dynamics (Schoennagel et al., 2004, Johnson et al., 2001, Chuvieco and Congalton, 1989, Liang et al., 2011). Forest fire, in turn, impacts climate conditions, plant ecosystems and human life (Flannigan et al., 2006, Conard and A Ivanova, 1997, EARSEL, 2008). As a result, vegetation will respond and adapt to changes in the environment by establishing appropriate structure and composition (Beuning et al., 2011, Kayes et al., 2011, Voepel et al., 2011, Russell-Smith et al., 2012). As with any endeavor involving different disciplines, an understanding of the terminology being used to study or describe a process and phenomenon of fire effects is essential within this study.

In relation to fire effects, there are a variety of terms used to describe the characteristics of fire and post-fire effects. The current research is associated with some of these terms: pre-fire environment, fire environment, active fire, post-fire environment, fire intensity, fire severity, burned scar and burn severity. Here we follow Jain et al. (2004) , Key & Benson(2006), Lentile et al. (2006), French et al. (2008), Kasischke et al.(2008) and Veraverbeke et al. (2010b) who accepted these terms as following (Table 1.1).

Table 1.1 Definitions of fire related environments and parameters used to measure fire effects

Fire related environment	Derived parameter	Definition of parameter
Pre-environment	-	The environmental characteristics of a site before the fire
Fire environment: the environmental characteristics of a site during the fire; this is the state involved with active fire	Fire frequency/fire recurrence	Number of fires per unit time in a specified area. This is the temporal aspect of fire regimes
	Fire intensity	A description of the fire behavior quantified by energy release such as the temperature and heat from burning organic matter
Post-environment: the environmental characteristics of a site after the fire including both the short and long term effects	Burned area and fire perimeter	The measurement of post fire effects in terms of dimension/area – fire - affected areas by fire, spatial extent of fire effect.
	Fire severity	The degree of environmental change caused directly by fire assessed immediately after the fire event (an initial assessment). This is the short-term severity assessment only, immediately after the fires.
	Burn severity	The degree of environmental change caused by the fire assessed by a certain amount of time elapses after the fire (an extended assessment). This includes both the short (e.g. pre-recovery phase after fire) and long term post fire severity (e.g. the observed changes in characteristics of vegetation regrowth after the fire such as re-sprouting, regeneration…); frequently used by the remote sensing applications.

As an agent of change to accelerate the modification of the vegetation landscape, forest fire controls both the environments for vegetation establishment and the vegetation succession (Furyaev, 2001, Brown et al., 1999, Schimmel and Granström, 1996). In coupling with both the

regional climates and ecotope conditions, fire characteristics determine post-fire forest structure, composition and function (Flannigan et al., 2000, Furyaev, 2001,Huang and Wang, 2010). Spatial arrangement and distribution of the forest components define the forest structure. The forest composition, however, is characterized by the species richness and abundance, as a description of forest biodiversity. Finally, the forest function refers to the production of organic matters (McElhinny et al., 2005).

In this study, we use a general term of forest pattern to represent the responses of forest ecosystem to disturbances by fire, in which the forest pattern is formed by forest structure and forest composition, and is measured by the distribution, arrangement, and species diversity or the forest types after the disturbance. Also, throughout this study, vegetation recovery, forest regeneration, and forest succession are occasionally used interchangeably. They all refer to the process of forest re-establishment from a stand clearing fire disturbance. More specifically, the forest succession is mainly observed in a broader context of forest ecosystem responses. Within this study, it refers to the different development stages of vegetation recovery after the fire disturbances, including bare land, herbaceous plants, grasses and shrubs dominated species, forest-tree seedlings and saplings, young and old forest stands. The forest regeneration is used to focus on the regenerating process of the pre-fire tree dominants in the post-fire environment.

1.4 Modeling post-fire effects and forest recovery patterns using remote sensing

1.4.1 Mapping burned area

Changes in spectral signatures that occur following a fire can be surrogates for identifying the ecological patterns of burned areas. Due to the loss of vegetation cover and the conversion of wood to charcoal by fire, the surface reflectance within the burned areas decreases dramatically in visible to near infrared wavelengths while it increases in short and middle

infrared bands of most satellite sensors (Miller and Thode, 2007, Lentile et al., 2006). For this reason, burned patches are relatively easy to discriminate visually (Bastarrika et al., 2011b). However, automatic monitoring of burned areas remains challenging due to uncertainties surrounding the heterogeneity of post-fire environment (Bastarrika et al., 2011b, Pereira, 1999, Loboda et al., 2011, Loboda et al., 2013).

Medium to coarse satellite data have been commonly used for regional and global analyses of burned areas, including boreal regions. For examples, the Moderate Resolution Imaging Spectroradiometer (MODIS) (Loboda et al., 2007, Chuvieco et al., 2008c, Roy et al., 2008, Giglio et al., 2009, Loepfe et al., 2012, Loboda et al., 2011, Giglio et al., 2010, Chuvieco et al., 2008a, Chuvieco et al., 2008b), and SPOT VEGETATION (Grégoire et al., 2003, Tansey et al., 2004, Fraser and Li, 2002, Tansey et al., 2008) have been widely used more recently for both detecting the active fires and mapping the burned scars due to its high quality of temporal and spectral resolution, and the data availability since 2000 and 1998 respectively. As the accuracy of long time-series data of burned areas is important for modeling fire emissions and assessing feedbacks between fire and global climate change, comparisons and critical reviews of the accuracy of different burned area products at global scale were also well reported in the literatures (Mouillot et al., 2014, Giglio et al., 2010, Kasischke et al., 2011). Giglio et al. (2010) found that there were considerable differences in many regions among burned area products of the Global Fire Emissions Database (GFED) derived from multi-sensor (http://www.falw.vu/~gwerf/GFED), the L3JRC global burned area data from SPOT VEGETATION (http://bioval.jrc.ec.europa.eu), the GLOBCARBON burned area product (http://www.geosuccess.net), and the Collection 5 MODIS MCD45A1 burned area product (http://modis-fire.umd.edu/Burned_Area_Products.html). The burned areas reported in the

L3JRC product were much higher than all other data sets in almost all regions, except for Africa, while the GFED product was most similar to the MCD45A1 data set. Similarly, Kasischke et al. (2011) found that the GFED version 3 burned area product was the most consistent with the fire management data in North America, while L3JRC and GLOBCARBON products significantly overestimated the burned areas. The MCD45A1 data set underestimated and resulted in higher fraction of burned areas when compared to GFED3 data (Kasischke et al., 2011). These results suggest that the use of global burned area products should be validated with other independent data sets to quantify omission and commission errors that requires a strong need to improve computer and earth observation facilities to achieve high quality of burned area products using remote sensing (Mouillot et al., 2014).

In addition, several studies in the boreal forest regions noted that mapping of the burned areas in such high northern latitudes using remote sensing should account for the variations of fire regime, vegetation phenomenon, timing of the burned area assessment, and climatic and environmental conditions in order to attain high quality data set of burned areas (Loboda et al., 2007, Loboda et al., 2011, Loboda et al., 2012, Loboda et al., 2013, Kasischke et al., 2010, Moreno Ruiz et al., 2012). All vegetation, fire, and environmental related information can be obtained from the remote sensing data (e.g., fire regimes from MODIS products (de Groot et al., 2012), vegetation phenology from the AVHRR-NDVI analysis (Delbart et al., 2006)), and can be subsequently incorporated into the mapping algorithms to improve the accuracy of mapping burned areas.

1.4.2 Mapping burn severity

Recent studies have demonstrated that the sensitivity of spectral bands and indices of remotely sensed data will change in burn severity classes, similar to mapping burned areas.

Spectral indices such as the Normalized Burn Ratio (NBR) and the Normalized Difference Vegetation Index (NDVI) have been widely used for assessing burn severity through remote sensing in boreal regions (Epting et al., 2005, Hall et al., 2008, Hoy et al., 2008, Barrett et al., 2010, Verbyla and Lord, 2008). Analyses of burn severity using multi-temporal satellite data and bi-temporal image differencing techniques have also resulted in the numerous differenced indices for burn severity assessment in boreal regions, such as the differenced Normalized Burn Ratio (dNBR) (Jin et al., 2012, Epting and Verbyla, 2005, Epting et al., 2005, Allen and Sorbel, 2008, Hall et al., 2008, Hoy et al., 2008, Murphy et al., 2008, Soverel et al., 2011, Cai et al., 2013), the differenced Normalized Difference Vegetation Index (dNDVI) (Epting et al., 2005, Wu et al., 2013) and a relative version of the dNBR (RdNBR) (Soverel et al., 2010). The above listed indices are often independent variables used to derive dependent field-based indices of burn severity, such as the Composite Burn Index (CBI) and the Geo Composite Burn Index (GeoCBI) (Epting et al., 2005, Sorbel and Allen, 2005, Allen and Sorbel, 2008, Hall et al., 2008, Soverel et al., 2010, Soverel et al., 2011) and the post-fire organic soil layer depth (Verbyla and Lord, 2008, Barrett et al., 2010), to estimate burn severity at pixel level.

Even though the field-based indices such as the CBI and the GeoCBI and the spectral indices such as the NBR, the dNBR and the RdNBR are the most widely adopted combination in the investigation of burn severity, they are not yet standard methods for evaluating burn severity in either remote sensing or fire science communities (Jain et al., 2012, French et al., 2008). Additionally, the assessment of burn severity from both in-situ and remotely sensed data are not always available in many boreal ecoregions (e.g. Siberian boreal forests) (Chu and Guo, 2013). As a result, there are a variety of methods beyond the models of CBI and vegetation regression indices to evaluate the burn severity using the remote sensing data, and the results vary widely.

For example, the percentile classifications of the MODIS dNBR and the change of spring albedo ($\Delta\alpha_0$) were employed by Jin et al (2012) to assign classes of low (20%-45% percentile), moderate (45%-75% percentile) and high (>75% percentile) severity in North American post-fire boreal forests. The authors mentioned that an alternative approach to measuring the burn severity is monitoring the changes in spring albedo since it depends on the mortality and recovery rate of post-fire vegetation. Epting and Verbyla (2005) applied similar Landsat dNBR threshold values (90, 275, and 680), calculated by Epting et al. (2005), to classify low, moderate, and high classes of burn severity in their Alaskan boreal forest study site. However, Cai et al. (2013) evaluated burn severity in eastern Siberia boreal forests according to the histogram of dNBR values with high severity (dNBR $\geq$743) and low severity (dNBR < 743). All these results suggest that the above proposed indices, spectral thresholds and methods of assessing burn severity can possibly be adjusted to local conditions with specific vegetation community. However, it is not clear whether they can be extended to other study sites. Additionally, characteristics of fire and burn severity have been very well documented in the boreal regions of North America(French et al., 2008, Chu and Guo, 2013). However, to the best of our knowledge, there have been no similar studies conducted in other boreal regions, such as the Eurasian boreal forests. Because the types of fire and vegetation properties are quite different from the boreal forests in North America and Russia similar patterns of burn severity may not be found among these boreal regions. Therefore, methods for mapping burn severity for the boreal forest regions around the world are necessary to be developed and validated to understand post-fire effects comprehensively, particularly for the remote boreal regions of Eurasia with little available data on the severity of fire disturbances.

1.4.3 Trajectory of post-fire forest regrowth patterns

The temporal and spatial variability of the post-fire forests can be characterized by the stages of forest succession, structure and regrowth of the forest composition since fire disturbance. The remote sensing of the disturbances for the express purpose of quantifying forest patterns enables the extraction of the independent variables to predict the dependent variables, such as the successional stages, stand age, tree diameter and height, biomass, canopy closure, species diversity and other structural parameters over large areas of the post-fire forest. In boreal forest ecosystems, there are very few studies using optical sensors, such as the Landsat TM/ETM+, to characterize the post-fire patterns of succession (Epting and Verbyla, 2005, Zhang et al., 2004, Hall et al., 1991, Steyaert et al., 1997). One known study of the post-fire succession through remote sensing was conducted by Epting and Verbyla (2005) over a 16 year post-fire period in interior Alaska. The Landsat TM/ETM+ images were used to categorize the two successional classes of self-replacement and relay floristic with respect to burn severity and pre-fire vegetation. The approach for monitoring successional stages by Epting and Verbyla relied on a similar method of change detection using post-classification maps. Pixels exhibiting the same class of vegetation in both pre- and post-fire images were classified as self-replacement succession, whereas areas that changed classes of vegetation from spruce-dominated to broadleaf-dominated were classified as relay floristic areas (Epting and Verbyla, 2005). The result showed that the post-fire patterns of succession in Alaskan boreal forests strongly depended on the types of pre-fire vegetation and burn severity. For example, most of the high burn severity areas with closed needle-leaf, open needle-leaf, and mixed forest classes shifted to woodland or shrubland, sixteen years after the fire (Epting and Verbyla, 2005).

In addition to classifying successional stages, remote sensing with time series data offers considerable potential in the trajectory of post-fire forest dynamics as well as estimation of the forest recovery rate. Many studies have addressed this issue by using moderate-to-low resolution time series of vegetation indices (Kasischke and French, 1997, Epting and Verbyla, 2005, Beck et al., 2011, Lyons et al., 2008, Tanase et al., 2011b, Hicke et al., 2003, Goetz et al., 2006, Jin et al., 2012, Jones et al., 2013, Magnussen and Wulder, 2012). The observations of the recovery rate of vegetation from these analyses varied greatly, even in the same eco-region, depending upon the data resolution, the pre-burn vegetation, the burn severity and the temporal and spatial variability of the vegetation indices within the burned and unburned areas. Goetz et al. (2006) used two NDVI time series derived from the Pathfinder AVHRR Land (PAL) and the Global Inventory Modeling and Mapping Studies (GIMMS) AVHRR to investigate the recovery of vegetation after fires in the boreal forests of Canada. Their results indicated that the recovery rates based on the NDVI of Canadian boreal forest were different between the PAL and GIMMS data sets but both were consistently shorter than previous studies (Kasischke and French, 1997, Hicke et al., 2003). Cuevas Gonzalez et al. (2009) found that it took more than 13 years for the burned Siberian boreal forest to recover fully to pre-fire conditions with respect to NDVI and Normalized Difference Shortwave Infrared Index (NDSWIR) extracted from the MODIS time series data. This recovery rate was longer than the 5-year recovery period reported by Goetz et al. (2006) and the 4-year period investigated by Hicke et al. (2003) in North America. Cuevas Gonzalez et al. (2009) assumed that the differences in fire regimes and fire types, growing conditions, species composition and data resolution between the Siberian and North American studies might have influenced these results. Similarly, Alcaraz-Segura et al. (2010) also mentioned that the low resolution data processing (1-8km observation), such as GIMMS-NDVI

data, may introduce a bias that tends to underestimate the positive NDVI trends in the Canadian boreal forest.

Even though many current studies have used optical vegetation indices such as NDVI, to describe forest recovery after disturbances, according to Frolking et al. (2009) the assumption that the index of vegetation recovery equates to forest recovery may be inappropriate. Buma (2011) examined this hypothesis using the MODIS time series data from 2000 to 2010 in the area of burned forest in Colorado's Routt National Forest, USA, and demonstrated that NDVI is poorly correlated with forest recovery represented by the seedling density in burned areas. Therefore, the studies on post-fire forest recovery should consider the inclusion of structural forest ground variables such as seedling recruitment, canopy cover, tree diameter and height directly to remotely sensed parameters (Buma, 2011, Leon et al., 2012, Gitas et al., 2012). To date, however, very few studies in the literature have attempted to tie the post-fire forest variables to the remotely sensed data with different metrics and spatial scales in either the boreal forests or other ecosystems. In addition to field based observations, the evaluation of satellite datasets in monitoring the post-fire forest recovery should include comparisons of the independent observations at the stage of results comparing the detected trends of different optical datasets (Alcaraz-Segura et al., 2010, Goetz et al., 2006), and optical and SAR/LiDAR datasets in different regions (Tanase et al., 2011b). Finally, as noted by some authors (e.g.,(Kasischke and French, 1997, Goetz et al., 2006, Cuevas Gonzalez et al., 2009, Alcaraz-Segura et al., 2010)), analyzing the patterns of vegetation cover in the boreal forests using the remote sensing data requires the development of approaches to account for the variations in spatial and spectral resolution of remotely sensed data, environmental conditions (e.g., clouds and haze, soil moisture, albedo, latitude, topography, climate), vegetation characteristics (e.g., species

composition, land cover type, vegetation phenology) and the disturbance regimes (e.g., fire and burn severity, fire type, fire frequency). A useful approach might be the stratification of those factors with similar conditions prior to applying the remote sensing tools (Chu and Guo, 2013).

1.4.4 Assessment of environmental factors affecting post-fire forest patterns

Forest regeneration patterns and the successional stages in post-fire environments are commonly heterogeneous across the landscape within burned areas (Casady et al., 2009, Johnstone et al., 2011,Lozano et al., 2012). The heterogeneous degree is strongly influenced by both the abiotic and biotic factors of pre- and post-fire environment, such as fire regimes, soil properties, landforms, regional climate, and species characteristics (Dube, 2009, Flannigan et al., 2006, Casady et al., 2009, Johnstone et al., 2010a). The fires can have either negative or positive influences on plant regrowth as determined by the changes in vegetation structure and composition, seed germination, and species recruitment depending on fire intensity, fire/burn severity, fire frequency and ecoregion (Shenoy et al., 2010, Mansuy et al., 2012, Cai et al., 2013, Veilleux-Nolin and Payette, 2012). The seedling density of black spruce and aspen in the North American boreal forest has positive correlation with the burn severity (Johnstone et al., 2010b, Veilleux-Nolin and Payette, 2012). On the other hand, burn severity has negative influence on the regeneration patterns of both conifer and broadleaf species (Cai et al., 2013).As a result of fire severity, there has been a potential shift in dominant forest cover in the Alaskan boreal forest in which the effect of large fire years, likely to be of higher severity, in the recent decade has reduced the black spruce stands by 4.2% and facilitated the growth of the deciduous forests by 20% (Barrett et al., 2011, Barrett and Kasischke, 2013). Regarding the fire frequency, the absence of fires during a very long period may lead to the increase in moss and duff layer and exacerbating the poor soil conditions and thus degrades forest ecosystem (Sofronov and

Volokitina, 2010). Fire frequency approximately once per century can act as a natural factor to enhance the forest biodiversity. However, high and very high fire frequency, occurring once per 20-30 years and 3-5 years, can lead to replacement of the forest vegetation by non-arboreal vegetation such as the meadow, the shrub, or the tundra or even take 50 to hundreds years to recover to pre-fire conditions (Bergeron et al., 2001, Zyryanova et al., 2010a).

In addition to the fire regimes, environmental factors such as the soil properties, the regional climate, the topography, and their interrelationships also alter the structure, functioning, and long-term successional dynamics of the boreal forest ecosystems, which depend on species characteristics. For example, larch *(Larix gmelini)* and birch *(Betula platyphylla)* only regenerate well in burned areas with good site conditions of shallow slopes and thick soil depth, whereas *Pinus pumila* seedlings can grow well in burned areas with either shallow slopes, thick soils or steep slopes and thin soils (Zhao et al., 2012). Similarly, organic layer depth in the burned areas has negative effects on the trembling aspen but positive effects on the black spruce successions (Shenoy et al., 2010). Other factors, the climatic conditions (Van Leeuwen et al., 2010, Mansuy et al., 2012), the topographic factors (Pausas et al., 2004, Oikonomakis and Ganatsas, 2012, Casady et al., 2009, Cai et al., 2013), and the pre-fire vegetation conditions (Leon et al., 2012, Lozano et al., 2012), also have significant effects on the seedling establishment and growth after the fire disturbances. Despite of the relevance of these factors for forest regeneration, few studies have assessed the integrated influence of these factors, leading to uncertainties in understanding of the forest ecosystems' responses to the environmental changes (Casady et al., 2009), particularly in the boreal larch forest ecosystems.

Both the field based and remote sensing based methods are much employed in the studies of post-fire regeneration patterns and driving factors. With remote sensing-based approaches;

however, the vegetation indices such as NDVI, EVI, and Tasseled Caps are mainly surrogates representing forest recovery (e.g. (Leon et al., 2012, Lozano et al., 2012) rather than the vegetation structural attributes. Similar to the trajectories of forest recovery mentioned above, this assumption may result in inappropriate assessments of the biotic and abiotic factors influencing the actual forest regenerations (Frolking et al., 2009, Buma, 2011). Therefore, the inclusion of forest structural variables, such as the seedling recruitment, canopy cover, diameter, height, and biomass as well as the use of remote sensing indices that accurately reflect the post-fire forest structure and composition is required for modeling the effects of fire and environmental changes on the vegetation responses and recovery. These types of analyses can be potentially conducted with the synergistic use of in-situ data and remotely sensed data in order to understand the response of post-fire forest ecosystems at landscape level comprehensively.

1.4.5 Summary and research gaps

The influences of fire disturbances generate a wide range of temporal and spatial forest heterogeneity, and hence the interpretation of fire effects, causal factors (e.g., fire regimes, soil properties, landforms), and ecological responses are a challenge to both scientists and managers. Availability and accuracy of the burned area and burn severity products in boreal regions are often confounded by the environmental conditions, limited instrument capabilities (e.g., resolution and cloud cover), methods of analysis (e.g. data resolution), and presence (or absence) of official data on burned areas and burn severity for validation of results. As boreal forests are located in high northern latitudes (generally at latitudes from 50^0 to 70^0N) with a very long period of snow and cloud cover annually, direct observation of clear land surface for mapping the burned areas and burn severity is thus limited by using remote sensing, particularly in using the optical remote sensing. This problem is particularly challenging for the goal of mapping

burned areas and burn severity during early and late-season fires when reflectance signatures of the burned areas are altered by snow cover and vegetation phenology. Even though a number of mapping algorithms have been developed for boreal regions, ranging from the visual interpretation to automatic burned area and burn severity classification algorithms, the accuracy of the burned area estimation and burn severity assessments in the boreal regions varied significantly among studies. Therefore, a selection of the operational data and methods might be difficult within the boreal regions, particularly for reconstructing the long time series of burned areas and burn severity. Remote sensing approaches for mapping the burned areas and burn severity also require overcoming limitations of the official fire statistics and the field-based assessment of burn severity. These data are urgently needed within some regions, such as the boreal forests located in Eurasia(Kukavskaya et al., 2012).

Modeling the complexity of post-fire forest patterns and their changes over time is a key issue in the spatial forest ecology that is related to fire. Even though remote sensing has been acknowledged as one of the most powerful methods to map components of vegetation and estimate their changes over time, this technique has sometimes been demonstrated as an unrealistic and biased representation of the post-fire forest patterns. For example, the optical remote sensing is less than ideal for the understory studies where the overstory canopy blocks the understory signal. Consequently, characterizing the stages of forest succession, including both early and late successional types, might be difficult using the optical sensors. This problem, coupled with the saturation issues of vegetation indices, limits the monitoring of post-fire forest patterns that might lead to an underestimation of the classes of forest succession and overestimation of forest recovery rate. Synthetic aperture radar systems and LiDAR systems are well designed to capture the forest structure and may address some issues of the passive optical

systems; however, application of these data may require higher costs and remain unavailable for mapping post-fire forest patterns at regional to continental scales, especially with lidar data. Additionally limitation of field observation as well as variations of environmental conditions (e.g., soil moisture, topography), vegetation characteristics (e.g., pre- and post- fire vegetation, species characteristic), and disturbance regimes (e.g., fire frequency, fire season, and severity) also alter the accuracy of modeling the recovery of post-fire forests because the recovery process is determined by the complex interaction of those biotic and abiotic factors.

In summary, the overall of research problems and gaps in studying the effects of forest fire and environmental conditions on the patterns of boreal larch forest recovery through remote sensing approach are illustrated in Figure 1.1.

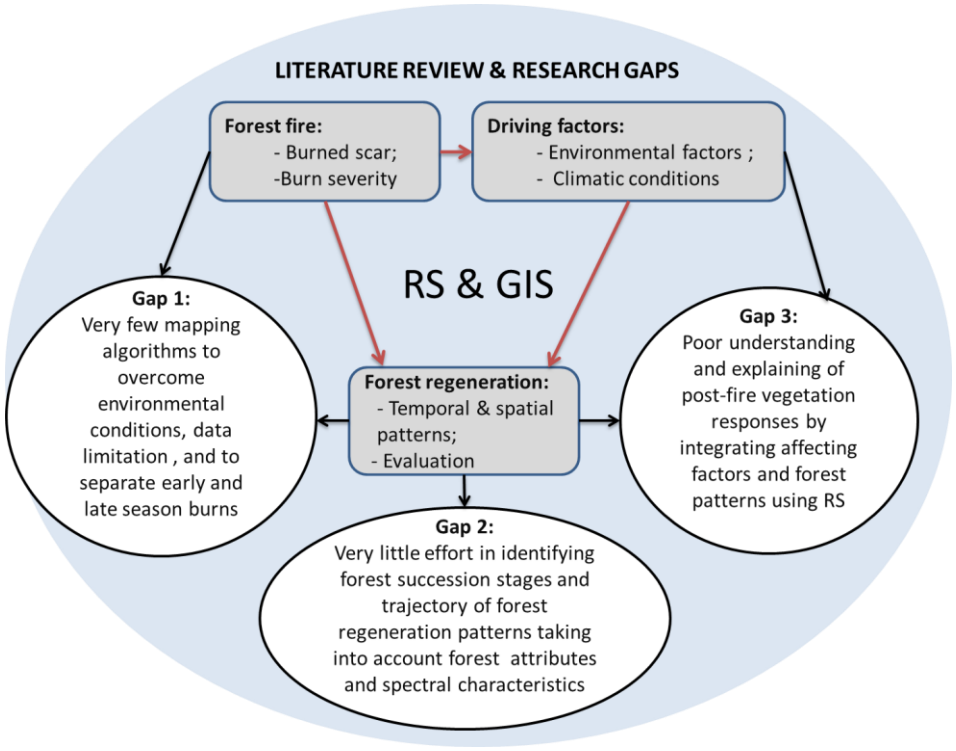

Figure 1.1 Research problems and research gaps in studying effects of forest fire and forest pattern.

1.5 Research hypothesis and objectives

The general hypothesis of this research is that forest regeneration patterns and their driving factors after fire can be characterized and evaluated using remote sensing approaches.

More specifically:

- ✓ The synergistic use of remote sensing data can overcome environmental conditions and data limitation for reconstructing the post-fire effects of burned areas and burn severity in high northern latitudes of boreal larch forests.
- ✓ The remote sensing data with abundant spectral information and time series data can be used to differentiate accurately some of the early forest succession stages and track the post-fire forest regrowth.
- ✓ The post-fire forest regeneration patterns depending upon various biotic and abiotic factors can be evaluated using remote sensing methods.

The purpose of this research is to model and evaluate forest regeneration patterns affected by fire in a boreal larch forest in permafrost ecosystems using remote sensing. To achieve this, the specific objectives are listed in the following points:

- ✓ To develop the methodology frameworks for reconstructing the burned areas and burn severity from remotely sensed data in a boreal larch forest ecosystem.
- ✓ To propose the trajectory method of temporal and spatial patterns of the post-fire forest regrowth at different levels of fire effects.
- ✓ To evaluate the regeneration patterns of the post-fire boreal larch forest ecosystem by analyzing driving factors using remote sensing and geospatial analyses.

1.6 Organization of this dissertation

This thesis follow a manuscript based format and is comprised of six chapters (Figure 1.2). Chapter 1 presents a brief introduction of the research background, hypothesis, objectives and general flowchart of the research methodology. Chapter 2 and chapter 3 are to achieve research objective 1 of mapping the burned areas and burn severity respectively. Chapter 4 fulfills the requirement of objective 2 on trajectory of the post-fire forest patterns as well as discrimination of early successional stages. To address objective 3 of modeling the post-fire forest patterns based on the fire and environmental factors, Chapter 5 investigates the influences of a number of fire and environmental predictor variables on the variations of post-fire forest patterns. Chapter 6 is the summary and conclusions for this thesis, which focuses on the overall contributions, current limitations, and potential opportunities in future research development.

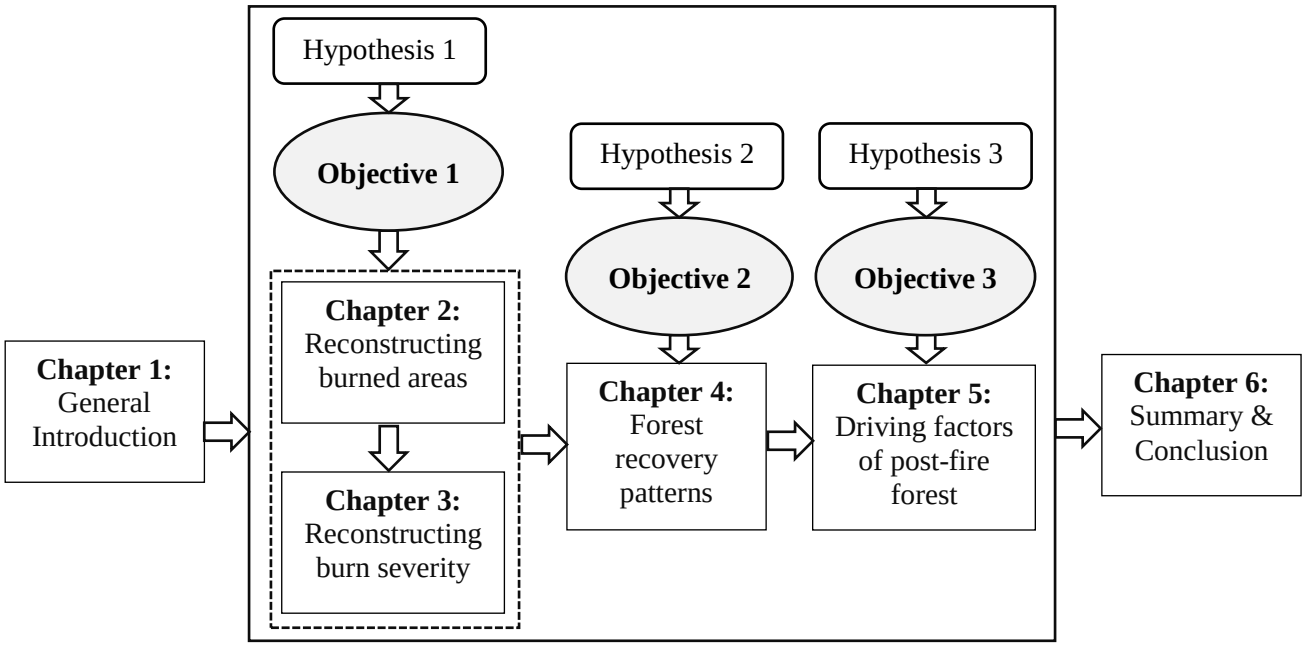

Figure 1.2 Flow chart of the thesis structure. See section 1.4 for the research hypotheses and objectives

CHAPTER 2: COMPOSITING MODIS TIME SERIES FOR RECONSTRUCTING BURNED AREAS IN THE TAIGA-STEPPE TRANSITION ZONE OF BOREAL LARCH FOREST

2.1 Preface

Chapter 2 is to fulfill the first objective of developing methodology framework for reconstructing the burned areas from remotely sensed data in the boreal larch forest ecosystem. The chapter presents the method of mapping burned areas from MODIS data to overcome limitations of data and environmental conditions in the boreal ecosystems. The results of this chapter have been published as a research paper:

> Chu, T. & Guo, X. (2015) Compositing MODIS time series for reconstructing burned areas in the taiga-steppe transition zone of northern Mongolia. *International Journal of Wildland Fire*, 24(3): 419-432, http://dx.doi.org/10.1071/WF14124.

Thuan Chu performed the data collection and analysis and wrote the manuscript. Dr. Xulin Guo supervised the research progress and provided comments on the manuscript. The last two paragraphs of the introduction section in the published paper has been used to form the section 2.3, and all other published sections have been entirely included in the sections from 2.4 to 2.7 of this chapter. The permission to re-use the published paper for the purpose of this chapter has been obtained from the CSIRO publisher by Thuan Chu.

2.2 Abstract

Estimations of areas burned by wildfires vary greatly depending on the environmental conditions, data availability, and methods used. This study aims to develop a framework for reconstructing the time series of burned areas in the taiga-steppe transition zone using MODIS

composites. The estimated accuracy of the developed mapping algorithm and other statistical indications denote that the clear-land surface composites of MODIS data in spring (JD 97 to 177), logistic regression, and MODIS active fire product can be integrated successfully for reconstructing the burned areas in the taiga-steppe transition zone. The time series of burned areas between 2000 and 2012 derived from the MODIS fire-season (or spring) composite algorithm were validated using Landsat based burned areas, showing average omission and commission errors of 18% and 31%, respectively. Compared with the MCD45A1 burned areas product, the developed algorithm significantly improved the prediction of burned areas, and successfully separated the late-season burns from early-season burns. The derived long term burned areas will assist to understand the complex relationships among the forest dynamics, forest recovery, and fires in the vulnerable boreal forest ecosystem as well as its transition zone under climate change in southern Siberia and Central Asia regions.

2.3 Introduction

Accurate mapping of burned areas is not only critical for forest and land managers to manage ecosystems but also important for the estimation of carbon emission and proposing resilience strategies. Fortunately, the MODIS has provided various products since 2000 that are globally available. However, as indicated in the chapter 1some uncertainties still remain when it comes to selecting the most suitable MODIS product as well as the MODIS composite for the discrimination of burned and unburned areas in studies of the fire effects at regional and local scales. For examples, the MODIS MCD45A1 and MODIS MCD64A1 (Boschetti et al., 2009), currently available online, have not yet been fully validated. Studies in the Mediterranean ecosystems (Bastarrika et al., 2011a), the arid regions in Southern Africa (Roy and Boschetti, 2009, Tsela et al., 2010), and the boreal ecosystems in North America and Eurasia (Giglio et al.,

2010, Kasischke et al., 2011, Loepfe et al., 2012, Chang and Song, 2009, Randerson et al., 2012) have shown a significant underestimation of the local and regional burned areas using these products. This finding is possibly attributable to the presence of clouds and smoke, low burning severity, heterogeneity in the background surface, the types of fire, and spatial resolution of the MODIS data (Giglio et al., 2013, Loepfe et al., 2012). The MODIS hotspot products (e.g. MOD14) are highly related to true burned areas, but estimation of the burned areas using only the hotspots also causes high omission errors (Hantson et al., 2013). Therefore, the use of those products derived from the global burned areas for local and regional scales requires validation and comparison with other independent datasets (e.g., higher resolution datasets and/or official fire data) prior to applying the products at local and regional studies.

The taiga-steppe transition zone separates boreal forests to the north from treeless steppe zone to the south. The latitudinal gradients of the forest types and tree cover, which are locally modified by the climate variability, topography and edaphic factors, make the taiga-steppe ecotone a more complex landscape than the forest-tundra and boreal forests (Zyryanova et al., 2010b). Similar to other high northern latitudes of the boreal forests, environmental conditions limit the mapping of burned areas using remote sensing in the taiga-steppe transition zone. This is due to the limitations of high zenith angles influencing the visible and infrared radiations, concentrations of high aerosol, cloud cover, cloud shadow, and snow cover at high northern latitudes (Loboda et al., 2011). These conditions require developing a suitable clear land surface composite as well as mapping algorithms to accurately detect burn scars in such areas. Although Loboda et al. (2011) proposed the burned area algorithm with the consideration of environmental conditions and effective time for mapping burned areas in the Alaska boreal region, the proposed algorithm has been adjusted to the local conditions. Thus, it is not clear whether the algorithm

can be accurately applied to the other ecoregions. In this paper, we aim to develop a framework of mapping the burned areas with improved accuracy in the taiga-steppe transition zone using the fire-season MODIS composites. To this aim, this study initially analyzed 13-years MODIS time series data to identify fire characteristics and atmospheric conditions in the transition zone of steppe and boreal forest. The clear-surface view composites of MODIS data were then developed with respects to the fire season to maximize the detection of the burned areas. Time series of the burned areas between 2000 and 2012 in the boreal forest ecotone in northern Mongolia was detected using the optimal clear-land MODIS composites in primary fire season, logistic regression model, and MODIS active fire data. Finally, time series of the burned areas were validated using the Landsat reference dataset and the MODIS MCD45A1 burn data.

2.4 Materials and methods

2.4.1 Study area

Mongolia is located in central Asia, which covers an area of 1 564 118 km^2 on the southern fringe of the great Siberian boreal larch forest. Forests and grasslands, which cover about 10% and 70% of all Mongolian territory respectively, play an important role in the country's economic development. About 92% of the total forested area (175 000 km^2) is currently growing trees (IFFN, 2007). Due to climate change, human activities, and inadequate management, forest resources in Mongolia are mainly suffering from overgrazing, mining, deforestation, and especially forest fires (Batkhuu et al., 2011, IFFN, 2007). According to Farukh et al. (2009) the worst fire losses were in 1996 with a burnt forest area of 23 636 km^2, and recently from 2001 to 2007, about 30% of the forest areas were affected by fires with the large scale fires in 2000-2002.

Mapping of the burned areas was conducted in Hovsgol province, the northern part of Mongolia ($49^0$38'N, $100^0$10'E) (Figure 2.1). The Hovsgol topography is characterized by the large Darhad valley at 1550 to 1600 masl (meters above sea level), Hovsgol lake, and surrounded by the high mountain ranges up to 3100 masl. Hovsgol province is the most densely forested area in Mongolia with 31 781 km^2 of closed forest with dominant species of *Larix sibirica* and *Picea obovata* accounting for 30% of Mongolia's total closed forest area (James, 2011). The Hovsgol forests are located on the widespread mountain permafrost between the Siberian taiga and the Central Asian steppe zones. The Siberian larch *(Larix sibirica)* dominantly contributes more than 90% to the forest composition in the area (IFFN, 2007). The average temperature in Hovsgol during winter months is -20.0^0C, while the average temperature in the summer is 11.8^0C (Murray, 2004). The area has been recently heavily affected by the severe fires caused by both human and lighting factors (Farukh et al., 2009, IFFN, 2007).

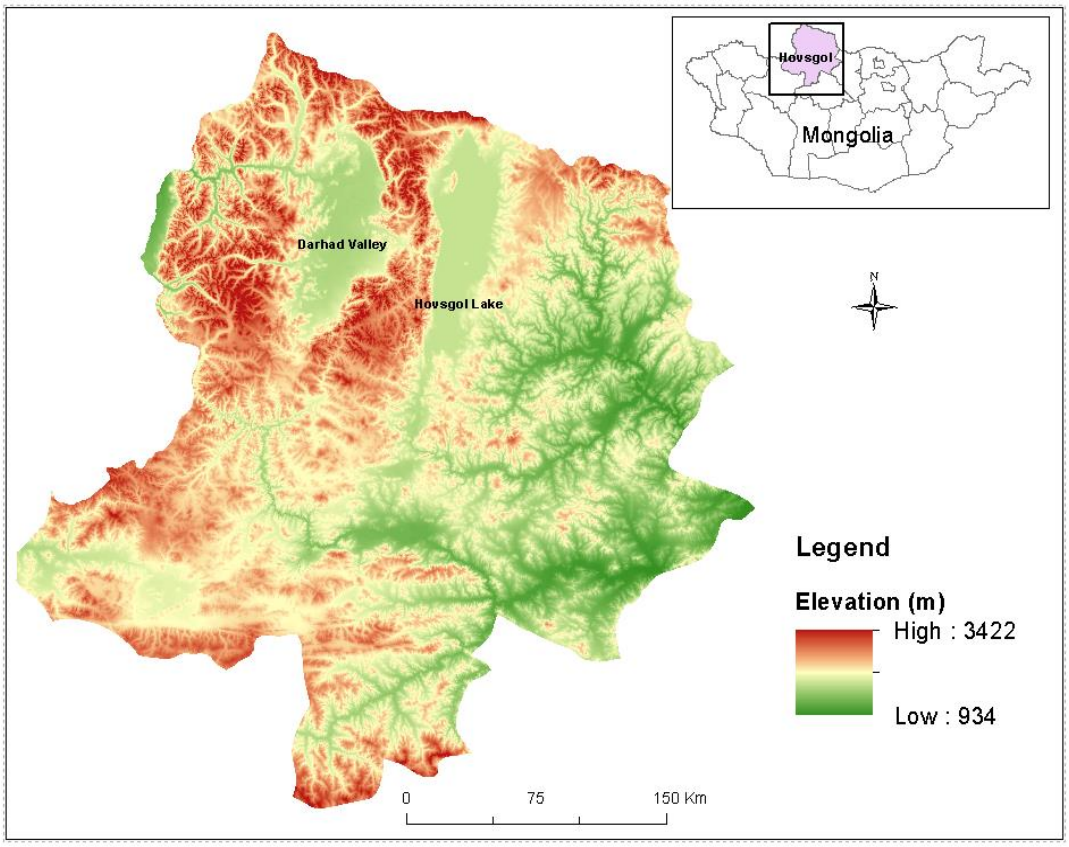

Figure 2.1 Hovsgol province, the northern part of Mongolia (49038'N, 100010'E).

2.4.2 Satellite data

The used MODIS and Landsat data products have been summarized in Table 2.1. Three basic MODIS products (tile h24v03) from 2000 to 2012 were used, including the 8-day surface reflectance composites (MOD09A1), the 8-day MODIS active fire product (MOD14A2), and the standard monthly burned area product (MCD45A1). All these products were downloaded from *http://reverb.echo.nasa.gov* and preprocessed using the MRT tool. In addition to the MODIS products, we used Landsat TM and ETM+ images, obtained from the USGS EROS Data Center at 30-m resolution for the period between 2000 and 2012, to develop a reference burn dataset for the validation of burned area maps (Table 2.1).

Table 2.1 The employed satellite data products for mapping burned areas

13-years' time series of burned areas were evaluated using fire-season (or spring) MOD09A1 composites and MOD14A2 data. Landsat and MCD45A1 were used to validate the derived burned areas. Landsat TM and ETM+ images were selected based on burned areas detected using spring MODIS composites in this study. All satellite images were clipped to the boundary of Hovsgol province.

Product name	**Tile /Path_row**	**Temporal coverage**	**Spatial resolution (m)**
MOD09A1	h24v03	Feb 18, 2000 – Dec 31, 2012	500
MOD14A2	h24v03	Feb 26, 2000 – Dec 31, 2012	1000
MCD45A1	h24v03	Apr 1, 2000 – Dec 31, 2012	500
Landsat ETM+	136_025	May 11, 2000	30
Landsat TM5	136_025	Jun 6, 2001	30
Landsat ETM+	137_025	Jun 8, 2002	30
Landsat TM5	137_025	Sept 21, 2002	30
Landsat TM5	137_025	Jun 3, 2003	30
Landsat ETM+	136_025	Jul 30, 2006	30
Landsat ETM+	136_024	Jul 17, 2007	30
Landsat ETM+	137_024	Jun 9, 2008	30
Landsat TM5	135_025	Jun 21, 2009	30
Landsat ETM+	135_025	Jul 2, 2010	30
Landsat ETM+	136_024	Jun 13, 2012	30
Landsat ETM+	136_025	Jun 13, 2012	30
Landsat ETM+	135_025	Jun 6, 2012	30

2.4.3 Analyzing fire occurrence patterns and reconstructing MODIS time-series composites

The monthly numbers of fires from February 2000 to December 2012 were analyzed to determine the fire occurrence tendencies in northern Mongolia. Hotspot data with high-confidence level (fire mask equals 9) in MOD14A2 product were selected to clarify the fire season and fire trends in the study area from 2000 to 2012. The fire season was then used to regenerate the new time series of fire-season MOD09A1 composite.

MOD09A1 is a seven-band product computed from the MODIS Level 1B land bands. It is a level-3 composite of the 500-m resolution MOD09GA with the correction for the effects of atmospheric gases, aerosols, and thin cirrus clouds (Vermote and Kotchenova, 2008). Even though the product contains the best possible observation during an 8-day period (Vermote and Kotchenova, 2008), challenges still remain to select clear land surface view for terrestrial studies, particularly in high northern latitudes. This was shown by the observation of data product quality in the 500-m resolution data state quality assurance layer in each of the downloaded MOD09A1 image (see *section 2.5.2*). Therefore, the new time series composites with the maximum of clear-surface view of MOD09A1 product were regenerated with respect to the primary fire season in the taiga forest-steppe transition zone. The accepted values of the environmental conditions and the clear land surface from MOD09A1 16 bit state flags layer(Vermote and Kotchenova, 2008) were analyzed (Table 2.2) in order to mask out the low quality pixels in each of the 8-day composite image. Consequently, 13-year mean seasonal trajectories (2000-2012) of the presence of clear land, snow, cloud cover, cloud shadow, and aerosol quality were analyzed to select an optimal period for the regenerating new MOD09A1 composite. The clear-land surface composited image of each year was finally developed by the combination of high quality pixels from each of the MOD09A1 8-day composite image with respect to the fire season in our study area that was derived from the number of fires using the MOD14A2 product.

Table 2.2 Accepted values from the MOD09A1 500m 16 bit state flags layer for the analysis of the environmental conditions in northern Mongolia

Bit number	Parameter	Accepted values	
		Environmental conditions analysis	Clear land surface
0-1	Cloud state	Cloudy, Mixed	Clear/assumed clear
2	Cloud shadow	Yes	No
3-5	Land/water flag	Land	Land
6-7	Aerosol quantity	Climatology, High	Low, Average
8-9	Cirrus detected	High	None, Small, Average
10	Internal cloud flag	Cloud	No cloud
12	MOD35 snow/ice flag	Yes	No
15	Internal snow mask	Snow	No snow

2.4.4 Sampling method for model calibration on clear-land MODIS composite

Among other approaches, the logistic regression models are valuable tools for predicting the fire occurrences as well as mapping out the burned areas (Mallinis and Koutsias, 2012, Lozano et al., 2007, Koutsias and Karteris, 2000). From a set of independent explanatory variables, a binary dichotomous variable of the burned and unburned pixels is estimated based on a static model of spectral probability. The MODIS active fire, 8-day MOD09A1 composite, and Landsat data in spring 2012 showed that there were large fires in spring 2012 on the east side of Hovsgol Lake, northern Mongolia (Figure 2.2). Therefore, the MOD09A1 composite of 2012 spring fire season, which was reconstructed from the 8-day MOD09A1 composites (see *section 2.5.2 & 2.5.3*), was selected to calibrate a logistic regression model.

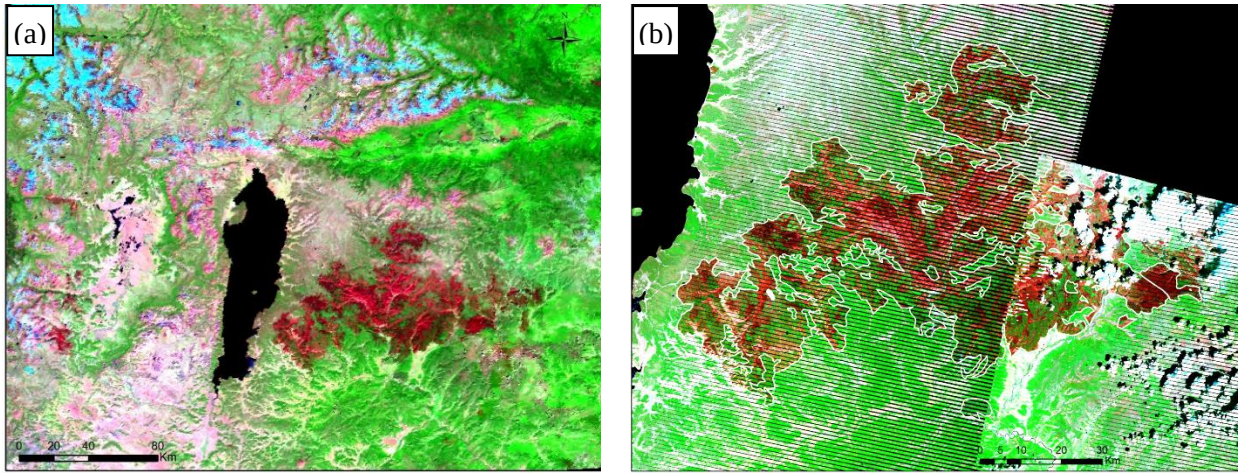

Figure 2.2 MOD09A1 image 8-days composited of the images acquired from 2 June to 9 June 2012 (R:G:B = B7:B2:B1/SWIR:NIR:R) (a).

Mosaic Landsat ETM+ images (path/row: 136/024, 136/025, and 135/025) acquired on 6 June and 13 June 2012 (R:G:B=B7:B4:B3/SWIR:NIR:R) (b). The large burned area (dark red pixels) caused by fires in May 2012 near Hovsgol lake (black pixels).

Ten explanatory variables including 7 reflectance channels, NDVI, NDMI, and NBR (Table 2.3) were extracted from the 2012 spring fire-season composite of MOD09A1 for logistic modeling. In this study, samples of the ten explanatory variables were collected based on the visual interpretation of the fire-season composited image since the burned and unburned areas can be easily distinguished based on the difference in spectral signatures. The easy recognition of burn scars was further facilitated by overlaying the MODIS active fire data that could eliminate other disturbances from the fire disturbances. The samples were coded with the value of 1 when they are located within the burned areas or 0 when they are outside the burned areas. Both the burn and unburned samples were collected with respects to spectral variability in the pre and post-fire environments to account for the different burn severity classes and land cover types. More specifically, within the burned areas, we created a number of polygons to include the potential burned pixels (e.g., dark red pixels in Figure 2.2), and then all the pixel values in the burned

polygons were extracted. More than 14 000 pixels representing the burned areas caused by fires in April and May 2012 were extracted spectral values from the 2012 spring fire-season MOD09A1composite. Subsequently, we selected randomly 5000 observations from those burned pixels to examine in the logistic regression. The same method was applied to collect the samples in unburned areas. The unburned polygons were trained in the vegetated areas and bare lands, which account for the spectral variability of the different land cover types. The five thousand unburned samples were extracted randomly from 19 000 pixels outside the burned areas. Consequently, the dataset consists of 10 000 observations, 1 response variable (0 for unburned, 1 for burned), and 10 independent explanatory variables.

Table 2.3 Ten spectral predictors from MOD09A1 spring composite used to characterize burned area using logistic regression

B1, B2, B3, B4, B5, B6, B7 are MODIS spectral reflectance as measured in band 1 - Red (620-670 nm); band 2 - NIR (841-876 nm); band 3 – Blue (459-479 nm); band 4 – Green (545-565 nm); band 5 - SWIR (1230-1250 nm); band 6 - SWIR (1628 – 1625 nm); band 7 - SWIR (2105 – 2155 nm)

Variable	Equation	Reference
Spectral bands		
Single MOD09A1 bands 1 to 7 (B1, B2, B3, B4, B5, B6, B7)		-
Spectral Indices		
Normalized Difference Vegetation Index	NDVI = $\frac{B2-B1}{B2+B1}$	(Namzalov et al., 2012)
Normalized Difference Moisture Index	NDMI = $\frac{B2-B6}{B2+B6}$	(Wilson and Sader, 2002)
Normalized Burned Ratio	NBR= $\frac{B2-B7}{B2+B7}$	(Key and Benson, 2006)

2.4.5 Statistic analysis and mapping time series of burned areas

A pool of 10 variables related to the burned and unburned areas was used for statistical analysis. In order to compare the difference between the burned and unburned samples using parametric test, normal distribution and outliers of the independent samples were tested using the histograms, along with the box plots. Logistic regression analysis with the maximal model of all 10 explanatory variables was ran twice, with and without the consideration of interactions of the variables to assess the performance of the explanatory variables for discriminating the burned and unburned pixels. The variance inflation factor (VIF) was used to identify possible high multicollinearity between the explanatory variables. One strategy for addressing this problem is to sequentially drop the covariate with the highest VIF, recalculate the VIFs and repeat this process until all VIFs are smaller than a pre-selected threshold (VIF<10). However, in order to avoid dropping the covariates with high variance explained the response variable; we also used Akaike's Information Criterion (AIC) and p-value (threshold 0.05) of independent variables to drop the non-significant as well as high multicollinearity covariates in prediction models. Model fit was assessed using graphical tests of the fit of the logistic to data – Area Under the Curve (AUC) obtained by the Receiver Operating Characteristic plot method (ROC-plot) (Lozano et al., 2007). Finally, the best minimum model in which non-significant and high multicollinearity covariates were eliminated was used to reconstruct the map of the burned areas from 2000 to 2012 in the study area. Since the results of the logistic regression range was between 0 (unburned) and 1 (burned) for every pixel from the input predictors, the cut-off level was chosen as 0.5. Values below the cut-off indicated unburned areas, while values higher than the cut-off value represented burned areas.

As indicated by Hantson et al. (2013), MODIS hotspot products such as the MOD14A2 are highly related to the true burned areas. We based on the assumption that all the burned areas in our study area are related to the detected hotspots by the MOD14A2 product. Therefore, the MOD14A2 data was not only used to eliminate the false detection of the burned areas intra-annually and instances of the surface reflectance changes due to reasons other than fire but also used to correct the year and season of the burned areas detected by using the primary fire-season (or spring-composite) logistic algorithm in this study. We used a two-phase filtering approach of burned areas to minimize both the omission and commission errors introduced by the fire-season logistic algorithm. In the first phase of filtering burned areas, after all the burn scars between 2000 and 2012 had been identified, only the burn polygons which contained the MODIS hotspots in the spring composites were selected and assigned as the spring burned areas corresponding to mapping years. The purpose of the second phase of filtering burned areas was to select the burned areas caused by late-season fires. Because the late-season burn scars ($year_n$) might be still visible and detected using a following fire-season composite ($year_{n+1}$), the remaining burn polygons, which were not selected by using the primary fire-season MOD14A2 composites, were continuously filtered by the late-season fires (MOD14A2 data in JD from 185 to 297) in $year_n$. Those burn scars were then assigned as the late-season burns in $year_n$. Figure 2.3 shows the overall algorithm processing flow of reconstructing the burned areas in the taiga-steppe transition zone.

2.4.6 Validation

The accuracy assessment was conducted using a sub-sample of the Landsat-based reference dataset for each year for which the cloud-free Landsat scenes were available and contained the burned areas detected by MODIS composites. We selected 13 Landsat TM and ETM+ scenes on

the path from 135 to 137 and row from 24 to 25 between 2000 and 2012 (Table 2.1) to digitize all the burned areas within each scene for the validation of the MODIS composite based burned areas. Similar to the training data selection, the validation data from the Landsat imagery were obtained easily by visual image interpretation. The visual interpretation of burned areas has been proved to be at least as precise as the automatic methods in many studies (Dubinin et al., 2010). Omission and commission errors were calculated for each year by combining the MODIS composite based burned areas and validation datasets. As noted that the MODIS MCD45A1 burned area data have underestimated the burned areas at local and regional scales, the derived MODIS burned areas and Landsat validation data in this study were also compared with the MCD45A1 data.

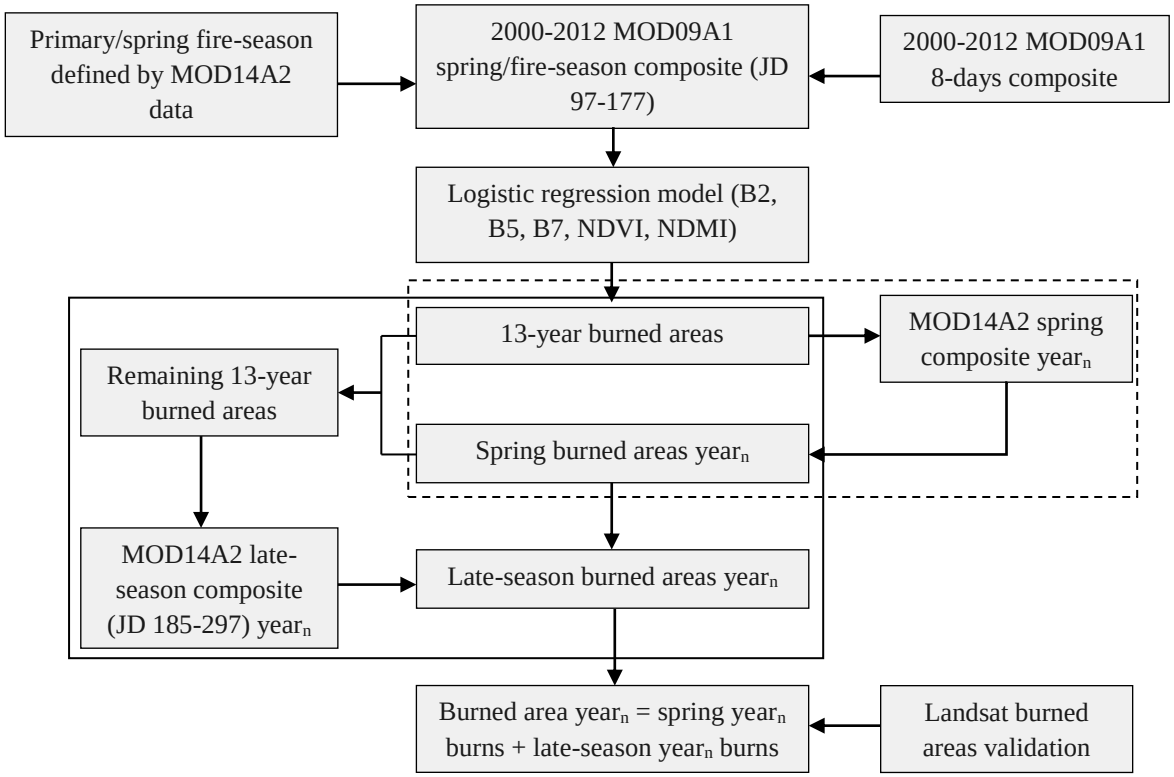

Figure 2.3 Overall processing flow of burned areas mapping for the taiga-steppe transition zone. The primary fire-season composite was also defined as the spring composite in this study.

(See *section 2.5* for more details on the reconstruction of MOD09A1 fire-season composite (JD 97-177) and the analysis of logistic regression model. The first and second phase filtering approaches were shown in the dash and solid boxes, respectively.)

2.5 Results

2.5.1 Characteristics of fire season in larch forest of taiga-steppe zone

Our analysis of the active fires derived from the MOD14A2 data across all of northern Mongolia demonstrated that the seasonal fire occurrences was from March to September annually (Table 2.4). Spring (March to June), summer (July to August), and autumn (September to October) fires comprised about 85%, 3%, and 12% of the total number of fires, respectively. Severe fire years were in 2002 (348 fires) and 2012 (1508 fires). In the primary fire season or spring fire season, almost all fires were observed in April and May. The majority of fires were out by the end of June, with few fires continuing into September, except for the 2002 late-season fires which accounted for 96% (262 fires) of all late-season fires in the area between 2000 and 2012.

Table 2.4 Characteristics of fire incidence in northern Mongolia (2000-2012)

Year	Month							Total
	Mar.	Apr.	May	Jun.	Jul.	Aug.	Sep.	
2000	0	40	42	21	0	0	0	103
2001	0	0	4	0	0	0	0	4
2002	1	1	19	0	64	1	262	348
2003	0	5	0	7	0	0	0	12
2004	0	0	0	0	0	0	0	0
2005	0	0	0	0	0	0	9	9
2006	0	3	32	4	0	0	0	39
2007	0	5	10	0	0	0	0	15
2008	5	13	122	0	0	0	0	140
2009	0	0	67	0	0	0	0	67
2010	0	0	18	0	0	0	0	18
2011	2	0	0	0	0	0	3	5
2012	0	733	722	53	0	0	0	1508
Monthly total (%)	8 (0.36%)	800 (35.3%)	1036 (45.7%)	87 (3.9%)	64 (2.8%)	1 (0.04%)	274 (12%)	2268 (100%)
Season fire (%)	**Spring (85%)**				**Summer (3%)**		**Autumn (12%)**	

2.5.2 Regeneration of clear land surface of MODIS time series

The observations of the clear land surface from MOD09A1 showed that mapping the burned areas in boreal larch forest of northern Mongolia is effectively limited to a seven-month period (April through October), with the best conditions during June, July, August, and September (Figure 2.4). The effective period of the clear land surface observation also overlapped with the fire season (Table 2.4).

In relation to the fire season characteristics, spring fires (late March to June) accounted for 85% of the fires in northern Mongolia (Table 2.4), and these fires are the most severe ones (IFFN, 2007). Therefore, a fire-season composite image defined as spring-composite image (Julian date from 97 to 177, April to June) of each year was created based on the highest quality pixels of the 8-day composite images acquired during this period. The spring-composite image was thus the optimal composite to detect all of the burned scars in the most severe fire seasons of each year in the study area. Similar approach as proposed by Loboda et al. (2011) was applied to create the spring-composite images. Firstly, all of the 8-day MOD09A1 composites between April and June (JD 97 to JD 177) were filtered out to select the clear land surface pixels. The masked-out pixels from a base 8-day composite (JD 177) were then filled with acceptable quality pixels from the 8-day composite of the previous date (JD 169). The process was repeated until the JD reached 97. Consequently, the 8-day MOD09A1 composites between JD 97 and 177 were combined in a single clear-land surface defined as the spring-composite image or fire-season composite image (Figure 2.5). Even though the spring composite was created from eleven 8-day composite images (e.g. MOD09A1 8-day composite in spring 2012), there were unclear (black) pixels existing in the image. Visual observations of those pixels in the spring composites between 2000 and 2012

showed that almost all of the pixels were located in the high to very high mountainous areas within the study area, which were still covered by snow during the spring (Figure 2.5).

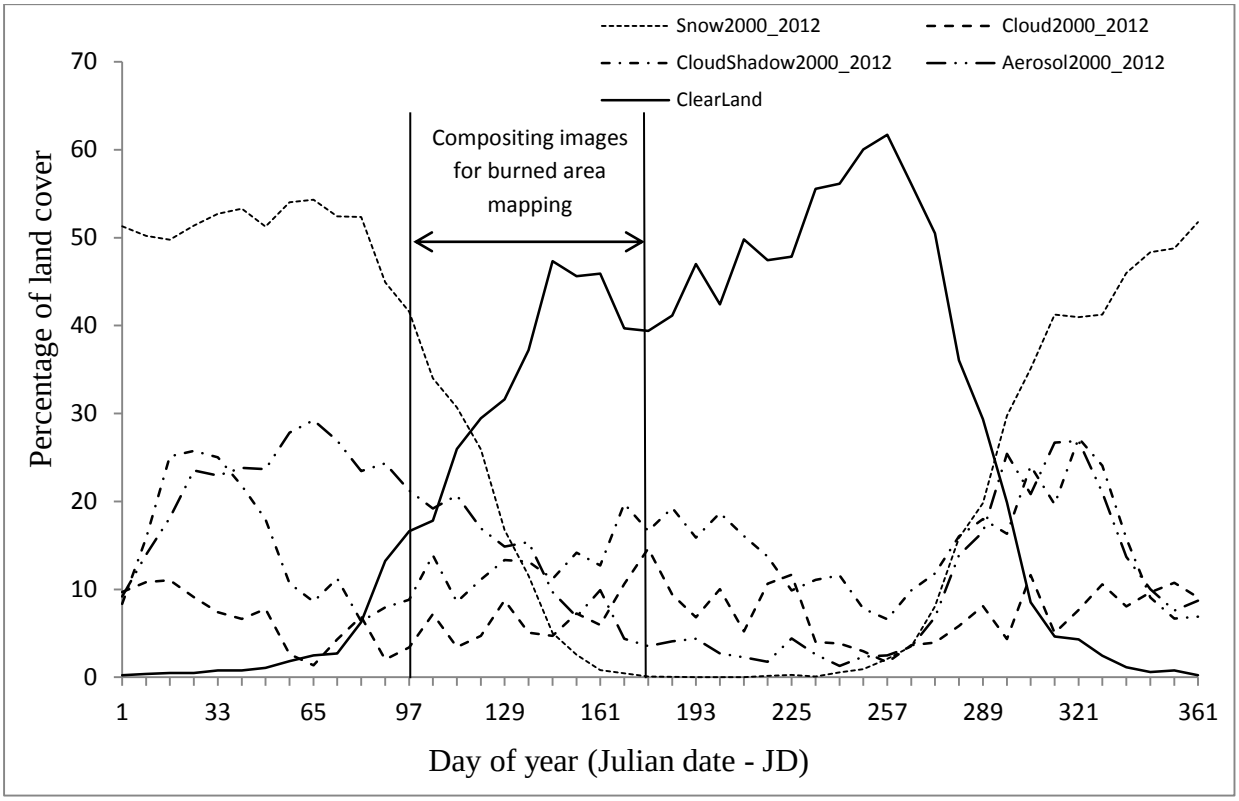

Figure 2.4 Thirteen year mean seasonal trajectories of environmental conditions using MOD09A1 500m 16 bit quality state flags.

The accepted values of each pixel to analyze the environmental conditions and clear land surfaces were shown in table 2.2. The spring-composite image was then created from the best pixels showing clear-land surface in the MOD09A1 imagery acquired during early April to June (97-177 JD) to develop the fire-season clear surface view.

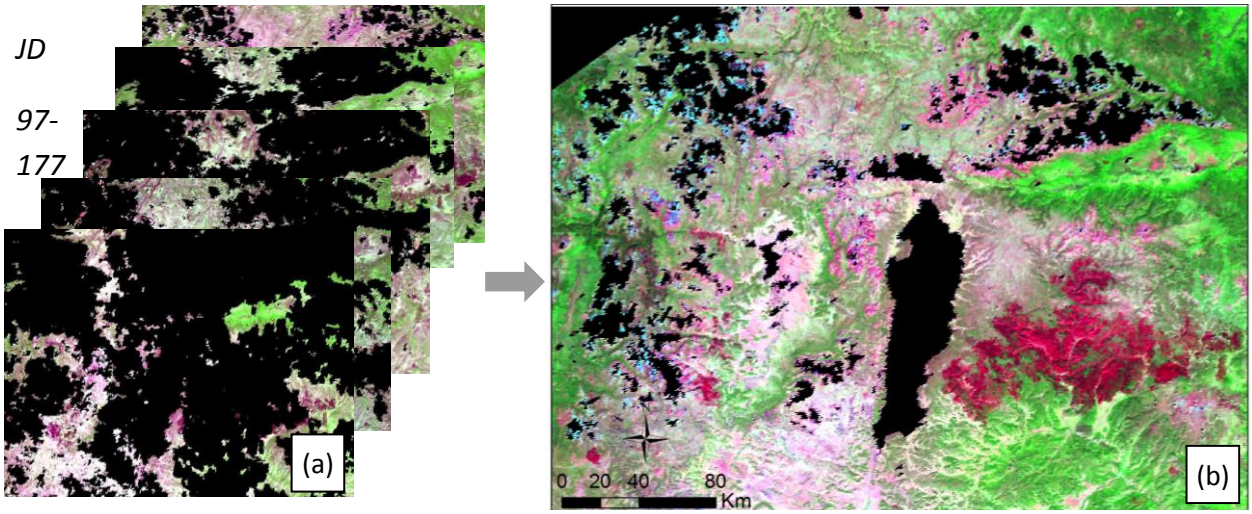

Figure 2.5 MOD09A1 fire-season composite image (JD from 97 to 177) (b) created by the mosaic of high quality pixels from each MOD09A1 8-day composite during the primary (spring) fire season (a).

2.5.3 Analysis of logistic regression model

All of the independent variables included in the univariate analysis showed significant differences between the burned and unburned points using the t-test ($p < 0.001$). The burned points had lower spectral reflectance in the visible and near infrared MODIS bands (band 1,2,3,4) and higher spectral reflectance in the mid-infrared band (band 7) as fire related decrease in chlorophyll content and vegetation moisture. Values of the independent spectral indices including the NDVI, NDMI, and NBR also decreased significantly in the burned samples, which illustrated the decrease of vegetation cover and surface moisture, and the increase of tree mortality after fires, respectively.

The minimal logistic regression model with 6 of the explanatory variables of MODIS bands 2, 5, 7, NDVI, and NDMI was selected as the best model with the AIC of 2440 and the area under ROC curves (AUC) of 0.99, indicating very good overall model fit. The result with the

consideration of the interactions between the predictors showed that all of the interactions terms were significant in the maximal model. However, the interaction model only showed slight improvement compared with the non-interaction models. In addition to the model complexity, the interaction models were thus not selected in this study. The estimated coefficients of the selected minimal model were shown in Eq. (2.1).

$$P(y) = \frac{1}{1 + e^{-(-7.3-0.008*B2-0.001*B5+0.004*B7+32.89*NDVI-19.80*NDMI)}} \quad (2.1)$$

Where *P(y)* indicates the probability of burned (*P(y)*> 0.5) and unburned pixels (*P(y)* ≤ 0.5);B2, B5, B7 are band 2 – NIR (841-876 nm), band 5 - SWIR (1230-1250 nm), and band 7 - SWIR (2105-2155 nm) MOD09A1 bands, respectively; NDVI – Normalized Difference Vegetation Index; NDMI – Normalized Difference Moisture Index.

2.5.4 Mapping time series of burned areas

The bands and indices based model (Eq. 2.1) defined as fire-season (or spring) composite logistic algorithm was used to detect all the burned areas between 2000 and 2012. As noted in the characteristics of the fire incidences in northern Mongolia, almost all of the fires occurred in spring (April to June), except for 2002 with serious fires in summer and autumn (see Table 2.4). With the use of the two-phase approach of filtering burned areas using the spring-composite logistic algorithm and the MOD14A2 data, not only spring burned areas but also late-season burned areas were detected. The result of mapping burned areas between 2000 and 2012 using the MOD09A1 spring-composite algorithm was reported and compared with MCD45A1 product (Figure 2.6).

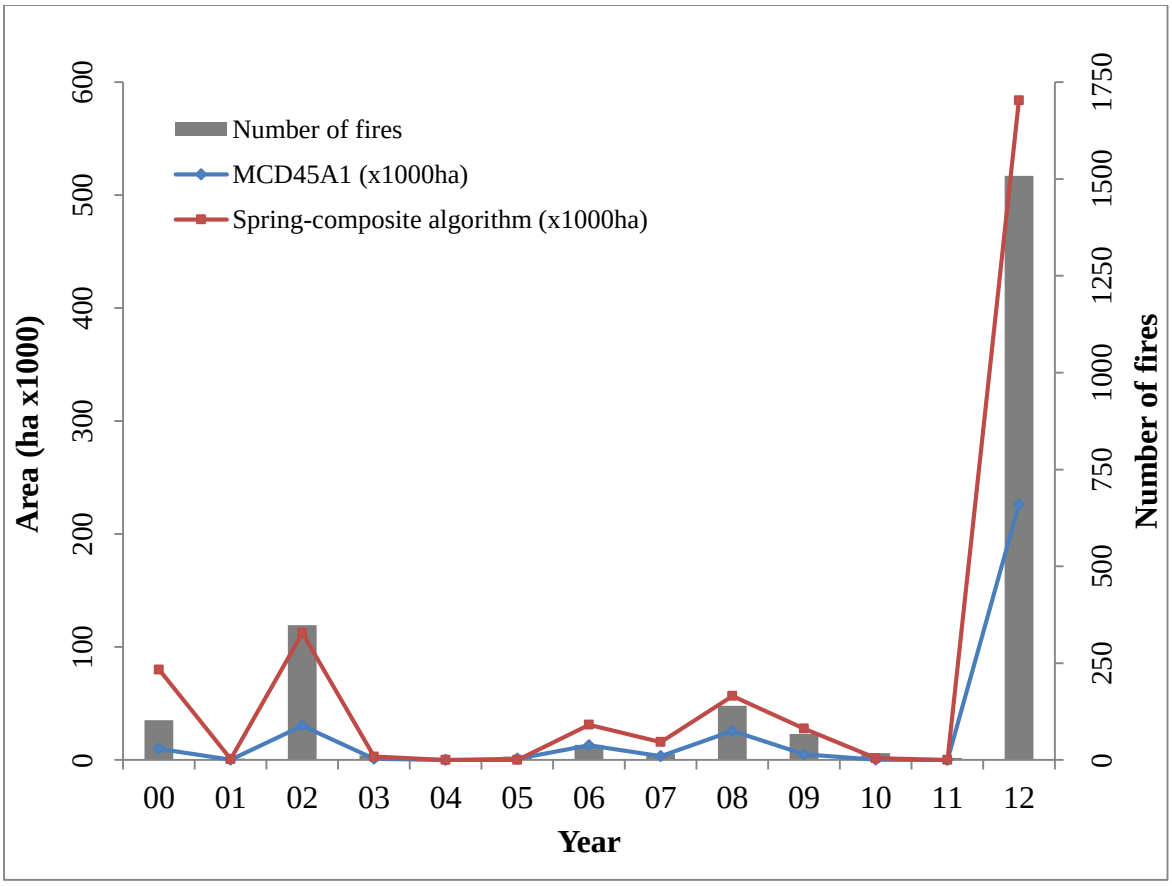

Figure 2.6 Time series (2000-2012) of burned area data from the developed algorithm (red) and MCD45A1 product (blue).

2.5.5 Validating burned area map

Validation of the burned area maps relied on the data from Landsat satellite sensors (TM and ETM+). For the burned area delineations, we used a total of 58 burns on 13 Landsat images, which were acquired in June and July between 2000 and 2012, except for the one image in September 2002 to detect 2002 late-season burns (Table 2.1). Consequently, 92% of the MOD09A1 spring-composite based burned areas (810 000 ha) was validated using the Landsat based reference dataset. Even though some of the Landsat ETM+ images acquired after 2003 contain some gaps due to the Scan Line Corrector (SLC) failure, burn scars were still clearly identified in those images (e.g. see figure 2.1). Average omission error of the MOD09A1 spring-

composite algorithm was 18%, while the average commission error was 31% (Table 2.5, Figure 2.7). No signs of the burned areas were found for 3 of 13 mapping years (2004, 2005, and 2011). These were similar results with the Landsat based burned areas, when cloud-free Landsat images in the same years were visually analyzed.

Table 2.5 Summary of confusion matrix results comparing Landsat based burned areas and MOD09A1 spring-composite based burned areas.

Year	Fire date	Landsat path/row (date)	Landsat (ha)	Spring MOD09A1 (ha)	Omission error (%)	Commission error (%)	% validated
2000	Apr & May	LE_136/025 (May 11)	42953	67517	12	44	84
2001	May	LT5_136/25 (Jun 6)	846	625	34	11	89
2002	Apr, May & Sept	LE_137/025 (Jun 8 & Sept 21)	72282	112562	14	45	100
2003	Apr & June	LT5_137/025(Jun 3)	2821	3063	44	49	100
2006	May	LE_136/025 (Jul 30)	22285	31285	8	35	100
2007	Apr & May	LE_136/024(Jul 17)	7437	12673	11	48	79
2008	May	LE_137/024 (Jun 9)	49447	51002	13	16	90
2009	May	LT5_135/025(Jun 21)	24733	27599	22	30	92
2010	May	LE_135/025(Jul 2)	1686	1580	19	14	100
2012	May	LE-136/024 & 136/025&135/025 (Jun 6 &Jun 13)	440591	502101	3	15	86
		Average			**18**	**31**	**92**

In order to evaluate how the performance of the spring-composite MODIS algorithm in this study improved the prediction of the burned areas compared with the MCD45A1 product, we also assessed the omission and commission errors of the MCD45A1 algorithm (Table 2.6) against the Landsat burn polygons. The results showed that the MCD45A1 algorithm significantly underestimated the burned areas with very high omission error, although the algorithm had low commission error, 71% and 18% respectively. Particularly, some of the burned areas in 2001,

which were detected by both the 2001 Landsat and the spring-composite logistic algorithm, were not identified in the MCD45A1 product.

Table 2.6 Summary of confusion matrix results comparing Landsat based burned areas and MCD45A1 burned areas

Year	Fire date	Landsat path/row (date)	Landsat (ha)	MCD45A1 (ha)	Omission error (%)	Commission error (%)
2000	Apr & May	LE_136/025 (May 11)	42953	9418	82	16
2001	May	LT5_136/25 (Jun 6)	846	235	100	100
2002	Apr & May	LE_137/025 (Jun 8 & Sept 21)	72282	29980	62	8
2003	Apr & June	LT5_137/025(Jun 3)	2821	85	97	5
2006	May	LE_136/025 (Jul 30)	22285	12914	59	30
2007	Apr & May	LE_136/024(Jul 17)	7437	3016	61	4
2008	May	LE_137/024 (Jun 9)	49447	22245	57	4
2009	May	LT5_135/025(Jun 21)	24733	4212	84	9
2010	May	LE_135/025(Jul 2)	1686	253	85	7
2012	May	LE-136/024 & 136/025&135/025 (Jun 6 &Jun 13)	440591	209399	33	1
		Average			**72**	**18**

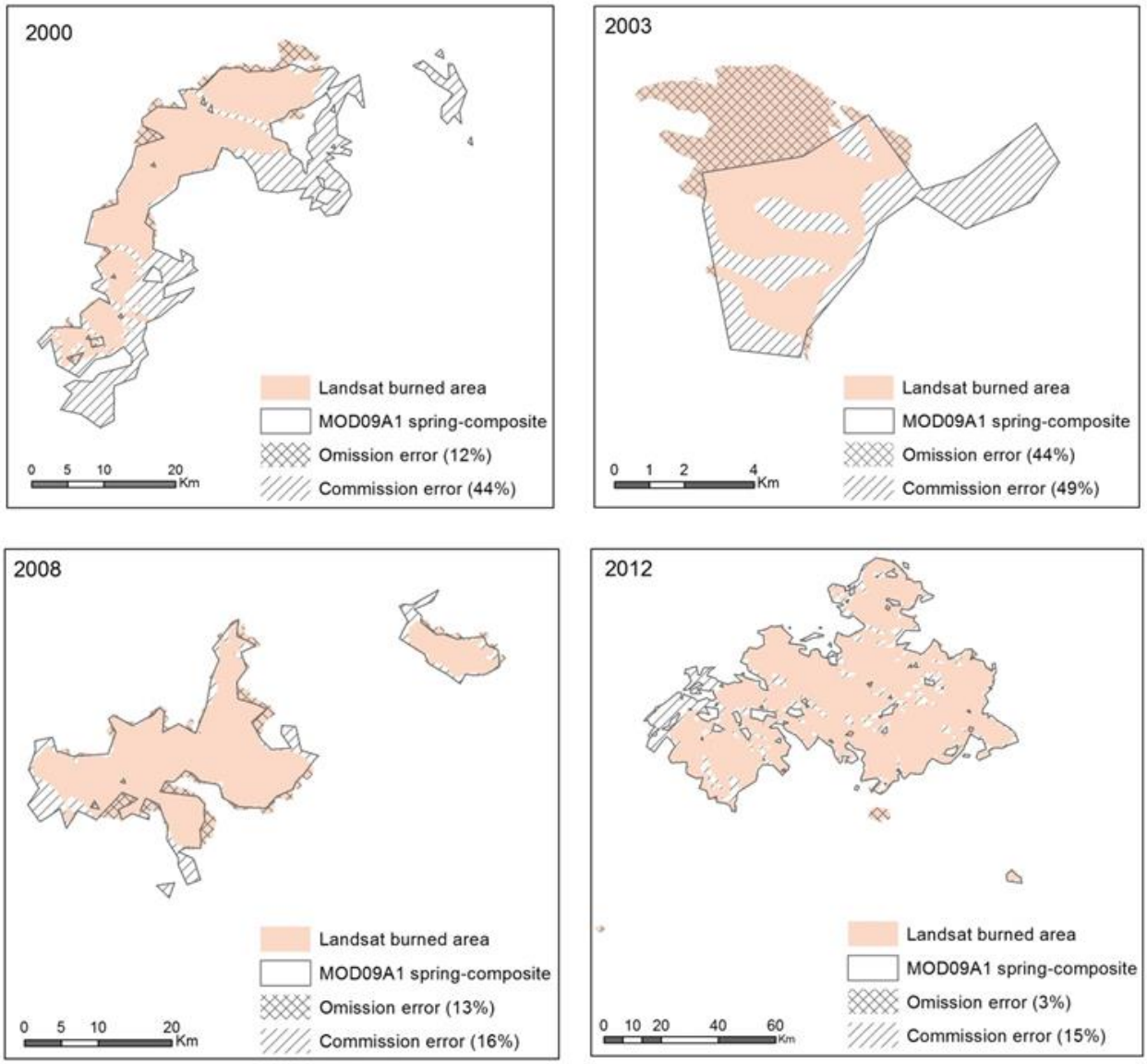

Figure 2.7 Examples of the result validation for the burned areas in 2000, 2003, 2008, and 2012.

2.6 Discussion

2.6.1 Clear-land spring MODIS composites and spectral signatures for mapping burned areas

Our analysis indicates that remote sensing observations of clear land for mapping burned areas in larch forest of the taiga-steppe transition zone in southern Siberia are effectively limited to a seven-month period (April through October), with the optimal conditions during June, July, August, and September. This result is similar to the findings by Loboda et al. (2011) for the

observation of clear land surface for mapping burned areas in the high northern latitudes in Alaska. However, the slightly lower northern latitudes such as Mongolia showed the longer optimal time period for the clear land observation. Even during the optimal period, only 45-65% of the clear land surfaces can be observed using remote sensing (Figure 2.4). Therefore, the developed fire-season composite images in this study were useful to maximize the surface information observed by the MODIS sensor in order for mapping and analyzing the burned areas as well as the biophysical parameters in such high northern latitudes.

The statistical indications of the developed algorithm denote that the logistic regression modeling with MODIS data can be used successfully for mapping the burned areas. The spectral bands and indices based model with the five predictors (B2/NIR, B5/SWIR, B7/SWIR, NDMI, and NDVI) was the most suitable model. In terms of ecological aspects, all of the selected variables in the best minimal model contribute different properties of the post-fire land surface as well as the significantly spectral variations to discriminate the burned and unburned areas. For example, fire related decreases in chlorophyll content, surface and vegetation moisture lead to decreases in the visible and near infrared wave length reflectance, and increases in the reflectance of infrared bands (De Santis and Chuvieco, 2007, Miller and Thode, 2007). It was also reported by Roy et al. (2005) that the separability of burned and unburned areas using MODIS band 2 (841-846 nm) and band 5 (1230-1250 nm) is much higher than the other land surface reflectance bands. Therefore, these bands were significant variables included in our logistic regression model to separate the two pixel domains of burned and unburned areas in the taiga-steppe ecotone. Even though, MODIS band 7 (2105-2155 nm) has small separability of burned and unburned pixels (Roy et al., 2005), this reflectance band accounts for important information of soil exposure as well as the surface moisture changes following fires. Similarly, the inclusion of the NDVI and

NDMI predictors in the minimal bands and indices based model was to enhance the observations of variations in the surface moisture and vegetation loss between the pre and post-fire environments, and thus improved the model prediction of the burned areas.

2.6.2 Contradiction between omission and commission error

The contradictions between omission and commission errors in mapping burned areas can be addressed by applying the two-phase approach in which core burned areas are first defined from the most severe burn pixels based on active fire pixels or threshold of vegetation indices, and then employs some contextual algorithms to refine the classification of burn scars (Chuvieco et al., 2008c, Stroppiana et al., 2012, Bastarrika et al., 2011b). Additionally, Hantson et al. (2013) found that the MODIS hotspots are very highly related to real burned areas, especially in the areas with vegetation cover prior to a fire. We used these notations to diminish the high commission error occurred by the developed algorithm by the inclusion of the MOD14A2 hotspot product. On the contrary, the MOD09A1 fire-season composite algorithm significantly reduced the omission error compared to the MCD45A1 product, 18% and 72% respectively (Table 2.5 & 2.6). The inclusion of the MODIS hotspots also helps to eliminate the potential confusion in the year and season of the burns.

The fire-season composite algorithm in this study consistently identifies burned areas for the time series between 2000 and 2012 and for a wide range of fire conditions from light to very severe years (e.g. 2001 and 2012 fires) with the low to moderate omission and commission errors (Table 2.5). Comparisons with the omission and commission errors introduced by the MCD45A1 data demonstrated these consistent errors. However, the fire-season composite algorithm also resulted in a clear tendency of higher commission errors compared with the omission errors in almost all mapping years. The higher commission errors may be caused by the spatial resolution

of the MODIS imagery used. It is apparent that the minimum area of burns detectable by the MODIS is much higher than that of the Landsat. Coupling the differences of the burn severity and spatial/spectral heterogeneity within the burn scars, the low resolution data tend to include small patches of unburned areas in burn scars. In this case, the term fire affected areas in using remote sensing to map burned areas might be more suitable than burned areas in order to account for the spatial and spectral heterogeneity of the burned areas.

Another source of error may be the separability of the burned and unburned areas of the developed algorithm in this study. For example, the manual interpretations of the burned areas within the Landsat images showed that some of the areas identified as burned areas by the fire-season composite algorithm were in fact bare land areas located in the high mountainous areas, or the areas caused by other disturbances rather than fires (e.g. logging). Therefore, applying a mask on those areas prior to mapping the burned areas is necessary to reduce commission errors. Finally, the higher omission and commission errors were observed in years for which no training data were collected (e.g. burns in 2000 to 2011). This poor inter-annual model transferability was likely due to a somewhat environmental and climatic conditions influenced the reflectance values of similar earth objects in different years. In spite of these issues, the time series of the burned areas presented in this paper showed a good agreement with other mapping algorithms in boreal regions, and our results were found to be more consistent, and had lower variation of omission and commission errors. For example, mapping of the burned areas in North America from NOAA/AVHRR by Pu et al. (2007) showed higher variation of omission and commission errors, ranging from 4% to 75% for omission and 18% to 32% for commission. Results from Chuvieco et al.'s (2008a) study showed lower commission error (10%), but much higher omission error (50% to 60%).

2.6.3 Importance of mapping late-season burned areas

Recent changes in fire regimes in some regions, for example in Alaska, showed that there has been an increase in the late-season burned areas over the last few decades (Kasischke et al., 2010). Several studies found that the late-season fires burned deeper organic layers than the spring fires due to seasonal increases in thaw depth and lower fuel moisture in late season (Kasischke et al., 2010, Kasischke and Johnstone, 2005). In addition, the depth of the post-fire surface organic layers has been shown to control the recruitment of post-fire seedling as well as the pattern of vegetation succession (Johnstone et al., 2010a). For example, higher rates of recruitment of broadleaf tree species has been observed in the Alaskan boreal forest in the sites with organic layers' depth less than 7.5cm, while higher rates of needleleaf tree recruitment were in the sites with organic layers deeper than 7.5cm (Kasischke et al., 2007). Therefore, separating late-season burned areas from the spring season burns is critical for understanding the ecological responses of the post-fire boreal ecosystems.

Examination of the Landsat and MODIS images in the severe late-season fire year in 2002 (Table 2.4) showed that the late-season burn scars on those satellite images were observable up to 3 to 5 years after the fires. This is shown in the low and gradual changes by the reflectance of the near infrared and short wave infrared bands (dark red pixels on satellite images). Particularly, the late-season burn scars in $year_n$ can be identified clearly in the following spring fire season in $year_{n+1}$ (Figure 2.8 & 2.9). The visibility of the late-season burn scars for a long time period, which were not interpretable for such long time period in almost all the early-season burns (e.g. spring burns in 2000), may be related to the high burn severity. This is because that higher burn severity (deeper organic layers burned) requires longer period for recovery of vegetation in the burned patches. An assessment of the pre-fire land cover and burn severity in both the early and

late season burns is thus necessary to confirm the variations of the spectral signatures following those burns, which in turn can be used to evaluate the patterns of the post-fire vegetation recovery in the taiga-steppe transition zone. In addition, similar to the burned areas in the Alaska region (Loboda et al., 2011), visual analysis of the multiyear burned area mapping showed that the new burn scars (e.g. late-season burns) were found to be adjacent to the previous burns (e.g. spring burns) (Figure 2.9b). In spite of these issues, the use of spring or fire-season MODIS composites in coupling with the MOD14A2 hotspots and the two-phase filtering approach of burned areas in this study not only detected burned areas in the primary fire season but also successfully separated the late-season burns from early-season burns. Consequently, more than 100 000 ha of burned areas detected on the 2003 spring composite (Figure 2.9d) was assigned as late-season burned areas in 2002, which were not available to identify on the 2002 spring composite.

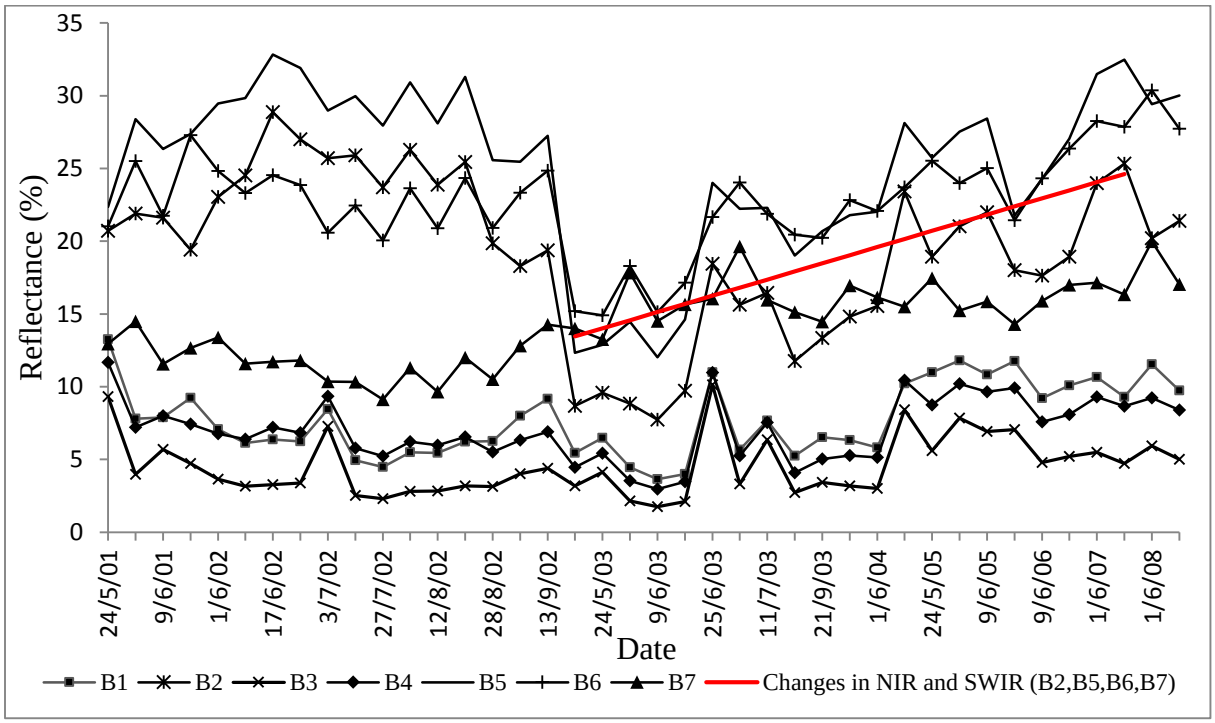

Figure 2.8 Example of 8-day MODIS reflectance values for a sample area affected by fire in September 2002 in larch forest of taiga-steppe transition zone.

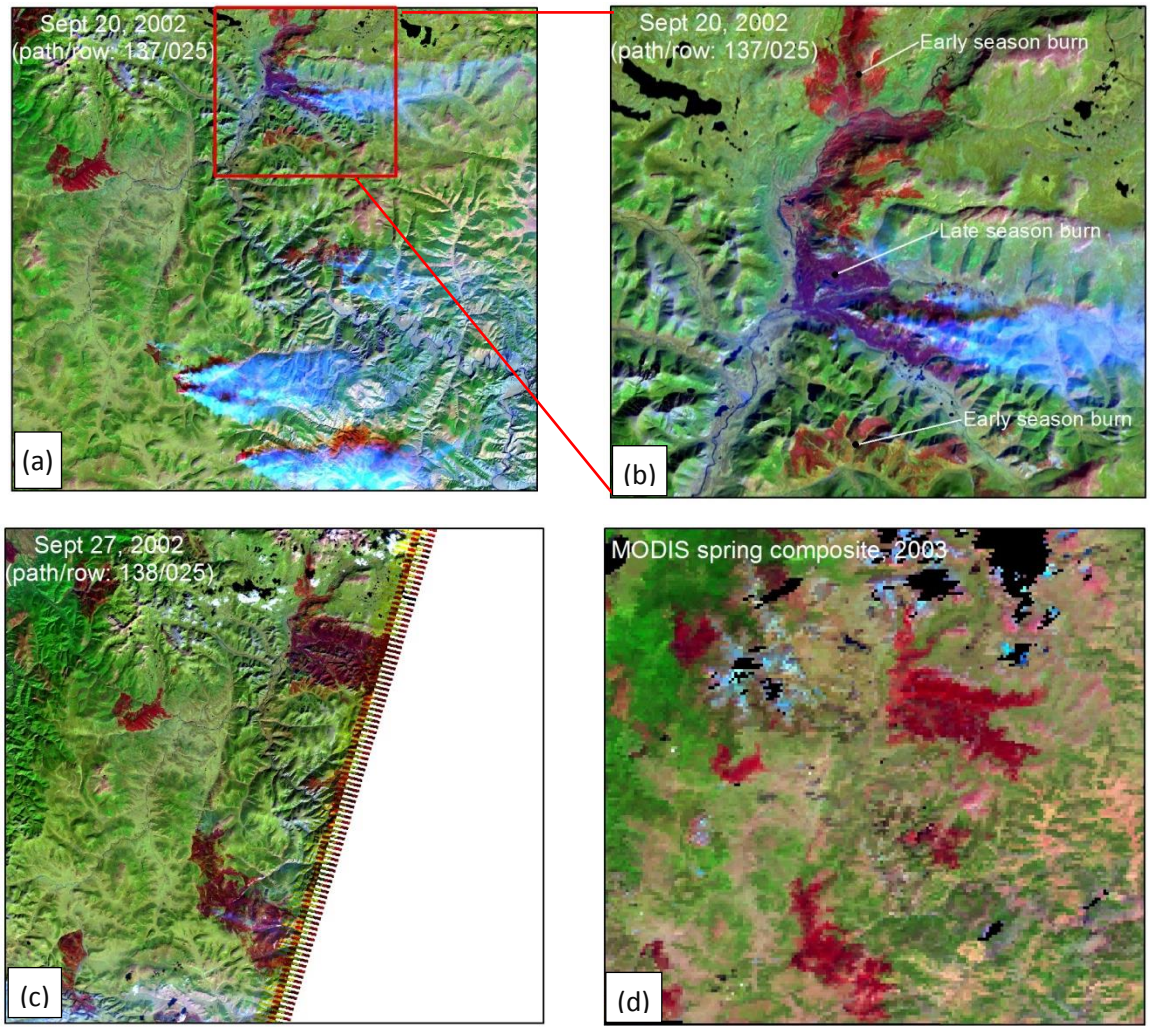

Figure 2.9 Early and late season burns on Landsat TM5 (a,b,c) and MODIS (d) images. Late-season burns on September 20, 2002 (a); The late-season burn was found to be adjacent to early-season burns (b); Late-season burn scars can be observed on both the late-season image (c) and following spring composite image (d). Fire date was confirmed by the MOD14A2 data as well as smokes on the Landsat images.

2.7 Conclusions

The reconstruction of the clear-land surface MODIS composites coupled with the logistic regression model and the MOD14A2 data presented in this chapter provided a suitable mapping tool of the burned areas compared with the existing MODIS burn product. However, the time series of the burned areas as well as the performance of the developed algorithm still require

further validating with other reference dataset and methods, and examination of different regions for longer periods to be implemented operationally in Mongolia and Central Asia regions. Furthermore, the burned areas should be classified into land cover types incorporating with an assessment of the burn severity to provide the opportunity to understand the vegetation responses after the fire disturbances in the transition zone of the taiga forest and steppe.

CHAPTER 3: TEMPORAL DEPENDENCE OF BURN SEVERITY ASSESSMENT IN SIBERIAN LARCH (*LARIX SIBIRICA*) FOREST USING REMOTELY SENSED DATA

3.1 Preface

Chapter 3 is to fulfill the first objective of developing methodology framework for reconstructing the burn severity from remotely sensed data in the boreal larch forest ecosystem. All sections of this chapter have been included in the manuscript and submitted in the International Journal of Wildland Fire as a research paper:

> Chu, T., Guo, X. & Takeda, K. (2015) Temporal dependence of burn severity assessment in the Siberian Larch *(Larix sibirica)* forest of northern Mongolia using remotely sensed data. *International Journal of Wildland Fire (Submitted).*

The manuscript now is under the first revision stage. Thuan Chu performed the data collection and analysis and wrote the manuscript. Dr. Xulin Guo supervised the steps of data processing as well as the research progress. Some field data (i.e. ground truth photos) were collected by Dr. Kazuo Takeda. The co-authors also provided comments and revised the manuscript.

3.2 Abstract

Assessing burn severity is critical for understanding both the short and long-term effects of fire disturbance on forest ecosystems. However, because of the remoteness and vastness of the Siberian boreal larch forest, there is very little available data on the severity of the fire disturbance. This study proposed a methodology framework to reconstruct the burn severity from the Landsat imagery at different time after the fire (lag timing up to 18 years) in the boreal larch

(*Larix sibirica*) forest. The estimated accuracy of the developed burn severity models denotes strong effects of the pre-fire conditions, fire ecology, date of the image acquisition and the remote sensing predictors on the assessment of the burn severity. In the first several years after the fire, the dNBR was the most important remotely sensed index for assessing burn severity, followed by the dNDMI (differenced Normalized Difference Moisture Index) and dNDVI (differenced Normalized Difference Vegetation Index). However, the dNDMI was more important than the dNBR and dNDVI in explanation of the severity levels when there is a dominance of the larch forest regrowth. The overall accuracy of the classification and regression tree (CART) models showed a decrease in accuracy from 83% to 62% depending on the lag timings of burn severity assessment. The high severity class had the lowest omission and commission errors followed by the low and moderate classes throughout the different lag timings. The evaluation of the model transferability and thresholds of the burn severity index demonstrates the advantage of the proposed methodology for assessing the fire effects in boreal larch forest that will assist to understand the complex relationships among the forest fires and ecological processes in the Eurasian boreal ecosystems.

3.3 Introduction

The severity of fire in a particular area can be assessed for short- and long-term periods. An initial assessment of the severity levels immediately after a fire event is often identified as fire severity. The burn severity quantifies the effect of the fire over extended time frames up to decades and is considered as the degree to which an ecosystem has changed because of the fire (Lentile et al., 2006, Barrett and Kasischke, 2013, Kasischke et al., 2008, Boby et al., 2010, Hoy et al., 2008, Veraverbeke et al., 2012a, Heward et al., 2013). Fire severity is often estimated by visual and/or measured field observation based on various ecological parameters (Key and

Benson, 2006, De Santis and Chuvieco, 2009, Cansler and McKenzie, 2012, Jain et al., 2012), or using post-fire remote sensing imagery acquired immediately after fire activities (Allen and Sorbel, 2008, Verbyla et al., 2008) . On the other hand, the measurement of burn severity is often based on the remote sensing techniques using the multi-temporal pre- and post-fire images acquired from weeks to years after the fire events had occurred (Lentile et al., 2006, Roy et al., 2006, French et al., 2008, Heward et al., 2013, Allen and Sorbel, 2008, Boer et al., 2008).

As a result of interaction between fire with vegetation and environmental conditions, the fire and burn severity are strongly influenced by both abiotic and biotic factors of the pre- and post-fire environment, such as other fire regimes (e.g. fire frequency, fire intensity, fire season), landforms, regional climate, species characteristics, and time since the fire occurred (Lentile et al., 2006, Kasischke et al., 2008, Verbyla et al., 2008, Barrett et al., 2010, Veraverbeke et al., 2010a, Heward et al., 2013, Keeley et al., 2008). According to Key (2006), these ecological conditions define the spatial and temporal constrains that generally affect the measurements of fire and burn severity in a landscape context. Regarding the temporal dimension, Key (2006) mentioned that the temporal factors including time of the year (seasonal timing) and time since the fire (lag timing) for sampling strongly influence the measure and detection of the severity. The first temporal factor, seasonal timing, can impact not only the radiometric quality of data but also the phenological characteristics of the post-fire vegetation that lead to bias in the analysis of fire and burn severity using the multi-temporal remote sensing method (Key, 2006). Verbyla et al. (2008) assessed the seasonal effect on estimating the fire severity, shortly after the fire event in black spruce stands, and found that there was high variation of the proportion of high fire severity class, ranged from 56 to 76% when there was one month change in either pre- or post-fire image acquisition dates. These significant effects of image acquisition dates on the fire

severity estimates were confounded by the changes in vegetation phenology and solar elevation (Verbyla et al., 2008). Thus, the multi-temporal remote sensing datasets should be matched with respects to the radiometric and seasonal qualities to reliably isolate the fire-specific responses in different levels (Key, 2006). To address the problem of the lag timing of an assessment, Allen and Sorbel (2008) found that there was significant difference between an initial and extended assessment of the post-fire effects, which is assessed shortly after the fire activity and one growing season after the fire event respectively within the tundra vegetation class. In contrast, these lag timing of the severity assessment had no effect for the black spruce forest (Allen and Sorbel, 2008). This was attributed to the rapid recovery of the post-fire tundra compared with the black spruce ecosystem (Allen and Sorbel, 2008). Similarly, Veraverbeke et al. (2010a) found that there was significant difference in post-fire severity levels in the initial assessment compared with the extended assessment in a quickly recovering Mediterranean ecosystem. As founded by Verbyla et al. (2008) in the black spruce stands, the seasonal timing of an assessment was also indicated as a significant factor contributing to the variation of fire and burn severity levels in the Mediterranean (Veraverbeke et al., 2010a). Apart from these studies, relatively little attention has been devoted to the longer lag timing (e.g. years to decades after fire) of burn severity assessment. Since the burn severity is defined as an indicator to characterize the degree to which an ecosystem has changed owing to the fire, longer lag timing of an extended assessment might reveal significant effect of the lag timing on the measurement of burn severity compared with the none significance, for example, as pointed by Allen and Sorbel (2008) using the immediate and one growing season after the fire assessments. This is critical assessment of the burn severity in relation to time since fire to account for an ecosystem change owing to the fire; particular in the forest ecosystems with low recovery rate after fire. Additionally, the assessment of burn severity

in different post-fire lag timing instead of only one growing season after the fire might also reveal the temporal sensitivity of the remote sensing indices in the assessment of burn severity as well as their ability to reconstruct the burn severity when there are available pre- and post-fire images.

Many studies have demonstrated the sensitivity of the spectral bands and indices of the remotely sensed data to changes in the fire and burn severity classes due to the reduction of the cover, density, greenness and water content of the vegetation as well as the change of the color and brightness of the soil (French et al., 2008, De Santis and Chuvieco, 2009, Veraverbeke et al., 2010b, Veraverbeke and Hook, 2013, Epting et al., 2005).The differenced Normalized Burn Ratio (dNBR) has been the most common method and outperformed other indices to assess the severity of fire, mostly from the Landsat imagery (Epting et al., 2005, Miller and Thode, 2007, Boer et al., 2008, Miller et al., 2009, Soverel et al., 2010, Veraverbeke et al., 2010b, Soverel et al., 2011, Veraverbeke et al., 2011). Although the relationship between the dNBR and field measures of the severity showed a moderate to high correlation in many study areas (De Santis and Chuvieco, 2007, Epting et al., 2005, Soverel et al., 2011, Picotte and Robertson, 2011, Tanase et al., 2011a), the dNBR empirical models are the data- and site-specific method, and the correlation varied and depended significantly on the vegetation cover types (De Santis et al., 2010, Soverel et al., 2011, Cansler and McKenzie, 2012, Hall et al., 2008, Allen and Sorbel, 2008, Epting et al., 2005). Particularly, some studies (Hoy et al., 2008, Murphy et al., 2008, Verbyla and Lord, 2008) criticized that the dNBR approach was sometimes unreliable and inconsistent in estimation of the fire and burn severity in Alaskan black spruce forests since it was unable to account for the depth of the post-fire organic layer, one of the important factors to evaluate the changes of post-fire forest ecosystem in Alaska (Kasischke et al., 2008, Kasischke et

al., 2007). In addition to the limitations of the imagery and field-severity data in many regions (Boer et al., 2008, Loboda, 2009, Loboda et al., 2011, Quintano et al., 2013), these results suggest that the approaches, which include multiple predictors (e.g. other vegetation indices), multiple remote sensing data (e.g. high resolution data) as an alternative approach for the extensive field sampling and stratification of the land cover prior to burn severity assessment should be further investigated in order to successfully model the severity caused by fire, particularly in the remote regions. To the best of our knowledge, very few studies on mapping the fire and burn severity have been conducted in the Eurasian boreal forests as well as the taiga-steppe transition zones (Chu and Guo, 2013). Because the types of fire and vegetation properties are quite different from the boreal forests in North America and Russia (de Groot et al., 2012), similar patterns of fire and burn severity may not be found among these boreal regions.

Here, we proposed to reconstruct the burn severity, defined as fire-induced changes in the vegetation cover and foliage status/color, and proportion of soil exposure, using different lag timing of pre- and post-fire Landsat image for the southern limit of the Siberia boreal larch forest. The objective of this assessment is to answer several questions: (i) how the sensitivity of the remote sensing indices changes in the assessment of the burn severity by time since fire?; (ii) which remote sensing index in addition to the dNBR is also important to account for both short- and long-term changes of an ecosystem responded to the fire?; (iii) how long after the fire can the burn severity still be accurately evaluated using the remote sensing approach?; and iv) what are possible thresholds of the burn severity index (e.g. dNBR) reflecting the post-fire effects in the boreal larch ecosystem. Because the removal of organic layers on land surface by fires results in significant decrease in the soil moisture for the first several years after the fire, especially with permafrost sites due to the increase of drainage (Yoshikawa et al., 2002, Kasischke and

Johnstone, 2005) and then the gradual increase due to the recovery of vegetation (Cuevas Gonzalez et al., 2009), the inclusion of the remote sensing indices such as the NDVI and the NDMI with the NBR were expected to account for the different properties of the post-fire environment as well as the degrees of the vegetation response in modeling the burn severity.

3.4 Materials

3.4.1 Study area

The similar study area of mapping the burned areas (see Chapter 2) was selected for mapping the burn severity in this chapter. However, we only focused on the two burned patches in 1996 and 2008 for model calibration and model assessment respectively (Figure 3.1).

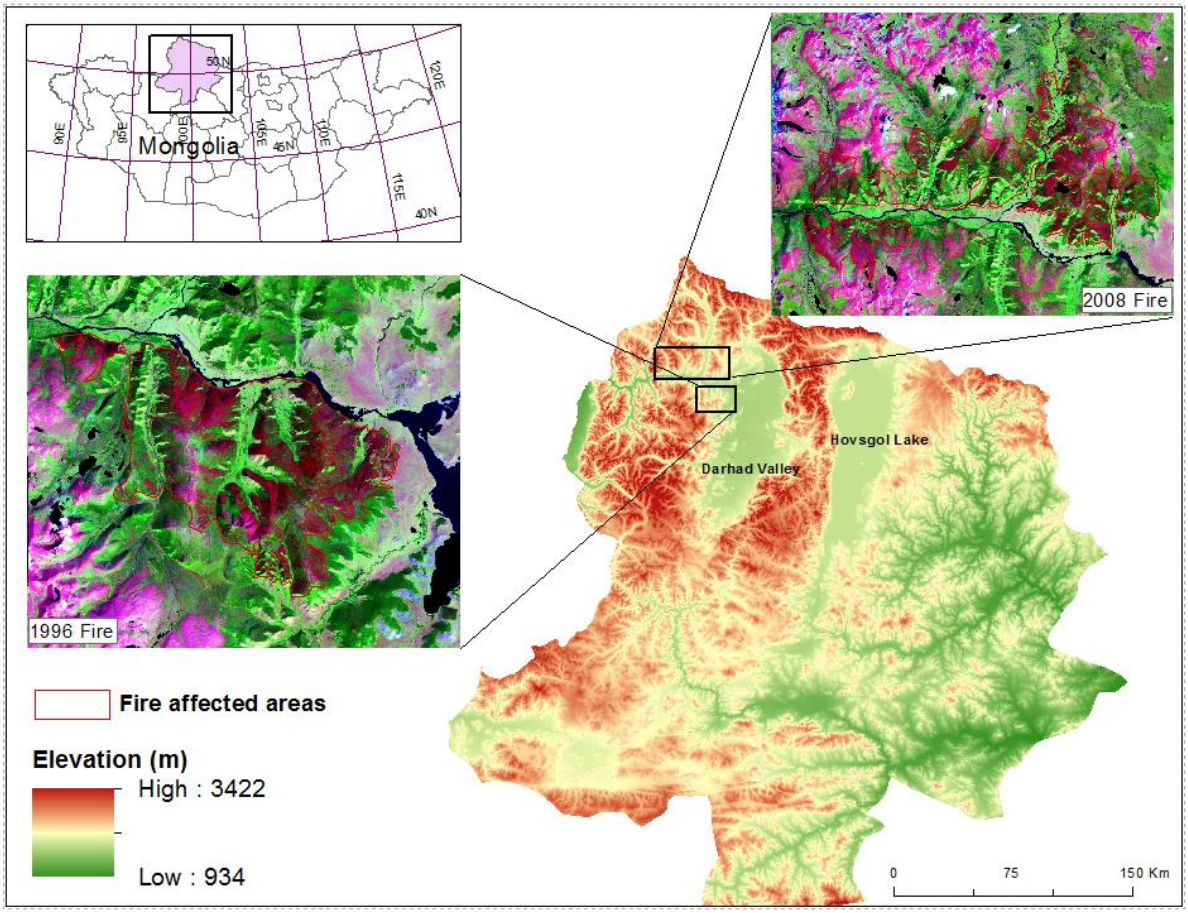

Figure 3.1 Location of the study area and burned patches for mapping burn severity.

Maps of the burned areas were unscaled, showing the 1996 burn scar on August 1998 Landsat 5 TM image (bottom left) and the 2008 burn scar on July 2009 Landsat 5 TM image (top right) (path/row: 137/024; R:G:B=TM7:TM4:TM1). Fire affected areas in 2008 was used to assess the transferability of the 1996 burn severity model (see section 3.5.7). The area is mainly covered by larch (*Larix sibirica*) forest.

3.4.2 Datasets

Our characterization of the burn severity patterns in the taiga-steppe transition zone focused on the analysis of a multi-temporal image series consisting of 16 peak-summer (July-August) Landsat TM, ETM+, and OLI images (WRS-2, path 137 row 24, http://glovis.usgs.gov/) between 1995 and 2014 (Table 3.1). There are no available or free clouds Landsat images for the post-fire period in 1996, 1997, 2006, and 2012 in the study area. The selection of the images acquired in the peak-summer months was considered to minimize the influences of the atmospheric conditions and the vegetation phenology (seasonal timing) differences on estimation of the burn severity levels (Key, 2006). Additionally, the available images were also screened based on the absence or low proportion of cloud cover. When cloud free or low cloud cover images were not available for a given peak-summer month, the image acquired closest to July and August was selected for the inclusion in the time-series (e.g. 1999 & 2013 images) (Table 3.1). Because the processing algorithms were based on the sampling plots (see section 3.5.5), images with partially clouded cover on the burned areas were still included (e.g. 2008, 2010, 2011 images) using the sampling points outside the cloud masks. Even though some of the Landsat ETM+ images acquired after 2003 contain some gaps due to the Scan Line Corrector (SLC) failure, burn scars in this study were outside the failure lines. In addition to the Landsat data, we used 50 cm WorldView-2 panchromatic image (Base map source: ESRI Inc.; DigitalGlobe) acquired on 21 August 2010 and our field observation in 2008 and 2011 to

develop a training and testing dataset for the calibration and validation of the burn severity models. The Landsat TM acquired in June 1995 was selected as the pre-fire image, whereas the post-fire images ranged from 1998 to 2014 excepted for three missing post-fire images in 1997, 2006, and 2012. Thus, there were 15 lag timings of the burn severity assessment, ranging from 1998 to 2014 (Table 3.1).

Table 3.1 List of the time-series Landsat images and the lag timings (or year since fire – YSF) of burn severity assessment.

The lag timings in 1st, 10th, and 16th year following the fire were not included because of the missing Landsat images in 1997, 2006, and 2012 respectively.

ID	Path_Row	Acquisition date	Sensor	Pre-Post Image	YSF/Lag timing
1	137_024	30/6/1995	TM	-	Pre-fire
2	137_024	25/8/1998	TM	95-98	2
3	137_024	5/9/1999	ETM+	95-99	3
4	137_024	29/7/2000	TM	95-00	4
5	137_024	16/7/2001	TM	95-01	5
6	137_024	19/7/2002	TM	95-02	6
7	137_024	6/7/2003	TM	95-03	7
8	137_024	16/7/2004	ETM+	95-04	8
9	137_024	4/8/2005	ETM+	95-05	9
10	137_024	9/7/2007	ETM+	95-07	11
11	137_024	12/8/2008	ETM+	95-08	12
12	137_024	6/7/2009	TM	95-09	13
13	137_024	25/7/2010	TM	95-10	14
14	137_024	12/7/2011	TM	95-11	15
15	137_024	3/9/2013	OLI	95-13	17
16	137_024	12/7/2014	ETM+	95-14	18

3.5 Methodology

3.5.1 Overall processing flow

We developed maps of the burn severity for the 1996 burned area in the larch (*Larix sibirica*) dominated forest of the taiga-steppe transition zone. Maps were created at different post-fire lag timing using the time-series collections of the Landsat imagery and classification

and regression tree (CART) algorithm (Figure 3.2). Model calibration and validation were developed based on the training and testing datasets extracted from the images of pre- and post-fire differenced vegetation indices, including the dNBR, the dNDVI, and the dNDMI.

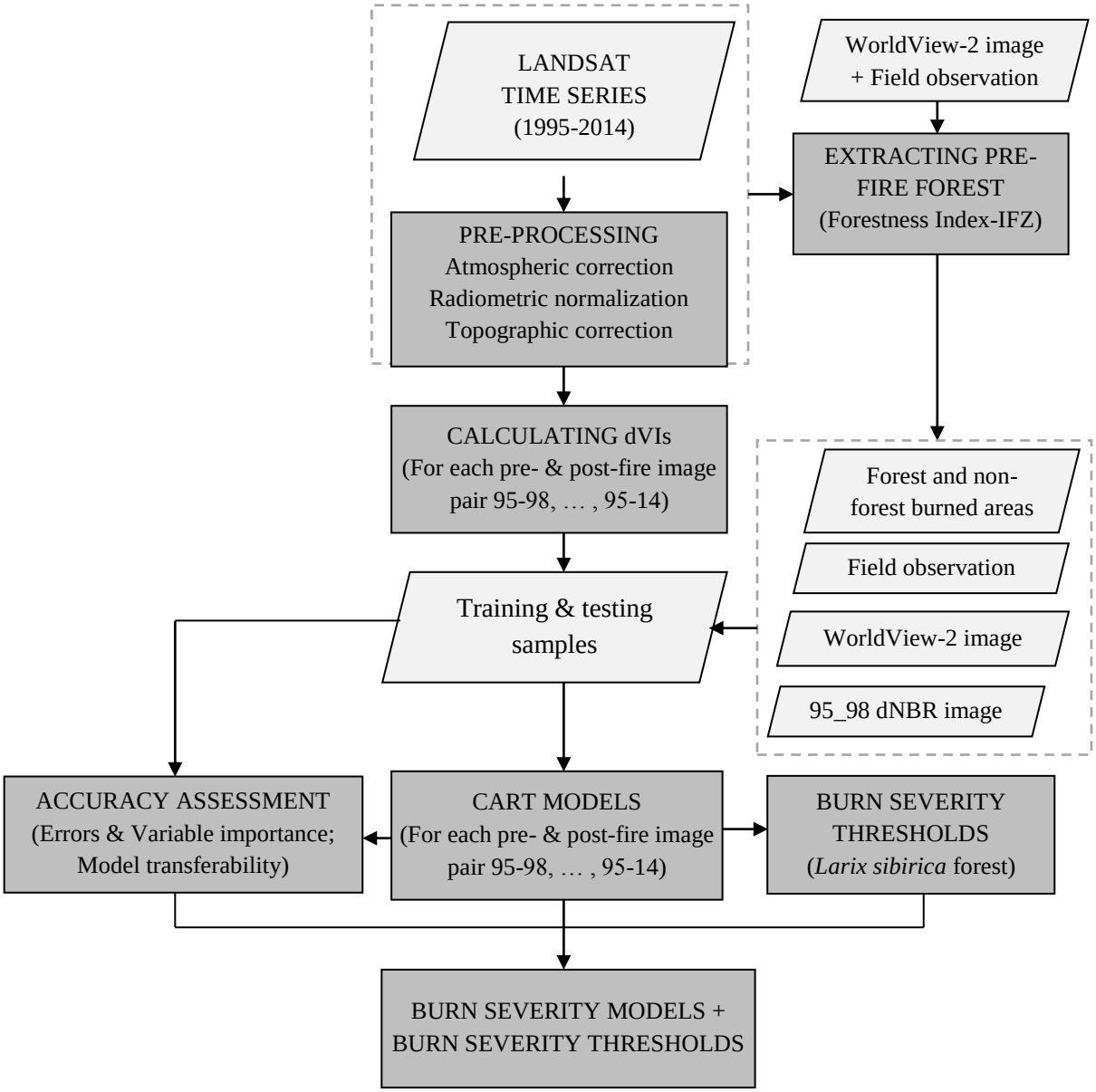

Figure 3.2 A conceptual flow of reconstructing burn severity at different post-fire lag timing in Larix sibirica forest.

3.5.2 Pre-processing

Pre-processing of the remotely sensed data included atmospheric correction and normalization, subsetting, and topographic correction. The "absolute-normalization" atmospheric correction method that matches all images in a time-series to an atmospherically corrected reference image(Schroeder et al., 2006) was used to correct the effects of atmosphere on the Landsat time-series data. The post-fire 1998 image was selected as a reference image due to its highly atmospheric and radiometric quality based on our visual interpretation. The reference image was conducted the absolute atmospheric correction of the surface reflectance using ATCOR algorithm (Richter, 1990). All other remaining images in the Landsat time series were then normalized to the reference image using the iteratively re-weighted MAD (multivariate alteration detection) algorithms of Canty et al. (2008), which identify the invariant pixels within a small subset of the larger image. The subset area was selected to cover both the 1996 and 2008 burned areas (Figure 3.1). Since the method is not limited to the cloud-free scenes, the normalized subset images were finally masked out cloud and cloud shadow using visual interpretation in coupling with automated cloud masking algorithm in the PCI Geomatica. Since the study area is located in mountainous region with high range of altitude, it was necessary to correct the Landsat time series for different illumination effects due to the topography. This was done based on the C correction method, an empirical modification of the cosine correction approach (Teillet et al., 1982). The digital elevation model of the Shuttle Radar Topography Mission (SRTM) was resampled and coregistered with the Landsat images, and then derived the topographical slope and aspect data. These two topographical variables and the solar zenith and azimuth angles at the time of image acquisition were used as input parameters for the C correction algorithm (Veraverbeke et al., 2010b).

3.5.3 Extraction of pre-fire forest and non-forest area

Because stratification of the different land cover types prior to the assessment of the burn severity is necessary (Cansler and McKenzie, 2012, Soverel et al., 2011,Allen and Sorbel, 2008), the pre-fire land cover was classified into the larch boreal forest and non-forest areas. Huang et al. (2009) proposed a forest z-score (IFZ) value to extract the forest pixels from a multi-spectral satellite images as follows (Eq. 3.1):

$$IFZ = \sqrt{\frac{1}{NB}\sum_{i=1}^{NB}(FZ_i)^2} \qquad (3.1)$$

where NB is the number of bands used, FZ_i is the forest z-score value for band i that can be calculated as the follows (Eq. 3.2):

$$FZ = \frac{b_{pi}-\bar{b_i}}{SD_i} \qquad (3.2)$$

where $\bar{b_i}$ and SD_i is the mean and standard deviation of the band i spectral values of the known forest pixels within an image respectively, b_{pi} is the spectral value for any pixel in that image. For the Landsat images, Red (630-690 nm), SWIR1 – Short Wave Infrared 1 (1550-1750 nm), and SWIR2 – Short Wave Infrared 2 (2080-2350 nm) are used to calculate the IFZ values (Huang et al., 2009). Since the IFZ is an inverse measure of the probability of a pixel being a forest pixel, pixels having low IFZ value closed to 0 have high probability of being the forest pixels, whereas those having high IFZ values are likely the non-forest pixels. We used the threshold of IFZ values less than 3 as proposed by Huang et al. (2010) to locate the forest pixels in the pre-fire Landsat TM image.

It is important to identify exactly the known forest pixels within an image in the determination of IFZ value. In this study, the confident forest samples were delineated using the

WorldView-2 image in combination with the stability of the spectral and spatial patterns of the forest patches closed to the burned area over the time series data (Figure 3.3). The visual interpretation within the time series Landsat data is necessary to confirm the unchanged-known forest pixels in the pre-fire image acquired in 1995. In addition to the WorldView-2 image, some of the known forest areas were also located based on our field observation in 2011.

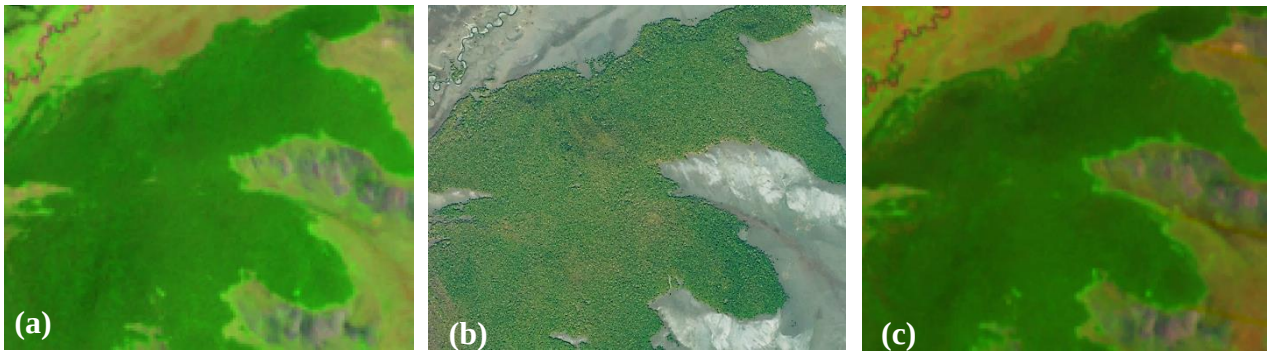

Figure 3.3 An example of unchanged-known larch forest patches closed to the 1996 burned area; (a) 1995 Landsat TM, (b) 2010 WorldView-2, and (c) 2014 Landsat ETM+ images.

Training samples were located on known larch forest patches of the 1995 image to calculate mean ($\overline{b_i}$) and standard deviation (SD_i) of the band i spectral values as inputs in equation (3.2).

3.5.4 Response and explanatory variables

Three remote sensing indices including the NBR (Key and Benson, 2006), the NDVI (Namzalov et al., 2012), and the NDMI (Wilson and Sader, 2002) were selected to assess the dependence of burn severity assessment on the post-fire lag timing. The selection of these indices in the model of burn severity assessment was expected to synergistically account for the different properties of the post-fire vegetation related to burn severity, which include percentage of tree mortality and soil exposure, changes in the canopy moisture content, and the ability of vegetation recovery to pre-fire condition.

To determine the degrees of change caused by fire, the post-fire image is subtracted from the pre-fire image resulted in the differenced image for the burn severity assessment (Table 3.2). After bi-temporal differencing, the burned area is associated with high values in the dNBR, the dNDVI, and the dNDMI images. These differenced indices were evaluated their performance in the model of lag-timing based burn severity assessment of the boreal larch forest using the classification and regression tree (CART) in this study. The response variable of the burn severity levels was categorized into four levels of unburned, low, moderate and high burn severity (*see section 3.5.5*).

Table 3.2 Pre/post-fire differenced spectral indices (dNBR, dNDVI, dNDMI) used as explanatory variables for burn severity assessment in this study

In Landsat TM and ETM+ images: R – Red (Band 3 – 630-690 nm); NIR – Near Infrared (Band 4 – 760-900 nm); SWIR1 – Short Wave Infrared 1 (Band 5 – 1550-1750 nm); and SWIR2 – Short Wave Infrared 2 (Band 7 – 2080-2350 nm).

Vegetation Index		**Pre/post-fire differenced index**
Normalized Burned Ratio (NBR)	$NBR = \frac{NIR - SWIR2}{NIR + SWIR2}$	$dNBR = (NBR)_{pre} - (NBR)_{post}$
Normalized Difference Vegetation Index (NDVI)	$NDVI = \frac{NIR - R}{NIR + R}$	$dNDVI = (NDVI)_{pre} - (NDVI)_{post}$
Normalized Difference Moisture Index (NDMI)	$NDMI = \frac{NIR - SWIR1}{NIR + SWIR1}$	$dNDMI = (NDMI)_{pre} - (NDMI)_{post}$

3.5.5 Sample design

The assessment of burn severity using the field-based indices such as the Composite Burn Index (CBI) and the Geo Composite Burn Index (GeoCBI) is not always available in many regions, particularly in remote regions. Thus, it is necessary to propose an alternative method for

field based measurement of burn severity. We used multi data for the process of sampling, which included the pre-fire (1995) and post-fire (1998) Landsat TM images, the difference of the pre- and post-fire NBR images, the 2010 WorldView-2 image, and the field observation. The sampling design was based on several assumptions of the post-fire environment that had the same pre-fire condition that: 1) higher burn severity results in lower spectral reflectance in near infrared band (760-900 nm) and higher spectral reflectance in short wave infrared band (2080-2350 nm) due to the loss of vegetation cover and the increase of soil exposure respectively, shown by the darker red color on the 1998 post-fire false RGB color composited image of the TM band 7 (SWIR), 4 (NIR), and 1 (Blue); 2) higher burn severity results in higher dNBR values; and 3) higher burn severity results in lower proportion of tree cover, higher proportion of soil exposure, and longer time for vegetation recovery to pre-fire condition. In this study, the first two assumptions were observed on the post-fire 1998 Landsat image as well as the difference in NBR values between pre- and post-fire images. The last assumption was evaluated using the high spatial resolution image of the WorldView-2 sensor in combination with the field observation in 2008 and 2011. Additionally, the visual inspection of the WorldView-2 image and observation from the field was also used to classify the burn severity into high, moderate, low, and unburnt classes. The classification of each training site into different burn severity levels was similar to the approach used by Quintano et al. (2013). Within each polygon of homogeneous spectral reflectance determined from the first two above steps, polygons where the proportion of the dead trees (inversed from alive standing trees) and bare soil exposure was over 90% were classified as the high severity class. Polygons where the proportion of the dead trees and bare soil exposure was between 50 and 90% were classified as moderate severity class, and polygons where the proportion of the dead trees and soil exposure was below 50%, showing a

heterogeneous patch of living and dead standing trees, were classified as the low severity class. The unburned samples were also determined surrounding the 1996 fire affected area included the larch forest and bare land areas that were unchanged between the pre- and post-fire images (Figure 3.4 & 3.5).

Each of the drawn polygons that determined unburned, low, moderate, or high severity level was then coded with the value of 0, 1, 2, or 3, respectively. However, in attempt to keep the samples equal and fully randomized among the burn severity classes, we used a stratified random design to select only approximately 300 pixels per burn severity level within the drawn polygons to be used as the training samples. An additional 250 samples per burn severity class were selected for the purpose of accuracy assessment of the developed CART models. For each sample location, the explanatory variables of dNBR, dNDVI, and dNDMI were extracted on a per pixel basis using the bilinear interpolation method. These samples were also equally stratified with the values of pre-fire conditions of the boreal larch forest and the non-boreal larch forest for the comparison of burn severity of the forest and non-forest areas. Consequently, each lag timing of the burn severity assessment included one response variable of the burn severity level, and the three explanatory variables with the same 1200 training samples, and 1000 testing samples in almost all lag timings, except for the lower number of samples in the lag timings of 12, 14, 15 years because of using the partially cloud post-fire 2008, 2010, and 2011 images, respectively.

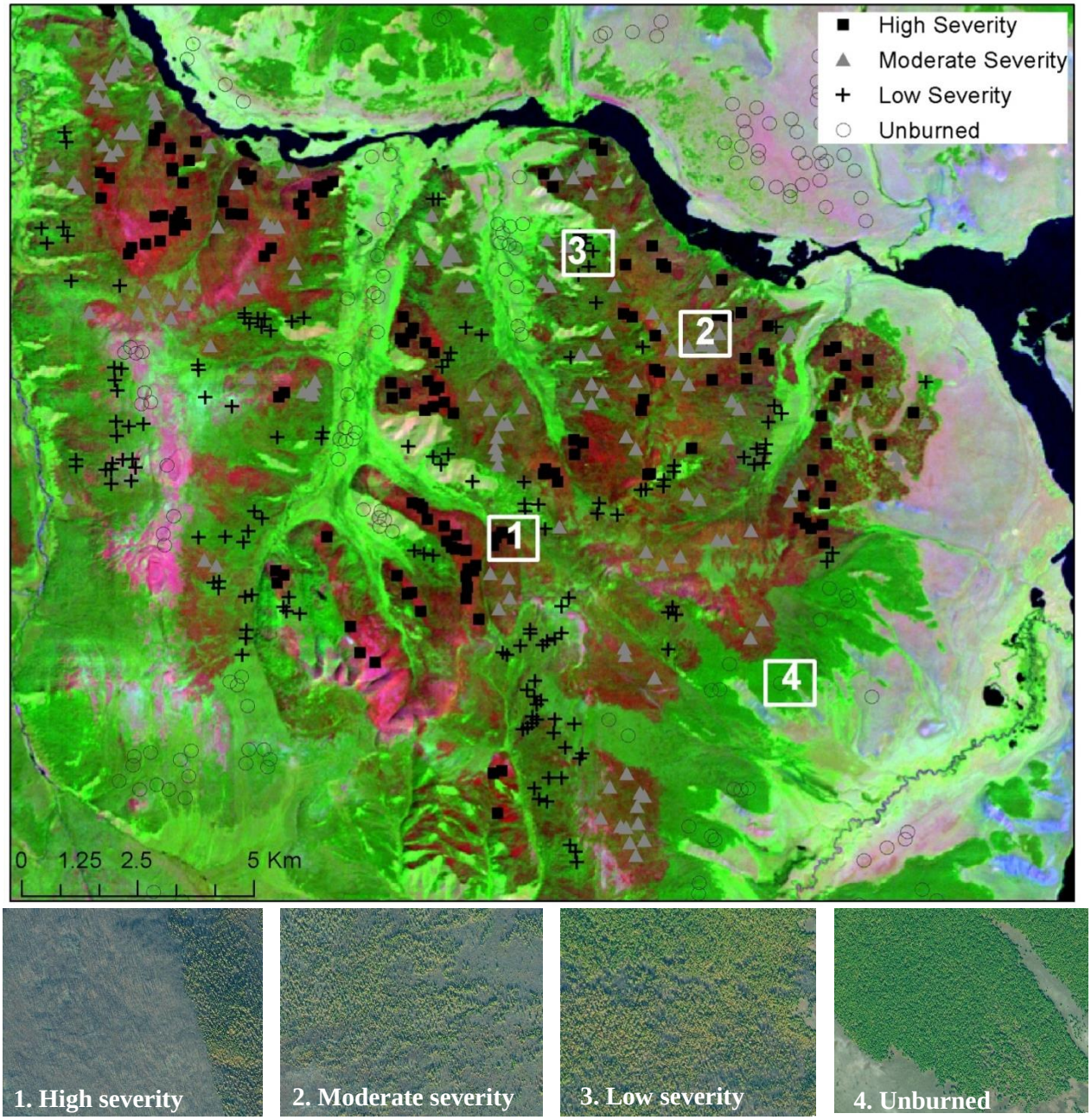

Figure 3.4 Locations of training samples on 1998 Landsat TM image and examples of four burn severity classes of boreal larch forest observed from WorldView-2 image.

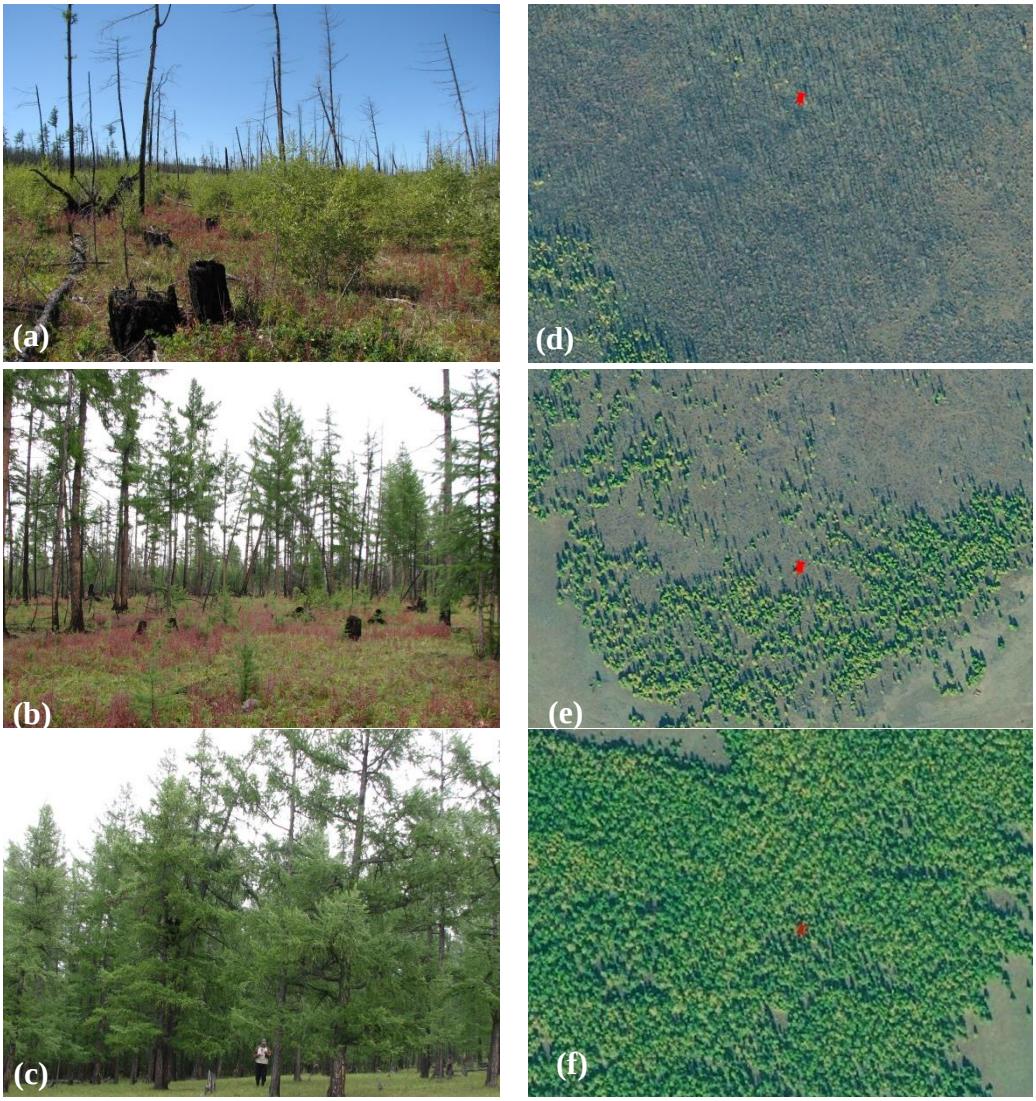

Figure 3.5 Example photos of burn severity levels in 1996 burned area.

High (a), moderate (b) severity, and unburned (c) plots of the 1996 burned area, and the corresponding samples (photos around red points) of high (d), moderate (e), and (f) unburned areas on the August 2010 WorldView-2 image. Photos were taken in August 2008 (Photos credit: Kazuo Takeda).

It should be noted that the results could be biased towards the use of samples from the visual inspection of the satellite data because our interpretation may be subjective, and the WorldView-2 image was acquired in 2010. However, from our field observation at timing of 3-years following the 2008 burned area, there was similar pre-fire condition with and closed to the

1996 burned area (Figure 3.1), the field based burn severity assessment was very similar to the assessment of the 1996 burned area and easily distinguished between the different burn severe levels (Figure 3.5 &3.6). This is possibly due to the low recovery rate of the post-fire vegetation in the boreal larch forest of the study area. In order to evaluate the possible biases in the sampling design for the 1996 burned area, a similar process of the sample design was conducted for the 2008 burned area closed to the 1996 burned area using the 2007 ETM+ (pre-fire), 2009 (post-fire) TM images and the same 2010 WorldView-2 scene. There were more than 400 samples selected within the 2008 burned area. These samples of the 2008 burned area were used not only to evaluate the possible biases in the sampling design of the 1996 burned area but also to examine how the developed CART model of the 1996 burned area can be transferred to the other burned areas (e.g. 2008 burned area) in the taiga-steppe transition zone (see *section 3.5.7*).

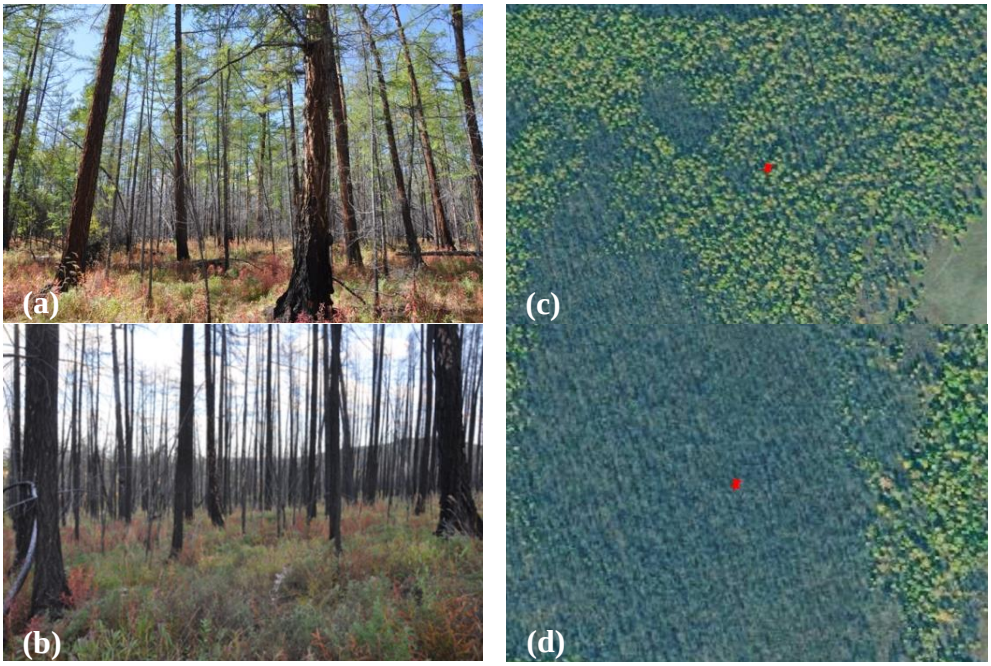

Figure 3.6 Example photos of burn severity levels in 2008 burned area.
Low (a), high (b) severity plots of the 2008 burned area, and the corresponding samples (photos at red points) of low (c), high (d) areas on the August 2010 WorldView-2 image. Photos were taken in August 2011 (Photos credit: Kazuo Takeda).

3.5.6 Classification of burn severity

The classification and regression tree (CART) model was selected for mapping the burn severity in this study as it is flexible, non-parametric, robust to complex non-linear relationship, and a number of explanatory variables can involve in the model (Schroeder et al., 2007). Additionally, since the selection of the training samples might result in the spatial autocorrelation, the CART is an appropriate method to avoid the effects of spatial autocorrelation in the dataset (Cablk et al., 2002, Collins et al., 2007). The CART is constructed by repeatedly splitting the data into increasingly homogeneous groups based on the response variable. Each split reduces the sum of the squares within the resulting groups. We used the tenfold cross-validation method to prune trees, and the smallest trees were selected using the one-standard error rule on the cross-validated relative error (Breiman et al., 1984). The CART was run 15 times corresponding to 15 post-fire lag timings of burn severity assessment (Table 3.1) to identify the four natural groups of unburned, low, moderate, and high burn severity within the continuous data of the dNBR, the dNDVI, the dNDMI of each lag timing of the assessment. The relative importance of three explanatory variables in the CART models was also derived to evaluate how these variables were sensitive and changed in the assessment of the burn severity levels at different timings following the fire. In this study, the assessment of the burn severity levels was conducted separately for the forested (*Larix sibirica*) and other vegetated areas. The analysis of the fire effects was reported and focused more on the burned forest area in the following sections.

3.5.7 Accuracy assessment and model transferability

To assess the accuracy of the CART models in classifying the severe levels of burned larch forest at different timings, we used the test samples within the burnt-forested area to

compute standard confusion matrices with overall accuracy, omission and commission errors of the derived burn severity classes. As mentioned in the section of sampling design that the results could be biased because the use of samples from the visual inspection of the WorldView-2 image acquired 14-years and the field observation (2008) 12-years after the 1996 fire, the burn severity model developed for the 1996 burned area was used to evaluate the severity of the 2008 burned area (Figure 3.1). Collecting samples based on the 2010 WorldView-2 image and 2011 field observation was only 2 and 3 years respectively delaying from the 2008 fire (Figure 3.6). The use of these samples were thus expected to evaluate the possible biases in the sampling design of the 1996 burned area as well as to examine how the developed CART model of the 1996 burned area can be transferred to other burned areas in the taiga-steppe region. In particular, the CART model with lagging of two of the 1996 burned area was used to classify the severity in the 2008 burned area, using the 2007 and 2009 images as the pre- and post-fire images respectively (see section 3.6.7). The accuracy of the transferred model was evaluated using the samples collected on the 2010 WorldView-2 images and our field observations in summer 2011.Both processes of the accuracy assessment and model transferability were only conducted using the samples and CART models within the boreal larch areas, and the unburned and low severity classes were combined to represent the "unburned to low" burn severity condition.

3.6 Results

3.6.1 Pre-fire vegetation condition

The pre-fire vegetation conditions were classified into the boreal larch forest dominated by the *Larix sibirica* species and other vegetation cover that included the broadleaf forest, shrub, and grass covers. Several patches of the known larch forest were located in the 1995 pre-fire image to calculate mean and standard deviation (SD) of the pre-fire Landsat TM band 3 (Red),

band 5 (SWIR1) and band 7 (SWIR2) (Table 3.3). The calculation of forest z-score (IFZ) and extraction of the larch forest was shown in figure 3.7.

Table 3.3 Mean and standard deviation values (% reflectance) used in Eqs. (3.1) and (3.2) for the extraction of larch forest

Band 3 (Red)		Band 5 (SWIR1)		Band 7 (SWIR2)	
Mean	SD	Mean	SD	Mean	SD
6.25	0.32	13.30	0.87	7.00	0.67

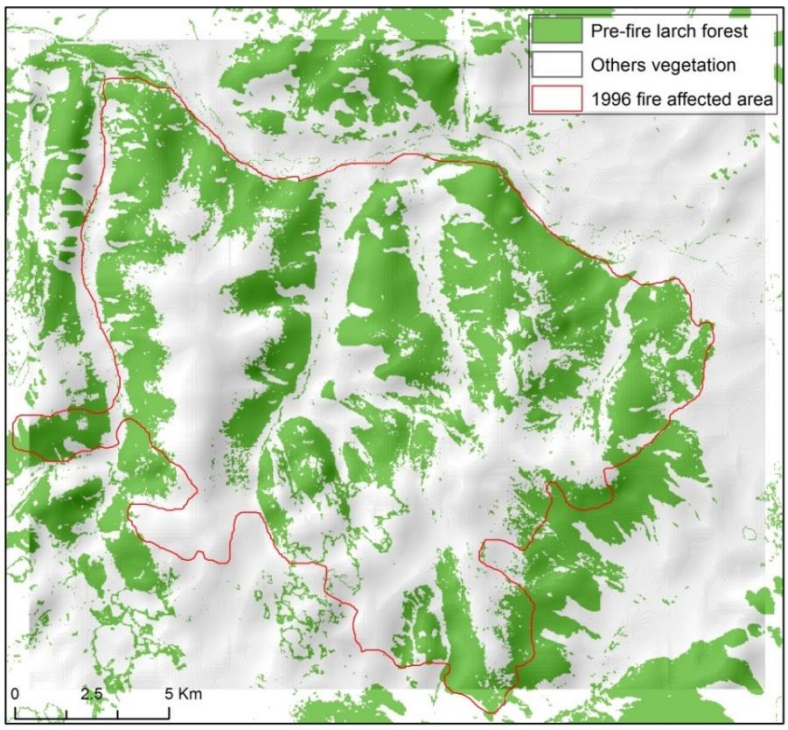

Figure 3.7 Extraction of 1995 larch forest area using forestness index (IFZ) prior to the burn in 1996.

The classification of the pre-fire larch forest and other land covers were used to stratify the samples as well as to compare the burn severity assessment of the different pre-fire conditions. Because the larch forest classification based on the known forest pixels interpreted from very high resolution image and field observations to calculate the likelihood of the larch

forest on the pre-fire image, the result of the larch forest map was reliable for the purpose of sampling design in this study. We only conducted a quick accuracy assessment of the map by visually comparing a number of the derived larch forest patches that were unburned and unchanged between 1995 and 2010 with the observations from the 2010 WorldView-2 image. The results showed very high consistency between the two data sources with respect to the larch forest boundary (Figure 3.8).

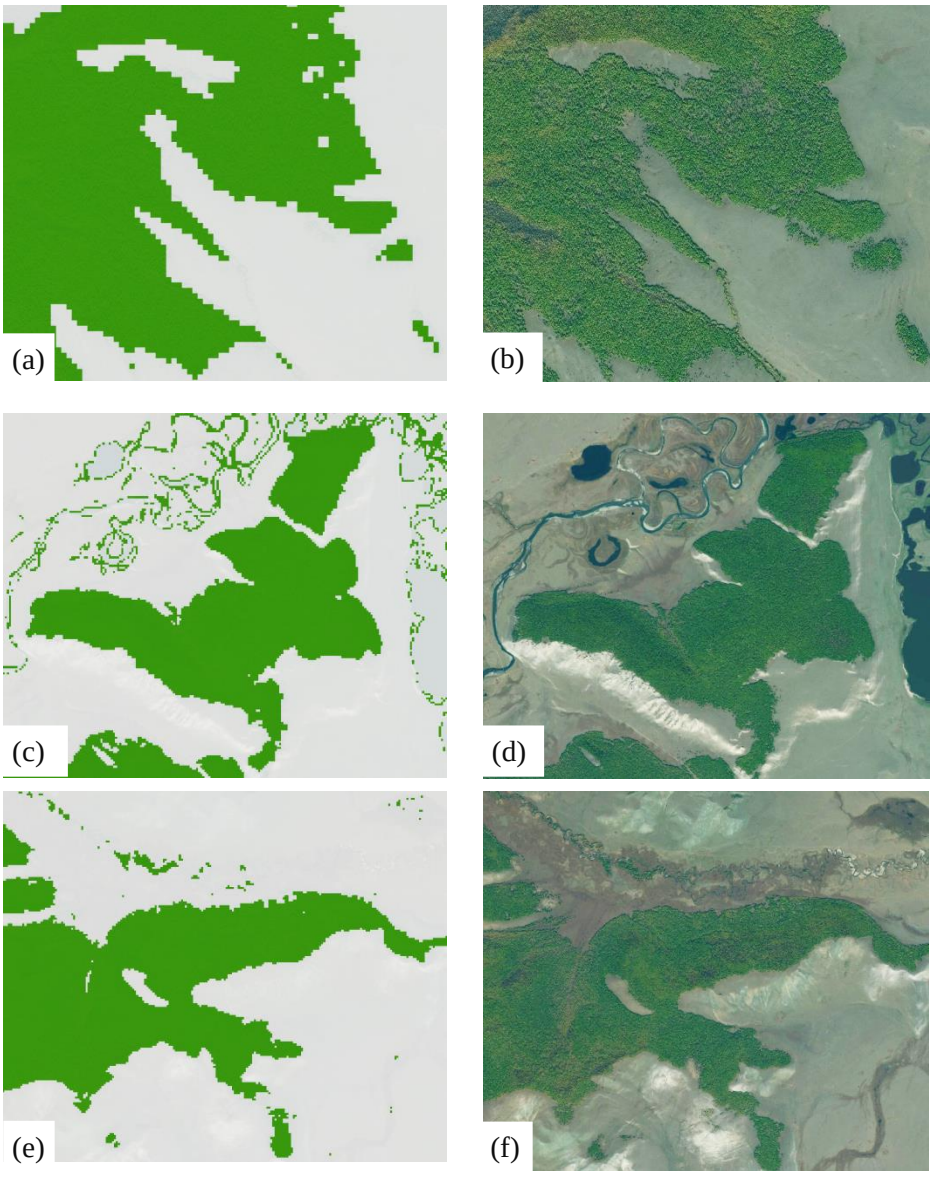

Figure 3.8 Visual assessment of the larch forest patches derived from Landsat TM forest z-score (IFZ) (a,c,e) using very high resolution image (b,d,f) respectively.

3.6.2 Burn severity of different pre-fire conditions

The box plots were used to compare the severity of burns in larch- and non-larch forest areas at different severity categories in respect to the magnitude of the dNBR, the dNDVI, and the dNDMI as severity indices (Figure 3.9). The results showed that the use of the dNBR, the dNDVI, and the dNDMI was necessary to classify burn severity into low, moderate, and high classes of both forest and non-forest burned areas at different lag timing of the burn severity assessments (e.g. lag timings of two in figure 3.9a, 3.9b, 3.9c and 18 in figure 3.9d, 3.9e, 3.9f). Within each burn severity categories, the dNBR and the dNDMI showed significant differences between the larch forest and non-larch forest samples of all the severity categories (Figure 3.9a, 3.9d, 3.9c, 3.9f). On the other hand, the dNDVI was insignificant between the two land cover classes particular in the high and moderate levels of lag timing of two (Figure 3.9b). The differenced vegetation indices of the long lag timing were much lower (Figure 3.9d, 3.9e, 3.9f) than that of the short lag timing (Figure 3.9a, 3.9b, 3.9c). These results suggest that the thresholds of the differenced vegetation indices such as the dNBR, the dNDVI and the dNDMI for assessing the burn severity levels should be proposed separately for different pre-fire land cover conditions as well as for different lag timing of the assessment. Additionally, the importance of the dNBR and the dNDMI was also revealed in both the short and long lag of burn severity assessments within and outside the forest burned patches.

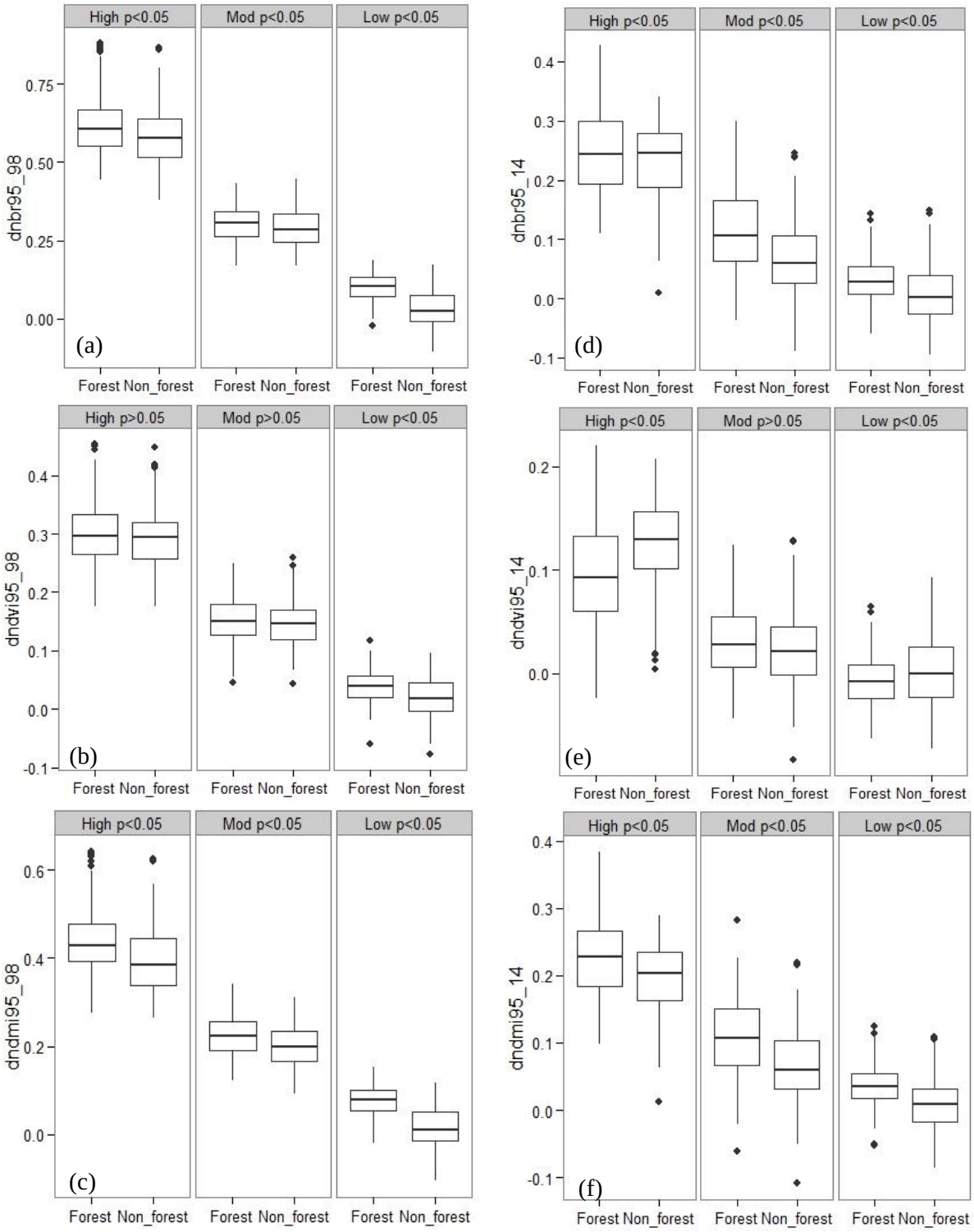

Figure 3.9 Assessment of 1996 burn severity using remote sensing indices. dNBR (a, d), dNDVI (b, e), and dNDMI (c, f) of forested area *(Larix sibirica)* and non-forested area; examples assessment of burn severity using the lag timing of 2 (a,b,c), and the lag timing of 18 (d,e,f).

3.6.3 Burn severity models of the burned larch forest

The samples of three explanatory variables (dNBR, dNDVI, dNDMI) were used to examine the CART models separately for the assessment of burn severity within and outside the larch forest area in the taiga-steppe transition zone. The number of explanatory variables involved in the CART models as well as the number of terminal nodes or classification decision rules varied depending on the lag timing of burn severity assessments (Figure 3.10). In almost all the CART models, moderate and high severity classes were generally classified at the terminal nodes using the dNBR and the dNDMI predictors. On the other hand, the dNDVI involved significantly in the terminal nodes to identify low and unburned classes. The cross validation of the CART models showed that longer lag timing of the assessment following the fire resulted in higher misclassification error rate. This might be due to the recovery of post-fire vegetation that leads to the difficult separation among the four severity classes defined by the percentage of tree mortality and soil exposure after fire. The accuracy assessment was further conducted using the independent testing samples to confirm the findings of misclassification error of the CART models using the cross validation (see section 3.6.6).

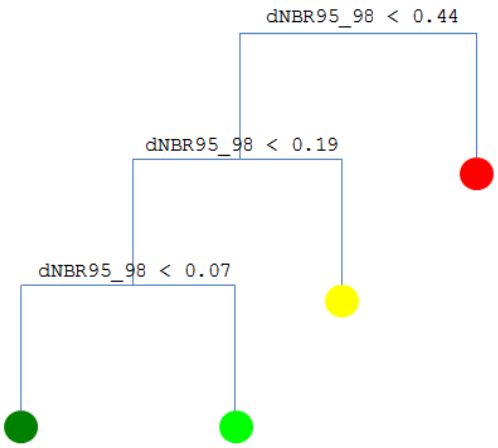

a) Lag timing of 2

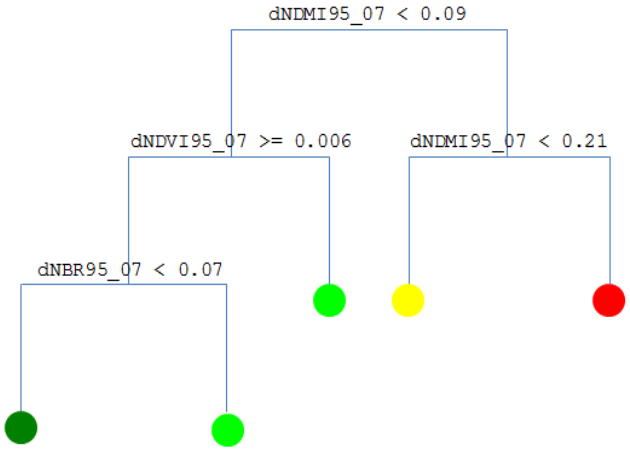

b) Lag timing of 11

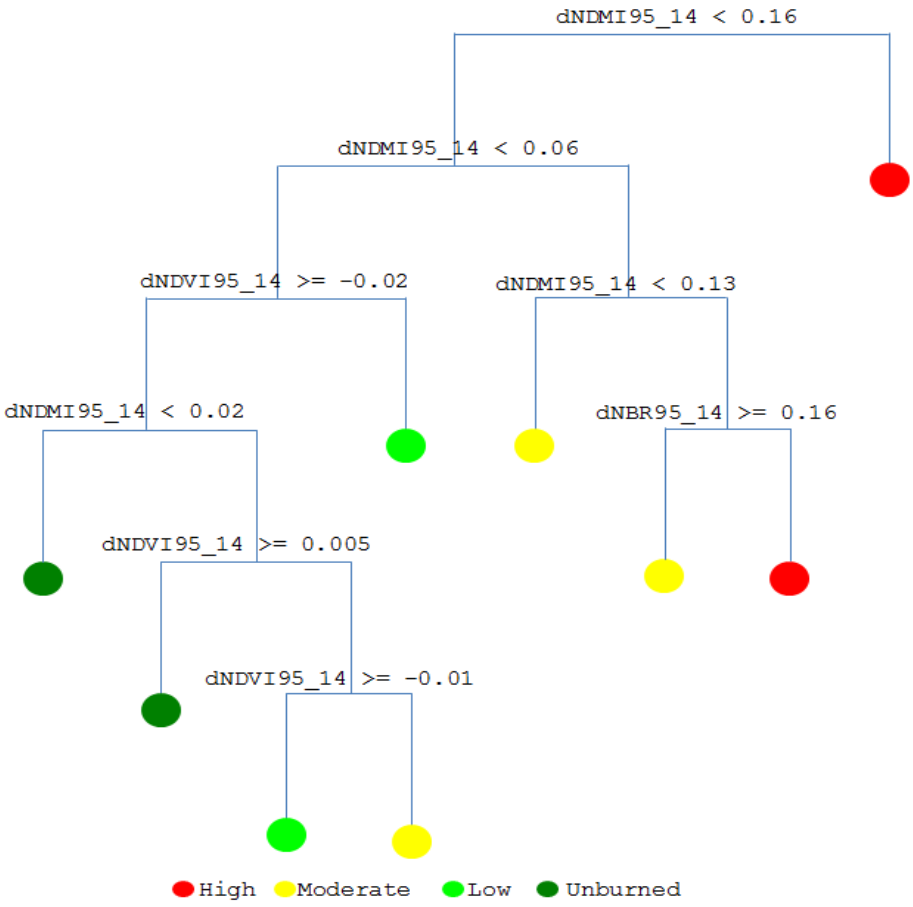

c) Lag timing of 18

Figure 3.10 Examples of CART models of burn severity assessment of larch forest at different timing of the assessment following the 1996 fire: 2 years (a), 11 years (b), and 18 years (c).

3.6.4 Variable importance

In addition to the branch length of the CART models, Figure 3.11 showed that the dNBR and dNDMI were more important than the dNDVI for the purpose of explaining four burn severity classes of both the larch and non-larch forest areas throughout different lag timings of the assessments. The dNDMI showed an increase trend of its importance in classifying burn severity, whereas the importance of the dNDVI decreased with increasing the lag timing of burn severity assessment. In the first seven years after the fire within the larch forest, the dNBR was the most important variable in determining burn severity (Figure 3.11b). However, the relative importance patterns of the three predictors, ranked in order of the importance, were dNDMI, dNBR, and dNDVI since the eighth year following the forest fire (Figure 3.11b).

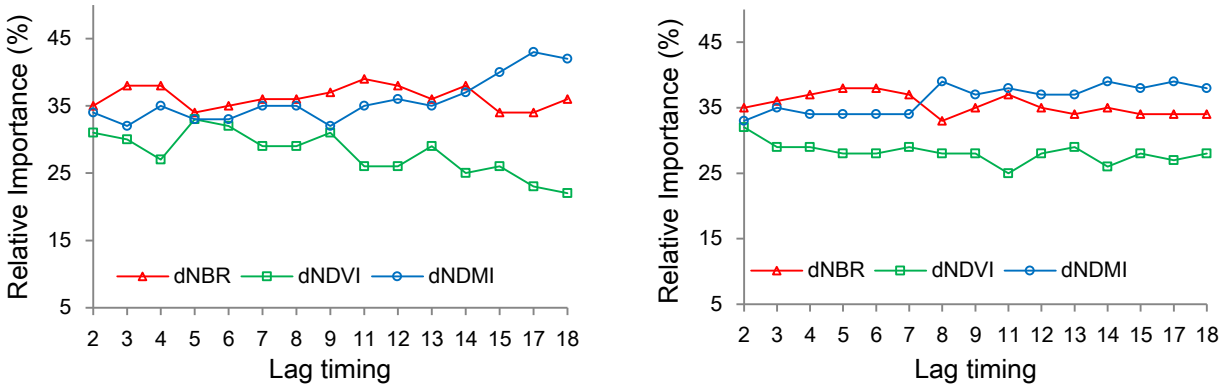

a) Non-forested burn b) Larch forest burn

Figure 3.11 Relative importance of three predictors (dNBR, dNDVI, dNDMI) in the CART models of non-larch forest (a) and larch (Larix sibirica) forest (b) at different lag timing of the assessment.

3.6.5 Burn severity classes at different lag timing

The proportion of each burn severity class within the burned larch-forest areas was computed to assess the influence of lag timings on the measurements of burn severity (Figure 3.12). The area of the severity classes varied, depending on the timing of post-fire images. In

particular, the high severity class increased substantially with longer lag timing of the assessments (e.g. from lag timing of 12 to lag timing of 18, Figure 3.12). Figure 3.13 shows examples of burn severity maps derived from the CART models of the larch forest at different lag timing of the assessments. It is possible to observe visually that there were similar spatial patterns of burn severity classes among the different lag timing based CART models.

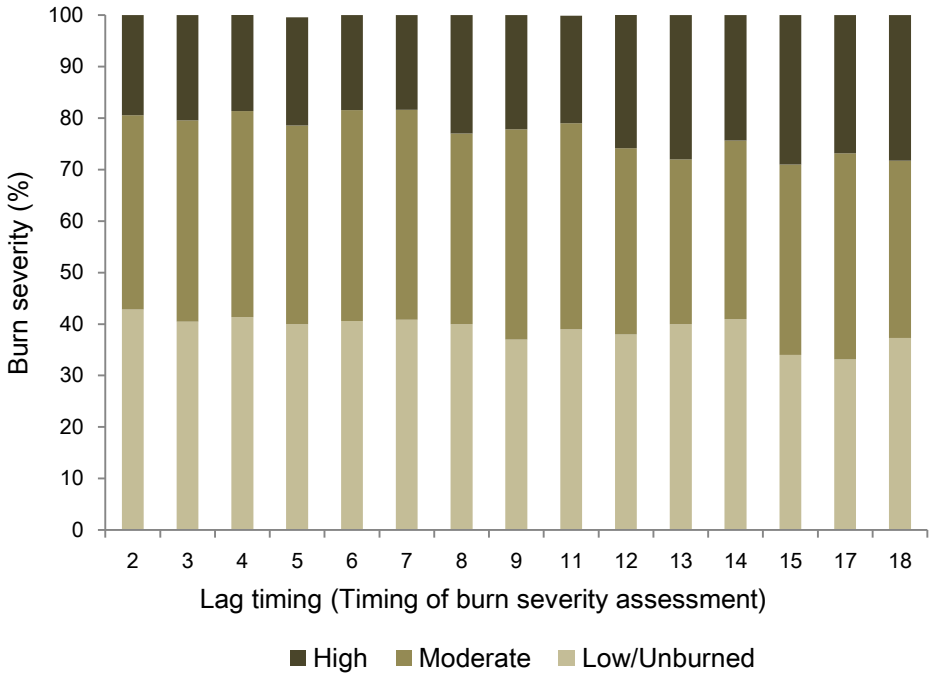

Figure 3.12 Proportion of burn severity classes within the larch forest area at different lag timings of burn severity assessment.

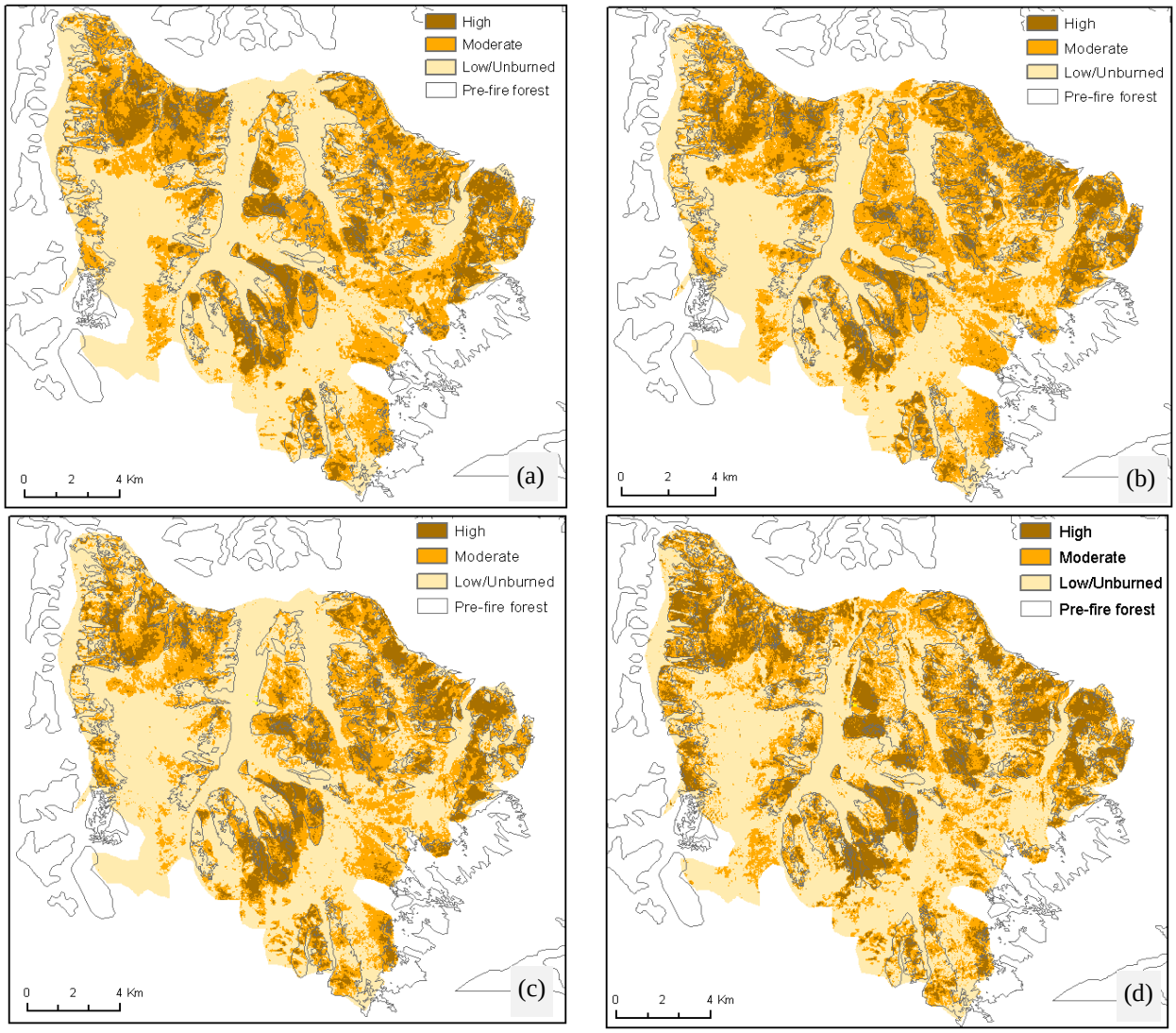

Figure 3.13 Examples of burn severity maps derived from CART models of larch forest with the use of the same 1995 pre-fire image and different post-fire images. Lag timing of two: post-fire image in 1998 (a); lag timing of six: post-fire image in 2002 (b); lag timing of 11: post-fire image in 2007 (c); and lag timing of 18: post-fire image in 2014 (d).

3.6.6 Accuracy assessment

The overall accuracy of the CART models within the larch forest areas ranged from 62% to 83% depending on lag timings of the burn severity assessments (Figure 3.14, Table 3.4). Generally, the overall accuracy decreased when the lag timing of the assessments increased.

Since the burn severity classes in this study were defined as the decrease of vegetation cover and increase of soil exposure, these results of overall accuracy suggested that the recovery of post-fire vegetation influenced the assessments of burn severity.

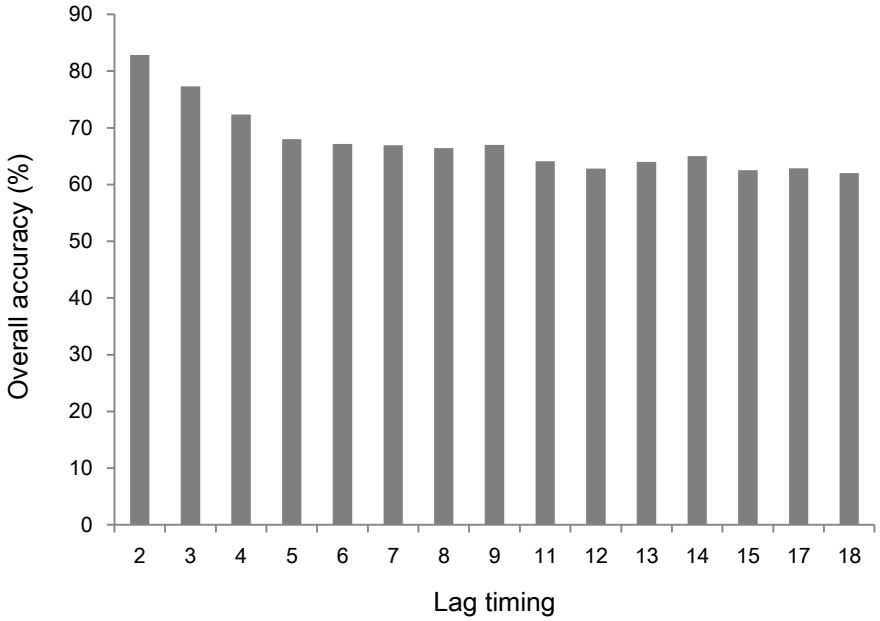

Figure 3.14 Overall accuracy of burn severity assessment at different lag timings.

The omission and commission errors (Table 3.4) indicated that the high burn severity class was predicted with greater accuracy than the classes of low and moderate severity in all the lag timings. This result suggested again that the possible relationship between the forest recovery and burn severity in which the high burn severity area can still be classified accurately using long lag-timing of the post-fire image due to the slow recovery of the larch forest. The errors of the moderate class have values relatively high throughout the lag timings. Since the moderate class was falling in between the low and high classes, the visual assessments of the moderate class during the selection of training and testing samples might be subjective and difficult to distinguish clearly with the other classes in a number of samples.

Table 3.4 Summary of confusion matrix results of CART models at different lag timing

Pre-Post Image	Lag timing	Omission Error (%)			Commission Error (%)			Omi. Average (%)	Com. Average (%)	Accuracy (%)
		Unburned /Low	Mod	High	Unburned /Low	Mod	High			
95-98	2	27	19	5	7	32	10	17	16	83
95-99	3	36	28	2	15	40	12	22	22	77
95-00	4	35	23	24	8	48	15	27	24	72
95-01	5	36	29	28	17	50	18	31	28	68
95-02	6	34	28	35	13	52	21	32	29	67
95-03	7	36	33	29	14	53	21	33	29	67
95-04	8	33	42	27	17	50	31	34	33	66
95-05	9	35	37	25	18	48	27	32	31	67
95-07	11	31	49	30	21	57	28	37	35	64
95-08	12	48	42	23	15	54	33	38	34	63
95-09	13	31	59	21	24	50	38	37	37	64
95-10	14	38	47	18	27	52	24	34	34	65
95-11	15	54	44	18	15	55	31	39	34	63
95-13	17	53	44	13	27	57	23	37	36	63
95-14	18	46	45	23	34	52	28	38	38	62

3.6.7 Model transferability

The highest accuracy CART model of the 1996 burned area was used to evaluate the burn severity for the 2008 burned area. Because these two burned areas were closed, we used the same Landsat scenes acquired in 2007 and 2009 shown in Table 3.1 as the pre- and post-fire images respectively for the calculation of the explanatory variable (dNBR) of the selected CART model (the CART model with lagging of two, see Figure 3.10a & Table 3.4). The result of burn severity assessment for the 2008 burned area was shown in Figure 3.15.

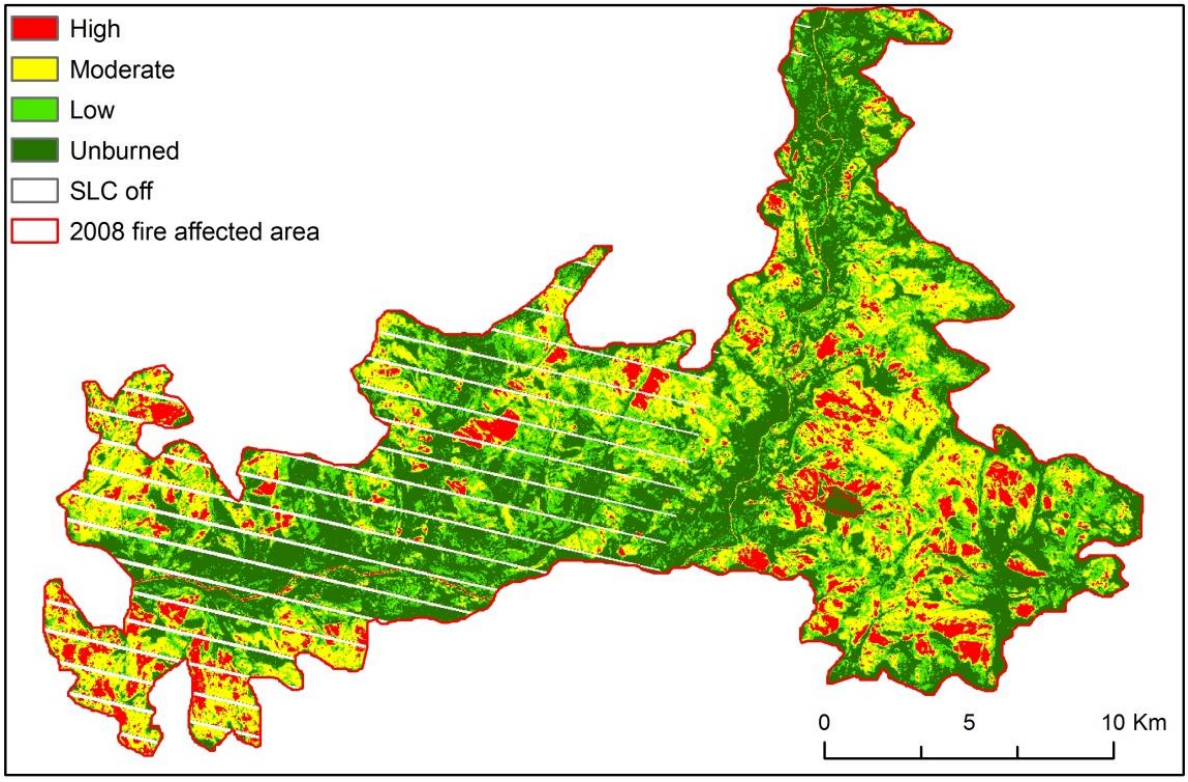

Figure 3.15 Burn severity of 2008 fire affected area using the 1996 CART model.

The overall accuracy of the transferred CART model was 79%. A kappa coefficient of 68% suggested "moderate agreement" between the predicted severity classes and the test samples. Ranging from 14 to 26%, the individual commission errors suggested that the unburned to low and high severity classes were predicted with greater accuracy than the class falling in between. This result was similar to the result of the severity assessments for the 1996 burned area. Figure 3.16 showed examples of the classification accuracy of the transferred model.

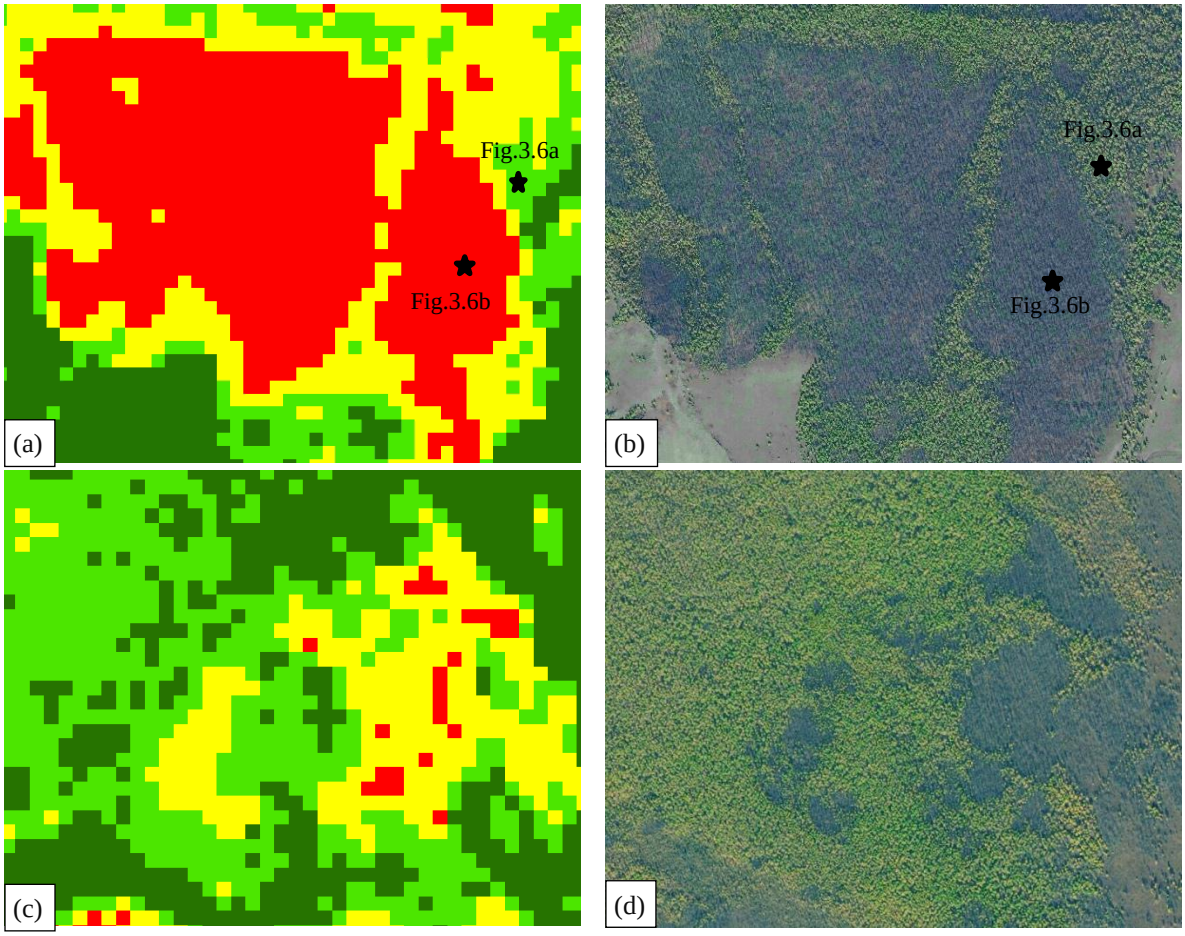

Figure 3.16 Examples of classification accuracy and errors of the 2008 burn severity using the 1996 burn severity model.

Locations of field photos in figure 3.6 were shown on the 2008 burn severity map (a) and 2010 WorldView-2 (b). Some high severity patches (black) on the WorldView-2 (d) were omitted on the classified image (c). See Figure 3.15 for color codes of burn severity classes.

3.7 Discussion

3.7.1 A data limitations-driven burn severity model

The results of this chapter highlight several important components. Assessments of the fire extent and burn severity using the remote sensing remain challenging at the northern boreal ecosystems due to the limitation of atmospheric conditions (e.g. high zenith angles,

concentration of high aerosol, cloud cover and cloud shadow) as well as the missing imagery and field survey data (Boer et al., 2008, Loboda, 2009, Loboda et al., 2011, Quintano et al., 2013, Kukavskaya et al., 2012). Thus, the methodology framework with the synergistic use of the multiple data (e.g. time series Landsat, WorldView2, field observation) proposed in this study strongly influences the outcome and success rate for the burn severity assessments in the boreal ecosystems, particularly in the Eurasia boreal forest. Similar to findings by the other researchers (e.g. (Key, 2006, Verbyla et al., 2008, Allen and Sorbel, 2008, Veraverbeke et al., 2010a), it is likely from our results that the accurate assessments of burn severity from our results is driven by both the ecological specifics of the pre-fire vegetation conditions, the fire ecology, as well as the date of image acquisition. Therefore, models of burn severity assessment should be proposed separately by taking into account these drivers as shown in this study.

Compared with the previous studies, our study conducted the assessments of the burn severity with much longer lag timing of the image acquisition (e.g. up to 18 years lag timing between pre- and post-fire images). The purpose of this longer lag timing assessment is not only to achieve models for the overcoming data limitation but also to understand the influence of the ecological processes on the assessments of the burn severity. As noted by Key and Benson (2006), the timing of image acquisition from different periods before and after the fire significantly affects how the remote sensing index is measuring severity. Our results showed significant decrease in terms of classification accuracy in the first five years of the post-fire assessments (Figure 3.14). In addition to the image acquisition date, the changes in the accuracy of mapping the burn severity might have causal link with the post-fire recovery of *Larix sibirica* species since our field observations revealed that the emergence of larch sapling density was 6 years after the fire at all low, moderate and high severity sites (Takeda et al., 2013). In other

words, the burn severity classes can be classified more accurately when the post-fire larch forest is regenerating at its early stages (e.g. grass, shrub, and seedling). On the other hand, the overall accuracy was slightly different at the different lag timings from year 6th following the fire as this is possibly due to the more stable conditions of the post-fire larch forest from year 6th with respects to the vegetation cover as well as the spectral reflectance. Our results also support our hypothesis that the longer lag timing (e.g. greater than one growing season after fire) of an extended assessment has significant effect on the measurement of burn severity compared with the insignificance as pointed by other researchers (e.g. Allen and Sorbel, 2008) using the post-fire image acquired immediately or one growing season for the assessments of burn severity. This is critical assessment of burn severity in relation to time since fire to account for an ecosystem change owing to the fire, particular in boreal ecosystems with low recovery rate of the forest species after the fire such as the black spruce and the larch stands.

Monitoring of the burn severity often classifies the post-fire environment into discrete classes of low, moderate and high severity (Lentile et al., 2006). The use of these categorical descriptions of burn severity might be very subjective and substantially changed depending on the definition of the severity thresholds as well as the date of post-fire image acquisition (Cocke et al., 2005, Lentile et al., 2006, Verbyla et al., 2008). Our results showed that there was an increase trend in the proportion of the high burn severity class, whereas the low to unburned and moderate classes were decreased when the lag timing of pre- and post-fire images increased (Figure 3.12). It is worth noting that this result might be misclassification of the CART models as shown by an increase trend of the commission error of high severity class as well as an increase omission error of the low and moderate classes (Table 3.4). Even though samples were fixed at the same locations for all the lag timing assessments, the distinction among the burn

severity classes using the extracted sample values at different lag timings might be blurred due to re-growth of vegetation after the fire. In contrast, the actual movements from the lower severity sites to the higher severity sites might happen due to the delay of vegetation mortality, revealing that plants green right after the fire had died by the post-fire growth periods. This might be evident in the boreal larch forest because the dominance of the surface fire regimes (de Groot et al., 2012). Under the low and moderate surface fires, overstory vegetation in the forested environment may only be damaged for long duration after the fire showing as the degree of the post-fire tree mortality. As a result, the satellite imagery with the strong capability of overstory observation will indicate the higher proportion of the high burn severity class through the use of older post-fire images. This assumption about the post-fire tree mortality to what degree and the capability of the remote sensing based assessment in the boreal larch (*Larix sibirica*) forest is still unknown and requires further investigation.

In terms of errors, our finding was complement to Cocke et al. (2005), showing decreasing trend of the overall accuracy when the older post-fire images was used, even though Cocke et al. used the shorter lag timings of extended assessments (e.g. post-fire images acquired in 1 and 2 years after fire). Similar to the previous studies in North America (e.g. (Cocke et al., 2005, Epting et al., 2005), our result also reveals that the high severity class had the highest degree of consistent classification with the lowest omission and commission errors throughout different lag timings of the assessments. The more spatially homogeneous of high severity fires (Hudak and Brockett, 2004) makes the classification algorithms easier to distinguish. As a result, the high severity class had the lower errors compared with the moderate and low burn sites.

3.7.2 Relative importance of explanatory variables

This study demonstrated that the different pre-fire conditions and the lag timings of the burn severity assessments lead to different relationships the between burn severity classes and the differenced vegetation indices (dNBR, dNDMI, and dNDVI). In almost all CART models of the burned larch forest, dNBR and dNDMI predictors were common at terminal nodes to classify moderate and high severity classes, while dNDVI involved more in terminal nodes to define low and unburned classes (Figure 3.10). In terms of the ecological aspects, these predictors in the burn severity models contributed different properties to the post-fire land surfaces as well as the significantly spectral variations to discriminate various levels of the burn severity. When vegetation and organic layers are consumed by fires, the surface albedo and the soil surface temperature increases (Jin et al., 2012). This will result in the significant decrease in the land surface moisture for several decades after fires, especially with permafrost sites due to the increased drainage (Yoshikawa et al., 2002, Kasischke and Johnstone, 2005), and then gradual increase due to the recovery of vegetation (Cuevas Gonzalez et al., 2009). Therefore, the inclusion of the dNBR and the dNDMI predictors in the CART models was important to enhance the observations of the variations in burn severity since the severity is defined as the percentage of tree mortality and soil exposure as well as the changes in canopy moisture content and the ability of vegetation recovery to the pre-fire condition in this study.

Compared with the dNBR and the dNDMI, the dNDVI variable was less important for the distinguishing the different degrees of severity, particularly in the high and moderate classes. Our results complement the findings of previous studies (e.g. (Epting et al., 2005, Veraverbeke et al., 2011, Hoy et al., 2008) that support the use of bi-temporal image differencing approach in mapping the burn severity. Veraverbeke et al. (2011) ranked dNBR as the first index with the

overall best correlation with the GeoCBI (Geo Composite Burn Index) field data, followed by the dNDMI and the dNDVI approach for the case study in a Mediterranean environment. Similar findings were obtained by Epting et al. (2005) and Hoy et al. (2008), reporting that the dNBR outperformed the dNDVI. Because the post-fire environment is often quickly recovered by grass and shrub, the use of the NDVI, showing the vegetation greenness, made it difficult to distinguish the different ranges of variation in the post-fire land surfaces. On the other hand, the reflectance of burned areas in Landsat band 7 (2080-2350 nm) is typically lower than that of Landsat band 5 (1550-1750 nm) due to a higher degree of water absorption by vegetation for longer wavelengths (Veraverbeke et al., 2011). Therefore, the fire-induced reflectance increase is likely to be more obvious in the Landsat band 7 than in band 5. Consequently, the dNBR index with band 7 instead of the dNDMI with band 5 is able to capture a larger range of variation in the post-fire effects. However, our results reveal that this pattern of variable importance changed from the lag timing (timing difference between pre- and post-fire images) of 15 and 8 years in evaluating the burn severity of the non-forested areas and forested areas respectively (Figure 3.11) in which the dNDMI was the most important factor in classifying the burn severity classes. As noted from our field observations, the larch sapling density emerged in year 6th after fire, the change in the variable importance of the CART models within the larch forest (Figure 3.11b) is likely driven by this ecological characteristics of the larch forest regeneration. In the retrospective mapping of the burned areas in Central Siberia, George et al. (2006) successfully identified and dated the burned areas up to 10 years prior to the image acquisition date using the MODIS normalized difference water index, calculated from the MODIS NIR (841-876 nm) and the SWIR (1628-1652 nm) bands that was similar to the Landsat NDMI in this study. This suggests an advantage in using the NDMI to detect old disturbances prior to the image

acquisition date as opposed to other vegetation indices. Additionally, the canopy moisture content and density of the regenerating forest differ not only from the surrounding unburned forest but also from the high and low severity sites showing lower NDMI values for many years after the fire event (George et al., 2006, Fraser and Li, 2002, Veraverbeke et al., 2011, Cuevas Gonzalez et al., 2009), while the greenness, soil exposure and charcoal, to which NDVI and NBR are more sensitive, might become more similar to the surrounding unburned forest after a few years of re-vegetation. As a result, the dNDMI increases its relative importance for explaining the post-fire effects following the year after the fire; particularly after the larch forest regenerated and covered the burned areas.

3.7.3 Thresholds of burn severity and management implications

Many studies have evaluated different ranges of the dNBR for the purpose of classifying burn severity into the discrete classes of low, moderate and high severity (Cocke et al., 2005, Epting et al., 2005, Key and Benson, 2006, Hall et al., 2008, Cai et al., 2013) and verified these classes using the field based measurement of burn severity such as the CBI and GeoCBI surveys. We found the discrete classification might be very subjective, and change substantially depending on the definition of severity thresholds, date of the post-fire image acquisition, and the vegetation type. The discrete burn severity classes, however, is often used and convenient for practical applications in the post-fire forest management (Hall et al., 2008, Lentile et al., 2006, Sunderman and Weisberg, 2011, Picotte and Robertson, 2011, Cai et al., 2013). This study employed the high resolution remote sensing data coupled with the field observations from which the burn severity classes in relation to the dNBR were used to map burn severity. Since the validation of the dNBR has been conducted in a wide range of environments, it would be expected that thresholding levels of the dNBR will be different if there are changes in the surface

properties that occur in the environment of interest (Lentile et al., 2006). Table 3.5 showed the thresholds for mapping the burn severity classes with respect to the degree of dNBR changes in the other forest environments compared with this study. We selected the best model of burn severity assessment with lag timing of two in our study (see Figure 3.10, Table 3.4) to propose the dNBR thresholds for mapping the burn severity in the Siberian boreal larch forest. To the best of our knowledge, there have been no available dNBR thresholds proposed for the boreal larch forest in Eurasia with the validation of either high resolution image or field survey data. Therefore, the proposed thresholds of the severity classes in this study are expected to contribute for convenience in mapping burn severity as well for practical applications of the post-fire management in the Eurasian boreal ecosystems. It is worth noting that the similar accuracy to this study might be achieved only if the same pre-fire vegetation conditions (e.g *Larix sibirica* forest), remote sensing data and preprocessing steps were considered prior to mapping the burn severity. Even though the burn severity model in this study was validated by an independent dataset of the burned area showing good complement with the field observations, the proposed thresholds still need further exploration before it could be applied operationally for the Eurasian boreal region. The thresholds we have derived here reflect how we defined our burn severity levels from the field observations and the visual interpretation of the high resolution satellite imagery. Any other definition of burn severity will most likely result in different thresholds.

Table 3.5 Comparison of differenced Normalized Burn Ratio (dNBR) values used in thresholding burn severity at different forest environments.

Study	Dominated vegetation	dNBR threshold of severity classes			
		UB	**L**	**M**	**H**
(Epting et al., 2005)	Black/white spruce (Alaska)	< 90	90-274	271-679	≥ 680
(Cocke et al., 2005)	Ponderosa pine (US)	< 51	51-240	241-570	≥ 571
(Key and Benson, 2006)	Boreal forest (US & Alaska)	< 100	100-269	270-659	≥ 660
(Miller and Thode, 2007)	Conifer & live oak (US)	< 41	41-176	177-366	≥ 367
(Hall et al., 2008)	Boreal forest (Canada)	< 41	41-283	284-513	≥ 514
This study	**Siberian larch (Eurasia)**	**< 70**	**70-190**	**190-439**	**≥ 440**

3.8 Conclusion

The Landsat dNBR, dNDMI and dNDVI, accounting for different properties of the post-fire effects, were selected as the explanatory variables in the lag timing CART models to evaluate the different levels of burn severity. The results showed these differenced remote sensing indices can be used to detect retrospectively the effects of the fire disturbances. In slowly recovering ecosystems, the regeneration processes, which can obscure the burn severity estimates, might not strongly influence observation of the fire effects at different post-fire lag timings. In the first several years after the fire, the dNBR was the most important variable followed by the dNDMI and dNDVI. It is likely that the dNDMI is more important than the dNBR and the dNDVI for explaining the severity levels when the larch forest regrowth is dominant. This reveals the influence of the lag timing of an assessment. Even though our model has not fully validated for the entire Eurasian boreal region, the result of the model transferability to another independent fire as well as the proposed dNBR thresholds demonstrates the advantage of the model in providing a better understanding of severity levels patterns that can be helpful to the fire management practices and the post-fire forest resilience efforts, particularly in the Eurasian taiga-steppe transition ecoregion. In addition, the different CART models can be used to assess retrospectively the burn severity at the timing in which the pre- and post-fire images are available.

CHAPTER 4: REMOTE SENSING APPROACH TO DETECT POST-FIRE VEGETATION REGROWTH IN BOREAL LARCH FOREST

4.1 Preface

Chapter 4 is to address the second objective of developing the remote sensing method for the trajectory of temporal and spatial patterns of the post-fire larch forest regeneration. All sections of this chapter have been submitted in the journal Ecological Indicators as a research paper:

Chu, T., Guo, X. & Takeda, K. (2015) Remote sensing approach to detect post-fire vegetation regrowth in Siberian boreal larch forest. *Ecological Indicators (Submitted)*.

The paper has been accepted for the second revision. Thuan Chu performed the collection and analysis of remote sensing data and wrote the manuscript. Dr. Xulin Guo supervised the steps of data processing as well as the research progress. The field data (i.e. ground truth data of the post-fire forest patterns) for the validation and discussion of the results were collected by Dr. Kazuo Takeda. Both co-authors also provided comments and revised the manuscript.

4.2 Abstract

Remote sensing with time series data offers considerable potential in the trajectory of post-fire forest dynamics, beyond the monitoring of the current structural attributes of forests after fires. Many studies have addressed this topic by using time series of remote sensing indices. However, this approach has sometimes been demonstrated as an unrealistic and biased representation of the post-fire forest patterns due to the saturation issues of vegetation indices which then leads to an underestimation of the forest successional stages and an overestimation of the forest recovery rate. This paper aims to develop a framework for trajectory of the post-fire

forest patterns in the Siberian boreal larch forest *(Larix sibirica)* with the synergistic use of different remote sensing based vegetation-cover indicators derived from the Landsat time series and the WorldView-2 images. A time-series of the forest recovery index (FRI) and fractional vegetation cover (FVC) has been analyzed to estimate the rates of forest regeneration and vegetation recovery across different burn severity levels in the Siberian larch forest. The results showed that the FRI method can be used to observe the regrowth of the larch forest from the year 10^{th} after the fire overlapping with the period of significant increase in the sapling stem volume. The post-fire larch forest canopy can fully recover to the pre-fire condition with respect to the magnitude of the FRI values after 30-47 years where the highest regeneration rate was observed in the moderate burn severity areas followed by the low and high burn severity. On the other hand, the FVC method was positively correlated with burn severity and more sensitive for evaluating the early stages of the forest succession in which the FVC dramatically increases after 5-6 years from the fire. The significant growth of FVC was complement with the maximum emergence of the saplings' density as well as the rapid growth of herbaceous plants, grasses, shrubs, and shade-intolerant trees immediately after the fire, which could not evaluate using the FRI. Both time series of the FRI and the FVC are valuable tools for determining the dominant stages of the post-fire larch forest succession in order to understand the relationships between fire disturbance and natural cycles of the boreal larch forest.

4.3 Introduction

Even though the patterns of post-fire boreal forest recovery have been very well demonstrated from field surveys (e.g. Johnstone et al., 2004, Johnstone et al., 2011, Zyryanova et al., 2010a, Dorisuren, 2008, Cai et al., 2013), observations of the post-fire forest succession using remote sensing are limited due to data availability and data resolution. However, remote

sensing with time-series data offers considerable potential in the trajectory of post-fire forest dynamics as well as the classification of the successional stages. Many studies have demonstrated the capability of remote sensing tool for studying vegetation dynamics in which indices such as the NDVI, the soil adjusted vegetation index (SAVI), the normalized difference shortwave infrared index (NDSWIR), the enhanced vegetation index (EVI), the albedo, the NDVI-based net primary productivity (NPP), and the fraction of absorbed photosynthetically active radiation (fAPAR) were the most common indicators representing the recovery of vegetation after fire disturbance (e.g. Hicke et al., 2003, Epting and Verbyla, 2005, Jin et al., 2012, Tanase et al., 2011b, Cuevas-González et al., 2008, Cuevas Gonzalez et al., 2009, Jones et al., 2013, Yi et al., 2013). Monitoring the patterns of post-fire vegetation using these indices is site specific and varied substantially depending on the indices (Chu and Guo, 2013). Additionally, an assumption that an index such as the NDVI of vegetation recovery equates to forest stand recovery (e.g. larch and black spruce forests) may be inappropriate as an unrealistic and biased representation of the actual post-fire forest recovery, particularly in early stages of the forest successions (Frolking et al., 2009). Therefore, selection of remote sensing indices to study actual forest recovery of the pre-fire tree recruitments must be relevant and correlated with the ground measurements in order to evaluate accurately how a forest ecosystem responds to a fire disturbance as well as the influences of fire disturbance on carbon storage and other natural cycles within the ecosystem.

Many studies have been conducted to quantitatively measure the forest-regeneration patterns from remote sensing data. The most common approach is to scale pixels between the bare soil and the dense vegetation index values to determine the fractional vegetation cover (FVC), which is defined as the vertical projection areal proportion of the landscape occupied by

green vegetation (Gitelson et al., 2002). The vegetation indices (e.g. NDVI) and the spectral mixture analysis (SMA) are two common techniques to estimate the FVC (Yang et al., 2013, Veraverbeke et al., 2012b). Studies of the FVC to monitor the post-fire environment have shown the promising results of this technique (Solans Vila and Barbosa, 2010, Roder et al., 2007). However, the accuracy of FVC estimate mainly depends on selection of the endmembers such as the bare soil and dense vegetation pixels, the saturation effect of the vegetation indices such as NDVI at high leaf area index (LAI) levels as well as the seasonal, topographic and atmospheric effects on satellite imagery (Solans Vila and Barbosa, 2010, Yang et al., 2013). In recent times, the integrated forest z-score (IFZ) proposed by Huang et al. (2008) has been used to automatically reconstruct forest disturbance using the dense Landsat time series stacks in the vegetation change tracker (VCT) algorithm (Huang et al., 2009, Huang et al., 2010). Since the IFZ indicates the probability of the non-forest pixel becoming a forest pixel, its temporal changes can be an indicator for the evaluation of the post-fire forest recovery (Huang et al., 2009). To the best of our knowledge, very few studies used the IFZ to determine whether the post-fire disturbance regrowth occurred for a given forest stand (e.g. boreal forest), and if it did occur, when it started and how long it took to recover to the pre-fire condition. This can be used to estimate accurately stand age of post-fire forest. In addition to the FVC estimate, the IFZ measurement is expected to account for and separate different characteristics of the post-fire forest patterns in which both forest (e.g. *Larix sibirica*) and non-forest species (e.g. grasses, shrubs) recover together.

The aim of this chapter is to propose the synergistic approach of remote sensing based vegetation cover indicators in determining different stages of the post-fire forest successions in the Siberian boreal larch *(Larix sibirica)* forest. More specifically, the FVC and the forest

recovery index (FRI) derived from the Landsat time-series and the WorldView-2 images were used to evaluate the temporal and spatial patterns of the post-fire forest regrowth under different burn severity effects. Since the integrated forest z-score (IFZ) has been originally designed for reconstructing the forest disturbance history by indicating how the forest pixels turn to non-forest pixels (Huang et al., 2009), we hypothesize that the forest recovery index (FRI) defined as the reciprocal of the IFZ values will track the recovery rate of the burned area to become pre-fire condition. We hypothesized that the FVC method can be used to monitor the early stages of post-fire forest succession while the FRI method can account for delaying of the forest species recruitments after the fire, and it can be used to monitor late recovery stages of the post-fire larch forest to pre-fire conditions. We evaluated the effectiveness and discussed any problems and challenges of these remote sensing indices in comparison with our field measurements and other studies in the boreal regions.

4.4 Materials and Methods

4.4.1 Study area

The burned area in 1996 located in Hovsgol province was selected to be the study models of post-fire forest recovery and successional stages (Figure 4.1). This is similar to the burned area for the assessment of the burn severity conducted in the previous chapter (see Chapter 3).

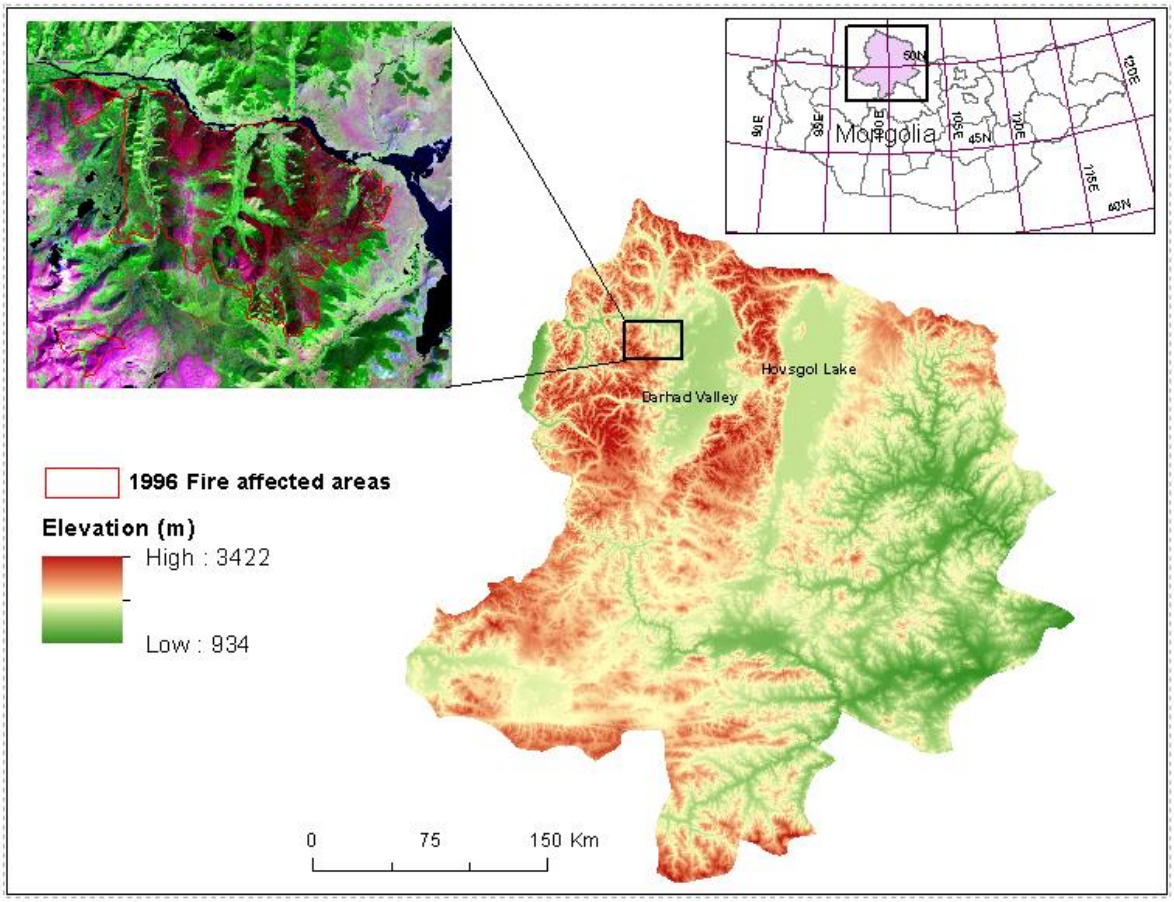

Figure 4.1 Location of the study area.

4.4.2 Overall processing flow

The processing flow (Figure 4.2) of this study contains steps of image selection, preprocessing, calculation and analysis of the FVC and the FRI derived from the IFZ, and the trajectory based approach of FVC and FRI representing the temporal and spatial patterns of the post-fire forest recovery. We used the Landsat imagery (http://glovis.usgs.gov/) as a primary product for the trajectory of post-fire forest patterns in the 1996 burned area.

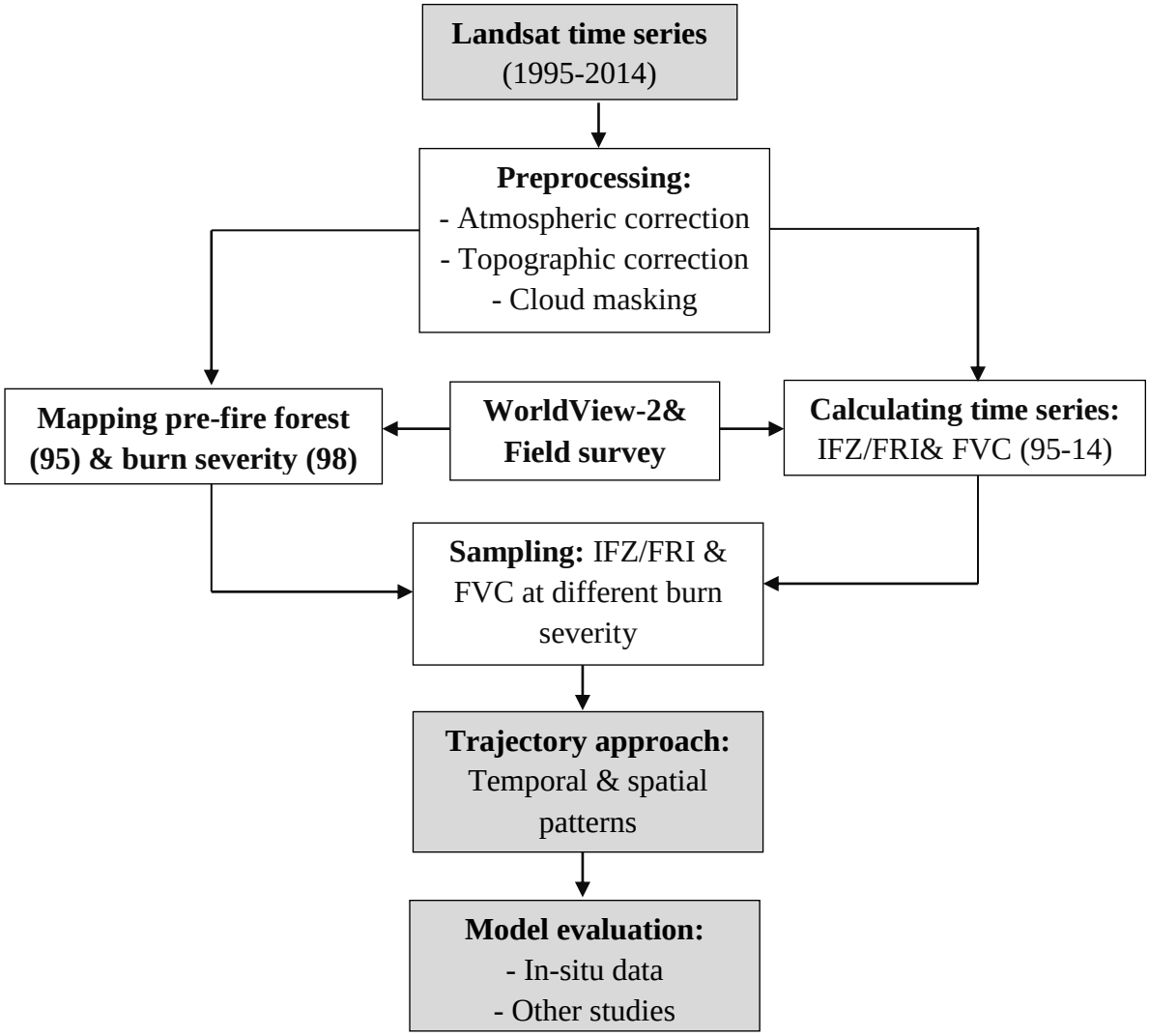

Figure 4.2 Overall processing flow for tracking the temporal and spatial patterns of post-fire forest regrowth in the Siberian larch (Larix sibirica) forest.

4.4.3 Datasets and pre-processing

We used similar Landsat dataset which was acquired for the assessment of burn severity in Chapter 3 for the objectives of this chapter (Table 4.1). Because the analysis of temporal pattern of the forest recovery were based on sampling plots, images with partially clouded cover on the burned area were still included (e.g. 2008, 2010, 2011 images) using sampling points outside the cloud masks. However, these high cloud cover images were excluded in the spatial analysis of the post-fire forest patterns (see Section 4.4.6). Even though some of the Landsat

ETM+ images acquired after 2003 contain some gaps due to the Scan Line Corrector (SLC) failure, burn scars in this study were outside the failure lines. The Landsat TM acquired in June 1995 was selected as the pre-fire image.

In addition to Landsat data, we used the 50 cm WorldView-2 panchromatic image (Base map source: ESRI Inc.; DigitalGlobe) acquired on 21 August 2010 and our field observation in 2008 and 2011 to develop a training dataset for the calculation of the FVC and the FRI as well as to evaluate the estimation of the forest regrowth based on these indices. In the field observation, we only investigated very few plots with the measurement of seedlings, saplings, mother trees in each plot. These field data were used to compare and discuss the results from the remotely sensed observations in this study.

Table 4.1 Time-series Landsat images for assessing post-fire recovery of Siberian larch forest in the 1996 burned area in northern Mongolia

No images in 1997, 2006, and 2012 were found for the study area. All images are in the same path 137 and row 24.

ID	Acquisition date	Sensor	Year since fire
1	30/6/1995	TM	Pre-fire
2	25/8/1998	TM	2
3	5/9/1999	ETM+	3
4	29/7/2000	TM	4
5	16/7/2001	TM	5
6	19/7/2002	TM	6
7	6/7/2003	TM	7
8	16/7/2004	ETM+	8
9	4/8/2005	ETM+	9
10	9/7/2007	ETM+	11
11	12/8/2008	ETM+	12
12	6/7/2009	TM	13
13	25/7/2010	TM	14
14	12/7/2011	TM	15
15	3/9/2013	OLI	17
16	12/7/2014	ETM+	18

In a time series of remote sensing data the atmospheric conditions, the illumunation angles and sensor calibration of each image may not be comparable. In order to extract the comparable reflectance values for temporal analysis, radiometric, atmospheric and topographic corrections were applied for the collected Landsat time series. The details of the pre-processing method of the satellite dataset can be found in Chapter 3 (section 3.5.2).

4.4.4 Calculation of FVC and FRI time series

We used both the FVC and FRI, whencombined, they should be able to highlight the changes in green vegetation abundance in the early successional stages and an indicator of the forest formation after fire. The time-series analysis of FVC and FRI was conducted to estimate both the temporal and spatial patterns of forest recovery.

4.4.4.1. Fractional vegetation cover (FVC)

Many studies have demonstrated that the FVC has a linear relationship with the NDVI (Eq. 4.1), showing a continuous scale from 0% (bare soil) to 100% (pure green vegetation) (Gitelson et al., 2002, Carlson and Ripley, 1997, Wittich and Hansing, 1995, Yang et al., 2013).

$$\text{FVC} = \frac{NDVI - NDVI_s}{NDVI_v - NDVI_s} \qquad (4.1)$$

where NDVI is given by: NDVI = $\frac{\rho_{nir} - \rho_{red}}{\rho_{nir} - \rho_{red}}$; ρ_{nir} and ρ_{red} are corrected reflectance obtained from the sensor bands located in the near infrared (NIR) and the red spectral regions for each pixel within an image (Namzalov et al., 2012). The $NDVI_s$ and $NDVI_v$ are values of the NDVI for bare soil (FVC=0) and pure green vegetation (FVC=1) within an image, respectively.

The primary problem when applying Eq. (4.1) is how to accurately estimate the $NDVI_s$ and $NDVI_v$ values on the Landsat imagery. In this study, the confident pure green vegetation and

the bare soil pixels were delineated using the WorldView-2 image in combination with our field observations and the stability of the spectral and spatial patterns of the pure green forest and bare soil patches close to the burned area throughout the time series data. Because the WorldView-2 image was acquired in 2010, the visual interpretation within the time series Landsat data and WorldView-2 image is necessary to confirm the unchanged-known pure green vegetation and bare soil patches on the images acquired prior to or after 2010 (Figure 4.3). The training samples within these known patches of pure green forest and bare soil were extracted for each year to calculate the $NDVI_s$ and the $NDVI_v$. In addition to the WorldView-2 image, some known forest areas were also located based on our field observations in 2008 and 2011. Consequently, a time series of FVC between 1995 and 2014 was derived for the study area in order to track the temporal and spatial patterns of the post-fire forest recovery.

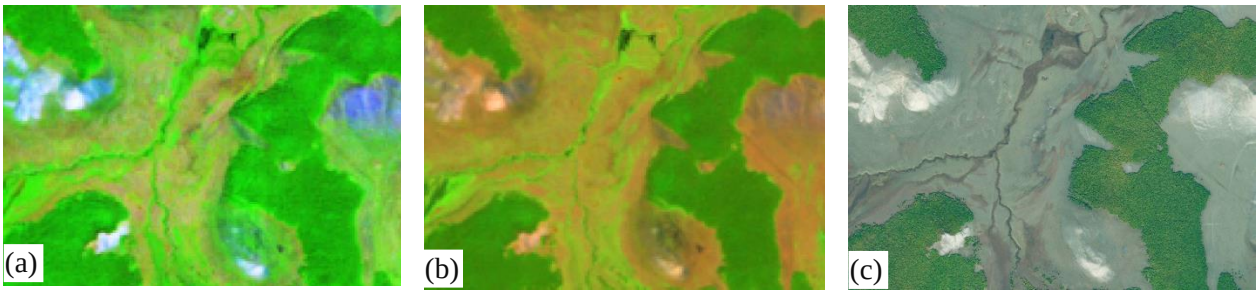

Figure 4.3 An example of bare soil and pure green larch forest patches on the time series data of (a) 1998 Landsat TM, (b) 2009 Landsat TM, and (c) 2010 WorldView-2 image.

4.4.4.2. Integrated forest-z score (IFZ) and forest recovery index (FRI)

In the chapter 3, we illustrated how to derive the IFZ from Landsat data. Similar to the calculation of the FVC, the identified forest samples (e.g. Figure 4.3) were used to calculate a number of indices that are indicative of a forest pixel (Huang et al., 2009). Because the purpose of this study was to monitor and predict how the larch forest recovers from different burn severity, we proposed the FRI defined as the reciprocal of the IFZ (Eq. 4.2). Both the FVC and the FRI variables were expected to have an increase trend in the years after fire, showing the rate

of the post-fire forest regeneration (Figure 4.4), and it was also calculated for all the images in the Landsat time series (1995-2014) based on the known forest samples (Figure 4.3).

$$FRI = \frac{1}{IFZ} \quad (4.2)$$ where IFZ is the integrated forest z-score estimated using Eq. (3.1).

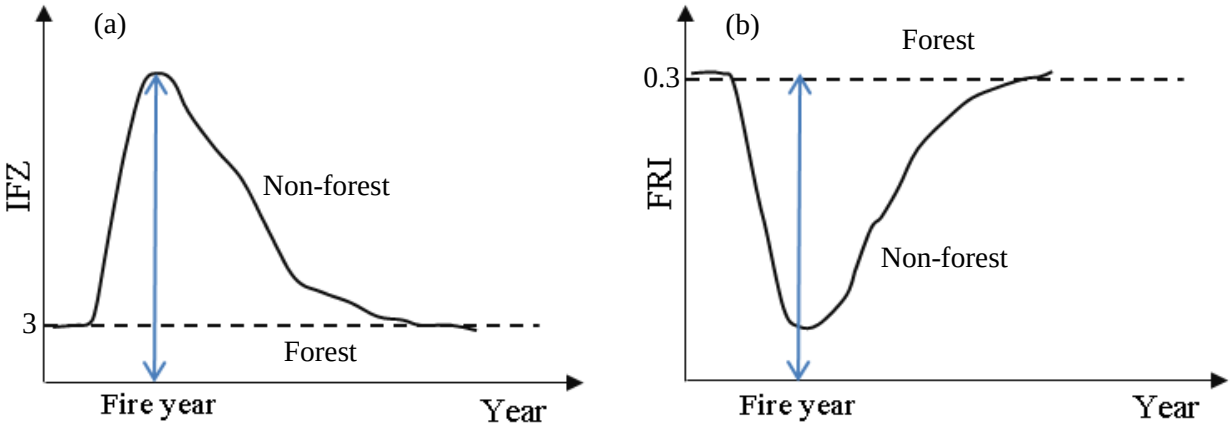

Figure 4.4 Temporal profiles of the integrated forest z-score (IFZ) (a) and forest recovery index (FRI) (b) of burned area.

The dash line indicates the threshold of the forest and non-forest values (Modified from (Huang et al., 2009)).If the IFZ value less than 3 is classified as forest pixel, the FRI value greater than 0.3 will be selected as the threshold for theregenerated forest pixel.

4.4.5 Mapping pre-fire forest and post-fire burn severity

Pre-fire land cover type is one of the important factors that influences post-fire forest recovery (Lozano et al., 2012, Leon et al., 2012). Stratification of the different pre-fire land cover types prior to the assessment of the post-fire effects is thus necessary. The pre-fire land cover in this study was classified into the larch dominated forest (*Larix sibirica*) and other vegetations using the integrated forest z-score (IFZ) of the pre-fire image as shown in the chapter 3 and section 4.4.4.2 of this chapter. The threshold of IFZ values less than 3 was selected to locate the forest pixels in the pre-fire Landsat TM image acquired in 1995. In this study, we

focused on sampling and analyzing the forest patterns within the boreal larch dominated forest of the 1996 burned area.

Burn severity, defined as the degree of ecosystem change due to fire disturbances(Key and Benson, 2006, Lentile et al., 2006), is another significant driver of the post-fire forest regeneration (French et al., 2008). Three discrete levels of low, moderate, and high burn severity were mapped using the thresholds of the dNBR proposed in our mapping burn severity algorithm for the study area (see Chapter 3).

4.4.6 Sampling and statistical analysis

Training samples of the FVC and FRI time series (1995-2014) were selected to evaluate the temporal patterns of forest recovery. In attempt to keep the samples equal and fully randomized among the severity classes of the burned larch forest, we used a stratified random design to create about 150 samples per burn severity level. For each sample location, the FVC and FRI values were extracted on a per pixel basis using the bilinear interpolation method. The mean values of the FVC and FRI were then derived for each severity level in each observed year between 1995 and 2014 for the trajectory of the temporal changes of the post-fire forest. The samples within the unburned larch forest were used as the controled data to compare with the burned area. Finally, the polynomial and logarithmic models were used to simulate the temporal patterns of forest recovery.

In terms of spatiotemporal patterns of the forest recovery, the pixel-wise linear regression approach was applied to detect the trend and rate of the post-fire forest recovery. Only time period (or images) showing an increasing trend in the temporal trajectory of the forest regeneration was selected to evaluate the spatial patterns in which the slope coefficient of the linear regression indicated the rate of change while its p-value revealed whether the trend was

statistically significant. Specifically, the area with significantly positive slope values was marked as the increase trend of forest cover. In contrast, the area with significantly negative slope values was identified as the decrease trend of forest cover. Throughout the paper, the terms FVC slope and FRI slope were used interchangeably with recovery rate to refer to the annual post-fire change in the fractional vegetation cover and the forest recruitment using the time series FVC, FRI and least squares regression. Statistical analysis of both the temporal and spatial patterns was conducted using the R and Matlab codes (R Team, 2008, MathWorks, 2008).

4.5 Results

4.5.1 Time series of FVC and FRI

The results of reconstructing the FVC and FRI time series are shown in Table 4.2, Figure 4.5, Table 4.3 and Figure 4.6.

Table 4.2 The values of NDVIs and NDVIv for all images analyzed in this study to derive FVC time series

Year	95	98	99	00	01	02	03	04	05	07	08	09	10	11	13	14
$NDVI_s$	0.09	0.10	0.12	0.07	0.07	0.07	0.07	0.05	0.08	0.08	0.06	0.05	0.05	0.10	0.05	0.08
$NDVI_v$	0.67	0.68	0.75	0.67	0.60	0.65	0.64	0.66	0.65	0.66	0.65	0.66	0.65	0.65	0.63	0.67

Compared with the pre-fire (1995) image, the fractional vegetation cover decreased dramatically after the fire in 1996 and then gradually increased in the years following the fire (Figure 4.5). These changes in the FVC based vegetation cover were visually observable on the post-fire FVC maps.

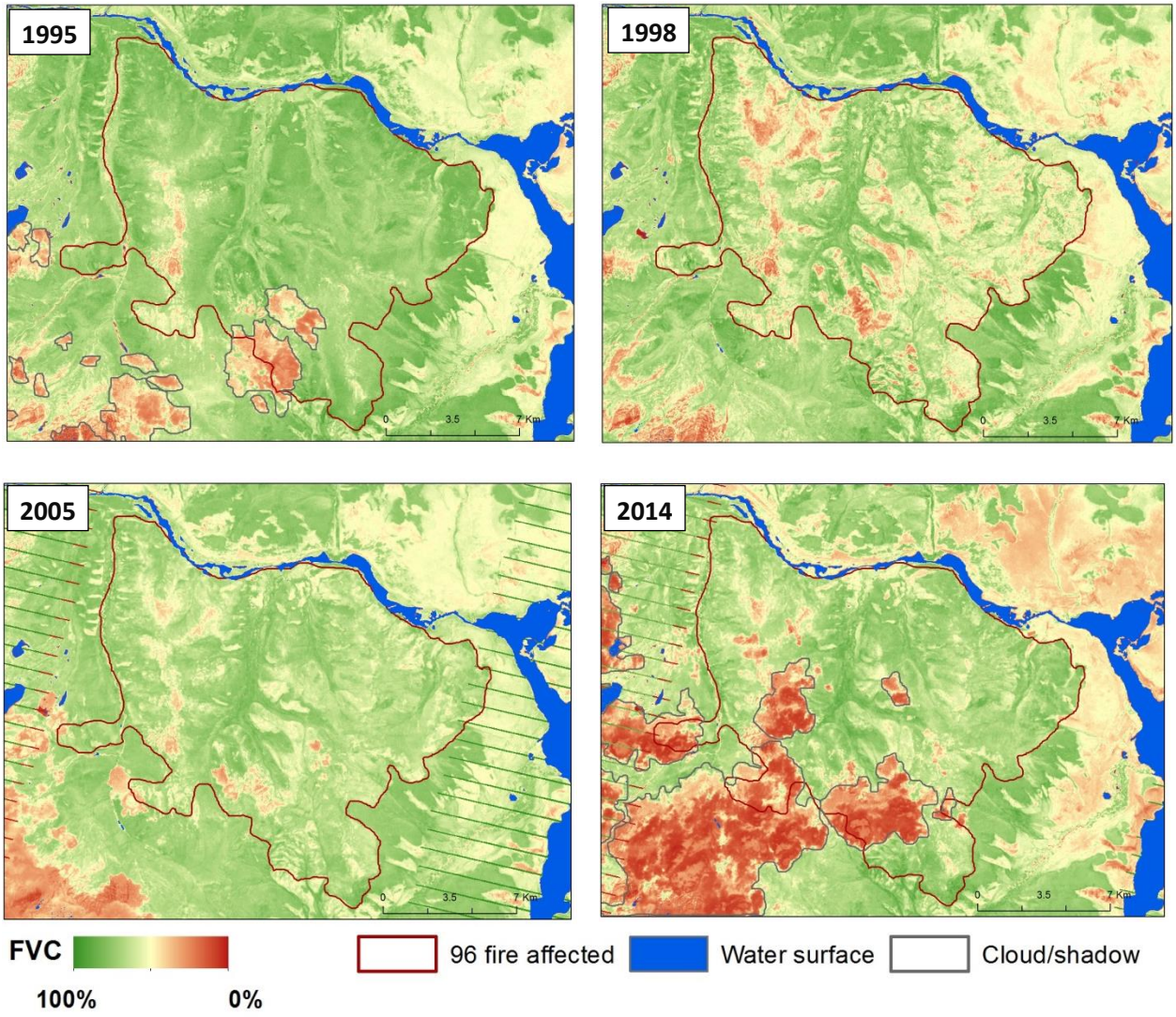

Figure 4.5 Examples of estimation of fractional vegetation cover (FVC) based on NDVIs and NDVIv, showing on pre-fire image (1995) and post-fire images (1998, 2005, and 2014).

Table 4.3 Mean and standard deviation of three Landsat bands.
Red (630-690 nm), SWIR1 – Short Wave Infrared 1 (1550-1750 nm), and SWIR2 – Short Wave Infrared 2 (2080-2350 nm) of known forest pixels, used to calculate forest recovery index (FRI).

Year	$\overline{b_{red}}$	SD_{red}	$\overline{b_{SWIR1}}$	SD_{SWIR1}	$\overline{b_{SWIR2}}$	SD_{SWIR2}
1995	5.80	0.25	12.01	0.68	6.16	0.55
1998	5.86	0.38	12.99	0.83	6.93	0.65
1999	5.70	0.45	13.28	0.89	7.89	0.77
2000	5.96	0.32	12.78	0.72	6.89	0.61
2001	6.24	0.26	13.02	0.76	7.38	0.57
2002	6.23	0.35	12.18	0.90	6.79	0.66
2003	6.08	0.27	12.87	0.84	7.16	0.64
2004	6.20	0.30	12.26	0.73	6.77	0.55
2005	6.01	0.26	12.85	0.70	6.98	0.55
2007	6.25	0.48	12.02	0.69	6.60	0.50
2008	6.44	0.32	13.15	0.68	7.17	0.49
2009	6.06	0.29	12.30	0.71	6.54	0.49
2010	5.83	0.39	12.06	0.68	6.35	0.60
2011	5.98	0.21	12.03	0.60	6.15	0.43
2013	6.08	0.45	13.45	0.78	7.26	0.50
2014	6.05	0.31	13.04	0.59	6.93	0.46

Because the FRI measures the likelihood of a pixel being a forest pixel, its values should change in response to the forest changes. Figure 4.6 shows the major land cover changes from forest to non-forest land, representing darker green to lighter green pixels respectively in response to the fire disturbance. A sequence of the gradually increasing FRI values following that disturbance (Figure 4.4b) represents the regeneration of a new forest stand. However, the process of the forest regeneration observed by the FRI maps (Figure 4.6) was not clear as the observation of the vegetation recovery using the FVC maps (Figure 4.5). This might suggest the low recovery rate of the *Larix sibirica* species in the study area that could not be visually observed using the FRI method. On the other hand, the FVC method could visually interpret the increase of post-fire vegetation cover that is often complement with the rapid regrowth of shrubs, grasses, and fire weeds after fires.

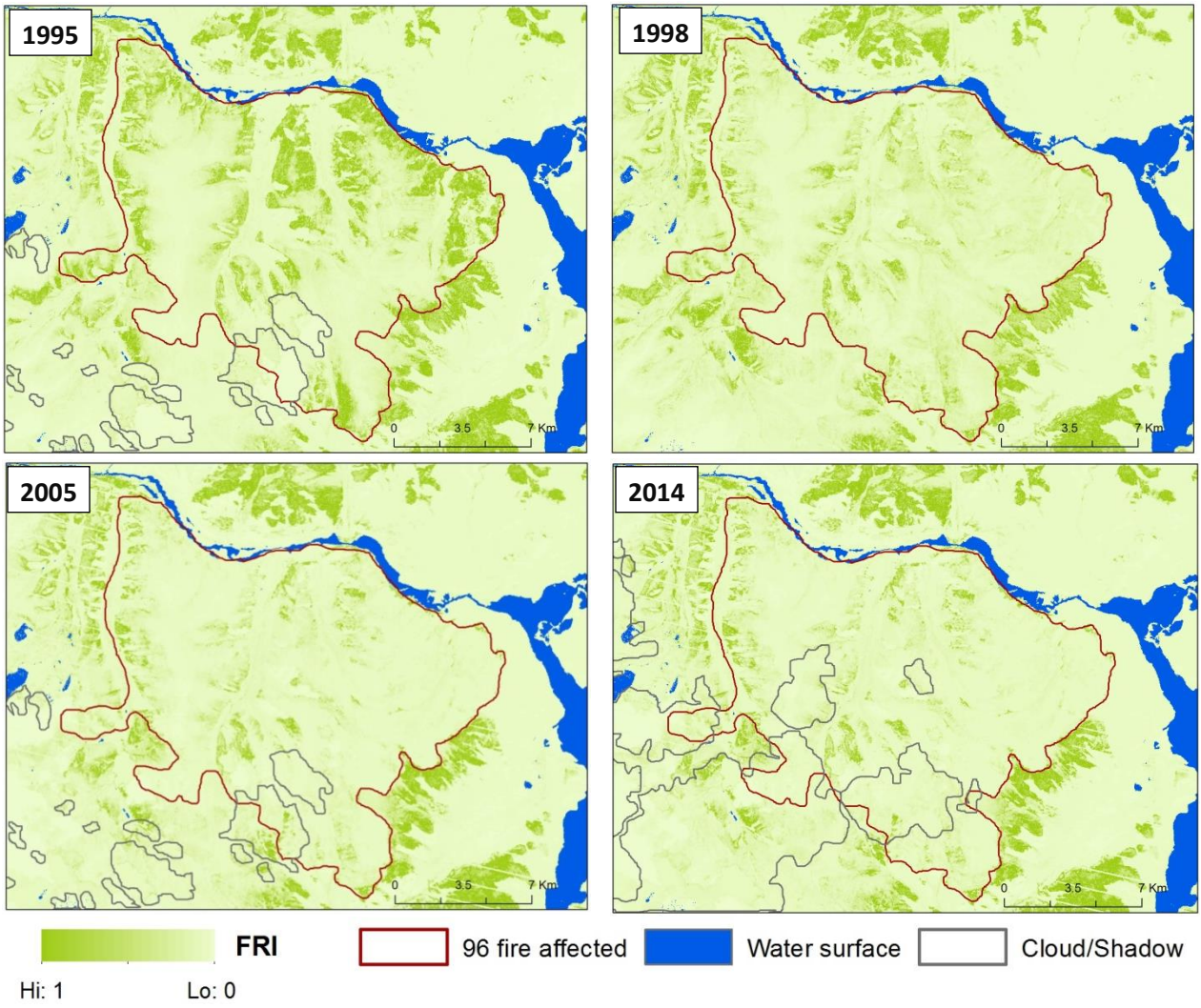

Figure 4.6 Examples of forest recovery index (FRI) maps derived from the integrated forest z-score using pre-fire image (1995) and post-fire images (1998, 2005, and 2014).

4.5.2 Pre-fire land cover and post-fire burn severity

The pre-fire land cover in 1995 and post-fire burn severity mapped in 1998 are illustrated in figure 4.7. These two maps were used to extract the FVC and FRI samples for tracking the temporal patterns of the Siberian larch forest (*Larix sibirica*) at different burn severity levels. Because the pre-fire larch forest was extracted using the IFZ, the high FRI values shown in the 1995 pre-fire FRI image (Figure 4.6) were found in the extracted larch forest areas (Figure 4.7).

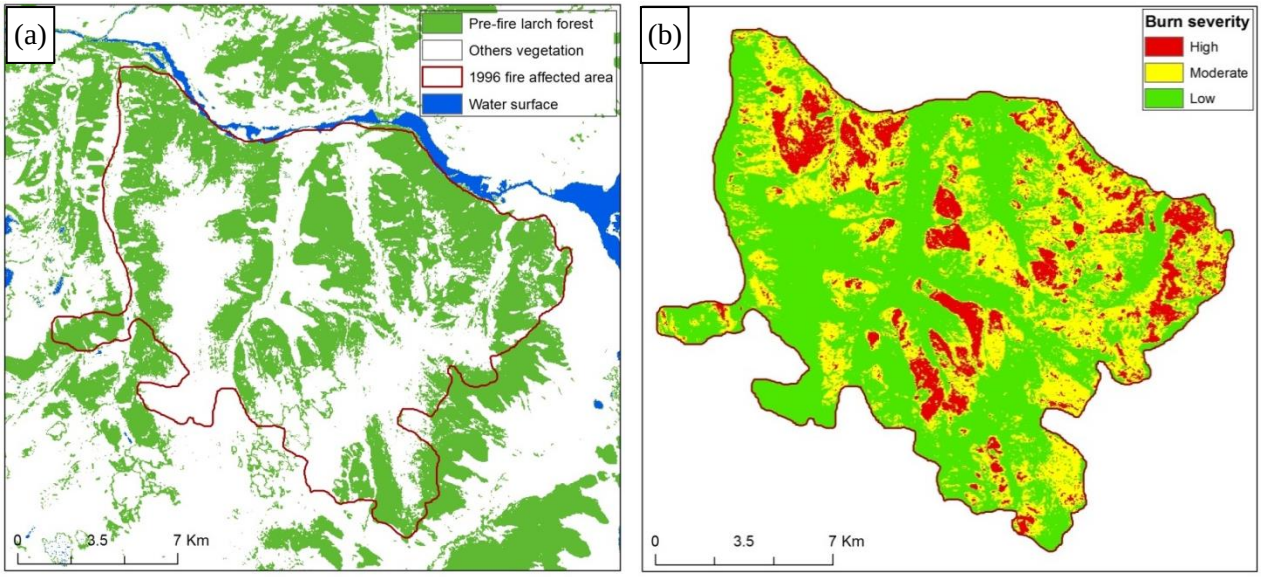

Figure 4.7 Classification of pre-fire land covers using 1995 integrated forest z-score (a) and the severity map of 1996 burned area (b).

4.5.3 Temporal pattern of post-fire forest recovery

Nineteen years of temporal profiles of the FVC and FRI were extracted at different burn severity levels (Figure 4.8 & 4.9). The unburned profile was selected as the controled profile to compare with the burn sites. Both the FVC and FRI decreased significantly after the fire disturbance (year 0). The FVC profiles showed a dramatic increase after 5 years of the disturbance suggest that the burned area was covered quickly by the green vegetation (i.e. grass, shrub and fire weed) after the fire. On the other hand, the FRI profiles were likely showing a decreasing trend in several years following the fire and then slightly increasing from year 10th after the fire, particularly in the moderate burn severity sites (Figure 4.9). As it was noted in the visual interpretation of post-fire FVC and FRI maps, these temporal patterns of the FVC and FRI suggest the capability of the FVC method to capture the regrowth of all the vegetation types (e.g. shrubs, grasses, fire weeds, and larix's seedlings) in the early stage of the post-fire forest succession, while the FRI might represent either the delay of the post-fire vegetation mortality

and the slow rate of forest regeneration, or the later stages of the larch forest succession such as young or mature larch forest.

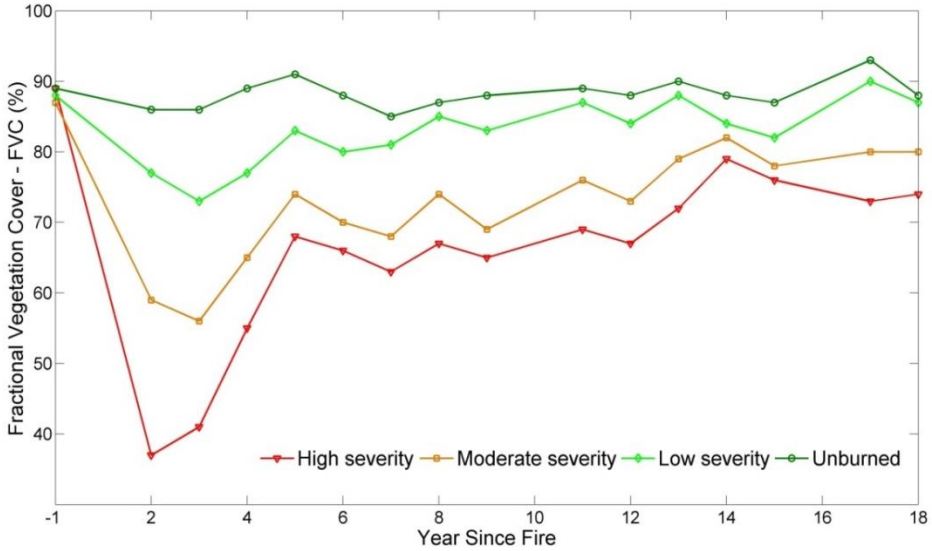

Figure 4.8 Temporal trajectory of the post-fire forest recovery defined by the fractional vegetation cover (FVC) at different burn severity levels.

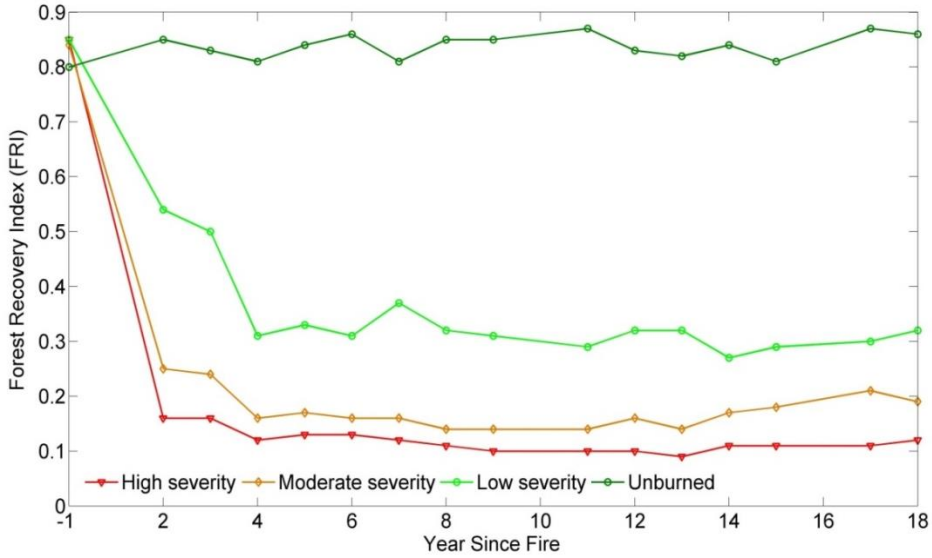

Figure 4.9 Temporal trajectory of post-fire forest recovery defined by forest recovery index (FRI) at different burn severity levels.

In order to understand clearly the temporal trend of the post-fire vegetation regrowth, the temporally observed FVC and FRI samples after the fire disturbance were fitted using the logarithmic and polynomial models respectively (Figure 4.10 & 4.11).

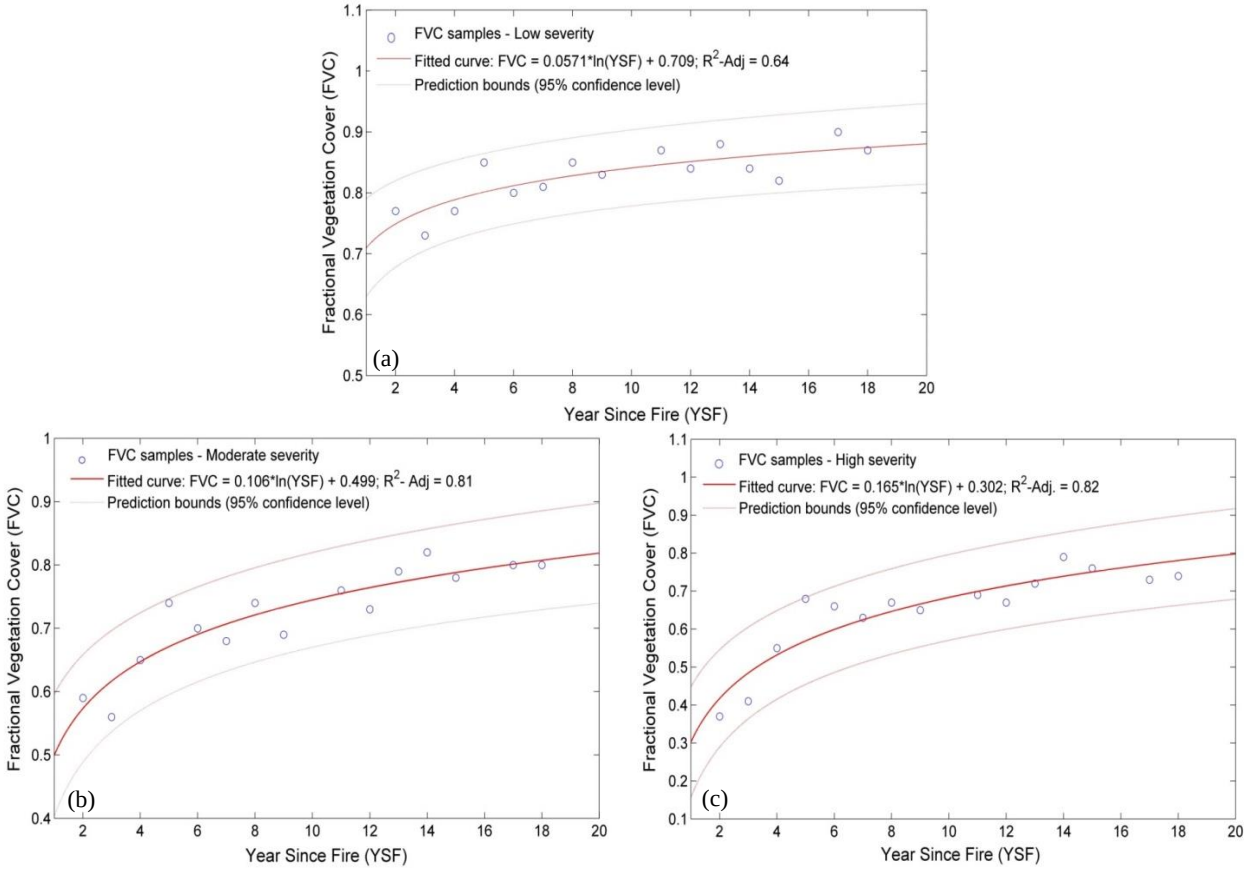

Figure 4.10 Relationship between fractional vegetation cover (FVC) and year since fire (YSF) at different burn severity levels of low (a), moderate (b), and high (c) severity.

The temporal trend of the FVC showed the highest recovery rate of post-fire vegetation, with respect to the slope coefficient of the logarithmic model, at high burn severity site, followed by moderate and low severity (Figure 4.10). Since the FVC measures the porportion of land surface covered by the pure green vegetation, it is not necessary to represent the burned area occupied by pre-fire tree recruitments (e.g. *Larix sibirica*) only. The pure green vegetation which recovered quickly after the fire can be shrubs, grasses, and broadleafs that are often dominant species following the fire.

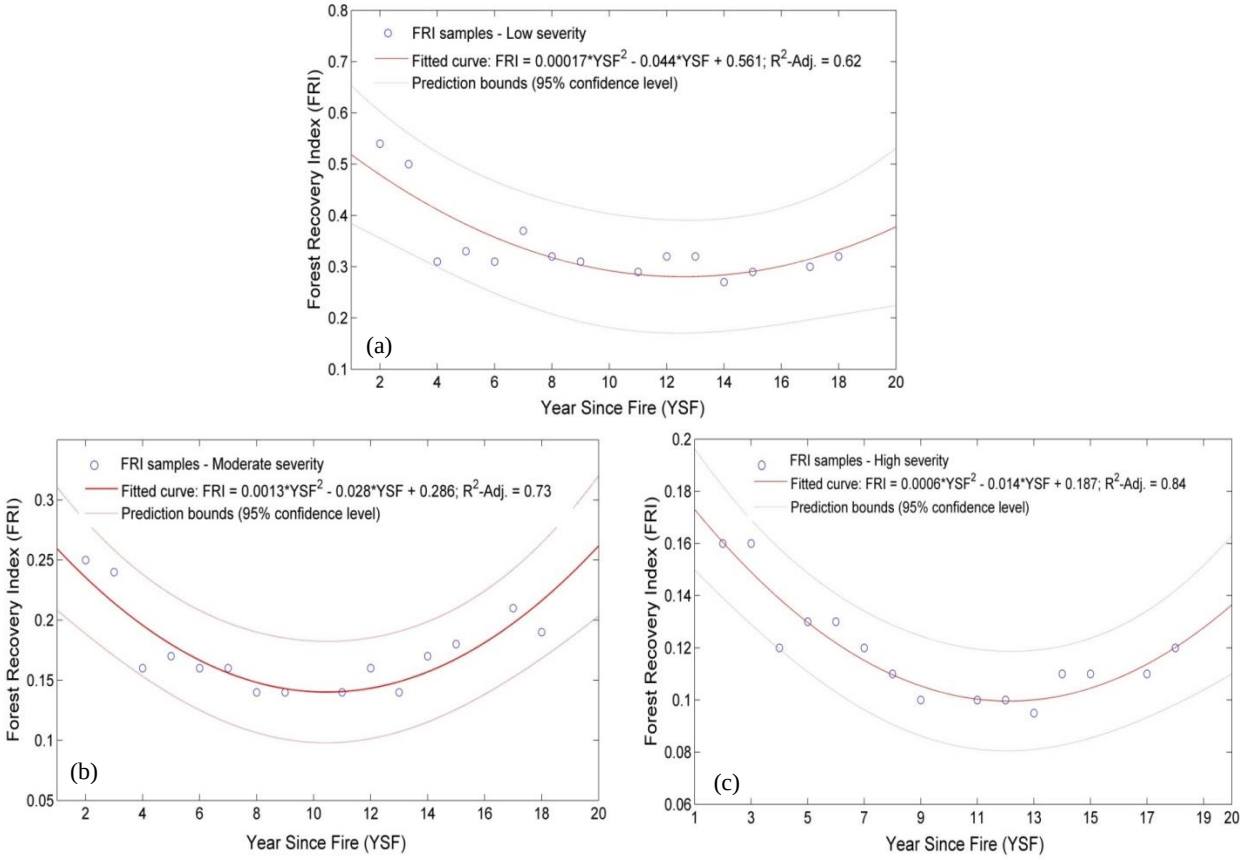

Figure 4.11 Relationship and prediction of forest recovery index (FRI) by year since fire (YSF) at different burn severity levels of low (a), moderate (b), and high (c) severity.

The post-fire FRI showed significantly decreasing trend in the first several years after the fire and then increased significantly from about year 10th after fire in both moderate and high severity sites (Figure 4.11b & 4.11c). The regrowth trend started later in the low burn severity (Figure 4.11a). Since the FRI indicates the movement of the non-forest pixel to become forest pixel, as it was expected, the increasing trend of the FRI at all severity levels suggests the capability of FRI in monitoring the post-fire forest recruitment (Figure 4.4) while the decrease trend might reflect the continuous delay in the post-fire tree mortality. It is noteworthy to mention that the regeneration process of the larch forest might happen in the first 10 years after the fire. However, the regrowth of the larch forest defined by the FRI is likely measured only

from year 10th after fire, particularly in moderate and high severity burns. In the low severity burn, only under storeys areaffected by surface fires. Therefore, the observation of post-fire forest regeneration using the remote sensing indices was affected by high density of alive standing trees of overstorey. As a result, the value of the FRI in low severity burn was much higher than that of the moderate and high burns, but the increasing started later as it also reflects the unburned mature overstorey forest.

4.5.4 Spatiotemporal pattern of post-fire forest recovery

4.5.4.1. FVC based spatiotemporal pattern

The estimated post-fire recovery rate defined by the FVC slopes for the study area is shown in Figure 4.12. The analysis of the pixel-wise linear regression between the FVC and year since fire also resulted in the p-value map, indicating whether the slope coefficient of the FVC fitted line in each pixel location is significant. Three classes of the significant increase trend, significant decrease trend and no change of vegetation regrowth patterns were derived from the combination of p-value map and FVC slope map (Figure 4.13).

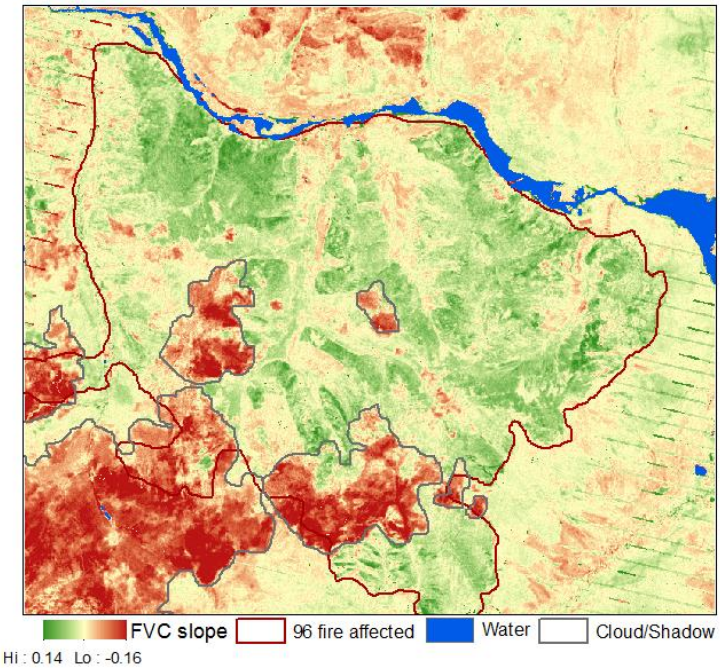

Figure 4.12 Spatiotemporal trajectory of the FVC based forest recovery illustrated by the slope coefficient (FVC slope) of the fitted linear regression between the FVC values and year since fire.

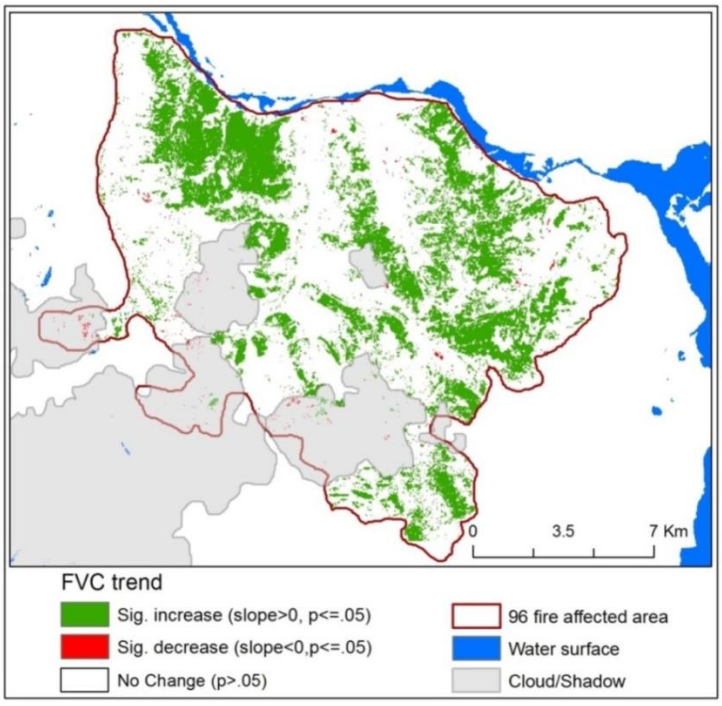

Figure 4.13 Spatiotemporal patterns of the FVC based forest recovery.

23.8% of the burned area showed significantly positive changes in the fractional vegetation cover, while 75.8% of the burned area was unchanged in vegetation cover after the fire. Up to 70% of the unchanged areas were located in the low severity burn sites. There was only 0.4% of the burned area with significantly negative trend. Annual positve changes in the post-fire FVC slope ranged from 0 to 0.13, representing about 2% annual increase in the mean annual vegetation cover.

4.5.4.2. FRI based spatiotemporal patterns

Similarly, the spatiotemporal pattern of the forest recovery with respect to the magnitude of the FRI change was derived using the most cloud-free FRI images (2005, 2007, 2009, and 2014) acquired after the fire in which an increase trend of the FRI was observed from the temporal analysis (see Figure 4.9 & 4.11). The results showed in figure 4.14 & 4.15.

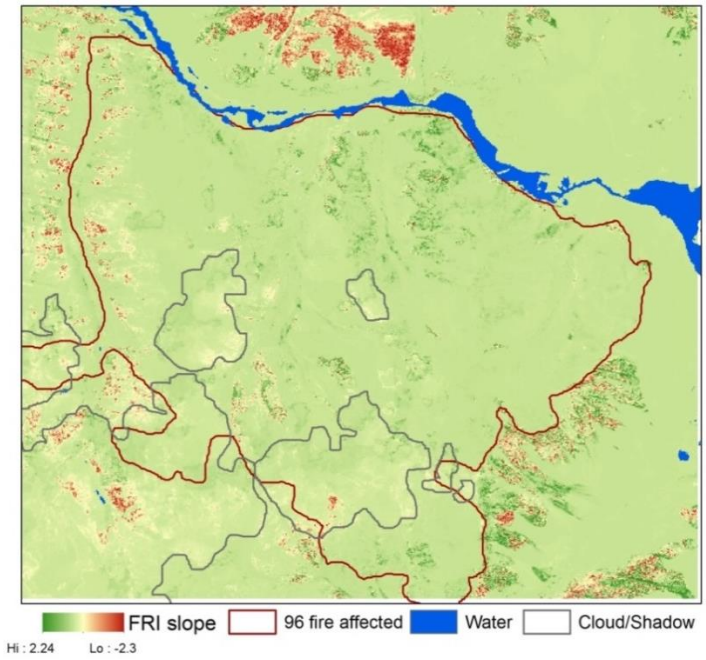

Figure 4.14 Spatiotemporal trajectory of the FRI based forest recovery illustrated by the slope coefficient (FRI slope) of the fitted linear regression between the FRI values and the year since fire.

There were 10% of the burned area with significant increase of the FRI values. The proportion of the burned area with significantly decrease and unchanged trend of the FRI values was 4% and 86% respectively. Similar to vegetation recovery measured by FVC, these negative and unchanged slopes of the FRI were commonly found in the sites with low burn severity, and some areas were particularly located in the high severity sites.

There is merit in mentioning that the unchanged areas measured by the FRI might still exist the regeneration process of the larch forest. However, the degree of forest regeneration was not significant enough to be observed by the remote sensing index such as the FRI. This suggests the limitation of the FRI in monitoring the early stages of forest regeneration, including seedlings, sapling, and young trees.

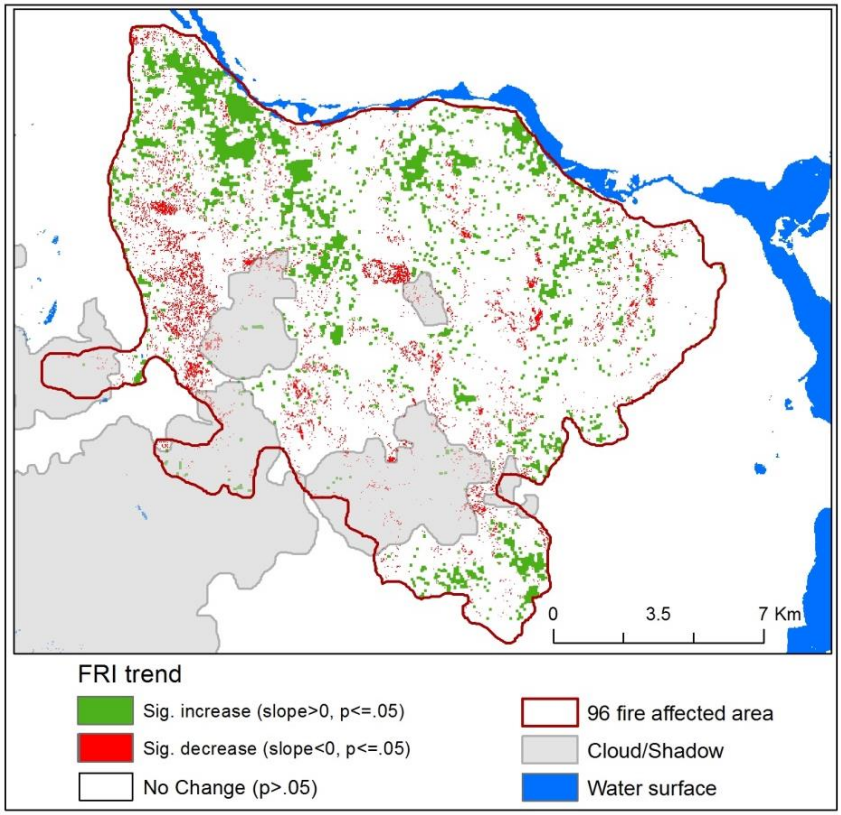

Figure 4.15 Spatiotemporal patterns of FRI based forest recovery.

The area with significant increases of the FRI values indicates the movement of the non-forest pixel to become forest pixels. Compared with the spatial patterns of the FVC that showed the percentage of all vegetation types occupied the burned area, almost all the areas with significant FRI increase were within the moderate and high burn severity sites and the areas with significant increase of the FVC values (Figure 4.13). On the other hand, the significant decrease areas of FRI were likely located in the sites with low burn severity and insignificant change of FVC.

4.6 Discussion

4.6.1 Potential use of the FVC and FRI methods to monitor different stages of post-fire forest succession

The two methods used in this study, the FVC and FRI, yielded different results in the post-fire forest dynamics over time. The FVC accounted for the amount of green vegetation distributed on an unit of land surface and it was not used to distinguish the different vegetation communities in this study, while the FRI was used to not only separate the forest and non-forest pixels but also to measure trees growth (Figure 4.4). Therefore, the difference in results of the post-fire forest regeneration using the FVC and FRI methods was expected to reveal different properties of the post-fire forest patterns as well as the successional stages and pathways (Figure 4.16).

Even though our field data were insufficient to match with the time-series remote sensing data for quantitative analysis, the findings of FVC and FRI based the spatiotemporal patterns of the post-fire larch forest were consistent with the field based observations. By doing the tree ring analysis of the saplings of several plots at different burn severity in our study area, it was revealed that the saplings of the dominant tree species *(Larix sibirica)* emerged and reached the maximum density in year 6^{th} after fire at all severity classes. This is similar to the turning up

period of the FVC values in the first 6 years after fire (Figure 4.8 & 4.10). However, it is worth mentioning that the significant increase of the FVC in several years after the fire might also reflect the regrowth of other post-fire dominant species such as grasses, shrubs and broadleaf trees commonly found in the early stage of the forest succession. For example, in the long term observations after fire based on permanent plots of pseudotaiga larch forests in Mongolia, Dorisuren (2008) found that the initial recovery phases following directly after fires were found to be connected to the rapid colonization of the herbaceous plants (e.g. *Corydalis sibirica, Chamaenerion angustifolium*) and then the stage of herbs-grasses community (e.g. *Marshantia polymorpha – Corydalis sibirica*) which lasted about 5 years after fire. From year 6 the larch forest already started to develop cereal stages of succession which lasted about 15 to 20 years. These mixed vegetation communities are able to recover quickly after fires, explaining the area of positive change in the FVC that was much higher than the area of negative change (Figure 4.13 & 4.16).

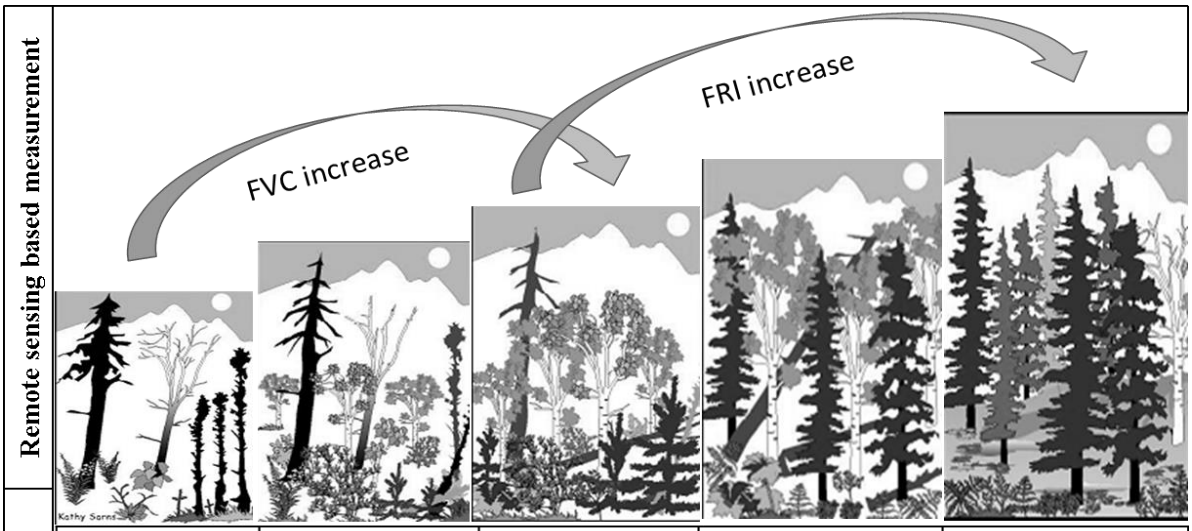

Field based based measurement	Herb Stage (0–5 years)	Grass–Shrub Stage (5–15 years)	Young Forest Stage (15–50 years)	Mature Forest Stage (50–100 years)	Climax Forest Stage (>100 years)
	Fire has burned the forest, illustrating "black burnt" spots. Herbaceous plants (wildflowers, grasses, sedges) may grow from seeds and sprout from unburned roots and stumps. Dead and living trees of pre-fire forest may still be standing.	Herb-moss association disappeared. Shrubs and tree seedlings of hardwoods and larch species become more widespread and abundant and begin shading the grasses and other small plants. Plant species composition of the ground vegetation recovers to the pre-fire level of plant diversity.	Sapling trees of larch begin growing faster among the hardwoods. The forest canopy has become more dense, shading the forest floor. Birch and larch trees overtop the shrubs. At the end of this stage, pre-fire dominant species become common in the storeys. Most tree snags have fallen.	Mature hardwood trees become less abundant, opening the canopy for larch forest to grow taller. Hardwoods, shrubs, herbs, mosses and lichens also grow in the openings. This is the final restoration stage of pre-fire plant species composition and cover percentage of the species.	The forest is mostly occupied by larch trees. Hardwoods, shrubs, herbs, mosses and lichens might still grow in the openings.

Figure 4.16 Post-fire forest successional stages of Siberian larch forest and the sensitivity of the remote sensing based FVC and FRI methods.
(Modified from (Zyryanova et al., 2010a, Dorisuren, 2008, Takeda et al., 2013, Taki et al., 2013,USFWS, 2003). Picture credit USFWS (2003).

On the other hand, the FRI seems to be less sensitive with either the dominant tree recruitment or the non-forest species recovery in the first several years after the fire. Compared with our field estimates and other field-based knowledge of experts (e.g. (Dorisuren, 2008, Zyryanova et al., 2010a) (Figure 4.16), the increase trend of the FRI from year 10th overlapped with the significant increase of sapling stem volume of *Larix sibirica*, particularly in the moderate burn severity site in which the increase of the stem volume showed highest rate. The

stem volume of saplings was measureable after 11 years of the fire event and reached about 5.5 m^3/ha for 18-years growing period after the fire. The stem volume in the low and high severity burn plots were negligible, about 0.01 m^3/ha for the post-fire 18 years growth (Takeda et al. 2013). Additionally, it was noted by many other studies (e.g. (Solans Vila and Barbosa, 2010, McHugh and Kolb, 2003) that the regrowth of the vegetation was heterogeneous within the burned areas. Some areas started to recover, while other areas are still regressing and the vegetation cover is still decreasing following the post-fire years. Sometimes, both the regrowth and mortality processes occur in the same area. Therefore, the use of the FRI method seems also to capture the patterns of the trees that survived after fire and then slowly perished by interactions between the crown damage and the bole char severity, which showed the decreasing FRI trend in the first several years after the fire (Figure 4.11). The certain areas of the FRI decrease were found in the low burn severity site (Figure 4.15). As a result of low severity, the onset of the tree mortality will increase (McHugh and Kolb, 2003) and hence the decrease of FRI might represent the process of the tree mortality. Particularly the low severity site illustrated longer period of FRI decrease (Figure 4.11a).

4.6.2 Prediction of larch forest recovery rate

Because forest succession is a long-term process and its observation is often based on the chronosequence approach in forest science. However, the initial forest conditions and tree recruitment immediately (e.g. $\leq$ 15 years) after the fire can be used to predict the future forest patterns (Johnstone et al., 2004). With respects to the magnitude of the FRI as the measurement of the larch tree recruitment, the recovery processes to the pre-fire condition of different burn severity areas were estimated in this study (Figure 4.17). The results showed that it takes from 30 to 47 years for the burned forest to recover to the pre-fire conditions, depending on the degree to

which the larch forest ecosystem has changed owing to the fire. Similar to our field observations, the recovery rate was highest in the moderate burn severity while it was slowest in the high burn severity (Figure 4.11). Even though the moderately burned site has higher recovery rate than the light burned site, the light burned forest still recovered to the pre-fire conditions earlier than the moderately burned site based on the FRI evaluation due to its proportion of the post-fire undamaged forest.

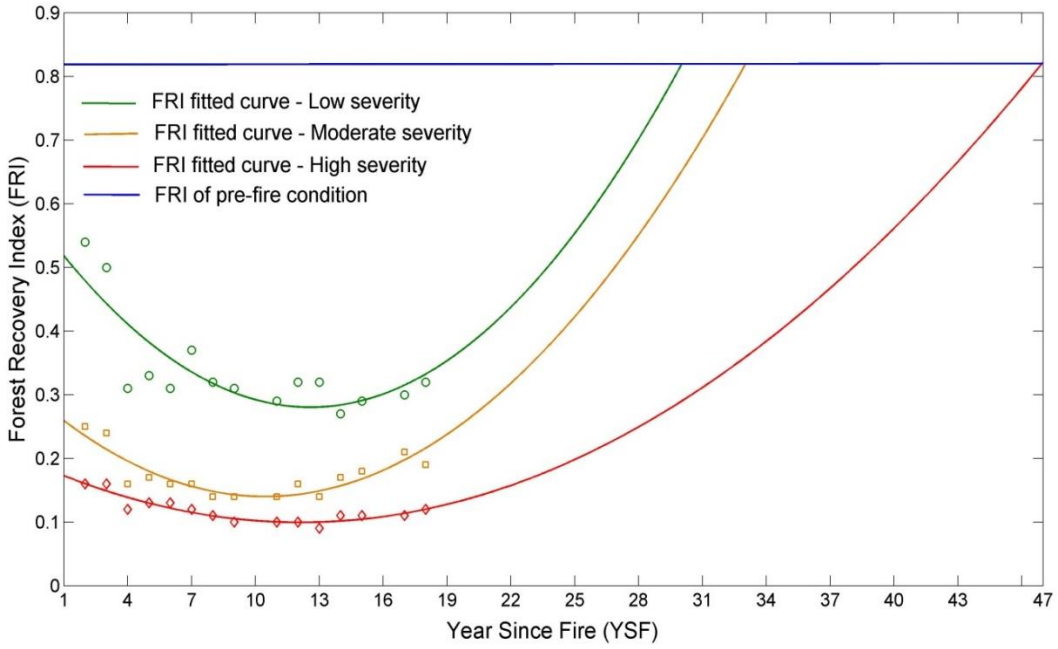

Figure 4.17 Estimates of forest recovery rate at different burn severity of Siberian larch forest with respect to the degree change of forest recovery index (FRI). The green, yellow and red dots are FRI values at low, moderate and high severity sites, respectively, that were extracted from FRI maps (See Figure 4.11 for fitted equations).

Compared with the field based measurements, there was a variability in the forest regrowth rate and lag at different fire-effect levels. Our field observations in the stage of the seedling and sapling regeneration (within 15 years after fire) in the study area showed that there was 6-years lag difference in stem volume growth of saplings between moderate and high severity fire plots (Takeda et al., 2013). Using the simulation models of the forest biomass at

different burn severity levels in the same study area, Taki et al. (2013) found that the larch forest subjected to light fire severity will take 25 years to recover to its pre-fire biomass while it takes up to 123 years and 170 years for the larch forests subjected to the moderate and high burn severity respectively to recover to their pre-fire biomass. From our remote sensing based prediction for 30 year onwards the fire, there was 14-year lag in forest regrowth with respect to the pre-fire FRI conditions between the high and moderate burn sites (Figure 4.17). The difference in the stages and variables of forest-regrowth measurement in these studies can account for the variablity of the forest regrowth rate as well as the regrowth lag timing at different burn severity levels. This suggests further studies to calibrate the FRI values with forest biophysical parameters such as the tree diameter, the tree height, the density and biomass to understand comprehensively the post-fire forest recovery with respect to the pre-fire conditions based on the remote sensing approach. There is merit in mentioning that the trends calculated using the time series analysis of the remote sensing data might be potentially affected by the different factors related to the processing and analysis steps. These include the accuracy of geometric correction of individual image, the influence of atmospheric conditions and the accuracy of its correction, and vegetation phenomenon at different image acquisition dates and stages of forest succession. Additionally, as shown in this study, the predicted trends of the forest regrowth might also be constrained by the limitation of the post-fire remote sensing images and monitoring time-frame in which the lack of a longer period of observations prevents us from identifying an actual time period for the full forest recovery. Therefore, the continuous observation with longer post-fire period is necessary to confirm the predicted trend of the post-fire FRI recovery in this study.

4.6.3 Trajectory of forest recovery at different burn severity classes

Regarding the influences of burn severity on the forest recovery, our findings of the FVC based vegetation-recovery monitoring agreed with other studies in the North American boreal forest. For instance, while investigating the vegetation recovery with NDVI in the Alaskan boreal forest, Epting and Verbyla (2005) found that the NDVI peaked 8 to 14 years after the fire with the largest increases in the high burn severity locations, followed by the moderate and low burn severity. Since the FVC in our study was calculated based on the NDVI, the similar pattern of vegetation recovery following fire was expected between these studies. However, the difference in the forest ecoregion might result in different patterns of the post-fire forest recovery from the NDVI measurement. For instance, Diaz-Delgado et al. (2003) used the NDVI method to investigate the effects of fire and environmental factors on the NDVI response in a fire in the Mediterranean environment. He found that the areas of high burn severity had lower levels of NDVI recovery compared to the low burn severity areas. Focusing on the spatial scales larger than a single fire, but not specifically in relation to the burn severity, Kasischke and French (1997) found that the NDVI of boreal forest was shown to decrease by over 50% immediately after a fire, but a dramatic increase was seen by the first year following the fire due to the growth of herbaceous vegetation. These results suggest the sensitivity of the NDVI method on monitoring the post-fire forest patterns, particularly in the early stage of forest succession. However, this method might not be suitable to describe the succession pathways of the post-fire forest as illustrated in this study as well as the other studies. Epting and Verbyla (2005) found that the self-replacement was the overall dominant successional pathway in the post-fire Alaskan boreal forest, with the pre-fire needle-leaf forest classes mostly succeeding to the needle-leaf woodland, and with the pre-fire broadleaf forest mostly succeeding to the broadleaf shrubland.

Within the burn severity classes, the areas of moderate severity in Epting and Verbyla's study had the highest percentage of self-replacement succession. In other words, this indicates the highest rate of pre-fire tree recruitment in the moderate burn severity sites. Their results are consistent with our findings of the forest regeneration pattern based on the FRI method in which the moderate burn severity results in the highest rate of forest recruitment as measured by the FRI. Additionally, the field based measurement of the forest regeneration in our study area also found that the moderate burn severity creates the most favourable condition for *Larix sibirica* to regenerate, showing the highest sapling density after 18 years of the fire (about 16000 saplings/ha), followed by low (740 saplings/ha) and high (630 saplings/ha) severity areas (Takeda et al., 2013). However, the burn severity might not be the unique driver defining the forest regeneration patterns in the *Larix sibirica* forest. Other environmental factors might also play important roles in determining the post-fire larch forest patterns and successional pathways that require further studies.

4.6.4 Comparison with other remote sensing indices

The use of remote sensing indices such as the NDVI, the SAVI, the NDSWIR, the EVI, and the fAPAR in monitoring the post-fire forest patterns demonstrated to yield different results, depending on the indices and data resolution (Hicke et al., 2003, Epting and Verbyla, 2005, Jin et al., 2012, Tanase et al., 2011b, Cuevas-González et al., 2008, Cuevas Gonzalez et al., 2009, Jones et al., 2013, Yi et al., 2013, Goetz et al., 2006). The results by Hicke et al. (2003) and Goetz et al. (2006) reported that the recovery period of the NDVI to pre-fire conditions in North America and Canada was 4 and 8 years after the fire, respectively. This recovery rate is shorter than the 13-year recovery time reported by Cuevas Gonzalez et al. (2009) for the central Siberia or at least the 20-year recovery period reported by our study depending on the methods and burn

severity levels (Figure 4.8 & 4.9). Goetz et al. (2006) and Cuevas Gonzalez et al. (2009) assumed that the differences found between their results were confounded by many factors such as the differences in fire regimes and fire types, the growing conditions and species composition between North America and Siberia, the remote sensing indices, and the data resolution among their studies. All these studies used much lower resolution data of AVHRR and MODIS compared with the Landsat data in our study, so nonlinearities in the aggregating NDVI over a large pixel (e.g. 8km in AVHRR PAL and 1km in MODIS data) may result in a faster predicted recovery than the real change observed on the ground (Hicke et al., 2003, Cuevas Gonzalez et al., 2009). In addition, the differences in recovery rate between our study and Cuevas Gonzalez et al. (2009), even in the similar condition of the Siberian boreal forest, might be due to the remote sensing indices used. Cuevas Gonzalez et al. (2009) used the NDVI and the NDSWIR that correlated to the leaf area index and water content of the canopy. As a result of rapid growth of the herbaceous plants, shrubs and grasses layers in the post-fire environment, these optical indices also reach their maximum quickly after the fire and saturate when the canopy is fully recovered (Tanase et al., 2011b, Berner et al., 2010, Jones et al., 2013). Therefore, monitoring of post-fire forest recovery using these indices might result in a faster rate of forest regeneration. This might also be problem for the use of NDVI based the FVC as shown in this study. As discussed previously, the FVC method is more sensitive to the early stages of forest succession. In this situation, the FRI method might be an alternative approach to continue monitoring the post-fire forest characteristics at later stages of the forest succession.

4.6.5 Implications for forest management

Modeling the post-fire regeneration pattern through the use of satellite based time-series data has the advantage of time-effective guidance and evaluating the management actions in the

post-fire ecosystems. The accurate distinguishing factors between the vegetation recovery in general and the actual forest tree recruitment is necessary to propose an appropriate silvicultural measures for obtaining the optimal biomass of the regenerated forest in the optimal period. This, in turn, maximizes the rate of return of the valuable goods and environmental services of the forest ecosystems after fire disturbances. Our results also indicated that the forest regeneration rate in the high severity areas was much lower than that of the moderate and low severity burns. In order to maintain the same forest structure at the different burn severity levels, the artificial seeding may be good management practice to accelerate the forest regeneration in high burn severity areas. However, other environmental factors influencing the forest regeneration process other than the burn severity should be also considered to enhance the effectiveness of the management actions.

4.7 Conclusion

The times series of the FVC and the FRI data in this study demonstrated their strengths in monitoring the different stages of the post-fire forest succession. Both variables were dramatically decreased immediately after the fire, showing good indicators to detect the forest disturbance. The FVC was then increased rapidly due to the growth of different vegetation layers such as the herbaceous plants, grasses, shrubs and seedling/sapling trees for several years after the fire. On the other hand, the FRI data showed a decrease trend for several years after the fire and then gradually increased at different rates depending on the burn severity levels. There was a consistent pattern of the FVC and FRI based the forest monitoring with the field-based measurements as well as the field-based knowledge of experts in post-fire studies.This suggests the potential integrated use of these methods to evaluate the different stages of forest succession after fire. Our analysis also indicated that in early stages of the forest succession the recovery

rate of dominated vegetation covers (e.g. herbaceous plants, shrubs, grasses, and fire weeds) was positively correlated with the burn severity. On the other hand, the growth rate at the later stage was highest in the moderate burn severity sites, showing the dominance of the larch species, followed by the low and high severity sites. More rigorous evaluations, including the ground-based and the remotely sensed methods with the longer post-fire period, would be valuable for determining the uncertainties in this study and describing the factors responsbile for the variability of the post-fire forest regeneration in the boreal larch forest ecosystems.

CHAPTER 5: EFFECTS OF BURN SEVERITY AND ENVIRONMENTAL CONDITIONS ON POST-FIRE REGENERATION VARIABILITY OF SIBERIAN BOREAL FOREST

5.1 Preface

Chapter 5 is to address the last objective of the thesis that is to evaluate the regeneration patterns of the post-fire boreal larch forest by analyzing driving factors. This chapter presents how driving factors of post-fire forest patterns can be extracted from remotely sensed data and then associate with the forest patterns. All sections of this chapter have been included in the manuscript and submitted in the journal Remote Sensing of Environment as a research paper:

> Chu, T., Guo, X. & Takeda, K. (2015) Effects of burn severity and environmental conditions on post-fire regeneration variability of Siberian boreal forest. *Remote Sensing of Environment (Submitted).*

The manuscript is now under review. Thuan Chu performed the collection and analysis of remote sensing data and wrote the manuscript. Dr. Xulin Guo supervised the steps of data processing as well as the research progress. The field data (i.e. ground truth data of the post-fire forest patterns) for the validation and discussion of the results were collected by Dr. Kazuo Takeda. Both co-authors also provided comments and revised the manuscript.

5.2 Abstract

Heterogeneity of post-fire forest environments is strongly influenced by both abiotic and biotic factors of pre- and post-fire environments, including: fire regimes, species characteristics, landforms, hydrology, regional climate and soil properties. Assessing these driving factors is critical for understanding the long-term effects of fire disturbances on forest succession. In this study, we aim to evaluate the several factors influencing the variability of the post-fire forest

patterns in the Siberian boreal larch forest *(Larix sibirica).* For this reason, a time-series of the remote sensing data was analyzed to estimate the post-fire recovery rate as a response variable across the burned area in 1996. The analysis results suggested that the burn severity and water content were the primary controls of both the larch forest recruitment and the green vegetation cover as defined by the forest recovery index (FRI) and the fractional vegetation cover (FVC) respectively. The high rate of larch forest recruitment was found in the site of moderate burn severity, while severer burn was the preferable condition for the burned land surface occupied quickly by vegetation that might include seral community of shrubs, grasses, conifer and broadleaf trees of the early successional stage. The sites close to water bodies that received higher total amount of solar energy during the summer months showed higher rate of both recovery types, which depend on the burn severity. In addition to these factors, the topographic variables and pre-fire condition were also important predictors of post-fire forest patterns. These results contribute directly to the post-fire forest managements in Siberian boreal larch region.

5.3 Introduction

The variation in forest regeneration patterns after a fire is strongly influenced by both abiotic and biotic factors of pre- and post-fire environments, including fire regimes (e.g. fire intensity, fire frequency, fire/burn severity, burned area), species characteristics, landforms, hydrology, regional climate and soil properties (Dube, 2009, Flannigan et al., 2006, Casady et al., 2009, Johnstone et al., 2010a). Advances in understanding of each of these factors will help us to manage and accelerate the forest resilience not only after fires but also other natural disturbances (Kasischke and Chapin III, 2008).

Depending on the forest composition and structure, the species ecology, the climate, and the ecotope condition, the boreal forest fire regimes influence the post-fire recovery patterns to

different degrees. An example of the burn severity influence is how the North American boreal conifer forests have gradually shifted to the broadleaf deciduous forests as well as the loss of permafrost as a result of the high burn severity (Barrett et al., 2011, Shenoy et al., 2010). Barret et al. (2011) found that the increasing numbers of large burned areas in the recent decades resulted in a decrease of the conifer forest by 4.2% accompanied by an increase of broadleaf stands by 20%. Higher burn severity also resulted in higher stem density and biomass of the aspen and lower stem density and biomass of the black spruce in the North American boreal forest (Shenoy et al., 2010). However, recent findings in eastern Siberia boreal larch *(Larix gmelinii*) forest by Cai et al. (2013) showed that the larch and birch recruit densities after the fire are both negatively related to burn severity. Burn severity is the most important factor for predicting the larch recruit density in eastern Siberia, followed by the understory cover, the soil moisture class, the soil organic depth, and the elevation (Cai et al., 2013). This finding is consistent with the other studies in other boreal regions (Schimmel and Granström, 1996, Johnstone and Chapin III, 2006b,Veilleux-Nolin and Payette, 2012) in which the burn severity is also the most important driver of the post-fire regeneration. Regarding succession pathways of the post-fire forest, areas of moderate severity seem to be the most suitable for "self-replacement" succession in which the post-fire vegetation returns successfully to its pre-fire condition (Epting and Verbyla, 2005, Tang et al., 2012). In addition to the burn severity, other factors, including: climatic conditions (Mansuy et al., 2012, James, 2011), the soil physical properties (Johnstone and Chapin III, 2006b, Johnstone et al., 2010a, Shenoy et al., 2010), the topographic factors (Pausas et al., 2004, Oikonomakis and Ganatsas, 2012, Casady et al., 2009, Zhao et al., 2012), the pre-fire vegetation conditions (Lozano et al., 2012, Leon et al., 2012), and

the water balance metrics (Kane et al., 2015) also have significant effects on the seedling establishment, the forest structure and regrowth after fire disturbances.

The southern limit of the Siberian taiga is located in northern Mongolia where the taiga forest-steppe is particularly vulnerable to climate change and fire disturbance (Dulamsuren et al., 2010a, Otoda et al., 2013). A growing demand for the wood products and environment services from the forests as well as increasing natural disturbances such as fire and climate change has highlighted the technical and scientific gaps in sustainable forest management of the taiga-steppe transition zone in northern Mongolia (James, 2011). *Larix sibirica* Ledeb. (Siberian larch) is dominant species covering up to 80% of stand composition in Mongolia followed by *Pinus sibirica* Du Tour (Siberian pine), *Pinus sylvestrus* L. (Scots pine), *Picea obovata* Ledeb. (Siberian spruce), *Betula platyphylla* Sukaczev. (Asian white birch), *Salix spp.* (willow), *Populus tremula* L. (trembling aspen) , and *Ulnus pumila* L. (Siberian elm) (Tsogtbaatar, 2004, James, 2011). Several field-based studies demonstrated that on forest composition and regrowth of the taiga-steppe forests in northern Mongolia are influenced by fire and climate change (Otoda et al., 2013, James, 2011, Dulamsuren et al., 2010b, Dulamsuren et al., 2010a). For instance, Otoda et al. (2013) found that the regeneration patterns after fire depend on the tree species. *Betula platyphylla* regenerates vigorously after fire and is not dependent on seed sources. Post-fire regeneration of *Larix sibirica* on the other hand is more dependent on the presence of nearby seed sources. Similar to the black spruce boreal forest, the higher fire frequency and larger burned areas are likely to promote the relative dominance of the broadleaf trees and threaten the existence of the coniferous species in the Siberian larch forest of the taiga-steppe transition zone (Otoda et al., 2013). In addition to fire, the climate trends underlie a remarkable regional variation of the forest growth in taiga-steppe forests even within the same mountain system

(Dulamsuren et al., 2010a). From tree-ring analysis, Dulamsuren et al. (2010a,2010b,2013) found that the annual tree-ring growth of *Larix sibirica* is negatively correlated with the summer temperature while it has positive relationship with the summer precipitation.

Despite of the relevance of various fire and environmental factors for regeneration of the Siberian larch forest, few studies have assessed the integrated influence of these factors, leading to uncertainties in understanding of the Siberian larch forest responses to the disturbances and the environmental changes, particularly in the taiga-steppe transition zone. Remote sensing with abundant data sources and time effectiveness offers considerable potential not only for tracking the forest patterns but also for evaluating the various driving factors of forest regeneration after fire disturbances. Additionally, compared with field-based method, remote sensing-based approach would enable forest researchers and managers to model the influence of biotic and abiotic factors on the post-fire forest patterns within a larger context such as landscape scale. The Landsat time-series based the fractional vegetation cover (FVC) and the forest recovery index (FRI) have been demonstrated to successfully capture the patterns of post-fire forest regeneration and vegetation recovery in the Siberian larch forest (see Chapter 4). In this chapter, we further assessed the effects of the burn severity and other environmental conditions on the post-fire forest patterns by using remote sensing tools. More specifically, our objectives in this chapter are: 1) to evaluate the influence of a selected set of environmental factors on the variability of the post-fire forest recovery rate at different stages of the forest succession, and 2) to examine the degree of interaction among the driving factors in determining the forest recovery pattern after fire disturbances. The burn severity, the pre- and post-fire environmental factors were expected to be the major drivers of the forest regeneration after fire in the Siberian boreal larch forest. In this study, we provide an example of the primary use of the remotely sensed data for the

evaluating post-fire forest regeneration, that present the opportunity for managers and scientist for the rapid evaluation and continuous monitoring of the vegetation responses after the fires, particularly in the remote and vast regions of the boreal forests.

5.4 Materials and methods

5.4.1 Study area and datasets

The 1996 burned area, which was assessed the burn severity and spatiotemporal patterns of the post-fire recovery (Chapter 3 & 4), was selected as the study area in this chapter (Figure 4.1). Additionally, similar Landsat, WorldView-2 satellite datasets, and field-based measurement used in Chapter 3 & 4 were used to obtain the research objectives in this chapter. See Chapter 3 (sections 3.4 & 3.5) for more details on how those data were collected and pre-processed.

5.4.2 Indicators of vegetation response after fire

To investigate how the environmental factors influence the variability of the post-fire forest regeneration, the forest regeneration rate at pixel level, which was defined by the evolution of the yearly FVC and the forest FRI of years following the fire, was used as the response variables. It has been demonstrated in our study (see Chapter 4) that the FVC method can be used to monitor the regrowth of the green vegetation cover in early stage of the forest succession while the FRI method is useful to represent the larch *(Larix sibirica)* forest regeneration in later stage of the post-fire forest succession. The use of both the FVC and FRI as response variables in this study was expected to account for the different characteristics of post-fire forest patterns, including both the early (i.e. herbaceous plants, grasses, shrubs, and larch's seedlings and saplings) and late (i.e. young and mature larch trees) stages of forest succession. It should be noted within this study that the term green vegetation recovery was sometimes referred to as the

regrowth of all the vegetation types immediately after the fire (e.g. herbaceous plants, shrubs, grasses, broadleaf trees, larch's seedlings and saplings), while the term forest regeneration or larch tree recruitment was defined as the dominance of larch species *(Larix sibirica)* in the later stage of post-fire forest succession. The time series of the FVC and FRI were calculated based on the Landsat time series data and the interpretation of high resolution WorldView-2 image and field data. See Chapter 4 for more details on how the time series of FVC and FRI were calculated.

Our temporal trajectory of FVC and FRI showed that the FVC increases dramatically after the fire disturbances while the FRI, showing both the post-fire tree mortality and the tree regeneration, decreases for the first 10 years after fire and then gradually increases (Figure 5.1). In this study, we only focused on how the larch forest and other vegetation recover spatiotemporally after the fire disturbances. Therefore, the only periods showing an increase trend of the FVC and the FRI were selected to establish least squares relationship using (Eq. 5.1& 5.2).

$$fFVC = \beta_{FVC} * YSF + \beta_1 \quad (5.1)$$

or

$$fFRI = \beta_{FRI} * YSF + \beta_2 \quad (5.2)$$

where the *f*FVC and the *f*FRI are annual growth of the green vegetation cover and forest tree recruitment of each post-fire year to the pre-fire level, and YSF is the number of years since the fire. The β_{FVC} and β_{FRI} were the slope of the post-fire trend of the FVC and FRI and defined as the rates of vegetation recovery and forest regeneration of the post-fire forest respectively in this study.

Consequently, all of the cloud-free FVC images from 1998 to 2014 (YSF 2 to 18) were used to estimate the rate of vegetation recovery while the cloud-free FRI images from 2005 to 2014 (YSF 9 to 18) were used to capture an increase trend of the FRI values illustrating the larch forest recruitment after fire. Throughout the remainder of the paper, we will use the terms green vegetation recovery rate and the forest recovery rate to refer to the annual post-fire change in the FVC and the FRI slopes (β_{FVC} and β_{FRI}) respectively as established using the time series FVC and FRI and the least squares regression at per pixel basis (Eq. 5.1& 5.2).

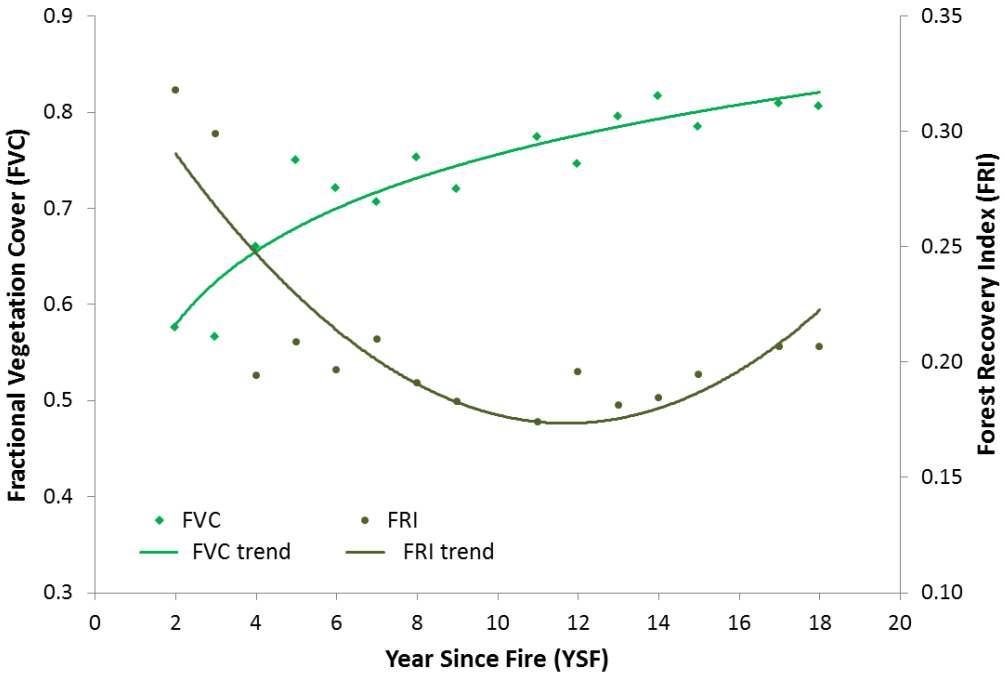

Figure 5.1 Temporal trend of post-fire forest patterns measured by FVC and FRI. The trends were fitted using the logistic and polynomial regressions based on the annual mean values of FVC and FRI and the year since fire (YSF) respectively. Only the periods showing an increasing trend of the FVC and FRI were selected to calculate the forest recovery rate after fire using the equations (5.1) and (5.2).

5.4.3 Exploring drivers of post-fire forest pattern

To find the local factors that influence the vegetation and forest recovery, we derived a total of 8 explanatory environmental variables from the Landsat imagery and other ancillary data sources. These variables were grouped into three categories of pre- and post-fire forest condition, local landscape, and topography (Table 5.1).

5.4.3.1. Pre- and post-fire forest condition

The pre-fire vegetation condition (e.g. tree density, tree age, basal area, biomass, and species composition) may influence post-fire forest regeneration due to its relationship with the fire burn severity, the post-fire seed availability and the seed germination (Keeley et al., 1999, Turner et al., 1999, Pausas et al., 2004, Shive et al., 2013, Lee et al., 2014, Lozano et al., 2012, Johnstone and Kasischke, 2005, Johnstone and Chapin III, 2006a). Since the NDVI is the most common remote sensing index that has shown consistent correlation with the vegetation condition and biophysical parameters (Pettorelli et al., 2005), we used this index to represent the pre-fire vegetation conditions. The NDVI is derived from the red (RED) and the near-infrared (NIR) reflectance ratio [NDVI=(NIR-RED)/(NIR+RED)] (Namzalov et al., 2012). Within the larch forest areas, higher pre-fire NDVI was expected to indicate better forest condition that can provide more suitable post-fire environments for the growth of the seedlings and saplings.

Burn severity is another significant driver of the post-fire forest regeneration (French et al., 2008). Four discrete levels of unburned, low, moderate, and high burn severity were mapped using the thresholds of the dNBR [dNBR= $NBR_{pre\text{-}fire} - NBR_{post\text{-}fire}$. The NBR was calculated using the equation (NIR-SWIR2)/(NIR+SWIR2), where the NIR and the SWIR2 are the near infrared and short wave infrared Landsat bands respectively (Key and Benson, 2006)]. The detail of burn severity mapping algorithm was presented in Chapter 3. The calculated dNBR was

scaled by 1000 and then reclassified into four levels according to the thresholds ofhigh severity (dNBR ≥ 440), moderate severity (190 ≤ dNBR < 440), low severity (70 ≤ dNBR < 190), and unburned (dNBR < 70).

Many studies have shown that the surface soil temperature and moisture determined by the organic layer depth after fire significantly controls the patterns of secondary succession in the boreal forest (Johnstone and Kasischke, 2005, Johnstone and Chapin III, 2006b, Kasischke and Johnstone, 2005, Kasischke et al., 2007). In remote sensing applications, the combination of the NDVI and land surface temperature (T_s) can provide information on the vegetation and soil moisture conditions and has been used widely in agricultural and forest meteorology (Sandholt et al., 2002, Wang et al., 2004, Chen et al., 2011, Son et al., 2012, Holzman et al., 2014). Sandholt et al. (2002) suggested a water stress index called the temperature-vegetation dryness index (TVDI) based on the analysis of a simplified triangular shape of NDVI-T_s space, in which the "wet edge" or T_{smin} (no-water-stress condition, TVDI=0) is treated as a constant value of the minimum land surface temperature and the "dry edge" or T_{smax} (no-water-available condition, TVDI=1) is described as having a negative relationship with the NDVI in the triangular shape of the NDVI-T_s space (Eq. 5.3).

$$\text{TVDI} = \frac{T_s - T_{smin}}{T_{smax} - T_{smin}} \qquad (5.3)$$

where the T_s is the observed surface temperature at a given pixel; the T_{smin} and T_{smax} is the minimum and maximum surface temperature respectively observed for a given NDVI, which defined as "wet edge" and "dry edge" respectively in the triangle shape of NDVI-T_s space. In many case studies, the minimum temperature extracted from the wet edge in the NDVI-T_s space does not remain constant with the changes of vegetation cover (Wang et al., 2004, Patel et al.,

2009, Petropoulos et al., 2009, Chen et al., 2011) and thus both the wet and dry edges are linearly regressed as follows:

$$T_{smax} = a_1 + b_1(NDVI) \qquad (5.4)$$

$$T_{smin} = a_2 + b_2(NDVI) \qquad (5.5)$$

where a_1 and a_2 are the intercepts for the dry and wet edges; b_1 and b_2 are the slopes for the dry and wet edges. This is also the case in our study, and we estimated the TVDI based on the equations (5.3, 5.4 & 5.5). The land surface temperature (T_s) was derived from the thermal band (10.4-12.5µm) of the Landsat data using the ATCOR algorithm in the PCI Geomatica. We used the interval of 0.01 of NDVI to determine the maximum and minimum T_S for regressing the dry and wet edge respectively. The TVDI has been demonstrated to be negatively correlated with the soil moisture, particularly in the soil depth from 0 to 10cm (Wang et al., 2004, Han et al., 2010, Chen et al., 2011, Holzman et al., 2014). The value of the TVDI is 1, indicating limited soil moisture avaiability and its value is 0, showing unlimited water access and maximum evapotranspiration. In this study, the time series of post-fire TVDI between 1998 and 2014 was estimated to calculate the post-fire mean TVDI as a predictor of vegetation recovery.

Table 5.1 Environmental factors as potential predictors of post-fire forest pattern

Variable group	Indicator	Description	Unit/Variable type	Source
Response variables				
Post-fire forest pattern/forest recovery rate	Fractional vegetation cover (FVC)	The FVC determines the proportion of burned land surface occupied by vegetation recovery. It not only represents larch forest recruitment but also seral community of shrubs, grasses, and broadleaf trees of early successional stage. The post-fire slopes of the fitted FVC by year since fire were used as the rate of post-fire vegetation recovery in general.	Continuous	Analysis of Landsat time series FVC data
	Forest recovery index (FRI)	The FRI determines whether a disturbed pixel is becoming a forest pixel. The post-fire slopes of the fitted FRI by year since fire were used as the rate of post-fire forest recruitment.	Continuous	Analysis of Landsat time series FRI data
Explanatory variables				
Pre- and post-fire forest condition	Pre-fire forest NDVI	Normalized Vegetation Difference Index (NDVI) is common indicator to evaluate vegetation health including tree density, tree age, and basal area. These variables have strong effect on forest regeneration. The pre-fire NDVI within larch forest locations was thus selected as an indicator of pre-fire forest condition.	Continuous ($0 \div 1$)	Derived from red and near infrared band of pre-fire Landsat image
	Burn severity	Burn severity is defined as the degree of ecosystem change owing to fire disturbance. Three burn levels of low, moderate and high severity were derived from our burn severity model of the study area.	Categorical with value of 1 (low), 2 (moderate) and 3 (high) severity	Burn severity model for the Siberian boreal larch forest in this study
	Post-fire vegetation and soil moisture	The TVDI is the remote sensing based index that provides a useful indication of drought condition. The TVDI is negatively related to vegetation and soil water content. Higher TVDI results from the combination of lower precipitation and higher evaporation rate. This study used 18-year mean of post-fire TVDI as indicator of post-fire vegetation and soil moisture condition.	Continuous ($0 \div 1$)	Derived from the relationship between surface temperature (T_s) and NDVI that were extracted from Landsat imagery
Topographic variables	Solar insolation	Solar insolation or solar radiation is the total amount of solar energy received at a particular location during a specified time period. It is an indicator of photosynthetically active radiation, soil moisture and soil temperature. The total amount of solar insolation in each location within the burned area was averaged during summer months in the study area.	Continuous (MWH/m^2)	Derived from digital elevation model (DEM)
	Elevation	Elevation within each pixel location of the burned area. SRTM digital elevation was interpolated and resampled to 30m resolution.	Continuous (m)	SRTM digital elevation model
	Slope	Slope within each pixel location of the burned area that was derived from DEM.	Continuous (deg.)	Digital elevation model
Local landscape	Distance to water body/Hydrology	Distance to water surface is an indicator of water content in the air and soil environment. Higher soil moisture and cooler air can be found near water surface. It was calculated by Euclidean distance to water body that masked from satellite imagery.	Continuous (km)	Analysis of Euclidean distance and masked water surface from Landsat imagery
	Land cover types	Pre-fire land cover types may indicate the potential for forest recovery due to post-fire seed availability and soil condition. The pre-fire land cover types of larch forest and non-larch forest were evaluated to compare recovery rate between these cover types.	Categorical with value of 1 (larch forest) and 0 (other)	Classification of pre-fire land covers type based on forest z-score (IFZ) from Landsat data

5.4.3.2. Topographic variables

In this study we consider the elevation, slope, and solar insolation as a proxy for the site conditions, as well as an indicator of the spatial arrangement of the land surface. According to previous findings, topography is also a significant factor related to the water availability, soil erosion, energy exchange and wind exposure that have direct or indirect influences on the response of the vegetation after the fire (Leon et al., 2012, Kane et al., 2015). In the boreal larch forest, the conifer species tends to regenerate faster in the sites with low land, shallow slope, mesic flat and thick soil (Cai et al., 2013, Zhao et al., 2012), while the upland and steep slope areas with moderate soil moisture content are ideal conditions for the broadleaf tree recruitments(Cai et al., 2013).

Incoming solar radiation (or solar insolation), defined as the total amount of solar energy received at a particular location during a specified time period, is fundamental to most physical and biophysical processes because of its influence on the energy and water balance at land surface, air and soil heating, evapotranspiration and photosynthesis of terrestrial ecosystems (Fu and Rich, 2002). Photosynthetically active radiation that vegetation is able to use in the process of photosynthsis has linear relationship with the solar insolation (Meek et al., 1984, Yu et al., 2015). Therefore, the solar insolation can be used as an indicator of the photosynthetically active radiation. The solar insolation varies significantly depending on the elevation, surface orientation (slope and aspect), and obstruction by surrounding topographic featuers. Several studies used aspect to represent solar radiation in studies of biophysical processes including the forest regeneration (Pausas et al., 2004, Oikonomakis and Ganatsas, 2012). However, an assumption of aspect as a sole indicator of the solar radiation may limit the interpretation of the vegetation dynamics driven by solar energy (Keating et al., 2007). In this study, we calculated

the solar insolation using digitial elevation model and solar analyst model developed in ArcGIS by Fu and Rich (1999). The total solar insolation of each summer month (June-August) in the post-fire years was calculated and then averaged to represent the mean solar insolation of the post-fire summer months, this is an indicator of the regrowth variability within the burned area.

5.4.3.3. Local landscape variables

The landscape variables such as land cover types, landscape heterogeneity, and water surface have significant effect not only on forest growth but also forest regeneration after the disturbances through their influences on seed availability, seed dispersion, water and energy balance (Fu and Burgher, 2015, Eckert et al., 2015, Lee et al., 2014, Christopoulou et al., 2014, Zhao et al., 2012). Zhao et al. (2012) found that the post-fire seed dispersal in the birch and larch is higher than in the *Pinus pumila*. As a result, more seedlings of the birch and larch is found in the burned areas than the seedlings of *Pinus pumila* (Zhao et al., 2012). We classified the pre-fire land cover into the larch dominated forest (*Larix sibirica*) and other vegetation using the integrated forest z-score (IFZ) of the pre-fire image acquired in 1995, similar to Chapter 3 & 4. The threshold of the IFZ values less than 3 was selected to locate the larch forest pixels in the pre-fire Landsat TM image. The regeneration of the larch forest was expected to have higher rate in the larch burned areas compared with the non-larch burned areas. Finally, because the study area is close to the water including rivers and lakes, we used the distance to water body as the last explanatory variable that can influence water content in the air and soil of the study area. The water body was extracted from the Landsat NDVI image and then the Euclidean distance to it was derived to define as a predictor of the forest regeneration.

5.4.4 Modeling post-fire forest pattern

In order to evaluate the influences of each of the environmental factors on the patterns of post-fire regeneration, we used the Random Forest (RF) algorithm (Breiman, 2001) to model the post-fire vegetation recovery rate (β_{FVC}) and the forest recovery rate (β_{FRI}) as a function of the factors related to the forest conditions, topography and local landscape variables (Table 5.1). The random forest modeling is an extension of the non-parametric classification and regression trees (CART). The random forest algorithm develops "forest" of the CART trees. For each CART model, a random portion of the data is selected to train the model and the remaining data are used for the model validation, and a random subset of the predictors are selected at each node split to ensure that the effects of all the predictors are tested. There are several advantages of the RF over the traditional classification techniques: (1) through a bootstrap approach, it can obtain higher accuracies than the single classification tree methods, (2) it develops accurate and unbiased predictions based on selections across bootstrap replicates, (3) it is non-parametric and thus unaffected by the distributional assumptions (Breiman, 2001, Falkowski et al., 2009).

The training and testing samples for the random forest algorithm in this study were randomly selected from a set of raster layers of the both response and predictor variables. In attempt to keep the samples equal and fully randomized among the categorical predictor variables (e.g. burn severity and pre-fire forest classes), we used a stratified random design to create about 450 samples for each the burn severity class and these samples were equally located in both the burned larch forest and burned non-larch forest. For each sample location, both responses (i.e. slope values of the FVC and the FRI recovery trend) and predictor variables (i.e. pre-fire forest NDVI, burn severity, distance to water body, land cover types, solar radiation, elevation, and slope) were extracted on a per pixel basis using the bilinear interpolation method.

Consequently, there were a total of 1400 samples and 70% of them were used as a training dataset and 30% of the samples were used for the validation purpose. We report the variance explained for each model as well as the importance of each predictor to the variance explained by the models. The variance explained for each model is similar to the coefficient of determination (R^2) for linear regressions that reports how well a statistical model fits a given dataset. We used the independent validation dataset of the response and explanatory variables for the purpose of calculating random forest variance explained. To measure the importance of the predictors, the random forest algorithm randomly excludes the values for a single predictor, and the remaining data are then used for the prediction across all trees within the random forest model. The resulting change in the mean square error from the original data was recorded and used as the variable importance measurement. In addition, we also report the interaction between the predictor variables in explaining response variable by using the interaction plot of each of the two specified predictor variables plotted on the X and Y axis for determining the response variable plotted on the Z axis from the independent validation dataset. The two sets of random forest models were run in this study. In the first set, we examined how the environmental factors influence the vegetation recovery rate defined by the FVC method. In the second set, the forest recovery rate defined by the FRI method was evaluated. It was expected that the influence degree of the predictor variables on the vegetation recovery rate is different from that of the forest recovery rate since each response variable accounts for the different stages of the post-fire forest recovery. We used the ModelMap package in the R statistical program (R Team, 2008) to develop and analyze our models. The overall processing steps of modeling drivers of the post-fire forest regeneration are shown in Figure 5.2.

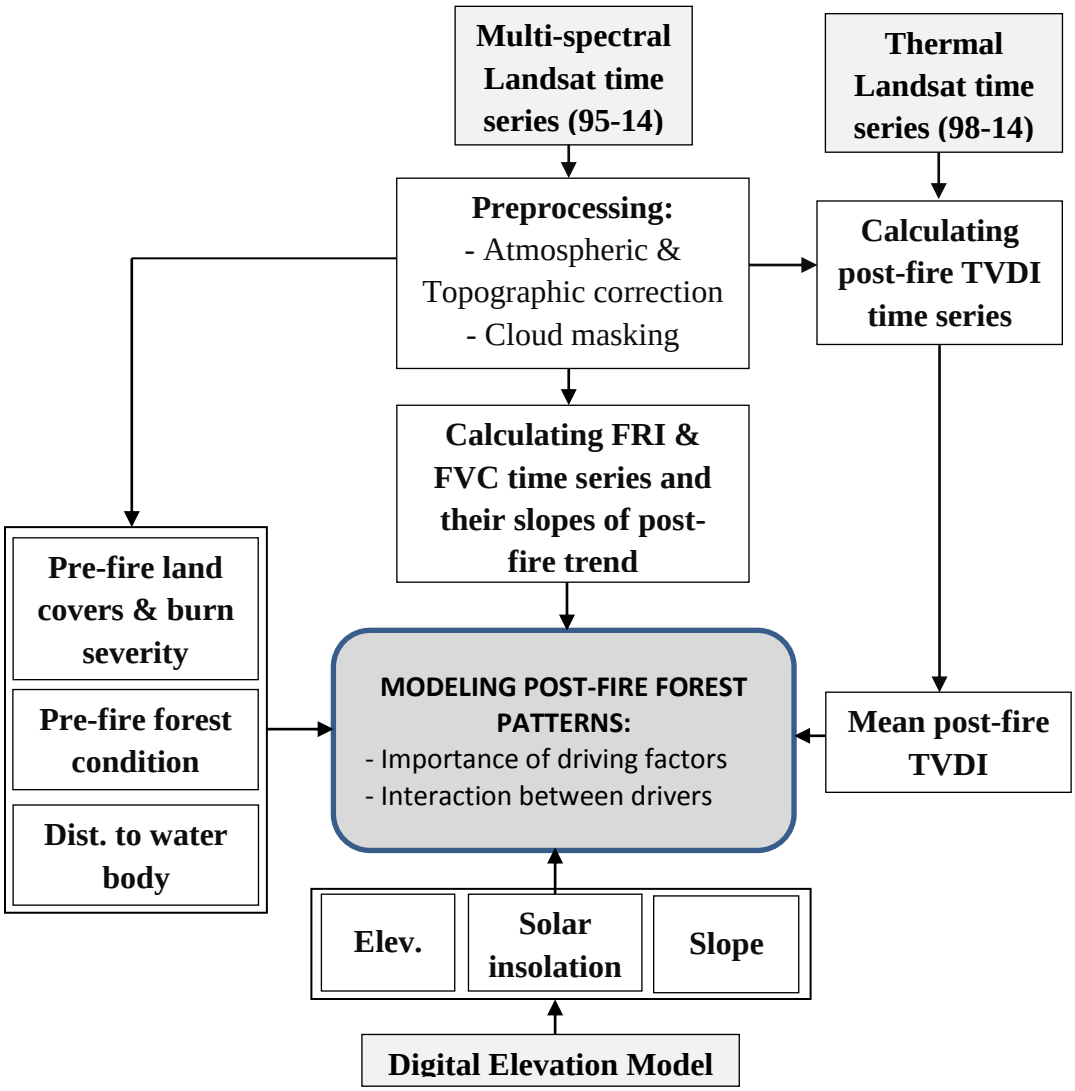

Figure 5.2 Overall processing flow of modeling drivers of post-fire forest regeneration in Siberian boreal larch forest.

5.5 Results

5.5.1 Patterns of post-fire forest recovery as response variable

As studied in chapter 4, the spatiotemporal patterns of forest recovery based on the FVC and FRI methods for the burned area in 1996 were shown in figure 5.3. The continuous values of both the FVC and FRI slopes at different recovery trends, which were defined as the vegetation recovery rate and forest recovery rate, were used as the response variables for modeling the post-

fire forest patterns.The positively higher value of the FVC and FRI slopes represents the higher rate of forest and vegetation recovery.

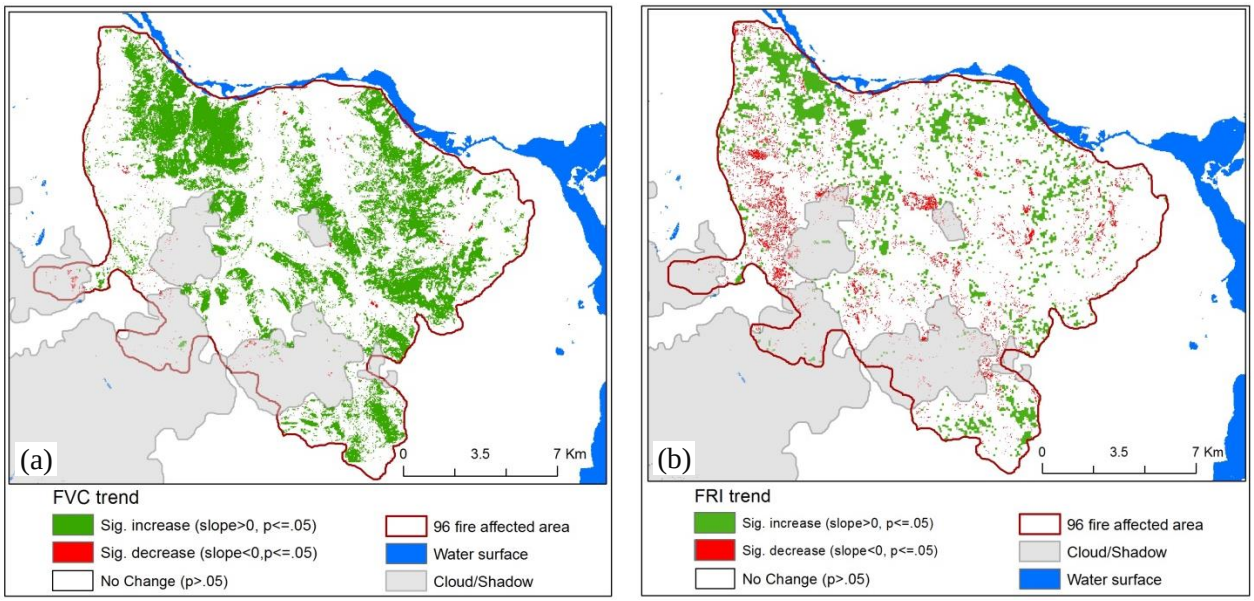

Figure 5.3 Response variables of post-fire forest pattern.

(a) Post-fire forest patterns estimated using the slope of the FVC trend and its p-value, an indicator of occupation rate of post-fire vegetation covers; and (b) the slope of the FRI trend and its p-value, an indicator of larch forest recruitment. The continuous values of both the FVC and FRI slopes were extracted randomly in different trends of forest recovery for modeling the post-fire forest patterns.

5.5.2 Calculation of driving factors

5.5.2.1. Pre- and post-fire vegetation conditions

The 1995 Landsat TM image was selected to calculate the pre-fire NDVI (Figure 5.4). The zonal statistic showed that the area of significant increase in the post-fire FVC and FRI slope had higher value of the pre-fire NDVI than the area of significant decrease in the FVC and FRI slope, 0.65 and 0.46 respectively. This suggests the importance of the pre-fire forest condition in the recovery of the forest after fire disturbances in which the healthier pre-fire forest conditions determined by the higher NDVI value may result in faster forest recovery rate.

The result of mapping burn severity based on the pre-fire Landsat image acquired in 1995 and the post-fire Landsat image acquired in 1998 is also shown in figure 5.4. 59% of the area with significant increase in the FVC trend (or significant increase of vegetation cover) after fire was found in the moderate severity areas, while 26% and 15% of that area was located in the high and low severity burns. However, the rate of vegetation recovery was highest in the high burn severity ($\beta_{FVCmean}$ = 0.04), followed by the moderate ($\beta_{FVCmean}$ = 0.024) and low burn severity ($\beta_{FVCmean}$ = 0.016). The results of the larch forest recovery measured by the FRI trend showed that 45% of the area with significant increase in the FRI trend (or significant increase of forest regeneration) after fire was found in the moderate burn severity, followed by the significant FRI increase area of low (35%) and high (20%) severity burns. In terms of forest recovery rate measured by the FRI slope within the area of significant FRI increase trend, the moderate burn severity sites had the highest recovery rate ($\beta_{FRImean}$= 0.01), followed by the low ($\beta_{FRImean}$= 0.006) and high ($\beta_{FRImean}$= 0.003) severity sites.

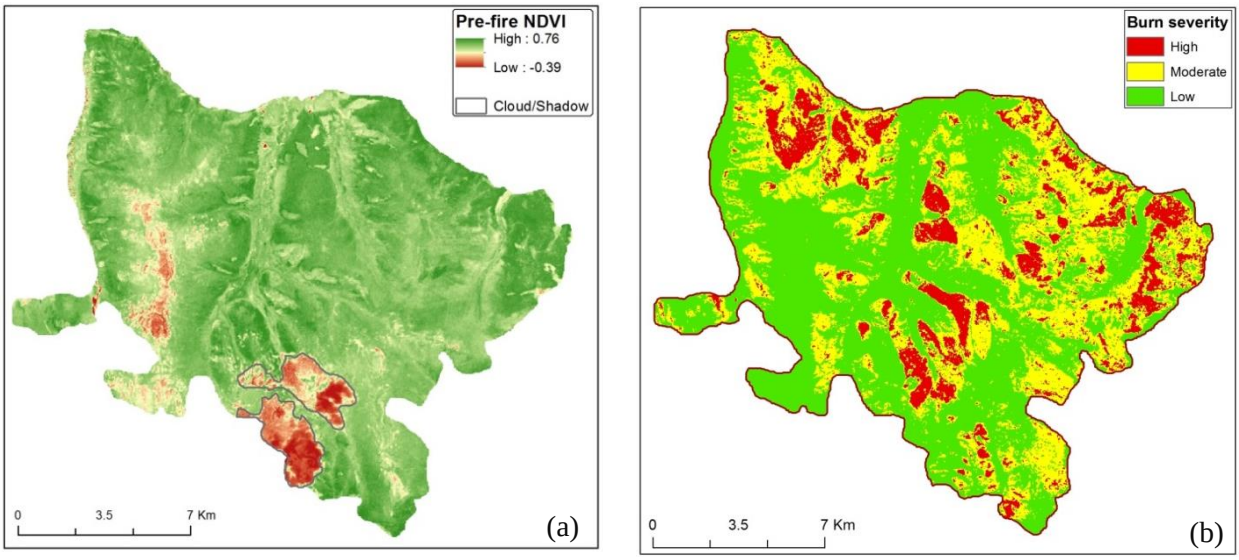

Figure 5.4 Pre-fire forest condition defined by NDVI (a) and post-fire forest effects defined by burn severity (b).

Regarding the vegetation and soil water content in the post-fire environment, the 18-years mean TVDI predictor variable of the post-fire years was estimated from the NDVI and land surface temperature (T_S) using NDVI-T_s space (Figure 5.5). The higher TVDI value indicates lower soil moisture. The forest regeneration is thus expected to have negative correlation with the TVDI variable.

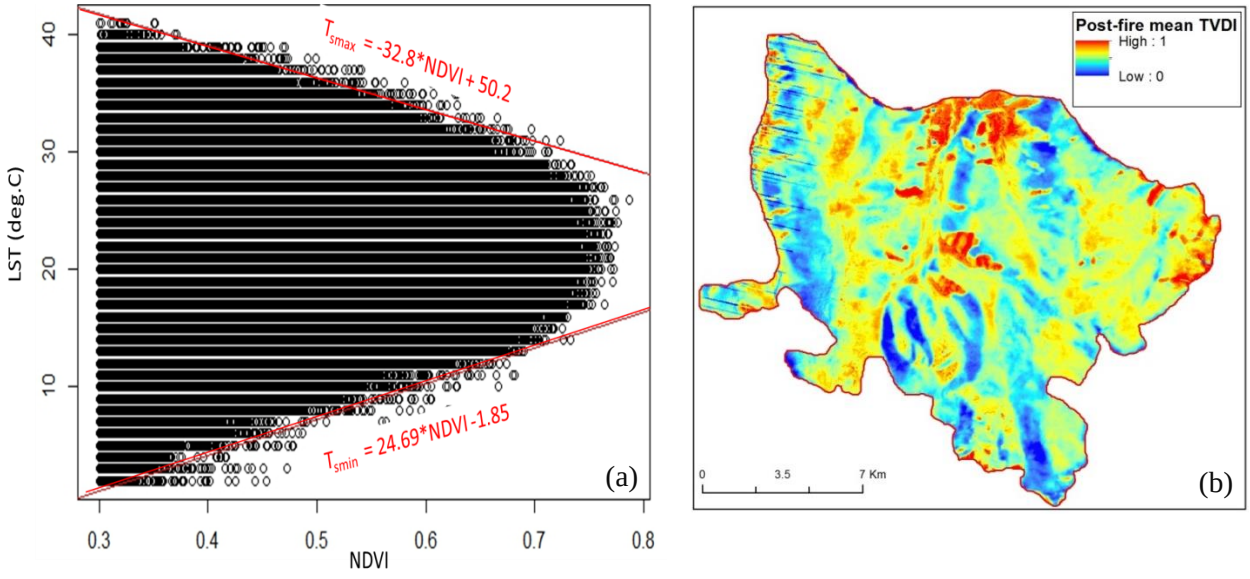

Figure 5.5 An example of NDVI-Ts space (a) and the mean TVDI of the post-fire 18-years (1998-2014) (b).

5.5.2.2. Topographic and local landscape variables

Topographic variables including the elevation, the solar insolation and slope were derived from the SRTM digital elevation model (DEM) (Figure 5.6a&b). Higher solar insolation in summer months was found in the south, southeast and southwest aspects that may results in the higher rate of vegetation recovery. The slope predictor variable not only affects the amount of solar radiation striking land surface, but also define physical properties and limitations (e.g. soil erosion, soil depth, soil moisture, and soil nutrient) of soil for vegetation growth (Renard et al., 1991, Liu et al., 1994, Kosmas et al., 2000). In the boreal larch forest, it is expected that the

broadleaf tree recruitment has higher rate in the upland sites with steep slopes compared with that of the needleaf recruitment (Cai et al., 2013).

Finally, the two landscape variables including the pre-fire land cover types and distance to water body were also derived for modeling the post-fire forest patterns (Figure 5.6c&d). The results of the zonal statistical analysis showed that there was a slight difference in the vegetation recovery rate measured by the FVC between the larch burned forest and non-larch burned forest with the mean FVC slopes ($\beta_{FVCmean}$) of 0.024 and 0.023 respectively. However, the forest recovery rate measured by the FRI in the larch burned area was much higher than that of the non-larch burn area, 0.013 and 0.0001 respectively. This not only suggests the influence of pre-fire land cover types on the post-fire tree recruitments but also confirmed our findings about the measurement of the post-fire vegetation and forest recovery using the FVC and FRI methods in which the FVC method is suitable to monitor the vegetation recovery (e.g. herbaceous plants, grasses, shrubs, broadleaf and needleaf trees), while the FRI method is suitable to estimate the pre-fire tree recruitment (e.g. larch trees).

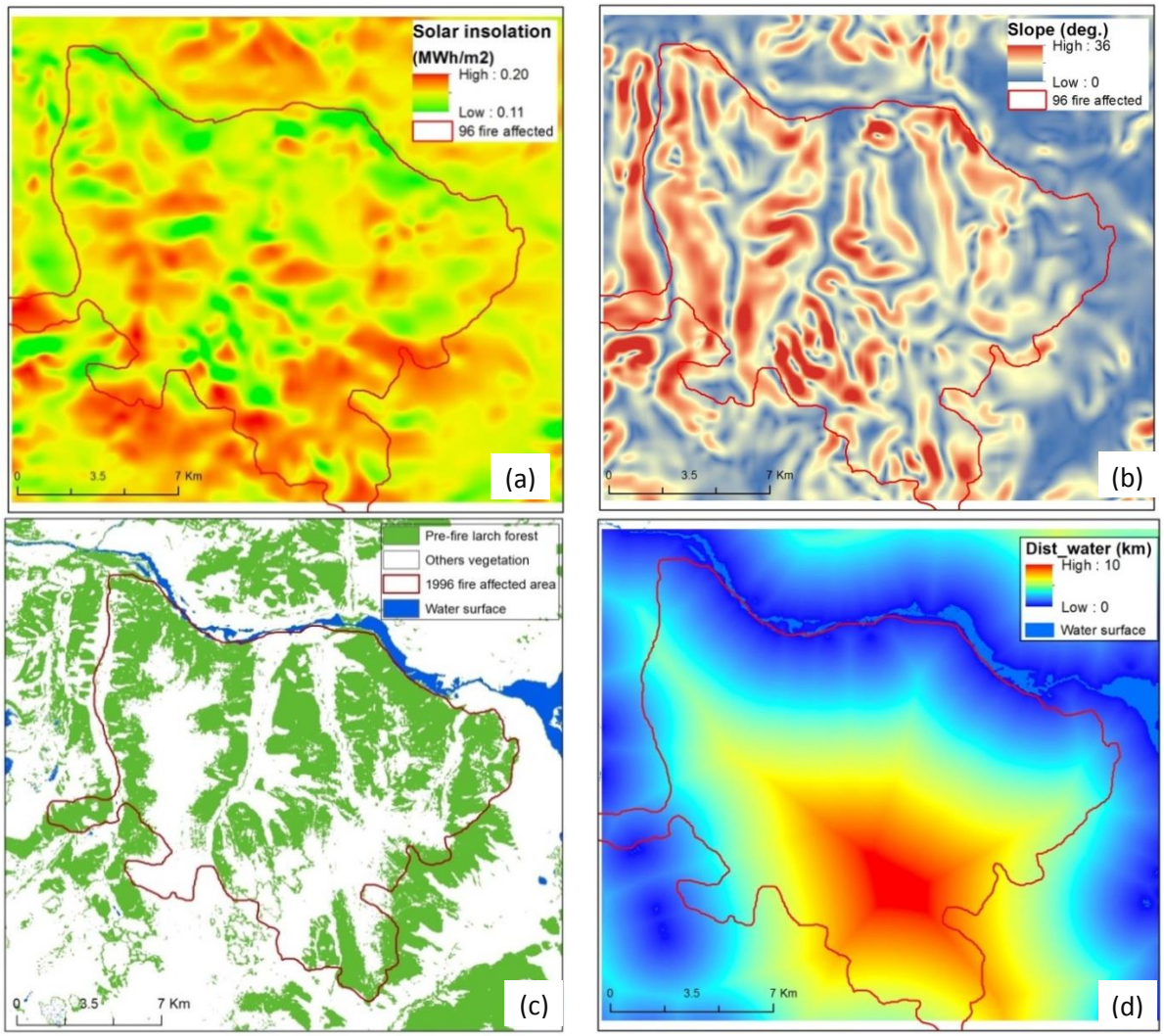

Figure 5.6 Examples of topographic and landscape variables.

Average solar insolation of summer months (a) and slope map (b) were derived from the surface analysis of digital elevation model. Classification of the pre-fire land covers using the 1995 integrated forest z-score (c) and the distance to water body using Euclidean distance (d). The water surfce was masked using the 1995 NDVI Landsat image.

5.5.3 Modeling post-fire forest recovery

5.5.3.1. Modeling FVC based vegetation recovery

The result of the random forest algorithm using a set of environmental predictors reveals that about 51% of the variation in vegetation recovery rate measured by the FVC can be

explained by the selected predictor variables in this study (e.g. burn severity, elevation, distance to water, dryness temperature, solar insolation, pre-fire NDVI, slope and land cover type, Table 5.1). The model validation using an independent dataset also showed a good fit between the observed and predicted values of the vegetation recovery rate defined by the FVC slope in which the burn severity was the most important factor for explaining the vegetation recovery, followed by the elevation, water and solar energy related variables (Figure 5.7). Since the recovery of vegetation in the post-fire environment includes not only the larch tree recruitment but also other vegetation types of the early successional stage, the pre-fire forest condition and land cover types which might determine the seed source availability of the larch forest were less important than other variables in classifying the FVC based vegetation recovery rate.

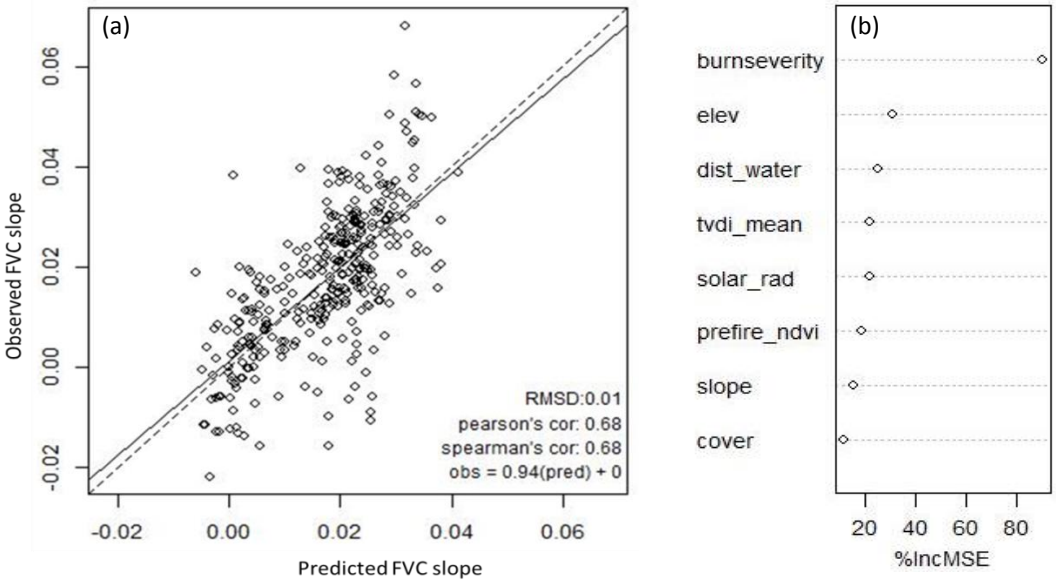

Figure 5.7 Observed and estimated FVC based vegetation recovery rate (or FVC slope) using random forest algorithm (a) and the importance of the predictors in classifying recovery rates (b).

The independent samples (or testing samples) were also used to estimate the vegetation recovery rate plotted in the z axis based on the interaction between the two specified predictor variables plotted in x and y axis (Figure 5.8). In this study, we observed the interaction of burn severity variable with other predictors in the determination of vegetation recovery. The

remaining predictor variables were fixed at their mean (for continuous predictors) or their most common value (for categorical predictors) in each interaction plot. The results showed that the FVC based vegetation recovery rate was positively correlated with the burn severity, pre-fire vegetation condition, solar radiation, and the slope factors (Figure 5.8, 5.8d, 5.8e & 5.8f). Similar to our temporal trajectory of the forest pattern in different burn severity classes (see Chapter 4), the post-fire vegetation recovery measured by the FVC slope had the highest rate in the high burn severity sites, followed by the moderate and low burn severity.The highest rate of vegetation recovery was also found in the altitude range from 1700m to 1900m and which had burned with high severity (Figure 5.8a). The distance to the water body seems to negatively correlate with the vegetation recovery where the highest recovery rate was found in the areas with the high burn severity and within 2km from the water body (Figure5.8b). Even though the relationship between the soil moisture measured by the TVDI and vegetation recovery rate was not clearly distinguished, the areas with high burn severity likely recovered quicker when they have higher soil moisture content defined by the lower TVDI values (Figure 5.8c).

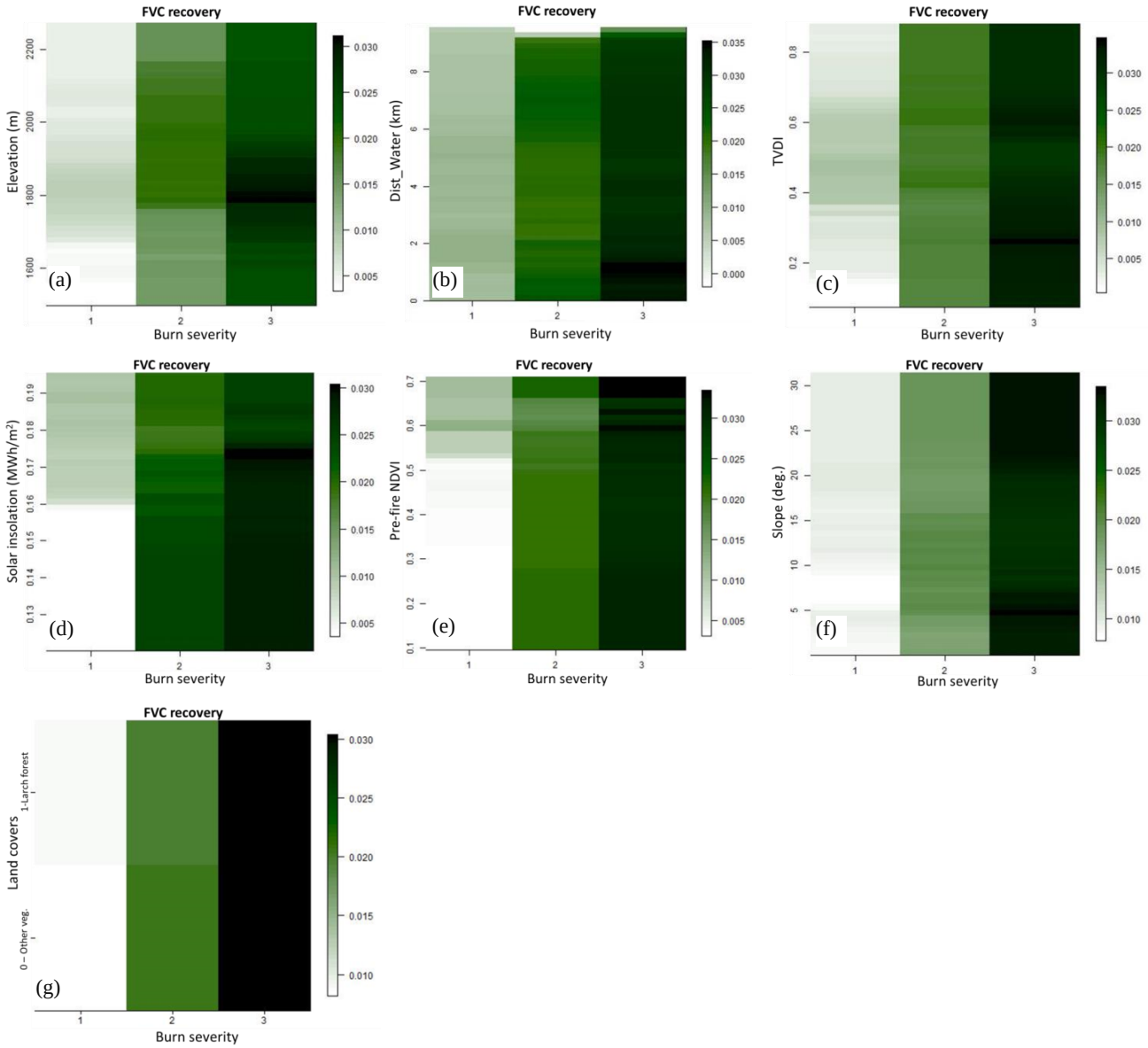

Figure 5.8 Interaction between burn severity and other environmental factors in predicting post-fire vegetation recovery rate defined by FVC.

In each interaction plot, the remaining predictor variables were fixed at their mean (for continuous predictors) or their most common value (for categorical predictors). The values in the plot legends shows the vegetation recovery rate measured by the FVC slope.

5.5.3.2. Modeling FRI based forest regeneration

The random forest model of the FRI based forest recovery indicated that about 40% of the variance in the post-fire forest recovery can be explained using the selected driving factors

related to the fire and environmental conditions (Table 5.1) in this study. Similar to the FVC based model, the variances explained in each model suggests that there are additional factors that should be included in the models in order to further explain the variations in the post-fire regeneration across the burned area. The validation result of the FRI based model using the independent dataset showed the good strength of the linear relationship between the observed and predicted values of the forest recovery rate (Figure 5.9a). The rate of the post-fire larch tree recruitment had the strongest correlation with burn severity, followed by the distance to water body, the pre-fire vegetation condition (or pre-fire NDVI), the solar radiation, the slope, the dryness temperature, the cover and elevation (Figure 5.9b). Compared with the FVC based vegetation recovery, the least important of the elevation factors for determining the larch forest recovery suggests that the classification of the larch forest recovery rate was more distinguishable by using other predictors rather than the elevation predictor.

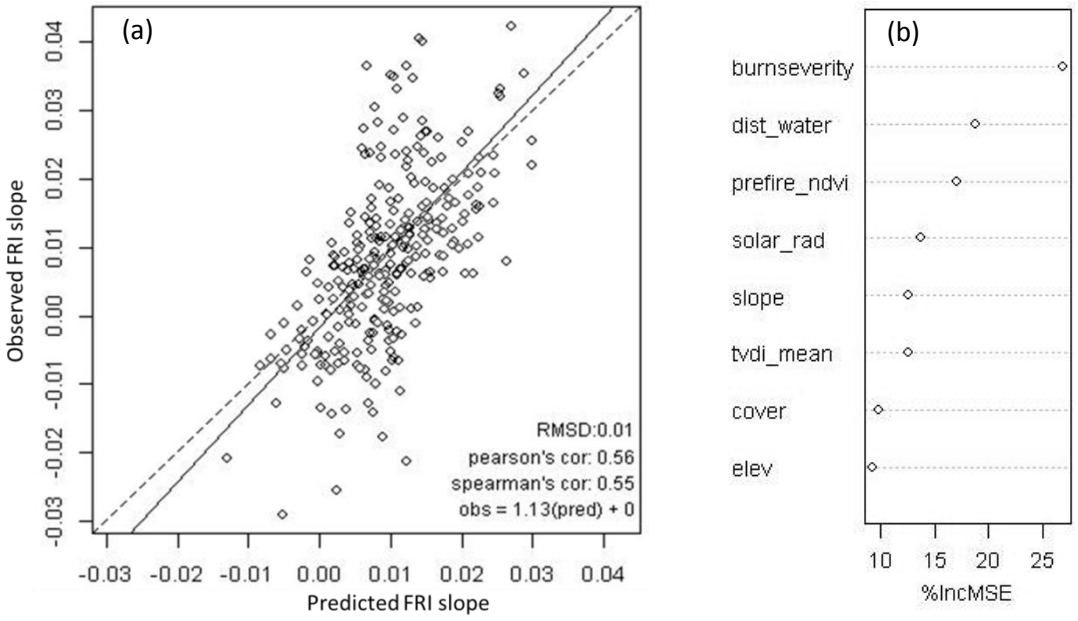

Figure 5.9 Observed and estimated FRI based forest recovery rate using random forest algorithm (a) and importance of predictors in classifying forest recovery rates (b).

The importance of the predictors measures the increase of the mean square error (MSE) in the classification of the response variable if one of these predictors is excluded from the prediction model.

The interaction plots of the FRI model showed more distinguishable patterns of relationship between the forest recovery rate and the predictor variables (Figure 5.9). The post-fire larch forest regeneration was strongly related to the burn severity in which the highest rate of the regeneration was found in the moderate severity areas, followed by low and high severity burns (Figure 5.10). The forest regeneration rate was positively correlated with the pre-fire vegetation condition (or pre-fire NDVI) (Figure 5.10b), photosynthetically active radiation defined by the solar insolation (Figure 11c), the slope (Figure 5.10d), and the soil moisture (Figure 5.10e). However, it had negative correlation with the distance to the water body (Figure 5.10a) at all burn severity classes. The highest rate of forest recruitment was found in the larch burned areas which are closed to water body (<3km), the healthy pre-fire vegetation condition (pre-fire NDVI>0.55) and the high soil moisture (TVDI<0.2). In addition to the burn severity factor, these results suggest the importance of microclimate, seed availability and soil water content within the burned area that can accelerate the regeneration of the larch forest.

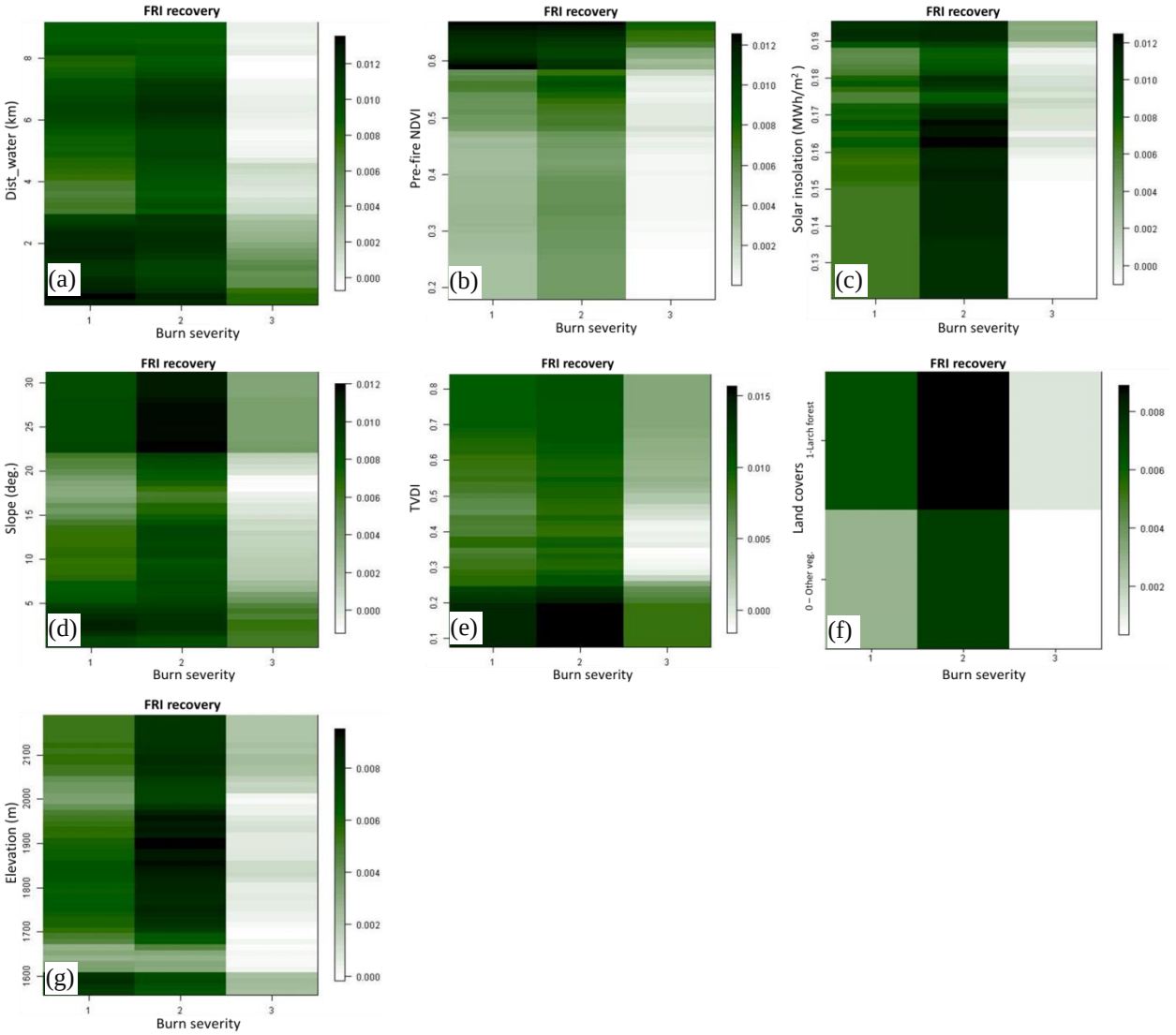

Figure 5.10 Interaction between burn severity and other factors in predicting post-fire forest recovery pattern defined by FRI.

In each interaction plot, the remaining predictor variables were fixed at their mean (for continuous predictors) or their most common value (for categorical predictors). The values in the plot legends shows the forest recovery rate measured by the FRI slope.

5.6 Discussion and conclusions

5.6.1 Influence of burn severity on post-fire vegetation response

Both the FVC and FRI slopes, accounting for the post-fire forest patterns in the early successional stage (<10 years since fire) and later dominant stage of the larch forest regeneration

(≥ 10 years since fire) respectively, were used as the response variables for evaluating the influence of fire and environmental factors on the forest variability. The rank of variables importance was generally consistent among the two models where the burn severity was by far the most important driver of both the vegetation recovery and the larch forest recruitment. This finding is consistent with other studies in the boreal regions (Johnstone and Chapin III, 2006b, Cai et al., 2013) which also indicate the primary control of burn severity on post-fire succession. However, our results reveal that the influence of the burn severity on early stage of forest succession differs from that of only larch dominated forest recruitment. More specifically, higher burn severity levels resulted in higher rate of green vegetation recovery determined by the FVC, while the moderate burn severity was the most favorable condition for the larch tree recruitment in the later stage defined by the FRI. These findings are similar to our field observations as well as other remote sensing based knowledge of experts. Regarding the green vegetation recovery, Epting and Verbyla (2005) found that the post-fire NDVI based green vegetation recovery in the Alaskan boreal forest has the largest increase in the high burn severity locations, followed by the moderate and low burn severity. Similarly, Jin et al. (2012) used the MODIS enhanced vegetation index (EVI) as an indicator of the post-fire vegetation recovery in the North American boreal forests, and found that more severe fires lead to more rapid post-fire EVI increases. Since our study used the NDVI method to calculate the FVC, the similar positive-correlation between the burn severity and the green vegetation recovery rate is thus expected among these studies in the boreal regions. According to Johnstone et al. (2010b) the higher consumption of organic layers in severe fires results in more exposure of the mineral soils, which favors the growth of herbaceous species and broadleaf trees. These shade-intolerant species often grow quickly in the early stage of post-fire forest succession (Dorisuren, 2008, Zyryanova et al., 2010a, Crotteau et

al., 2013) and respond positively to increased burn severity (Johnstone and Chapin III, 2006b, Johnstone and Kasischke, 2005, Crotteau et al., 2013). As a result, the vegetation indices such as the NDVI, EVI, and NDVI based FVC which are sensitive to the changes of green vegetation canopy several years after the fire (Goetz et al., 2006, Jin et al., 2012) are positively correlated with burn severity.

In terms of the larch forest regeneration, our remote sensing based estimates of larch *(Larix sibirica)* forest recovery rate in the later successional stage (≥10 years since fire) found that the moderate burn severity sites had the highest rate, followed by low and high severity sites (Figure 5.10). This pattern of larch regeneration with respect to burn severity is consistent with our field-based assessment conducted 13-years after the fire in which the moderate burn severity was the most suitable condition for the larch forest regeneration with the highest density of $16x10^3$ saplings/ha, followed by low and high burn severity sites with 740 saplings/ha and 630 saplings/ha respectively. Even though the seed and seedling density was highest ($92x10^4$ seeds/ha and $5x10^4$ seedlings/ha) in the low severity sites, these seeds and seedlings could hardly grow to become saplings due to the competition of high density of undamaged adult trees (526 trees/ha) which resulted in low light availability for photosynthesis in the understorey of low severity sites (Takeda et al., 2013). Compared with the low and moderate burn severity sites, the seed density in the high severity burns was very low due to both the limitation of seed dispersion from the very few remaining adult trees (<42 trees/ha) and the high consumption of seed source by the severe fires. Consequently, the moredate burn severity sites with the high number of disseminated seeds ($40x10^4$ seeds/ha) and the light availability due to the low to moderate density of adult trees (101 trees/ha) seem to create favourable conditions for seed germination

and sapling growth compared with the high and low severity burned forest. This highlights the characteristics of Siberian larch species that is shade-tolerant species with low recovery rate.

The relationship between the burn severity and the larch regeneration in our study is different from the studies in the Alaska interior boreal black spruce forest where the burn severity is positively correlated with the seedling establishment (Johnstone et al., 2010b) and in the northeast China boreal larch forest where the density of the tree recruitment (both conifer and broadleaf trees) is negatively correlated with the burn severity (Cai et al., 2013). These differences are likely confounded by several factors such as the experiment design, the fire ecology, the soil organic layer depth and the regeneration ecology of the dominant tree species. Cai et al. (2013) only used two burn severity classes (low and high severity) and accounted both the seedling and the sapling density for the post-fire tree recruitment density. If both the seedlings and saplings, the low and moderate burn severity had been combined in our field-based and remote sensing based study respectively, a similar pattern of negative relationship between the post-fire tree-recruitment and the burn severity would also have observed as shown in Cai et al.'s study. Regarding our remote sensing based study, the remotely sensed observation is often highly correlated with the overstorey properties. Distinguishing between the seedling and sapling density is thus necessary to be able to capture the overstory forest by remote sensing method. It should also be noted that, from our field observations, the growth of seedlings to become saplings in the low burn severity sites was negligible possibly due to the competition of high density of remaing adult trees. Regarding the fire ecology and regeneration ecology of the dominant tree species, the North American boreal conifers survive in the crown-fire dominated ecosystems by storing seeds in the serotinous cones, which can disseminate seeds after fire and thus are able to regenerate as a shade tolerant species growing in the understory of pioneer

species (de Groot et al., 2012). In our study area, increased burn severity decreases the larch seed availability dramatically for regeneration ($92x10^4$ seeds/ha in low severity sites and $4x10^4$seeds/ha in high severity sites). The lack of seed availability in high burn severity can thus limit the post-fire larch recruiment. However, as discussed previously, our finding of the green vegetation recovery in early successional stage as measured by the FVC is consistent with the studies in North America. The FVC is sensitive to early stage of forest succession with the dominance of species with high regrowth rate such as grasses and shrubs, while the FRI is more suitable to monitor the larch regeneration in the later successional stages (see Chapter 4). These results suggest the different response to the burn severity levels of the deciduous conifer and broadleaf trees in Siberian boreal larch forest compared with that of the North American forests.

5.6.2 Influence of other environmental factors on post-fire vegetation response

Even though the burn severity has been determined as a primary factor influencing the post-fire forest patterns (Johnstone and Chapin III, 2006b, Johnstone et al., 2010b, Shenoy et al., 2010, Cai et al., 2013, Crotteau et al., 2013, Jin et al., 2012 , this study), other environmental factors also affect the response of post-fire vegetation. In this study, we investigated the influence of other factors related to the site conditions on variations of the post-fire forest patterns. The results showed that the water content in soil and air which was defined by the distance to water body and TVDI variables is likely the second most important driver of the recovery patterns of both early and late forest succession stage. In particular, the larch forest regeneration clearly had positive relationship with the water content (Figure 5.10a&e). Even though we did not measure the soil moisture in the field, the results of field investigation showed that much higher number of saplings was found in the plots close to the lake surface. This suggests the importance of water balance for the larch forest growing. This finding is similar to

the studies in North American boreal forest in which the dramatically lower levels of tree recruitment (both broadleaf and conifer trees) were found in the sites with lower soil moisture levels (Kasischke et al., 2007, Johnstone et al., 2010b). For the long term growth of the larch forest, changes in water related factors such as the temperature, precipitation, soil moisture and water potential due to climate change are also important factors for influencing the larch forest growth and regeneration (Dulamsuren et al., 2009, Dulamsuren et al., 2010a, Dulamsuren et al., 2010b, Dulamsuren et al., 2013). For example, the young larch trees growing at the taiga-steppe forest are more susceptible to drought than the mature trees at the same sites (Dulamsuren et al., 2009). Similarly, the recent growth declines of the larch forests at the southern limit of the Siberian boreal forest is also attributed to the decreasing effective moisture due to the increasing summer temperature and decreasing summer precipitation in the course of climate warming (Dulamsuren et al., 2010a, Dulamsuren et al., 2013).

Regarding the topographic variables, our results showed that elevation was the least important variable in the predicting the regeneration rate of the larch forest while it was the second most important variable for explaining patterns of the earlier forest succession. This suggests that the recovery rate is more identical in the early stages of forest succession with respect to the elevation than that of the larch dominated regrowth. Even though our field observations (Takeda et al., 2013) and other studies (Johnstone et al., 2010b, Cai et al., 2013) showed that the conifer recruit density in the boreal forests is negatively correlated with the elevation, other factors related to the burn severity, the soil water content, the pre-fire vegetation condition and solar insolation are the foremost requirements for predicting the forest regeneration rate (Cai et al., 2013, Lozano et al., 2012, Otoda et al., 2013 , this study) which obscured the elevation predictor variable for determining the larch regeneration rate. In relation

to the topographic condition, the solar insolation was also an important factor which showed the positive correlation with the green vegetation recovery rate at low burn severity (Figure 5.8d) and the larch regeneration rate (Figure 5.10c), while it was negatively correlated with the green vegetation recovery rate at moderate and high burn severity (Figure 5.8d). The solar insolation is not only relates to the soil temperature and soil moisture (Fu and Rich, 2002) but also have linear relationship with the photosynthetically active radiation (Yu et al., 2015). The negative or positive responses of both the early and late forest successional stages to the total summer solar insolation depending on the burn severity in our study suggests the requirement of light availability for photosynthesis of the post-fire vegetation to regrow. In the early stage of post-fire forest succession, the low burn severity sites are still dominated by the undamaged remaing adult trees. Therefore, an increase of solar insolation in the low burn severity sites (Figure 5.8d) is necessary for the light penetration through the closed canopy of overstorey, and thus promotes the photosynthetic activity for the growth of all species in understory canopies or the tree-fall gaps. Since the Siberian larch is a shade-intolerant species, the positive response of the FRI and FVC (Figure 5.8d & 5.10c) to solar insolation shows the larch's physiology during the regrowth stages. In the case of the likely negative response to the solar insolation of the FVC in the moderate and high burn severity sites (Figure 5.8d), this might associate with the availability of soil moisture for the growth of green vegetation. In addition, the high solar insolation in those sites might also result in the increase of leaf temperature of the dominant species in the early stage (i.e. grasses, shrub and fire weeds) that leads to a decrease of net photosynthetic rate (Koike et al., 2010).

In terms of the pre-fire forest conditions defined by the pre-fire NDVI, both the early and late recovery stages of the post-fire forest were positively correlated with the pre-fire forest

conditions (Figure 5.8e, 5.10b). The importance of the pre-fire NDVI, particularly in predicting the larch regeneration, may be related to the basal area of the pre-fire larch forest. The seed production and seedling densities have been shown to be positively correlated with the pre-fire basal areas (Greene et al., 2004, Chen et al., 2009, Johnstone et al., 2010b, Pausas et al., 2004). Higher pre-fire NDVI thus results in higher seed productivity which can promote post-fire regeneration. The high recruitment rate in early successional stage after the fire was also expected in the areas with higher pre-fire NDVI, as they can provide more roots and stumps bank for asexual recovery of these species. Similarly, the higher forest recovery rate in the larch burned areas not only suggests the importance of the seed availability but also the conditions of the microclimate and soil properties in the post-fire larch environment for seed germination and growth (Figure 5.10f).

Even though we evaluated several factors related to the fire and environmental conditions that affect the patterns of post-fire forest succession in the boreal larch forest, many other unstudied parameters might also have strong direct- or indirect-influences on the post-fire forest patterns. In addition to the burn severity, other paramaters of the fire regime such as fire intensity, fire severity and fire frequency are also significant factors in determining the heterogeneity of post-fire landscape as well as species composition (Otoda et al., 2013, Lozano et al., 2012, Zyryanova et al., 2007, Zyryanova et al., 2010a, Sofronov and Volokitina, 2010). For example, the high and very high fire frequency may lead to replacement of the forest vegetation by the non-arboreal vegetation such as the meadow, the shrub, or the tundra, and may even take 50 to hundreds years to recover to the pre-fire conditions (Bergeron et al., 2001, Zyryanova et al., 2010a). The fire intensity and fire severity may be important variables that might have higher correlation with vegetation recovery than the burn severity predictor variable.

Unfortunately, estimates of fire intensity and fire severity by means of remote sensing were not feasible in this study as they require satellite images acquired shortly after the fire event. However, it should be noted that burn severity that is measured in an extended assessment using remote sensing can be used as a surrogate of the fire intensity and fire severity in monitoring the post-fire effects (Veraverbeke et al., 2010a, French et al., 2008, Keeley, 2009, Heward et al., 2013). Additionally, the post-fire soil properties, the soil organic layer depth and the permafrost conditions are also major factors that can determine the patterns of the boreal forest recovery. Kasischke et al. (2007) found that the organic layer depth remaining after fire is positively correlated with the post-fire conifer seedling density, while it is negatively affected by the broadleaf recruitment and growth in the North American boreal forest. These patterns of tree recruitment in the post-fire boreal forests are further affected by the soil moisture (Kasischke et al., 2007), the soil burn severity, the pre-fire conifer and broadleaf basal area and drainage (Johnstone and Kasischke, 2005). Siberian boreal larch forests typically have pre-fire organic layer much lower the North American boreal forest, about 10cm and 25cm respectively (Sofronov et al., 2004, Cai et al., 2013). The organic layer depth significantly affects the depth of soil thawing that, in turn, can drive larch forest growth and regeneration (Sofronov et al., 2004). In addition to the difference in fire types and species characteristics (de Groot et al., 2012), the response of the post-fire vegetation with respect to the organic layer depth as well as the soil thawing depth is thus expected to be different between these two boreal ecoregions that requires further investigation, particularly by the means of remote sensing.

5.6.3 Implications for post-fire forest succession and forest management

Post-fire successional trajectories in larch forests are highly sensitive to variations in fire regimes, physical environmental conditions and species characteristics. With the sensitivity of

the FVC and FRI to differentiate stages of post-fire forest recovery, an assessment of the driving factors that influence changes in the FVC and FRI based forest recovery rates as shown in this study has demonstrated consistent results with the field-based studies. Even though the monitoring of all successional stages after disturbances requires an effort in long period and/or the considerations of all the biotic and abiotic factors in the post-fire environment, the initial forest conditions and tree recruitment immediately (e.g. ≤ 15 years) after the fire can provide a critical observational window to predict the canopy patterns and stand dynamics up to a few decades (Johnstone et al., 2004). Therefore, using the prediction models of the early (i.e. grasses, shrubs, fire weeds and larch germinations) and later (i.e. dominant regrowth of larch species) successional stage based on our selected predictor variables can be useful to identify further successional pathways such as from the young to climax larch forest successions. For example, the high density of larch saplings as well as its high recovery rate measured by the FRI slope in the moderate burn severity sites for the first 20 years after fire can be a surrogate of the "self-replacement" succession in these sites. On the other hand, the low recovery rate and lack of seed source for the larch regeneration in the high burn severity sites can shift the larch dominated forest to the broadleaf dominated forest in the course of fire effects.

The variation in the initial stages of post-fire tree recruitment at different burn severity could result in large, long-term negative impacts on the forest carbon storage (Turner et al., 2004, Liu and Yang, 2014). As shown in this study, the larch forest in the areas of severe burns will take a longer recovery period to attain the pre-fire level of net primary productivity. This, in turn, will exacerbate climate change and thus the fire disturbances. Additionally, the transformation of closed to open forest or even grassland caused by fires could also result in changes of other natural cycles such as hydrological and biogeochemical cycles (Mayor et al.,

2007, Woods and Balfour, 2010, Certini, 2005). Therefore, our study suggests that incorporating the fire and environmental factors into the way that environmental conditions are classified in the management guidelines would improve their ability to guide restoration towards desired fire behavior, the forest composition and struture and landscape patterns. The landscapes could be evaluated to identify where the existing forest communities are significantly different than those expected for their environmental conditions to propose priority areas for the silvicultural treatments. We note, however, that our results for the single burned area should be examined for other burned areas in the same ecoregion to predict comprehensively the behavior of fires and forest responses at regional scales.

CHAPTER 6: SUMMARY AND CONCLUSIONS

6.1 Research contributions

The purpose of this research was to model and evaluate fire effects and forest regeneration patterns in a boreal larch forest ecosystem using remote sensing. As many of the remotely sensed data used in this research were collected at different spatial and temporal scales, new methodology frameworks have been developed to effectively and accurately characterize the post-fire effects of the burned area, the burn severity, and the environmental conditions that result in variability of forest regeneration. Modeling the post-fire forest patterns to answer ecological questions of the fire effects often requires a number of variables related to the fire regimes and environmental conditions which have causal links with the forest patterns. As such, each chapter presented in this dissertation builds on the concepts developed in the previous chapters, resulting in the entirely conceptual framework for evaluating and understanding the responses of the larch forest ecosystem to the environmental changes caused by fire through the remote sensing approach.

To overcome the challenges surrounding the environmental conditions and data limitations of the high northern latitudes as well as the remote regions of the boreal forests in quantifying the post-fire effects, the synergistic use of the multi-temporal and multi-sensor satellite data would be a useful approach. In Chapter 2 and Chapter 3 we developed methods for reconstructing the burned area and burn severity from remotely sensed data. We found that the mapping algorithm of the spring/fire season composites of the MODIS multispectral (MOD09A1) and the active-fire (MOD14A2) data not only accurately estimates the annual burned areas in the taiga-steppe transition zone of the boreal larch forest but also successfully categorizes the seasonal burned areas. Similarly, a data limitations-driven model of monitoring

the burn severity in the boreal larch forest was proposed using the multi-temporal Landsat images in coupling with the available high-resolution data of the WorldView-2 image and field-based measurements. The results of burn severity models showed strong effects of the pre-fire conditions, fire ecology, date of image acquisition and remote sensing indices on the assessment of burn severity. The potential use of mapping algorithms of the burned area and burn severity is not only to improve the prediction of carbon emission from the forest fire but also to better understand the complex interactions among the forest fire and ecological processes in the boreal ecosystems, particularly in the southern limit of the Siberian boreal larch forest.

Modeling the complexity of the post-fire forest patterns and their changes over time is a key issue in spatiotemporal forest management that is related to fires. Even though remote sensing has been acknowledged as one of the most powerful approaches to monitor terrestrial ecosystems, this technique has sometimes been demonstrated as an unrealistic and biased representation of the post-fire forest patterns due to the saturation issues of the vegetation indices as well as the lack of incorporation with forest structural parameters (Frolking et al., 2009, Buma, 2011, Chu and Guo, 2013). In Chapter 4 and Chapter 5, we overcame these limitations by proposing an integrated approach for monitoring and modeling the spatiotemporal patterns of post-fire forest recovery. The results in Chapter 4 showed that the Landsat time-series of the fractional vegetation cover (FVC) and the forest recovery index (FRI) can be used simultaneously to evaluate the different patterns of post-fire forest recovery, which can account for the early recovery stage of the shade-intolerant species (e.g. herbaceous plants, grasses, shrubs, broadleaf trees, and larch germination) and the late regeneration stage of the dominant larch forest regrowth. The recovery rate at different stages of the forest succession, which was revealed in Chapter 5, was significantly dependent upon the burn severity and site conditions of

the post-fire environments in which burn severity was the key factor of larch forest regeneration. The regeneration of larch forest is fastest in moderate burn severity. However, both the low and high severity fire disturbance reduced the regeneration rate of the larch tree recruitment and regrowth. Other environmental factors such as the distance to water body, the solar energy and the soil moisture condition also play important roles in determining the post-fire forest patterns in both the early successional stage and the larch-dominated regrowth stage. Our results of the post-fire successional trajectory and its driving factors will contribute direct implications for the post-fire forest managements in the Siberian boreal larch forest as well as provide the remote sensing tools for monitoring and modeling of the post-fire forest patterns.

6.2 Limitations and future research

Even though we achieve several important results in monitoring and modeling the post-fire effects and forest patterns through the remote sensing approach, several limitations remain in our research that need to be addressed in future research. As we now have a better understanding of how and why successional variability is occurring on the local burned areas in the boreal larch forest, the further stages of this research are to ascertain a greater understanding of the uncertainty surrounding the prediction models of the temporal and spatial post-fire forest structure and successional stages using satellite imagery, particularly on the landscape levels. This can be addressed by the quantitative analysis of post-fire spatiotemporal forest patterns derived from remote sensing observations with field-based inventory plots at the landscape scale as well as the extent of monitoring the time frame up to several decades after the fire disturbances. Additionally, many other biotic and abiotic factors (e.g. fire intensity, fire frequency, grazing intensity, permafrost depth, soil organic depth) also need to be measured for comprehensively understanding the influences of the fire and environmental conditions on the

resilience of the post-fire forest ecosystems. Finally, the differences in the temporal, spatial and radiometric resolution of the satellite data also limit monitoring and modeling the post-fire effects in our research. MODIS products with high temporal resolution are appropriate to monitor the occurrence of the fire events and the burned areas, but their low spatial resolution and short temporal coverage (from 2000 onwards) lead to high uncertainty of the post-fire effects as well as the ecological processes. On the other hand, the Landsat imagery with better spatial resolution and longer temporal coverage has lower temporal resolution and is not always available as the cloud-free images that limit the monitoring of the post-fire effects, particularly in mapping the immediately burned areas and burn severity. In addition to optical remote sensing, LiDAR and SAR data that have the ability to penetrate cloud cover are more appropriate for capturing vertically distributed elements and textures of land cover structure and change and are thus expected to improve the prediction models of the post-fire forest responses. Therefore, applying the approaches of data fusion is necessary to utilize the advantages of each satellite data to overcome the challenges and uncertainties in the courses of mapping, monitoring, and modeling the post-fire effects and responses of the forest ecosystems.

Different disturbances (e.g. fire, grazing, mining and logging) will have dissimilar mechanisms and result in the disparate temporal and spatial patterns of the landscapes. Understanding and modeling the mechanisms and patterns of various disturbances in the natural resources through the use of the remote sensing and GIS techniques are necessary for time and cost effectiveness of the management measures. For future applications, our methodology frameworks can be used to compare and project the recovery process in the boreal forest following the different natural disturbances (e.g. fire, climate change, and insect-borne diseases) and anthropogenic disturbances (e.g. harvesting, gas and oil exploitation, and land use practices).

Similarly, the responses of forest ecosystems to the disturbances differ in different ecoregions. Future research to test how our models for the fire disturbances can be applied to the other disturbances as well as the other boreal forest ecosystems around the world would be welcome.

REFERENCES

Alcaraz-Segura, D., Chuvieco, E., Epstein, H. E., Kasischke, E. S. & Trishchenko, A. 2010. Debating the greening vs. browning of the North American boreal forest: differences between satellite datasets. *Global change biology,* 16**,** 760-770.

Allen, J. L. & Sorbel, B. 2008. Assessing the differenced Normalized Burn Ratio's ability to map burn severity in the boreal forest and tundra ecosystems of Alaska's national parks. *International Journal of Wildland Fire,* 17**,** 463-475.

Babintseva, R. & Titova, Y. V. 1996. Effects of fire on the regeneration of larch forests in the Lake Baikal Basin. *FORESTRY SCIENCES,* 48**,** 358-365.

Barrett, K., Kasischke, E., Mcguire, A., Turetsky, M. & Kane, E. 2010. Modeling fire severity in black spruce stands in the Alaskan boreal forest using spectral and non-spectral geospatial data. *Remote Sensing of Environment,* 114**,** 1494-1503.

Barrett, K. & Kasischke, E. S. 2013. Controls on variations in MODIS fire radiative power in Alaskan boreal forests: Implications for fire severity conditions. *Remote Sensing of Environment,* 130**,** 171-181.

Barrett, K., Mcguire, A., Hoy, E. & Kasischke, E. 2011. Potential shifts in dominant forest cover in interior Alaska driven by variations in fire severity. *Ecological Applications,* 21**,** 2380-2396.

Bastarrika, A., Chuvieco, E. & Martãn, M. P. 2011a. Automatic Burned Land Mapping From MODIS Time Series Images: Assessment in Mediterranean Ecosystems. *Geoscience and Remote Sensing, IEEE Transactions on Geoscience and Remote Sensing,* 49**,** 3401-3413.

Bastarrika, A., Chuvieco, E. & Martãn, M. P. 2011b. Mapping burned areas from Landsat TM/ETM+ data with a two-phase algorithm: Balancing omission and commission errors. *Remote Sensing of Environment,* 115**,** 1003-1012.

Batkhuu, N. O., Lee, D. K. & Tsogtbaatar, J. 2011. Forest and Forestry Research and Education in Mongolia. *Journal of Sustainable Forestry,* 30**,** 600-617.

Beck, P. S., Goetz, S. J., Mack, M. C., Alexander, H. D., Jin, Y., Randerson, J. T. & Loranty, M. 2011. The impacts and implications of an intensifying fire regime on Alaskan boreal forest composition and albedo. *Global change biology,* 17**,** 2853-2866.

Bergeron, Y., Gauthier, S., Kafka, V., Lefort, P. & Lesieur, D. 2001. Natural fire frequency for the eastern Canadian boreal forest: consequences for sustainable forestry. *Canadian Journal of Forest Research,* 31**,** 384-391.

Berner, L. T., Beck, P. S. A., Bunn, A. G., Lloyd, A. H. & Goetz, S. J. 2010. High-latitude tree growth and satellite vegetation indices: correlations and trends in Russia and Canada (1982-2008). *Journal of Geophysical Research,* 116**,** G01015.

Beuning, K. R. M., Zimmerman, K. A., Ivory, S. J. & Cohen, A. S. 2011. Vegetation response to glacial-interglacial climate variability near Lake Malawi in the southern African tropics. *Palaeogeography, Palaeoclimatology, Palaeoecology,* 303**,** 81-92.

Boby, L. A., Schuur, E. A., Mack, M. C., Verbyla, D. & Johnstone, J. F. 2010. Quantifying fire severity, carbon, and nitrogen emissions in Alaska's boreal forest. *Ecological Applications,* 20**,** 1633-1647.

Boer, M. M., Macfarlane, C., Norris, J., Sadler, R. J., Wallace, J. & Grierson, P. F. 2008. Mapping burned areas and burn severity patterns in SW Australian eucalypt forest using remotely-sensed changes in leaf area index. *Remote Sensing of Environment,* 112**,** 4358-4369.

Boschetti, L., Roy, D. & Hoffmann, A. 2009. MODIS Collection 5 Burned Area Product-MCD45. *User's Guide. Ver,* 2.

Boyd, D. & Foody, G. 2010. An overview of recent remote sensing and GIS based research in ecological informatics. *Ecological Informatics,* 6**,** 25-36.

Breiman, L. 2001. Random forests. *Machine learning,* 45**,** 5-32.

Breiman, L., Friedman, J., Stone, C. J. & Olshen, R. A. 1984. *Classification and regression trees*, CRC press.

Brown, P. M., Kaufmann, M. R. & Shepperd, W. D. 1999. Long-term, landscape patterns of past fire events in a montane ponderosa pine forest of central Colorado. *Landscape ecology,* 14**,** 513-532.

Buma, B. 2011. Evaluating the utility and seasonality of NDVI values for assessing post-disturbance recovery in a subalpine forest. *Environmental Monitoring and Assessment***,** 1-12.

Cablk, M., White, D. & Kiester, A. 2002. Assessment of spatial autocorrelation in empirical models in ecology. *Predicting species occurrences: issues of scale and accuracy. Island Press, Washington DC***,** 429-440.

Cai, W., Yang, J., Liu, Z., Hu, Y. & Weisberg, P. J. 2013. Post-fire tree recruitment of a boreal larch forest in Northeast China. *Forest Ecology and Management,* 307**,** 20-29.

Cansler, C. A. & Mckenzie, D. 2012. How Robust Are Burn Severity Indices When Applied in a New Region? Evaluation of Alternate Field-Based and Remote-Sensing Methods. *Remote Sensing,* 4**,** 456-483.

Canty, M. J. & Nielsen, A. A. 2008. Automatic radiometric normalization of multitemporal satellite imagery with the iteratively re-weighted MAD transformation. *Remote Sensing of Environment,* 112**,** 1025-1036.

Carlson, T. N. & Ripley, D. A. 1997. On the relation between NDVI, fractional vegetation cover, and leaf area index. *Remote Sensing of Environment,* 62**,** 241-252.

Carmenta, R., Parry, L., Blackburn, A., Vermeylen, S. & Barlow, J. 2011. Understanding human-fire interactions in tropical forest regions: a case for interdisciplinary research across the natural and social sciences. *Ecology and society,* 16**,** -.

Casady, G. M., Van Leeuwen, W. J. D. & Marsh, S. E. 2009. Evaluating post-wildfire vegetation regeneration as a response to multiple environmental determinants. *Environmental Modeling and Assessment,* 15**,** 295-307.

Certini, G. 2005. Effects of fire on properties of forest soils: a review. *Oecologia,* 143**,** 1-10.

Chang, D. & Song, Y. 2009. Comparison of L3JRC and MODIS global burned area products from 2000 to 2007. *Journal of Geophysical Research: Atmospheres,* 114**,** D16106.

Chen, H. Y., Vasiliauskas, S., Kayahara, G. J. & Ilisson, T. 2009. Wildfire promotes broadleaves and species mixture in boreal forest. *Forest Ecology and Management,* 257**,** 343-350.

Chen, J., Wang, C., Jiang, H., Mao, L. & Yu, Z. 2011. Estimating soil moisture using Temperature–Vegetation Dryness Index (TVDI) in the Huang-huai-hai (HHH) plain. *International Journal of Remote Sensing,* 32**,** 1165-1177.

Christopoulou, A., Fyllas, N. M., Andriopoulos, P., Koutsias, N., Dimitrakopoulos, P. G. & Arianoutsou, M. 2014. Post-fire regeneration patterns of Pinus nigra in a recently burned area in Mount Taygetos, Southern Greece: The role of unburned forest patches. *Forest Ecology and Management,* 327**,** 148-156.

Chu, T. & Guo, X. 2013. Remote sensing techniques in monitoring post-fire effects and patterns of forest recovery in boreal forest regions: A Review. *Remote Sensing,* 6**,** 470-520.

Chu, T., Guo, X. 2015. Compositing MODIS time series for reconstructing burned areas in the taiga-steppe transition zone of northern Mongolia. International Journal of Wildland Fire, *24*(3), 419-432, http://dx.doi.org/10.1071/WF14124

Chu, T., Guo, X. & Takeda, K. 2015. Temporal dependence of burn severity assessment in the Siberian Larch *(Larix sibirica)* forest of northern Mongolia using remotely sensed data. *Submitted to International Journal of Wildland Fire.*

Chu, T., Guo, X. & Takeda, K. 2015. Remote sensing approach to detect post-fire vegetation regrowth in Siberian boreal larch forest. *Submitted to Ecological Indicators.*

Chu, T., Guo, X. & Takeda, K. 2015. Effects of burn severity and environmental conditions on post-fire regeneration variability of Siberian boreal forest. *Submitted to Remote Sensing of Environment.*

Chuvieco, E. & Congalton, R. G. 1989. Application of remote sensing and geographic information systems to forest fire hazard mapping. *Remote Sensing of Environment,* 29**,** 147-159.

Chuvieco, E., Englefield, P., Trishchenko, A. P. & Luo, Y. 2008a. Generation of long time series of burn area maps of the boreal forest from NOAA - AVHRR composite data. *Remote Sensing of Environment,* 112**,** 2381-2396.

Chuvieco, E., Giglio, L. & Justice, C. 2008b. Global characterization of fire activity: toward defining fire regimes from Earth observation data. *Global change biology,* 14**,** 1488-1502.

Chuvieco, E., Opazo, S., Sione, W., Valle, H. D., Anaya, J., Bella, C. D., Cruz, I., Manzo, L., Lopez, G. & Mari, N. 2008c. Global burned-land estimation in Latin America using MODIS composite data. *Ecological Applications,* 18**,** 64-79.

Cocke, A. E., Fulã©, P. Z. & Crouse, J. E. 2005. Comparison of burn severity assessments using Differenced Normalized Burn Ratio and ground data. *International Journal of Wildland Fire,* 14**,** 189-198.

Collins, B. M., Kelly, M., Van Wagtendonk, J. W. & Stephens, S. L. 2007. Spatial patterns of large natural fires in Sierra Nevada wilderness areas. *Landscape Ecology,* 22**,** 545-557.

Conard, S. G. & A Ivanova, G. 1997. Wildfire in Russian Boreal Forests--Potential Impacts of Fire Regime Characteristics on Emissions and Global Carbon Balance Estimates. *Environmental Pollution,* 98**,** 305-313.

Crotteau, J. S., Morgan Varner Iii, J. & Ritchie, M. W. 2013. Post-fire regeneration across a fire severity gradient in the southern Cascades. *Forest Ecology and Management,* 287**,** 103-112.

Cuevas-González, M., Gerard, F., Balzter, H. & Riaño, D. 2008. Studying the change in fAPAR after forest fires in Siberia using MODIS. *International Journal of Remote Sensing,* 29**,** 6873-6892.

Cuevas Gonzalez, M., Gerard, F., Balzter, H. & Riano, D. 2009. Analysing forest recovery after wildfire disturbance in boreal Siberia using remotely sensed vegetation indices. *Global change biology,* 15**,** 561-577.

De Groot, W. J., Cantin, A. S., Flannigan, M. D., Soja, A. J., Gowman, L. M. & Newbery, A. 2012. A comparison of Canadian and Russian boreal forest fire regimes. *Forest Ecology and Management,* 294**,** 23-34.

De Santis, A., Asner, G. P., Vaughan, P. J. & Knapp, D. E. 2010. Mapping burn severity and burning efficiency in California using simulation models and Landsat imagery. *Remote Sensing of Environment,* 114**,** 1535-1545.

De Santis, A. & Chuvieco, E. 2007. Burn severity estimation from remotely sensed data: Performance of simulation versus empirical models. *Remote Sensing of Environment,* 108**,** 422-435.

De Santis, A. & Chuvieco, E. 2009. GeoCBI: A modified version of the Composite Burn Index for the initial assessment of the short-term burn severity from remotely sensed data. *Remote Sensing of Environment,* 113**,** 554-562.

Delbart, N., Le Toan, T., Kergoat, L. & Fedotova, V. 2006. Remote sensing of spring phenology in boreal regions: A free of snow-effect method using NOAA-AVHRR and SPOT-VGT data (1982–2004). *Remote Sensing of Environment,* 101**,** 52-62.

Diaz-Delgado, R., Lloret, F. & Pons, X. 2003. Influence of fire severity on plant regeneration by means of remote sensing imagery. *International Journal of Remote Sensing,* 24**,** 1751-1763.

Dorisuren, C. Post-fire successions of the larch forests in Mongolia. First International Central Asian Wildland Fire Joint Conference and Consultation, 2008 Ulaanbaatar, Mongolia. 24.

Dube, O. P. 2009. Linking fire and climate: interactions with land use, vegetation, and soil. *Current Opinion in Environmental Sustainability,* 1**,** 161-169.

Dubinin, M., Potapov, P., Lushchekina, A. & Radeloff, V. C. 2010. Reconstructing long time series of burned areas in arid grasslands of southern Russia by satellite remote sensing. *Remote Sensing of Environment,* 114**,** 1638-1648.

Dulamsuren, C., Hauck, M., Bader, M., Osokhjargal, D., Oyungerel, S., Nyambayar, S., Runge, M. & Leuschner, C. 2009. Water relations and photosynthetic performance in Larix sibirica growing in the forest-steppe ecotone of northern Mongolia. *Tree physiology,* 29**,** 99-110.

Dulamsuren, C., Hauck, M., Khishigjargal, M., Leuschner, H. H. & Leuschner, C. 2010a. Diverging climate trends in Mongolian taiga forests influence growth and regeneration of Larix sibirica. *Oecologia,* 163**,** 1091-1102.

Dulamsuren, C., Hauck, M. & Leuschner, C. 2010b. Recent drought stress leads to growth reductions in Larix sibirica in the western Khentey, Mongolia. *Global Change Biology,* 16**,** 3024-3035.

Dulamsuren, C., Wommelsdorf, T., Zhao, F., Xue, Y., Zhumadilov, B. Z., Leuschner, C. & Hauck, M. 2013. Increased summer temperatures reduce the growth and regeneration of Larix sibirica in southern boreal forests of eastern Kazakhstan. *Ecosystems,* 16**,** 1536-1549.

Earsel. Disaster Management and Emergency Response in the Mediterranean Region. *In:* OLUIC, M., ed. 1st International Conference on Remote Sensing Techniques in Disaster Management and Emergency Response in the Mediterranean Region, 2008 Croatia. European Association of Remote Sensing Laboratories (EARSEL).

Eckert, S., Hüsler, F., Liniger, H. & Hodel, E. 2015. Trend analysis of MODIS NDVI time series for detecting land degradation and regeneration in Mongolia. *Journal of Arid Environments,* 113**,** 16-28.

Epting, J. & Verbyla, D. 2005. Landscape-level interactions of prefire vegetation, burn severity, and postfire vegetation over a 16-year period in interior Alaska. *Canadian Journal of Forest Research,* 35**,** 1367-1377.

Epting, J., Verbyla, D. & Sorbel, B. 2005. Evaluation of remotely sensed indices for assessing burn severity in interior Alaska using Landsat TM and ETM+. *Remote Sensing of Environment,* 96**,** 328-339.

Falkowski, M. J., Evans, J. S., Martinuzzi, S., Gessler, P. E. & Hudak, A. T. 2009. Characterizing forest succession with lidar data: An evaluation for the Inland Northwest, USA. *Remote Sensing of Environment,* 113**,** 946-956.

Fao 2010. Global Forest Resources Assessment 2010 - Main report. *Food and Agriculture Organization of the United Nations (FAO) Forestry Paper,* 163, Rome, Italia.

Farukh, M. A., Hayasaka, H. & Mishigdorj, O. 2009. Recent Tendency of Mongolian Wildland Fire Incidence: Analysis Using MODIS Hotspot and Weather Data. *Journal of Natural Disaster Science,* 31**,** 23-33.

Flannigan, M., Amiro, B., Logan, K., Stocks, B. & Wotton, B. 2006. Forest fires and climate change in the 21 st century. *Mitigation and Adaptation Strategies for Global Change,* 11**,** 847-859.

Flannigan, M., Cantin, A. S., De Groot, W. J., Wotton, M., Newbery, A. & Gowman, L. M. 2013. Global wildland fire season severity in the 21st century. *Forest Ecology and Management,* 294**,** 54-61.

Flannigan, M., Stocks, B. J. & Wotton, B. 2000. Climate change and forest fires. *Science of the total environment,* 262**,** 221-229.

Fraser, R. H. & Li, Z. 2002. Estimating fire-related parameters in boreal forest using SPOT VEGETATION. *Remote Sensing of Environment,* 82**,** 95-110.

French, N. H. F., Kasischke, E. S., Hall, R. J., Murphy, K. A., Verbyla, D. L., Hoy, E. E. & Allen, J. L. 2008. Using Landsat data to assess fire and burn severity in the North American boreal forest region: an overview and summary of results. *International Journal of Wildland Fire,* 17**,** 443-462.

Frolking, S., Palace, M., Clark, D., Chambers, J., Shugart, H. & Hurtt, G. 2009. Forest disturbance and recovery: A general review in the context of spaceborne remote sensing of impacts on aboveground biomass and canopy structure. *Journal of Geophysical Research,* 114**,** G00E02.

Fu, B. & Burgher, I. 2015. Riparian vegetation NDVI dynamics and its relationship with climate, surface water and groundwater. *Journal of Arid Environments,* 113**,** 59-68.

Fu, P. & Rich, P. M. Design and implementation of the Solar Analyst: an ArcView extension for modeling solar radiation at landscape scales. Proceedings of the 19th annual ESRI user conference, 1999. San Diego, USA, 1-33.

Fu, P. & Rich, P. M. 2002. A geometric solar radiation model with applications in agriculture and forestry. *Computers and electronics in agriculture,* 37**,** 25-35.

Furyaev, V. V. V., Eugene A.; Tchebakova, Nadejda M.; Valendik, Erik N. 2001. Effects of fire and climate on successions and structural changes in the Siberian Boreal forest. *Eurasian Journal of Forest Research,* 2**,** 1-15.

George, C., Rowland, C., Gerard, F. & Balzter, H. 2006. Retrospective mapping of burnt areas in Central Siberia using a modification of the normalised difference water index. *Remote Sensing of Environment,* 104**,** 346-359.

Giglio, L., Csiszar, I., Restã¡S, Ã., Morisette, J. T., Schroeder, W., Morton, D. & Justice, C. O. 2008. Active fire detection and characterization with the advanced spaceborne thermal emission and reflection radiometer (ASTER). *Remote Sensing of Environment,* 112**,** 3055-3063.

Giglio, L., Loboda, T., Roy, D. P., Quayle, B. & Justice, C. O. 2009. An active-fire based burned area mapping algorithm for the MODIS sensor. *Remote Sensing of Environment,* 113**,** 408-420.

Giglio, L., Randerson, J., Werf, G., Kasibhatla, P., Collatz, G., Morton, D. & Defries, R. 2010. Assessing variability and long-term trends in burned area by merging multiple satellite fire products. *Biogeosciences,* 7**,** 1171-1186.

Giglio, L., Randerson, J. T. & Van Der Werf, G. R. 2013. Analysis of daily, monthly, and annual burned area using the fourth-generation global fire emissions database (GFED4). *Journal of Geophysical Research: Biogeosciences,* 118**,** 317-328.

Gitas, I., Mitri, G., Veraverbeke, S. & Polychronaki, A. 2012. Advances in Remote Sensing of Post-Fire Vegetation Recovery Monitoring–A Review. *In 'Remote Sensing of Biomass – Principles and Applications'. (Ed. L Fatoyinbo) (InTech) Available at* *http://www.intechopen.com/books/remote-sensing-of-biomass-principles-and-applications/advances-in-remote-sensing-of-post-fire-monitoring-a-review*.

Gitelson, A. A., Kaufman, Y. J., Stark, R. & Rundquist, D. 2002. Novel algorithms for remote estimation of vegetation fraction. *Remote Sensing of Environment,* 80**,** 76-87.

Goetz, S. J., Fiske, G. J. & Bunn, A. G. 2006. Using satellite time-series data sets to analyze fire disturbance and forest recovery across Canada. *Remote Sensing of Environment,* 101**,** 352-365.

Greene, D., Noel, J., Bergeron, Y., Rousseau, M. & Gauthier, S. 2004. Recruitment of Picea mariana, Pinus banksiana, and Populus tremuloides across a burn severity gradient following wildfire in the southern boreal forest of Quebec. *Canadian Journal of Forest Research,* 34**,** 1845-1857.

Grégoire, J.-M., Tansey, K. & Silva, J. 2003. The GBA2000 initiative: developing a global burnt area database from SPOT-VEGETATION imagery. *International Journal of Remote Sensing,* 24**,** 1369-1376.

Hall, F. G., Botkin, D. B., Strebel, D. E., Woods, K. D. & Goetz, S. J. 1991. Large-scale patterns of forest succession as determined by remote sensing. *Ecology***,** 628-640.

Hall, R. J., Freeburn, J. T., De Groot, W. J., Pritchard, J. M., Lynham, T. J. & Landry, R. 2008. Remote sensing of burn severity: Experience from western Canada boreal fires. *International Journal of Wildland Fire,* 17**,** 476-489.

Han, Y., Wang, Y. & Zhao, Y. 2010. Estimating soil moisture conditions of the greater Changbai Mountains by land surface temperature and NDVI. *Geoscience and Remote Sensing, IEEE Transactions on,* 48**,** 2509-2515.

Hansen, M. C. & Loveland, T. R. 2011. A review of large area monitoring of land cover change using Landsat data. *Remote Sensing of Environment*.

Hantson, S., Padilla, M., Corti, D. & Chuvieco, E. 2013. Strengths and weaknesses of MODIS hotspots to characterize global fire occurrence. *Remote Sensing of Environment,* 131**,** 152-159.

Heward, H., Smith, A. M., Roy, D. P., Tinkham, W. T., Hoffman, C. M., Morgan, P. & Lannom, K. O. 2013. Is burn severity related to fire intensity? Observations from landscape scale remote sensing. *International Journal of Wildland Fire,* 22**,** 910-918.

Hicke, J. A., Asner, G. P., Kasischke, E. S., French, N. H., Randerson, J. T., James Collatz, G., Stocks, B. J., Tucker, C. J., Los, S. O. & Field, C. B. 2003. Postfire response of North American boreal forest net primary productivity analyzed with satellite observations. *Global change biology,* 9**,** 1145-1157.

Holzman, M., Rivas, R. & Piccolo, M. 2014. Estimating soil moisture and the relationship with crop yield using surface temperature and vegetation index. *International Journal of Applied Earth Observation and Geoinformation,* 28**,** 181-192.

Hoy, E. E., French, N. H., Turetsky, M. R., Trigg, S. N. & Kasischke, E. S. 2008. Evaluating the potential of Landsat TM/ETM+ imagery for assessing fire severity in Alaskan black spruce forests. *International Journal of Wildland Fire,* 17**,** 500-514.

Huang, C., Goward, S. N., Masek, J. G., Thomas, N., Zhu, Z. & Vogelmann, J. E. 2010. An automated approach for reconstructing recent forest disturbance history using dense Landsat time series stacks. *Remote Sensing of Environment,* 114**,** 183-198.

Huang, C., Goward, S. N., Schleeweis, K., Thomas, N., Masek, J. G. & Zhu, Z. 2009. Dynamics of national forests assessed using the Landsat record: Case studies in eastern United States. *Remote Sensing of Environment,* 113**,** 1430-1442.

Huang, F. & Wang, P. 2010. Vegetation change of ecotone in west of Northeast China plain using time-series remote sensing data. *Chinese Geographical Science,* 20**,** 167-175.

Hudak, A. & Brockett, B. 2004. Mapping fire scars in a southern African savannah using Landsat imagery. *International Journal of Remote Sensing,* 25**,** 3231-3243.

Iffn 2007. The Forest Fire Situation in Mongolia. *International Forest Fire News (IFFN),* 36**,** 46-66.

Jain, T. B., Graham, R. T. & Pilliod, D. S. 2004. Tongue-tied: confused meanings for common fire terminology can lead to fuels mismanagement. *Wildfire June/July, 22-26.*

Jain, T. B., Pilliod, D. S., Graham, R. T., Lentile, L. B. & Sandquist, J. E. 2012. Index for Characterizing Post-Fire Soil Environments in Temperate Coniferous Forests. *Forests,* 3**,** 445-466.

James, T. M. 2011. Temperature sensitivity and recruitment dynamics of Siberian larch (Larix sibirica) and Siberian spruce (Picea obovata) in northern Mongolia's boreal forest. *Forest Ecology and Management,* 262**,** 629-636.

Jin, Y., Randerson, J. T., Goetz, S. J., Beck, P. S. A., Loranty, M. M. & Goulden, M. L. 2012. The influence of burn severity on postfire vegetation recovery and albedo change during early succession in North American boreal forests. *Journal of Geophysical Research,* 117**,** G01036.

Johnson, E., Miyanishi, K. & Bridge, S. 2001. Wildfire regime in the boreal forest and the idea of suppression and fuel buildup. *Conservation Biology,* 15**,** 1554-1557.

Johnstone, J. & Chapin Iii, F. 2006a. Fire interval effects on successional trajectory in boreal forests of northwest Canada. *Ecosystems,* 9**,** 268-277.

Johnstone, J. F., Chapin, F. S., Hollingsworth, T. N., Mack, M. C., Romanovsky, V. & Turetsky, M. 2010a. Fire, climate change, and forest resilience in interior Alaska *Canadian Journal of Forest Research,* 40**,** 1302-1312.

Johnstone, J. F., Chapin Iii, F., Foote, J., Kemmett, S., Price, K. & Viereck, L. 2004. Decadal observations of tree regeneration following fire in boreal forests. *Canadian Journal of Forest Research,* 34**,** 267-273.

Johnstone, J. F. & Chapin Iii, F. S. 2006b. Effects of soil burn severity on post-fire tree recruitment in boreal forest. *Ecosystems,* 9**,** 14-31.

Johnstone, J. F., Hollingsworth, T. N., Chapin, F. S. & Mack, M. C. 2010b. Changes in fire regime break the legacy lock on successional trajectories in Alaskan boreal forest. *Global change biology,* 16**,** 1281-1295.

Johnstone, J. F. & Kasischke, E. S. 2005. Stand-level effects of soil burn severity on postfire regeneration in a recently burned black spruce forest. *Canadian Journal of Forest Research,* 35**,** 2151-2163.

Johnstone, J. F., Rupp, T. S., Olson, M. & Verbyla, D. 2011. Modeling impacts of fire severity on successional trajectories and future fire behavior in Alaskan boreal forests. *Landscape Ecology,* 26**,** 487-500.

Jones, M. O., Kimball, J. S. & Jones, L. A. 2013. Satellite Microwave Detection of Boreal Forest Recovery from the Extreme 2004 Wildfires in Alaska and Canada. *Global change biology*.

Justice, C. O., Giglio, L., Roy, D., Boschetti, L., Csiszar, I., Davies, D., Korontzi, S., Schroeder, W., Oâ€™Neal, K. & Morisette, J. 2011. MODIS-Derived Global Fire Products. *Land Remote Sensing and Global Environmental Change***,** 661-679.

Kane, V. R., Lutz, J. A., Alina Cansler, C., Povak, N. A., Churchill, D. J., Smith, D. F., Kane, J. T. & North, M. P. 2015. Water balance and topography predict fire and forest structure patterns. *Forest Ecology and Management,* 338**,** 1-13.

Kasischke, E. & French, N. 1997. Constraints on using AVHRR composite index imagery to study patterns of vegetation cover in boreal forests. *International Journal of Remote Sensing,* 18**,** 2403-2426.

Kasischke, E. S., Bourgeau-Chavez, L. L. & Johnstone, J. F. 2007. Assessing spatial and temporal variations in surface soil moisture in fire-disturbed black spruce forests in Interior Alaska using spaceborne synthetic aperture radar imagery—Implications for post-fire tree recruitment. *Remote Sensing of Environment,* 108**,** 42-58.

Kasischke, E. S. & Chapin Iii, F. S. 2008. Increasing vulnerability of Alaska's Boreal forest as a result of climate warming and the changing fire regime. *Sudden and disruptive climate change: its likelihood, character and significance. Edited by MC MacCracken, F. Moore, and JCJ Topping. Earthscan Publications, London, UK***,** 175-192.

Kasischke, E. S. & Johnstone, J. F. 2005. Variation in postfire organic layer thickness in a black spruce forest complex in interior Alaska and its effects on soil temperature and moisture. *Canadian Journal of Forest Research,* 35**,** 2164-2177.

Kasischke, E. S., Loboda, T., Giglio, L., French, N. H., Hoy, E., De Jong, B. & Riano, D. 2011. Quantifying burned area for North American forests: Implications for direct reduction of carbon stocks. *Journal of Geophysical Research,* 116**,** G04003.

Kasischke, E. S. & Stocks, B. J. 2000. *Fire, climate change, and carbon cycling in the boreal forest*, Springer-Verlag NewYork.

Kasischke, E. S., Turetsky, M. R., Ottmar, R. D., French, N. H., Hoy, E. E. & Kane, E. S. 2008. Evaluation of the composite burn index for assessing fire severity in Alaskan black spruce forests. *International Journal of Wildland Fire,* 17**,** 515-526.

Kasischke, E. S., Verbyla, D. L., Rupp, T. S., Mcguire, A. D., Murphy, K. A., Jandt, R., Barnes, J. L., Hoy, E. E., Duffy, P. A. & Calef, M. 2010. Alaskas changing fire regime

implications for the vulnerability of its boreal forests. *Canadian Journal of Forest Research,* 40**,** 1313-1324.

Kayes, L. J., Puettmann, K. J. & Anderson, P. D. 2011. Short term bryoid and vascular vegetation response to reforestation alternatives following wildfire in conifer plantations. *Applied Vegetation Science, 14(3), 326-339.*

Keating, K. A., Gogan, P. J., Vore, J. M. & Irby, L. R. 2007. A simple solar radiation index for wildlife habitat studies. *The Journal of wildlife management,* 71**,** 1344-1348.

Keeley, J. E. 2009. Fire intensity, fire severity and burn severity: a brief review and suggested usage. *International Journal of Wildland Fire,* 18**,** 116-126.

Keeley, J. E., Brennan, T. & Pfaff, A. H. 2008. Fire severity and ecosytem responses following crown fires in California shrublands. *Ecological Applications,* 18**,** 1530-1546.

Keeley, J. E., Keeley, M. B. & Bond, W. J. 1999. Stem demography and post-fire recruitment of a resprouting serotinous conifer. *Journal of Vegetation Science,* 10**,** 69-76.

Key, C. H. 2006. Ecological and sampling constraints on defining landscape fire severity. *Fire Ecology,* 2**,** 34-59.

Key, C. H. & Benson, N. C. 2006. Landscape assessment: ground measure of severity, the Composite Burn Index; and remote sensing of severity, the Normalized Burn Ratio. *In 'FIREMON: Fire Effects Monitoring and Inventory System'.* (Eds. DC Lutes, RE Keane, JF Caratti, CH Key, NC Benson, S Sutherland, LJ Gangi) USDA Forest Service, Rocky Mountain Research Station, General Techincal Report RMRS-GTR-164-CD: LA, pp. 1-15. (Ogden, UT).

Koike, T., Mori, S., Zyryanova, O., Kajimoto, T., Matsuura, Y. & Abaimov, A. 2010. Photosynthetic Characteristics of Trees and Shrubs Growing on the North-and South-Facing Slopes in Central Siberia. In *Permafrost Ecosystems (pp. 273-287).* Springer Netherlands.

Kosmas, C., Danalatos, N. & Gerontidis, S. 2000. The effect of land parameters on vegetation performance and degree of erosion under Mediterranean conditions. *Catena,* 40**,** 3-17.

Koutsias, N. & Karteris, M. 2000. Burned area mapping using logistic regression modeling of a single post-fire Landsat-5 Thematic Mapper image. *International Journal of Remote Sensing,* 21**,** 673-687.

Kukavskaya, E. A., Soja, A. J., Petkov, A. P., Ponomarev, E. I., Ivanova, G. A. & Conard, S. G. 2012. Fire emissions estimates in Siberia: evaluation of uncertainties in area burned, land cover, and fuel consumption. *Canadian Journal of Forest Research,* 43**,** 493-506.

Lee, J.-M., Lee, S.-W., Lim, J.-H., Won, M.-S. & Lee, H.-S. 2014. Effects of heterogeneity of pre-fire forests and vegetation burn severity on short-term post-fire vegetation density and regeneration in Samcheok, Korea. *Landscape and ecological engineering,* 10**,** 215-228.

Lentile, L. B., Holden, Z. A., Smith, A. M. S., Falkowski, M. J., Hudak, A. T., Morgan, P., Lewis, S. A., Gessler, P. E. & Benson, N. C. 2006. Remote sensing techniques to assess active fire characteristics and post-fire effects. *International Journal of Wildland Fire,* 15**,** 319-345.

Leon, J. R. R., Van Leeuwen, W. J. D. & Casady, G. M. 2012. Using MODIS-NDVI for the Modeling of Post-Wildfire Vegetation Response as a Function of Environmental Conditions and Pre-Fire Restoration Treatments. *Remote Sensing,* 4**,** 598-621.

Liang, J., Zhou, M., Verbyla, D. L., Zhang, L., Springsteen, A. L. & Malone, T. 2011. Mapping forest dynamics under climate change: A matrix model. *Forest Ecology and Management,* 262**,** 2250-2262.

Liu, B., Nearing, M. & Risse, L. 1994. Slope gradient effects on soil loss for steep slopes. *Transactions of the ASAE,* 37**,** 1835-1840.

Liu, Z. & Yang, J. 2014. Quantifying ecological drivers of ecosystem productivity of the early-successional boreal Larix gmelinii forest. *Ecosphere,* 5**,** art84.

Loboda, T., French, N., Hight-Harf, C., Jenkins, L. & Miller, M. 2013. Mapping fire extent and burn severity in Alaskan tussock tundra: An analysis of the spectral response of tundra vegetation to wildland fire. *Remote Sensing of Environment,* 134**,** 194-209.

Loboda, T., O'neal, K. & Csiszar, I. 2007. Regionally adaptable dNBR-based algorithm for burned area mapping from MODIS data. *Remote Sensing of Environment,* 109**,** 429-442.

Loboda, T. V. 2009. Modeling fire danger in data-poor regions: a case study from the Russian Far East. *International Journal of Wildland Fire,* 18**,** 19-35.

Loboda, T. V., Hoy, E. E., Giglio, L. & Kasischke, E. S. 2011. Mapping burned area in Alaska using MODIS data: a data limitations-driven modification to the regional burned area algorithm. *International Journal of Wildland Fire,* 20**,** 487-496.

Loboda, T. V., Zhang, Z., O'neal, K. J., Sun, G., Csiszar, I. A., Shugart, H. H. & Sherman, N. J. 2012. Reconstructing disturbance history using satellite-based assessment of the distribution of land cover in the Russian Far East. *Remote Sensing of Environment,* 118**,** 241-248.

Loepfe, L., Lloret, F. & Romãn-Cuesta, R. M. 2012. Comparison of burnt area estimates derived from satellite products and national statistics in Europe. *International Journal of Remote Sensing,* 33**,** 3653-3671.

Lozano, F. J., Suárez-Seoane, S. & De Luis-Calabuig, E. 2012. Does fire regime affect both temporal patterns and drivers of vegetation recovery in a resilient Mediterranean landscape? A remote sensing approach at two observation levels. *International Journal of Wildland Fire,* 21**,** 666-679.

Lozano, F. J., Suárez-Seoane, S. & De Luis, E. 2007. Assessment of several spectral indices derived from multi-temporal Landsat data for fire occurrence probability modelling. *Remote Sensing of Environment,* 107**,** 533-544.

Lyons, E. A., Jin, Y. & Randerson, J. T. 2008. Changes in surface albedo after fire in boreal forest ecosystems of interior Alaska assessed using MODIS satellite observations. *Journal of Geophysical Research,* 113**,** G02012.

Magnussen, S. & Wulder, M. A. 2012. Post-Fire Canopy Height Recovery in Canada's Boreal Forests Using Airborne Laser Scanner (ALS). *Remote Sensing,* 4**,** 1600-1616.

Mallinis, G. & Koutsias, N. 2012. Comparing ten classification methods for burned area mapping in a Mediterranean environment using Landsat TM satellite data. *International Journal of Remote Sensing,* 33**,** 4408-4433.

Mansuy, N., Gauthier, S., Robitaille, A. & Bergeron, Y. 2012. Regional patterns of postfire canopy recovery in the northern boreal forest of Quebec: interactions between surficial deposit, climate, and fire cycle. *Canadian Journal of Forest Research,* 42**,** 1328-1343.

Masek, J. G., Huang, C., Wolfe, R., Cohen, W., Hall, F., Kutler, J. & Nelson, P. 2008. North American forest disturbance mapped from a decadal Landsat record. *Remote Sensing of Environment,* 112**,** 2914-2926.

Mathworks 2008. MATLAB – The Language of Technical Computing. *The MathWorks, Inc., Natick, Massachusetts (2008).*

Mayor, A., Bautista, S., Llovet, J. & Bellot, J. 2007. Post-fire hydrological and erosional responses of a Mediterranean landscpe: Seven years of catchment-scale dynamics. *Catena,* 71**,** 68-75.

Mcelhinny, C., Gibbons, P., Brack, C. & Bauhus, J. 2005. Forest and woodland stand structural complexity: its definition and measurement. *Forest Ecology and Management,* 218**,** 1-24.

Mchugh, C. W. & Kolb, T. E. 2003. Ponderosa pine mortality following fire in northern Arizona. *International Journal of Wildland Fire,* 12**,** 245-245.

Meek, D., Hatfield, J., Howell, T., Idso, S. & Reginato, R. 1984. A generalized relationship between photosynthetically active radiation and solar radiation. *Agronomy journal,* 76**,** 939-945.

Miller, J. D., Knapp, E. E., Key, C. H., Skinner, C. N., Isbell, C. J., Creasy, R. M. & Sherlock, J. W. 2009. Calibration and validation of the relative differenced Normalized Burn Ratio (RdNBR) to three measures of fire severity in the Sierra Nevada and Klamath Mountains, California, USA. *Remote Sensing of Environment,* 113**,** 645-656.

Miller, J. D. & Thode, A. E. 2007. Quantifying burn severity in a heterogeneous landscape with a relative version of the delta Normalized Burn Ratio (dNBR). *Remote Sensing of Environment,* 109**,** 66-80.

Moreno Ruiz, J. A., Riaño, D., Arbelo, M., French, N. H., Ustin, S. L. & Whiting, M. L. 2012. Burned area mapping time series in Canada (1984–1999) from NOAA-AVHRR LTDR: A comparison with other remote sensing products and fire perimeters. *Remote Sensing of Environment,* 117**,** 407-414.

Mouillot, F., Schultz, M. G., Yue, C., Cadule, P., Tansey, K., Ciais, P. & Chuvieco, E. 2014. Ten years of global burned area products from spaceborne remote sensing—A review: Analysis of user needs and recommendations for future developments. *International Journal of Applied Earth Observation and Geoinformation,* 26**,** 64-79.

Mulder, V., De Bruin, S., Schaepman, M. & Mayr, T. 2011. The use of remote sensing in soil and terrain mapping--A review. *Geoderma,* 162(1), 1-19.

Murphy, K. A., Reynolds, J. H. & Koltun, J. M. 2008. Evaluating the ability of the differenced Normalized Burn Ratio (dNBR) to predict ecologically significant burn severity in Alaskan boreal forests. *International Journal of Wildland Fire,* 17**,** 490-499.

Murray, M. 2004. Dynamics of Biodiversity Loss and Permafrost Melt in Lake Hovsgol National Park, Mongolia. *Hovsgol GEF/WB Project TF028988,* Geo-Ecology Institute 301, Mongolia.

Namzalov, B. B., Kholboeva, S. A., Korolyuk, A. U., Baskhaeva, T. G., Tsirenova, M. G. & Mongush, A. M. 2012. Features of structure in zonal forest-steppe ecotone of South Siberia and Central Asia. *Arid Ecosystems,* 2**,** 78-85.

Oikonomakis, N. & Ganatsas, P. 2012. Land cover changes and forest succession trends in a site of Natura 2000 network (Elatia forest), in northern Greece. *Forest Ecology and Management,* 285**,** 153-163.

Otoda, T., Doi, T., Sakamoto, K., Hirobe, M., Nachin, B. & Yoshikawa, K. 2013. Frequent fires may alter the future composition of the boreal forest in northern Mongolia. *Journal of Forest Research,* 18**,** 246-255.

Patel, N., Anapashsha, R., Kumar, S., Saha, S. & Dadhwal, V. 2009. Assessing potential of MODIS derived temperature/vegetation condition index (TVDI) to infer soil moisture status. *International Journal of Remote Sensing,* 30**,** 23-39.

Pausas, J., Ribeiro, E. & Vallejo, R. 2004. Post-fire regeneration variability of Pinus halepensis in the eastern Iberian Peninsula. *Forest Ecology and Management,* 203**,** 251-259.

Pereira, J. M. C. 1999. A comparative evaluation of NOAA/AVHRR vegetation indexes for burned surface detection and mapping. *Geoscience and Remote Sensing, IEEE Transactions on,* 37**,** 217-226.

Petropoulos, G., Carlson, T., Wooster, M. & Islam, S. 2009. A review of Ts/VI remote sensing based methods for the retrieval of land surface energy fluxes and soil surface moisture. *Progress in Physical Geography,* 33**,** 224-250.

Pettorelli, N., Vik, J. O., Mysterud, A., Gaillard, J.-M., Tucker, C. J. & Stenseth, N. C. 2005. Using the satellite-derived NDVI to assess ecological responses to environmental change. *Trends in ecology & evolution,* 20**,** 503-510.

Picotte, J. J. & Robertson, K. M. 2011. Validation of remote sensing of burn severity in south-eastern US ecosystems. *International Journal of Wildland Fire,* 20**,** 453-464.

Pierce Jr, K. B., Ohmann, J. L., Wimberly, M. C., Gregory, M. J. & Fried, J. S. 2009. Mapping wildland fuels and forest structure for land management: A comparison of nearest

neighbor imputation and other methods. *Canadian Journal of Forest Research,* 39**,** 1901-1916.

Powell, S. L., Cohen, W. B., Healey, S. P., Kennedy, R. E., Moisen, G. G., Pierce, K. B. & Ohmann, J. L. 2010. Quantification of live aboveground forest biomass dynamics with Landsat time-series and field inventory data: A comparison of empirical modeling approaches. *Remote Sensing of Environment,* 114**,** 1053-1068.

Pu, R., Li, Z., Gong, P., Csiszar, I., Fraser, R., Hao, W.-M., Kondragunta, S. & Weng, F. 2007. Development and analysis of a 12-year daily 1-km forest fire dataset across North America from NOAA/AVHRR data. *Remote Sensing of Environment,* 108**,** 198-208.

Quintano, C., Fernández-Manso, A. & Roberts, D. A. 2013. Multiple Endmember Spectral Mixture Analysis (MESMA) to map burn severity levels from Landsat images in Mediterranean countries. *Remote Sensing of Environment,* 136**,** 76-88.

Randerson, J. T., Chen, Y., Van Der Werf, G. R., Rogers, B. M. & Morton, D. C. 2012. Global burned area and biomass burning emissions from small fires. *Journal of Geophysical Research: Biogeosciences,* 117**,** G04012.

Renard, K. G., Foster, G. R., Weesies, G. A. & Porter, J. P. 1991. RUSLE: Revised universal soil loss equation. *Journal of soil and Water Conservation,* 46**,** 30-33.

Richter, R. 1990. A fast atmospheric correction algorithm applied to Landsat TM images. *International Journal of Remote Sensing,* 11**,** 159-166.

Roder, A., Hill, J., Duguy, B., Alloza, J. A. & Vallejo, R. 2007. Using long time series of Landsat data to monitor fire events and post-fire dynamics and identify driving factors. A case study in the Ayora region (eastern Spain). *Remote Sensing of Environment,* 112**,** 259-273.

Roy, D., Boschetti, L., Justice, C. & Ju, J. 2008. The collection 5 MODIS burned area product - Global evaluation by comparison with the MODIS active fire product. *Remote Sensing of Environment,* 112**,** 3690-3707.

Roy, D., Jin, Y., Lewis, P. & Justice, C. 2005. Prototyping a global algorithm for systematic fire-affected area mapping using MODIS time series data. *Remote Sensing of Environment,* 97**,** 137-162.

Roy, D. P. & Boschetti, L. 2009. Southern Africa validation of the MODIS, L3JRC, and GlobCarbon burned-area products. *Geoscience and Remote Sensing, IEEE Transactions on,* 47**,** 1032-1044.

Roy, D. P., Boschetti, L. & Trigg, S. N. 2006. Remote sensing of fire severity: assessing the performance of the normalized burn ratio. *Geoscience and Remote Sensing Letters, IEEE,* 3**,** 112-116.

Russell-Smith, J., Gardener, M. R., Brock, C., Brennan, K., Yates, C. P. & Grace, B. 2012. Fire persistence traits can be used to predict vegetation response to changing fire regimes at expansive landscape scales - an Australian example. *Journal of Biogeography*.

Sandholt, I., Rasmussen, K. & Andersen, J. 2002. A simple interpretation of the surface temperature/vegetation index space for assessment of surface moisture status. *Remote Sensing of Environment,* 79**,** 213-224.

Schimmel, J. & Granström, A. 1996. Fire Severity and Vegetation Response in the Boreal Swedish Forest. *Ecology,* 77**,** 1436-1450.

Schoennagel, T., Veblen, T. T. & Romme, W. H. 2004. The interaction of fire, fuels, and climate across Rocky Mountain forests. *BioScience,* 54**,** 661-676.

Schroeder, T. A., Cohen, W. B., Song, C., Canty, M. J. & Yang, Z. 2006. Radiometric correction of multi-temporal Landsat data for characterization of early successional forest patterns in western Oregon. *Remote Sensing of Environment,* 103**,** 16-26.

Schroeder, T. A., Cohen, W. B. & Yang, Z. 2007. Patterns of forest regrowth following clearcutting in western Oregon as determined from a Landsat time-series. *Forest Ecology and Management,* 243**,** 259-273.

Schroeder, W., Prins, E., Giglio, L., Csiszar, I., Schmidt, C., Morisette, J. & Morton, D. 2008. Validation of GOES and MODIS active fire detection products using ASTER and ETM+ data. *Remote Sensing of Environment,* 112**,** 2711-2726.

Seidl, R., Fernandes, P. M., Fonseca, T. F., Gillet, F. O., Johnsson, A. M., Mergania • Ova, K., Netherer, S., Arpaci, A., Bontemps, J.-D., Bugmann, H., Gonzã¡Lez-Olabarria, J. R., Lasch, P., Meredieu, C. L., Moreira, F., Schelhaas, M.-J. & Mohren, F. 2010. Modelling natural disturbances in forest ecosystems: a review. *Ecological Modelling,* 222**,** 903-924.

Shenoy, A., Johnstone, J. F., Kasischke, E. S. & Kielland, K. 2010. Persistent effects of fire severity on early successional forests in interior Alaska. *Forest Ecology and Management,* 261**,** 381-390.

Shive, K. L., Kuenzi, A. M., Sieg, C. H. & Fulé, P. Z. 2013. Pre-fire fuel reduction treatments influence plant communities and exotic species 9 years after a large wildfire. *Applied Vegetation Science,* 16**,** 457-469.

Sofronov, M. & Volokitina, A. 2010. Wildfire ecology in continuous permafrost zone. *Permafrost Ecosystems.* Springer, Netherlands.

Sofronov, M. A., Volokitina, A. V., Kajimoto, T. & Uemura, S. 2004. The Ecological role of moss-lichen cover and thermal amelioration of larch forest ecosystems in the northern part of Siberia. *Eurasian Journal of Forest Research,* 7**,** 11-19.

Solans Vila, J. P. & Barbosa, P. 2010. Post-fire vegetation regrowth detection in the Deiva Marina region (Liguria-Italy) using Landsat TM and ETM+ data. *Ecological Modelling,* 221**,** 75-84.

Son, N., Chen, C., Chen, C., Chang, L. & Minh, V. 2012. Monitoring agricultural drought in the Lower Mekong Basin using MODIS NDVI and land surface temperature data. *International Journal of Applied Earth Observation and Geoinformation,* 18**,** 417-427.

Sorbel, B. & Allen, J. 2005. Space-based burn severity mapping in Alaska's National Parks. *Alaska Park Science,* 4**,** 5-11.

Soverel, N. O., Coops, N. C., Perrakis, D. D. B., Daniels, L. D. & Gergel, S. E. 2011. The transferability of a dNBR-derived model to predict burn severity across 10 wildland fires in western Canada. *International Journal of Wildland Fire,* 20**,** 518-531.

Soverel, N. O., Perrakis, D. D. B. & Coops, N. C. 2010. Estimating burn severity from Landsat dNBR and RdNBR indices across western Canada. *Remote Sensing of Environment,* 114**,** 1896-1909.

Steyaert, L., Hall, F. & Loveland, T. 1997. Land cover mapping, fire regeneration, and scaling studies in the Canadian boreal forest with 1 km AVHRR and Landsat TM data. *Journal of Geophysical Research,* 102**,** 29581-29,598.

Stroppiana, D., Bordogna, G., Carrara, P., Boschetti, M., Boschetti, L. & Brivio, P. 2012. A method for extracting burned areas from Landsat TM/ETM+ images by soft aggregation

of multiple Spectral Indices and a region growing algorithm. *ISPRS Journal of Photogrammetry and Remote Sensing,* 69**,** 88-102.

Sunderman, S. O. & Weisberg, P. J. 2011. Remote sensing approaches for reconstructing fire perimeters and burn severity mosaics in desert spring ecosystems. *Remote Sensing of Environment,* 115**,** 2384-2389.

Takeda, K., Torita H., Nobori Y., Lopez C.M.L & J., I. Regeneration in burned Larch forests of Hovsgol region, northern Mongolia. *In:* TAKEDA, K., ed. Multidisciplinary Research on Mongolian Ecosystem, 2013 Ulaanbaatar, Mongolia. Japan Society of Forest Planning Press.

Taki, S., Nobori Y., Lopez C.M.L, Takeda, K., Ishida S. & C., M. A simulation of larch forest dynamics associated with fire in northern Mongolia. *In:* TAKEDA, K., ed. Multidisciplinary Research on Mongolian Ecosystem, 2013 Ulaanbaatar, Mongolia. Japan Society of Forest Planning Press.

Tanase, M., De La Riva, J. & Pérez-Cabello, F. 2011a. Estimating burn severity at the regional level using optically based indices. *Canadian Journal of Forest Research,* 41**,** 863-872.

Tanase, M., De La Riva, J., Santoro, M., Pérez-Cabello, F. & Kasischke, E. 2011b. Sensitivity of SAR data to post-fire forest regrowth in Mediterranean and boreal forests. *Remote Sensing of Environment,* 115**,** 2075-2085.

Tang, C. Q., He, L.-Y., Su, W.-H., Zhang, G.-F., Wang, H.-C., Peng, M.-C., Wu, Z.-L. & Wang, C.-Y. 2012. Regeneration, recovery and succession of a Pinus yunnanensis community five years after a mega-fire in central Yunnan, China. *Forest Ecology and Management,* 294**,** 188-196.

Tansey, K., Grégoire, J. M., Defourny, P., Leigh, R., Pekel, J. F., Van Bogaert, E. & Bartholomé, E. 2008. A new, global, multi-annual (2000–2007) burnt area product at 1 km resolution. *Geophysical Research Letters,* 35.

Tansey, K., Grégoire, J. M., Stroppiana, D., Sousa, A., Silva, J., Pereira, J., Boschetti, L., Maggi, M., Brivio, P. A. & Fraser, R. 2004. Vegetation burning in the year 2000: Global burned area estimates from SPOT VEGETATION data. *Journal of Geophysical Research: Atmospheres (1984–2012),* 109.

Team, R. D. C. 2008. R: A Language and Environment for Statistical Computing. *3-900051-07-0R Foundation for Statistical Computing, Vienna, Austria (2008).*

Teillet, P., Guindon, B. & Goodenough, D. 1982. On the slope-aspect correction of multispectral scanner data. *Canadian Journal of Remote Sensing,* 8**,** 84-106.

Tsela, P., Van Helden, P., Frost, P., Wessels, K. & Archibald, S. Validation of the MODIS burned-area products across different biomes in South Africa. International Geoscience and Remote Sensing Symposium (IGARSS), 2010 IEEE International, 2010. IEEE, 3652-3655.

Tsogtbaatar, J. 2004. Deforestation and reforestation needs in Mongolia. *Forest Ecology and Management,* 201**,** 57-63.

Turner, M. G., Romme, W. H. & Gardner, R. H. 1999. Prefire heterogeneity, fire severity, and early postfire plant reestablishment in subalpine forests of Yellowstone National Park, Wyoming. *International Journal of Wildland Fire,* 9**,** 21-36.

Turner, M. G., Tinker, D. B., Romme, W. H., Kashian, D. M. & Litton, C. M. 2004. Landscape patterns of sapling density, leaf area, and aboveground net primary production in postfire lodgepole pine forests, Yellowstone National Park (USA). *Ecosystems,* 7**,** 751-775.

Usfws 2003. Role of Fire in Alaska. February 2003 ed. National Wildfire Refuge System, 1011 E. Tudor Road, Anchorage, Alaska.

Van Leeuwen, W. J. D., Casady, G. M., Neary, D. G., Bautista, S., Alloza, J. A., Carmel, Y., Wittenberg, L., Malkinson, D. & Orr, B. J. 2010. Monitoring post-wildfire vegetation response with remotely sensed time-series data in Spain, USA and Israel. *International Journal of Wildland Fire,* 19**,** 75-93.

Veilleux-Nolin, M. & Payette, S. 2012. Influence of recent fire season and severity on black spruce regeneration in spruce–moss forests of Quebec, Canada. *Canadian Journal of Forest Research,* 42**,** 1316-1327.

Veraverbeke, S., Hook, S. & Hulley, G. 2012a. An alternative spectral index for rapid fire severity assessments. *Remote Sensing of Environment,* 123**,** 72-80.

Veraverbeke, S. & Hook, S. J. 2013. Evaluating spectral indices and spectral mixture analysis for assessing fire severity, combustion completeness and carbon emissions. *International Journal of Wildland Fire,* 22**,** 707-720.

Veraverbeke, S., Lhermitte, S., Verstraeten, W. W. & Goossens, R. 2010a. The temporal dimension of differenced Normalized Burn Ratio (dNBR) fire/burn severity studies: The

case of the large 2007 Peloponnese wildfires in Greece. *Remote Sensing of Environment,* 114**,** 2548-2563.

Veraverbeke, S., Lhermitte, S., Verstraeten, W. W. & Goossens, R. 2011. Evaluation of pre/post-fire differenced spectral indices for assessing burn severity in a Mediterranean environment with Landsat Thematic Mapper. *International Journal of Remote Sensing,* 32**,** 3521-3537.

Veraverbeke, S., Somers, B., Gitas, I., Katagis, T., Polychronaki, A. & Goossens, R. 2012b. Spectral mixture analysis to assess post-fire vegetation regeneration using Landsat Thematic Mapper imagery: Accounting for soil brightness variation. *International Journal of Applied Earth Observation and Geoinformation,* 14**,** 1-11.

Veraverbeke, S., Verstraeten, W. W., Lhermitte, S. & Goossens, R. 2010b. Evaluating Landsat Thematic Mapper spectral indices for estimating burn severity of the 2007 Peloponnese wildfires in Greece. *International Journal of Wildland Fire,* 19**,** 558-569.

Verbyla, D. & Lord, R. 2008. Estimating post-fire organic soil depth in the Alaskan boreal forest using the Normalized Burn Ratio. *International Journal of Remote Sensing,* 29**,** 3845-3853.

Verbyla, D. L., Kasischke, E. S. & Hoy, E. E. 2008. Seasonal and topographic effects on estimating fire severity from Landsat TM/ETM+ data. *International Journal of Wildland Fire,* 17**,** 527-534.

Vermote, E. & Kotchenova, S. 2008. MOD09 (Surface Reflectance) User's Guide. *http://modis-sr.ltdri.org/products/MOD09_UserGuide_v1_2.pdf*.

Voepel, H., Ruddell, B., Schumer, R., Troch, P. A., Brooks, P. D., Neal, A., Durcik, M. & Sivapalan, M. 2011. Quantifying the role of climate and landscape characteristics on hydrologic partitioning and vegetation response. *Water Resources Research,* 47**,** W00J09.

Wang, C., Qi, S., Niu, Z. & Wang, J. 2004. Evaluating soil moisture status in China using the temperature-vegetation dryness index (TVDI). *Canadian journal of remote sensing,* 30**,** 671-679.

Wang, S., Miao, L. & Peng, G. 2012. An Improved Algorithm for Forest Fire Detection Using HJ Data. *Procedia Environmental Sciences,* 13**,** 140-150.

Wilson, E. H. & Sader, S. A. 2002. Detection of forest harvest type using multiple dates of Landsat TM imagery. *Remote Sensing of Environment,* 80**,** 385-396.

Wittich, K. & Hansing, O. 1995. Area-averaged vegetative cover fraction estimated from satellite data. *International Journal of Biometeorology,* 38**,** 209-215.

Woods, S. W. & Balfour, V. N. 2010. The effects of soil texture and ash thickness on the post-fire hydrological response from ash-covered soils. *Journal of Hydrology,* 393**,** 274-286.

Wooster, M., Xu, W. & Nightingale, T. 2012. Sentinel-3 SLSTR active fire detection and FRP product: Pre-launch algorithm development and performance evaluation using MODIS and ASTER datasets. *Remote Sensing of Environment, 120, 236-254.*

Wu, Z., He, H., Liang, Y., Cai, L. & Lewis, B. 2013. Determining Relative Contributions of Vegetation and Topography to Burn Severity from LANDSAT Imagery. *Environmental Management,* 52**,** 821-836.

Yang, G., Pu, R., Zhang, J., Zhao, C., Feng, H. & Wang, J. 2013. Remote sensing of seasonal variability of fractional vegetation cover and its object-based spatial pattern analysis over mountain areas. *ISPRS Journal of Photogrammetry and Remote Sensing,* 77**,** 79-93.

Yi, K., Tani, H., Zhang, J., Guo, M., Wang, X. & Zhong, G. 2013. Long-Term Satellite Detection of Post-Fire Vegetation Trends in Boreal Forests of China. *Remote Sensing,* 5**,** 6938-6957.

Yoshikawa, K., Bolton, W. R., Romanovsky, V. E., Fukuda, M. & Hinzman, L. D. 2002. Impacts of wildfire on the permafrost in the boreal forests of Interior Alaska. *Journal of Geophysical Research: Atmospheres (1984–2012),* 107**,** FFR 4-1-FFR 4-14.

Yu, X., Wu, Z., Jiang, W. & Guo, X. 2015. Predicting daily photosynthetically active radiation from global solar radiation in the Contiguous United States. *Energy Conversion and Management,* 89**,** 71-82.

Zhang, Q., Pavlic, G., Chen, W., Latifovic, R., Fraser, R. & Cihlar, J. 2004. Deriving stand age distribution in boreal forests using SPOT VEGETATION and NOAA AVHRR imagery. *Remote Sensing of Environment,* 91**,** 405-418.

Zhao, F. J., Shu, L. F., Wang, M. Y., Liu, B. & Yang, L. J. 2012. Influencing factors on early vegetation restoration in burned area of Pinus pumila - Larch forest. *Acta Ecologica Sinica,* 32**,** 57-61.

Zyryanova, O., Abaimov, A., Bugaenko, T. & Bugaenko, N. 2010a. Recovery of forest vegetation after fire disturbance. In *Permafrost Ecosystems* (pp. 83-96). Springer, Netherlands.

Zyryanova, O., Abaimov, A., Daimaru, H. & Matsuura, Y. 2010b. Floristic diversity and its geographical background in central Siberia. in *Permafrost Ecosystems (*pp. 17-39). Springer, Netherlands.

Zyryanova, O. A., Yabarov, V., Tchikhacheva, T. L., Koike, T., Makoto, K., Matsuura, Y., Satoh, F. & Zyryanova, V. 2007. The structure and biodiversity after fire disturbance in Larix gmelinii (Rupr.) Rupr. forests, northeastern Asia. *Eurasian J For Res,* 10**,** 19-29.